



Guanylate cyclase-activating protein 5 from the zebrafish retina binds ferrous iron and is a redox-sensitive regulator of retinal guanylate cyclases

Von der Fakultät für Mathematik und Naturwissenschaften der
Carl von Ossietzky Universität Oldenburg
zur Erlangung des Grades und Titels einer

Doktorin der Naturwissenschaften (Dr. rer. nat.)

angenommene Dissertation

von

Frau Sarah-Karina Menke-Sell
geboren am 16.06.1991 in Oldenburg (Oldb)

Betreuender Gutachter: Prof. Dr. Karl-Wilhelm Koch

Zweitgutachterin: apl. Prof. Dr. Ulrike Janssen-Bienhold

Tag der Disputation: 04.05.2023

Zusammenfassung

Guanylatcyclase-aktivierende Proteine (GCAPs) sind neuronale Calciumsensoren, die Ca^{2+} -abhängig Photorezeptor-spezifische Guanylatcyclasen (GCs) aktivieren und somit die Produktion von cyclischem Guanosinmonophosphat (cGMP) regulieren. Der Zebrafisch (*Danio rerio*) exprimiert in der Retina insgesamt sechs GCAP-Isoformen: GCAP1, 2, 3, 4, 5 und 7. Frühere Studien haben gezeigt, dass GCAP5 sich anders verhält als die übrigen zebrafisch GCAPs und dass ein nicht konservierter Cysteincluster am *N*-Terminus, genauer Cys15 und Cys17, daran beteiligt sein könnte. In dieser Studie zeige ich, dass diese Cysteine kritische Aminosäuren sind, die die biochemischen Charakteristiken und regulatorischen Eigenschaften von GCAP5 kontrollieren. Wildtyp GCAP5 hat zwar auf Änderungen der Ca^{2+} -Konzentration reagiert, aber nur sehr geringe Ca^{2+} -Abhängigkeiten bezüglich der Konformationsänderung und der GC-Regulierung gezeigt. Die Mutation von Cys15 and Cys17 zu Alanin durch zielgerichtete Mutagenese stellte Ca^{2+} -abhängige Eigenschaften, wie sie für andere GCAP-Isoformen bekannt sind, wieder her. Eine *N*-terminale Myristoylierung hatte nur kleine Effekte auf GCAP5, erhöhte aber in Ca^{2+} -unabhängiger Weise geringfügig die GC-Aktivierung. Cystein-Reste können an redox-abhängigen Prozessen beteiligt sein und Eisen-Schwefel-Cluster bilden. Tatsächlich unterschied sich unter reduzierenden Bedingungen gereinigtes GCAP5 (reduziertes GCAP5) signifikant von unter normalen Bedingungen gereinigtem GCAP5. Die bereits geringe Ca^{2+} -Abhängigkeit von nicht reduziertem GCAP5 war bei reduziertem GCA5 fast vollständig aufgehoben und reduziertes GCAP5 aktivierte eine retinale GC etwa sechs Mal stärker als nicht reduziertes GCAP5. Außerdem konnten wir zusammen mit dem Department für Chemie der *UC Davis* (Kalifornien, USA) zeigen, dass GCAP5 mit nanomolarer Affinität zweiwertiges Eisen bindet (Lim et al. 2017, *Biochemistry* 56(51): 6652-6661). Zwei GCAP5-Moleküle koordinieren ein zweiwertiges Eisenion mit Cys15 und Cys17, indem sie einen $[\text{Fe}(\text{SCys})_4]$ -Komplex bilden. Im Gegensatz zu eisenfreiem GCAP5 unterschied sich die Aktivität der GC, wenn sie von eisenbeladenem GCAP5 reguliert wurde, nicht von der Basalaktivität der GC. Ob GCAP5 in seiner eisengebundenen Form verhindert, dass die GC aktiviert wird oder gar nicht erst an die GC bindet, ist unklar. Eisen und Licht können jeweils oxidativen Stress verursachen und cGMP-abhängige Prozesse Photorezeptoren davor schützen, zu degenerieren. Ich vermute, dass GCAP5 an zellschützenden Prozessen unter oxidativen Stresssituationen beteiligt ist, indem es die cGMP-Produktion in redox- und/oder eisenabhängiger Weise limitiert. Das könnte außerdem erklären, warum die GCAP5-Expression in den kurzen Einzelzapfen, die auf energiereiches UV-Licht reagieren, besonders hoch ist.

Abstract

Guanylate cyclase-activating proteins (GCAPs) are neuronal calcium sensors that activate photoreceptor specific guanylate cyclases (GCs) in a Ca^{2+} -dependent manner and thus regulate cyclic guanosine monophosphate (cGMP) production. The zebrafish (*Danio rerio*) expresses a total of six GCAP isoforms in its retina: GCAP1, 2, 3, 4, 5, and 7. Previous studies suggested that GCAP5 behaves different from the other zebrafish GCAPs and that a non-conserved cysteine cluster at its *N*-terminal, namely Cys15 and Cys17, might be involved. Here, I present that the two cysteines are critical residues controlling biochemical characteristics and target regulation of GCAP5. Wildtype GCAP5 did react to changing Ca^{2+} -concentrations but showed only low Ca^{2+} -dependencies regarding the conformational change and GC regulation. Mutation of Cys15 and Cys17 to alanine by site directed mutagenesis restored Ca^{2+} -dependent properties as known from other GCAP isoforms. *N*-terminal myristoylation had only minor effects on wildtype GCAP5 but slightly enhanced GC activation in a Ca^{2+} -independent manner. Cysteine residues can be involved in redox-dependent processes and form iron-sulfur clusters. Indeed, GCAP5 purified under reducing conditions (reduced GCAP5) showed significant differences from GCAP5 purified under normal conditions. The already low Ca^{2+} -dependency of GCAP5 was abolished nearly completely, and reduced GCAP5 activated a retinal GC around six times stronger than non-reduced GCAP5. Together with the Department of Chemistry at the *UC Davis* (California, USA), we could further show that GCAP5 binds ferrous iron with nanomolar affinity (Lim et al. 2017, *Biochemistry* 56(51): 6652-6661). Two GCAP5-molecules coordinate one ferrous iron with Cys15 and Cys17, forming an iron-sulfur cluster in a $[\text{Fe}(\text{SCys})_4]$ complex. In contrast to GCAP5 under iron-free conditions, GC activity regulated by iron-loaded GCAP5 did not differ significantly from GC basal activity. Whether GCAP5 prevents retinal GCs from activation or does not even bind to retinal GCs in its iron-bound form is unclear. Iron and light can both induce oxidative stress, and cGMP-dependent processes can protect photoreceptors from degenerating. I propose that GCAP5 is involved in cell protection under oxidative stress conditions by limiting cGMP production in a redox- and/or iron-dependent manner. This could further explain why GCAP5 expression is especially high in short single cones, which sense energetic UV-light.

Table of Contents

Zusammenfassung.....	I
Abstract	II
Table of Contents	III
Abbreviations.....	VI
Figures	IX
Tables.....	X
Equations.....	X
1 Introduction.....	1
1.1 Photoreceptors of the vertebrate retina.....	1
1.2 Phototransduction in vertebrate photoreceptors.....	3
1.3 Importance of the GC-GCAP system in photoreceptor outer segments.....	6
1.3.1 Retinal guanylate cyclases (GCs)	8
1.3.2 Guanylate cyclase-activating proteins (GCAPs).....	11
1.4 The GC-GCAP system and ribbon synapses.....	13
1.5 GCs and GCAPs in photoreceptors of the zebrafish (<i>Danio rerio</i>).....	16
1.6 Zebrafish GCAP5	19
1.7 Aims of the thesis	22
2 Material and methods.....	24
2.1 Devices and consumables.....	24
2.1.1 Devices.....	24
2.1.2 Chemicals.....	26
2.1.3 Consumables, media, sera, enzymes, antibiotics	27
2.1.4 Antibodies.....	28
2.1.5 Bacterial strain.....	29
2.1.6 Vectors and plasmids.....	29
2.1.7 Mammalian cell line	29
2.2 Heterologous expression and purification of GCAPs.....	30

2.2.1	Retransformation, preparation of glycerol stocks, inoculation of overnight cultures.....	31
2.2.2	Expression in <i>E. coli</i>	31
2.2.3	Cell lysis, ultracentrifugation, denaturation.....	32
2.2.4	Dialysis and ultracentrifugation.....	32
2.2.5	Concentrating of protein	33
2.2.6	Fast-performance liquid chromatography (FPLC)	34
2.2.7	Buffer exchange and lyophilization	36
2.3	Purification of reduced protein	36
2.4	Determination of protein concentration.....	36
2.4.1	UV-absorbance at 280 nm	36
2.4.2	Bradford Assay.....	37
2.5	Specific proof of proteins	38
2.5.1	SDS-PAGE.....	38
2.5.2	Western blot (“blue method”)	39
2.5.3	Immunoassay and antigen detection with ECL technique	40
2.6	Determination of the Cysteine accessibility with the Ellman’s Reagent.....	40
2.7	Tryptophan fluorescence spectroscopy	41
2.7.1	Determination of $[Ca^{2+}]_{free}$ with fura-2	42
2.7.2	Tryptophan fluorescence spectroscopy with GCAP5	43
2.8	Cell culture conditions of HEK293-human GC-E cell line and cell harvesting	43
2.9	GC assay.....	44
2.9.1	Preparation of the GC.....	44
2.9.2	Preparation of GCAPs	45
2.9.3	Enzymatic assay	45
2.9.4	GC assay with $FeSO_4$	46
2.9.5	GC assay under reducing conditions	46
2.10	High performance liquid chromatography (HPLC)	46
2.10.1	Analytical SEC	47
2.10.2	Reversed phase-HPLC.....	48

2.11	Preparation of adult zebrafish retinæ	49
2.11.1	Subcellular fractionation	49
2.11.2	Tissue fixation	50
2.11.3	Preparation of cryosections.....	50
2.11.4	Immunohistochemistry on cryosections	51
2.11.5	Image acquisition by confocal microscopy.....	51
3	Results	52
3.1	Purification of recombinant GCAP5.....	52
3.2	Analytical SEC	54
3.3	Myristoylation rate	58
3.4	Cysteine accessibility	61
3.5	Tryptophan fluorescence.....	62
3.6	GC assay.....	64
3.7	Localization of GCAP5 in photoreceptors of the zebrafish retina	67
4	Discussion	71
4.1	Purification of GCAP5	71
4.2	Fine-tuning of GCAP5 by myristoylation	72
4.3	Ca ²⁺ -sensitivity of GCAP5 is influenced by myristoylation, reduction, and cysteines	75
4.4	GCAP5 is a redox-sensor.....	77
4.5	Fe ²⁺ -bound GCAP5 inhibits GC-E activity despite reduction	80
4.6	GCAP5 in the adult zebrafish retina	83
4.7	Conclusion	84
	References.....	87
	Appendix.....	109
	Publikationen.....	128
	Danksagung	129
	Erklärung.....	131

Abbreviations

λ_{\max}	wavelength of the fluorescence intensity maximum
$(\text{NH}_4)_2\text{SO}_4$	ammonium sulfate
$[\text{Ca}^{2+}]$	calcium-ion concentration
AEC	anion exchange chromatography
ATP	adenosine 5'-triphosphate
AU	absorbance unit
BAPTA	1,2-bis(2-Aminophenoxy)ethane-N,N,N',N'-tetraacetic acid
C15A-C17A	myristoylated zebrafish GCAP5-D3N-C15A-C17A
Ca^{2+}	calcium-ion
CaCl_2	calcium chloride
CaCl_2	calcium chloride
CD	catalytic domain
cGMP	cyclic guanosine monophosphate
CO	carbon monoxide
CtBP	C-terminal binding protein
CTE	C-terminal extension
CV	column volume
DD	dimerization domain
DMEM	Dulbecco's Modified Eagle Medium
DNA	deoxyribonucleic acid
dpf	days post fertilization
DTNB	5,5'-dithio-bis-(2-nitrobenzoic acid)
DTT	dithiothreitol
<i>E. coli</i>	<i>Escherichia coli</i>
ECD	extracellular domain
ECL	enhanced chemiluminescence
EDTA	ethylenediaminetetraacetic acid
EGTA	ethylene glycol-bis(β -aminoethyl ether)-N,N,N',N'-tetraacetic acid
Fe^{2+}	ferrous ion, iron-ion
F_{\max}	fluorescence intensity maximum
FPLC	fast-performance liquid chromatography
GC	guanylate cyclase

GCAP	guanylate cyclase-activating protein
GDP	guanosine 5'-diphosphate
GMP	guanosine 5'-monophosphate
GTP	guanosine 5'-triphosphate
H18E-Y21E	myristoylated zebrafish GCAP5-D3N-H18E-Y21E
H ₂ O ₂	hydrogen peroxide
HCl	hydrochloric acid
HEK293	Flp-In™-293 Cell Line
HEPES	<i>N</i> -2-Hydroxyethylpiperazine- <i>N'</i> -2-ethane sulphonic acid
HIC	hydrophobic interaction chromatography
HPLC	high-performance liquid chromatography
IC ₅₀	half maximal inhibitory concentration
IPTG	Isopropyl β-d-1-thiogalactopyranoside
ITC	isothermal titration calorimetry
JMD	juxta membrane domain
KCl	potassium chloride
KH ₂ PO ₄	potassium dihydrogen phosphate
KHD	kinase homology domain
LB	lysogeny broth
Mes	2-(<i>N</i> -Morpholino)-ethane sulphonic acid
Mops	3-(<i>N</i> -Morpholino)propane sulfonic acid
myr	myristoylated
NaCl	sodium chloride
NAD(H)	nicotinamide adenine dinucleotide
NC-membrane	nitrocellulose-membrane
NBD	NAD(H)-binding domain
NH ₄ HCO ₃	ammonium hydrogen carbonate
NMR	nuclear magnetic resonance
NO	nitric oxide
non-myr	non myristoylated
non-myr WT	non-myristoylated zebrafish GCAP5-D3N
OD	optical density
OGP	Octyl β-D-glucopyranoside

PBS	phosphate buffered saline
PDE	phosphodiesterase
PMSF	phenylmethylsulfonyl fluoride
PVDF	polyvinylidene difluoride
RD3	retinal degeneration 3
Rec	recoverin
redox	reduction/oxidation
reduced WT	reduced purified myristoylated zebrafish GCAP5-D3N
Rh	rhodopsin
Rh*	meta rhodopsin II
ROS	rod outer segment
SBD _a and SBD _b	discontinuous substrate-binding domain part a and part b
SDS-gels	sodium dodecyl sulfate-polyacrylamide gels
SDS-PAGE	sodium dodecyl sulfate-polyacrylamide gel electrophoresis
SEC	size exclusion chromatography
TBS	tris buffered saline
TBST	tris buffered saline with Tween-20
TEMED	N,N,N',N'-tetramethylethylenediamine
TFA	trifluoroacetic acid
TNB	2-nitro-5-thiobenzoic acid
Tris	tris(hydroxymethyl)aminomethane
T α -subunit	α -subunit of the G-protein transducin
V76E	myristoylated zebrafish GCAP5-D3N-V76E
WT	myristoylated zebrafish GCAP5-D3N

Figures

Figure 1: Schematic overview of vertebrate photoreceptors and their photocurrents after light stimulation.	1
Figure 2: Schematic overview of the phototransduction cascade in rods.	5
Figure 3: The GC-GCAP system as a negative feedback mechanism in phototransduction.....	6
Figure 4: ERGs of wildtype and GC knockout mice.....	7
Figure 5: Light responses of mouse rods and cones with normal GCAPs expression levels or GCAPs knockout.....	8
Figure 6: Domain structure of mature retinal guanylate cyclase homodimers, GC-E and GC-F.	10
Figure 7: Structure and Ca ²⁺ -dependent dynamics of myristoylated chicken GCAP1 and non-myristoylated bovine GCAP2.	12
Figure 8: Photoreceptor ribbon synapse – schematic overview, RIBEYE domain structure, and Ca ²⁺ - and light-dependent dynamics of ribbons.	14
Figure 9: Photoreceptors of the zebrafish (<i>Danio rerio</i>) - schematic overview, spectral sensitivity, and mosaic.....	16
Figure 10: Ca ²⁺ -relay model of the mammalian GC-GCAP system.	18
Figure 11: Immunohistochemistry against GCAP5 in cryosections of adult zebrafish retina.	19
Figure 12: Color-forming reaction of Ellman’s reagent with sulfhydryl groups.	41
Figure 13: Coomassie-stained SDS-gels after SEC and AEC of successful GCAP5 purification.	53
Figure 14: Analytical SEC chromatograms of GCAP5.....	56
Figure 15: Relative integrals of the analytical SEC chromatogram peaks.	57
Figure 16: Reversed phase-HPLC chromatograms of GCAP5.	60
Figure 17: Cysteine accessibility of GCAP5.....	62
Figure 18: Ca ²⁺ -dependent tryptophan fluorescence of GCAP5.....	63
Figure 19: Ca ²⁺ -dependent human GC-E activation profile by GCAP5.	66
Figure 20: Fe ²⁺ -dependent human GC-E activation by GCAP5 WT and C15A-C17A mutant.....	67
Figure 21: GCAP5 immunoreactivity in the zebrafish retina and in photoreceptors.	69
Figure 22: Localization of GCAP5 in double cones of the zebrafish retina.....	70
Figure 23: NMR-derived structure of Mg ²⁺ -bound, Ca ²⁺ -free, and Fe ²⁺ -free myristoylated GCAP5.	74
Figure 24: Modeled structure of the Fe ²⁺ -bound GCAP5 dimer.....	81
Figure 25: Putative involvement of GCAP5 in cell protection against light-/iron-induced oxidative stress. ...	85

Tables

Table 1: Antibodies used for immunohistochemistry or immunodetecting after western blotting.....	28
Table 2: Purification protocols for GCAP5 of the Division of Biochemistry (<i>University of Oldenburg</i>) and variations.	30
Table 3: Purification protocols for GCAP5 of the Department of Chemistry (<i>UC Davis</i>) and variation.	30
Table 4: AEC columns with flow rates and fraction sizes.	35
Table 5: Molar extinction coefficients and molar masses of GCAP3 and GCAP5.....	37
Table 6: Yields achieved for GCAP5 variants.	54
Table 7: GCAP5 protein states observed on the BioSep-SEC-S2000 column.	54
Table 8: Possible myristoylation rates of GCAP5.....	61
Table 9: Effect of myristoylation on GCAP5.	73
Table 10: Ca ²⁺ -dependency of GCAP5.	76
Table 11: Redox-dependency of GCAP5.....	78

Equations

Equation 1: Calculation of the required mass of ammonium sulfate for a certain percentage of saturation.	33
Equation 2: Lambert-Beer law.....	37
Equation 3: Calculation of the mass of a protein in a solution.	37
Equation 4: Calculation of the mass concentration of the protein with the BSA calibration line.	37
Equation 5: Calculation of the number of accessible cysteines.	41
Equation 6: Calculation of the [Ca ²⁺] _{free} with the fura-2 excitation spectrum.....	42
Equation 7: Calculation of the [Ca ²⁺] _{free} for the tryptophan fluorescence with the Ca ²⁺ -EGTA buffer system.	42
Equation 8: Calculation of the retention factor k _r	47

1 Introduction

1.1 Photoreceptors of the vertebrate retina

Vision begins with the detection of light. In vertebrates, the photosensitive cells are the photoreceptors of the retina, the rods and the cones (Figure 1 A). They can adapt to a broad range of light intensities spanning ten orders of magnitude (Arshavsky and Burns 2012).

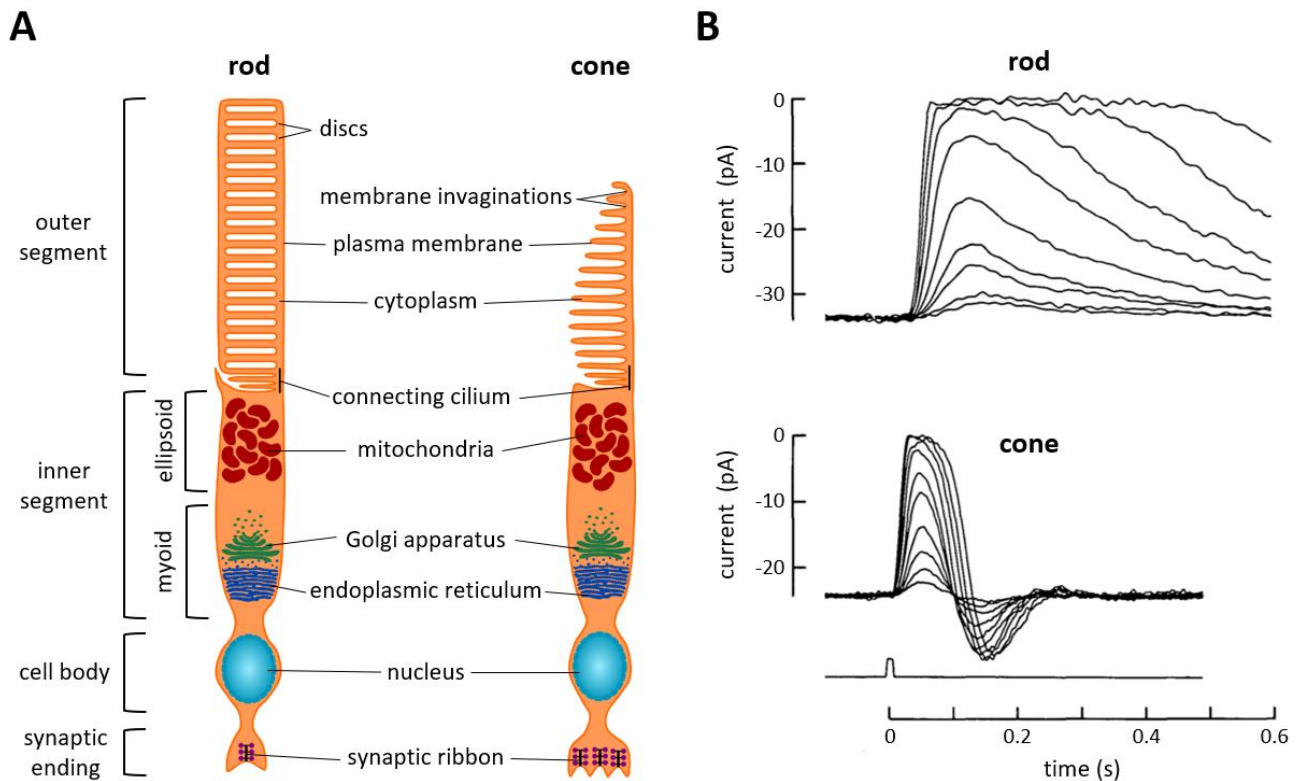


Figure 1: Schematic overview of vertebrate photoreceptors and their photocurrents after light stimulation.

(A) Photoreceptor cells can be categorized into rods and cones. Both consist of an outer segment connected to an inner segment via the connecting cilium, a cell body containing the nucleus, and a synaptic terminal. The outer segments of rods are densely packed with discs, whereas the plasma membranes in cone outer segments form invaginations. The inner segments can be subdivided into an ellipsoid and a myoid. The ellipsoid is close to the outer segment and densely packed with mitochondria. The myoid contains the Golgi complex and the endoplasmic reticulum. The synaptic endings are specialized ribbon synapses with one or several synaptic ribbons in rods or in cones, respectively. Based on Mavlyutov et al. (2002); Wässle (2004); Fu and Yau (2007). (B) Photocurrent families of rod (upper graph) and red cone outer segments (lower graph) of the monkey *Macaca fascicularis* recorded by suction electrode. Light flashes were increased by factors of two. X-axis: time in seconds beginning with the light stimulus (lower trace); y-axis: current in picoampere. Modified from Baylor (1987).

Rods are very sensitive. They can detect a single photon and, therefore, are important for night vision (Rieke and Baylor 1998, Fu and Yau 2007; Lamb 2016). Cones mediate day vision, as they are operating at bright light conditions and not saturating due to adaptation mechanisms (Kawamura and Tachibanaki 2012; Imamoto and Shichida 2014; Lamb 2016). Since they express different pigments sensitive to specific light wavelengths, they enable color vision. For example, humans and closely related primates are trichromats, possessing three different cone types sensitive to blue, green, and red light, respectively (Surrridge et al. 2003). The zebrafish (*Danio rerio*), a tetrachromat model organism for vertebrate retina research, like many

other fishes and birds, owns an additional cone type allowing it to sense UV light (Imamoto and Shichida 2014; Franke et al. 2019). Most mammals possess only two cone types and, therefore, are dichromats (Imamoto and Shichida 2014).

The light sensitive pigment consists of an opsin covalently bound to a retinal chromophore via a Schiff base (Stryer 1991; Luo et al. 2008; Korenbrot 2012). Opsins are specific for the photoreceptor type and determine the absorbance spectrum of the pigments. Independent of the photoreceptor type, the chromophore is always 11-*cis*-retinal. The opsins are embedded in the disc membranes of the rod outer segments or in the invaginations of the plasma membrane in cone outer segments, respectively. Upon light absorption, they start a transduction cascade generating a change of the plasma membrane potential. This phototransduction cascade will be explained further in the next section. In contrast to other cells of the nervous system, which are hyperpolarized in their resting state and are depolarized after being stimulated, photoreceptors hyperpolarize upon light detection (Baylor 1987). The associated photocurrents differ between rods and cones (Figure 1 B). In suction electrode experiments with rods and cones of the *Macaca fascicularis*, cones respond faster to a light stimulus, and the response duration is shorter in comparison to rods. Furthermore, the cone photocurrent of some species shows an undershoot.

The change in membrane potential is transduced from the outer segment to the synaptic terminal, where the glutamic acid release is adjusted according to the incoming light intensity. Photoreceptor synaptic terminals are specialized ribbon synapses (Wässle 2004; Heidelberger et al. 2005; Schmitz 2009). They allow a continuous transmitter release that can be accelerated or reduced depending on the membrane potential. The synaptic terminal of a rod photoreceptor, the rod spherule, possesses only one ribbon synapse (Wässle 2004) supporting the high acuity of the photon response. Cone synaptic terminals, the cone pedicles, contain 20 to 50 ribbons (Wässle 2004). These ribbon synapses will be explained further in section 1.4.

The photoreceptor cell signals are further processed by other retinal cells in a highly complex network (for review see e. g. Wässle 2004; Masland 2012; Baden et al. 2020). Final retinal processing is performed by the ganglion cells relaying the visual signal to the brain. In this thesis, however, I will focus on the retinal photoreceptors.

1.2 Phototransduction in vertebrate photoreceptors

The phototransduction cascade is the process in which a light stimulus is converted into an electrical signal. Rods and cones have similar sets of proteins involved in the phototransduction cascade and located in the outer segments of the photoreceptors (see Figure 1 for location) (Luo et al. 2008; Kawamura and Tachibanaki 2012). However, the phototransduction in rods is much better understood (Kawamura and Tachibanaki 2012) and, therefore, will be described in the following.

In the dark state of the photoreceptor (Figure 2, dark state), the free cyclic guanosine monophosphate (cGMP) concentration ([cGMP]) in the outer segment is relatively high with ca. 2-6 μM (Nakatani and Yau 1988; Kaupp and Koch 1992). cGMP opens the cyclic nucleotide gated (CNG)-channel, allowing the influx of sodium (Na^+) and calcium-ions (Ca^{2+}). This cation inward current, also termed dark current, generates a membrane potential around -40 mV (Baylor and Nunn 1986; Pugh and Lamb 2000). The Na^+/K^+ , Ca^{2+} exchanger transports Ca^{2+} out of the cell, leading to a species dependent free [Ca^{2+}] between 200 and 800 nM (Pugh and Lamb 2000; Nakatani et al. 2002; Woodruff et al. 2002). The G-protein coupled receptor rhodopsin (Rh), the light sensitive pigment of rods, is inactive. The PDE is inhibited by its γ -subunit (Hurley and Stryer 1982). Ca^{2+} is bound to the calcium sensor proteins recoverin (Rec) and guanylate cyclase-activating protein (GCAP). Rec has a covalently attached fatty acid, which is mostly the myristic acid (Dizhoor et al. 1992). In the Ca^{2+} -free state of Rec, its myristoyl group is buried inside a hydrophobic pocket in the protein interior (Hughes et al. 1995; Tanaka et al. 1995). In the Ca^{2+} -bound state like in the dark state of the photoreceptor, the myristic acid of Rec is exposed, associating Rec to the disc membrane (Lange and Koch 1997). The free hydrophobic pocket and the C-terminus of Rec are suggested to interact with and inhibit the G-protein coupled receptor kinase 1 (GRK1) (Chen et al. 1995; Ames et al. 2006; Weiergräber et al. 2006; Abbas et al. 2019). The second messenger cGMP is synthesized by membrane bound guanylate cyclases (GCs), GC-E and GC-F (also termed GC1/GC2, RetGC-1/RetGC-2 or ROS-GC1/ROS-GC2). GCAPs bind to the GC and inhibit it in their Ca^{2+} -bound state (Koch and Stryer 1988; Gorczyca et al. 1994; Palczewski et al. 1994; Olshevskaya et al. 1997). However, a basal activity of the GC remains, providing sufficient cGMP to keep a fraction of CNG-channels open (Luo et al. 2008).

If light hits Rh, the chromophore 11-*cis*-retinal isomerizes to all-*trans*-retinal, inducing a conformational change of Rh to its activated form meta rhodopsin II (Rh^*) (Figure 2, illuminated state) (Luo et al. 2008). Rh^* activates the heterotrimeric G-protein transducin (T) by catalyzing the exchange of guanosine 5'-diphosphate (GDP) for guanosine 5'-triphosphate (GTP) at the $\text{T}\alpha$ -subunit. The GTP bound $\text{T}\alpha$ -subunit dissociates from the $\text{T}\beta\gamma$ -subunits and activates the phosphodiesterase (PDE) by binding to the $\text{PDE}\gamma$ -subunit (Wensel and Stryer 1986, Burns and Pugh 2010). The PDE now hydrolyzes cGMP to guanosine 5'-monophosphate (GMP), which leads to a decrease of the cGMP concentration. Therefore, the CNG-channel closes, resulting in a hyperpolarization of the photoreceptor plasma membrane due to the reduced inward cation current. After saturating flashes, the hyperpolarization can reach around -65 mV

(Baylor and Nunn 1986; Baylor 1987). Ca^{2+} cannot enter the photoreceptor cell anymore but is expelled by the Na^+/K^+ , Ca^{2+} -exchanger.

The resulting decrease of the local intracellular $[\text{Ca}^{2+}]$ to around 50 nM (Gray-Keller and Detwiler 1994) starts three of four shut off mechanisms of the phototransduction cascade (Figure 2, recovery phase). This recovery of the dark state is important for the detection of a new light stimulus after a former photon activated Rh (Fu and Yau 2007; Burns and Pugh 2010).

Deactivation of Rh^* : The Deactivation of Rh^* involves Rec and the GRK1. Ca^{2+} dissociates from Rec, and Rec undergoes the Ca^{2+} -myristoyl switch, burying the myristoyl moiety inside a hydrophobic pocket (Zozulya and Stryer 1992; Ames and Lim 2012). This causes Rec to dissociate from the disc membrane and to set the GRK1 free. The GRK1 now can phosphorylate Rh^* at its C-terminal, which facilitates the competitive binding of arrestin (Arr) to Rh^* (Maeda et al. 2003). Arr competes with T and prevents Rh^* from further activating T. Therefore, the phototransduction cascade is terminated.

Inhibition of the PDE: The deactivation of the PDE relies on the “RGS9-complex”, which consists of RGS9-1, $\text{G}\beta_5\text{L}$ and R9AP (Anderson et al. 2009; Arshavsky and Wensel 2013). RGS9-1 is a retina specific GTPase activating protein. It enhances the intrinsic GTPase activity of the $\text{T}\alpha$ -subunit to hydrolyze the bound GTP to GDP. The GDP bound $\text{T}\alpha$ -subunit dissociates from the PDE, allowing the $\text{PDE}\gamma$ -subunit to inhibit the PDE activity.

Increase of the cGMP-sensitivity of the CNG-channels: At high $[\text{Ca}^{2+}]$, calmodulin (CaM) binds to the CNG-channels and decreases its sensitivity to cGMP (Arshavsky and Burns 2012). The drop in the $[\text{Ca}^{2+}]$ after the light stimulus causes CaM to dissociate from the CNG-channels. The CNG-channels are now more sensitive to cGMP, even though this effect is relatively small in rod photoreceptors (Pugh and Lamb 2000).

Recovery of the photoresponse: For the recovery of the photoresponse, the so-called GC-GCAP system is important. The decreasing $[\text{Ca}^{2+}]$ leads to GCAPs losing their bound Ca^{2+} and binding magnesium-ions (Mg^{2+}) instead (not shown in Figure 2; see section 1.3.2). The $[\text{Mg}^{2+}]$ in photoreceptor outer segments of amphibians lies around 800 μM (Chen et al. 2003). The GCAPs undergo a conformational change and enhance the activity of the GC (Dizhoor and Hurley 1996; Peshenko and Dizhoor 2006; Peshenko and Dizhoor 2007; Peshenko et al. 2008; Lim et al. 2009; Lim et al. 2016). This locally increases the [cGMP] in the photoreceptor outer segment, which reopens the CNG-channel. Ca^{2+} and Na^+ can enter the cell again, and the membrane potential repolarizes.

The GC-GCAP system was of special interest for this thesis and will be explained further.

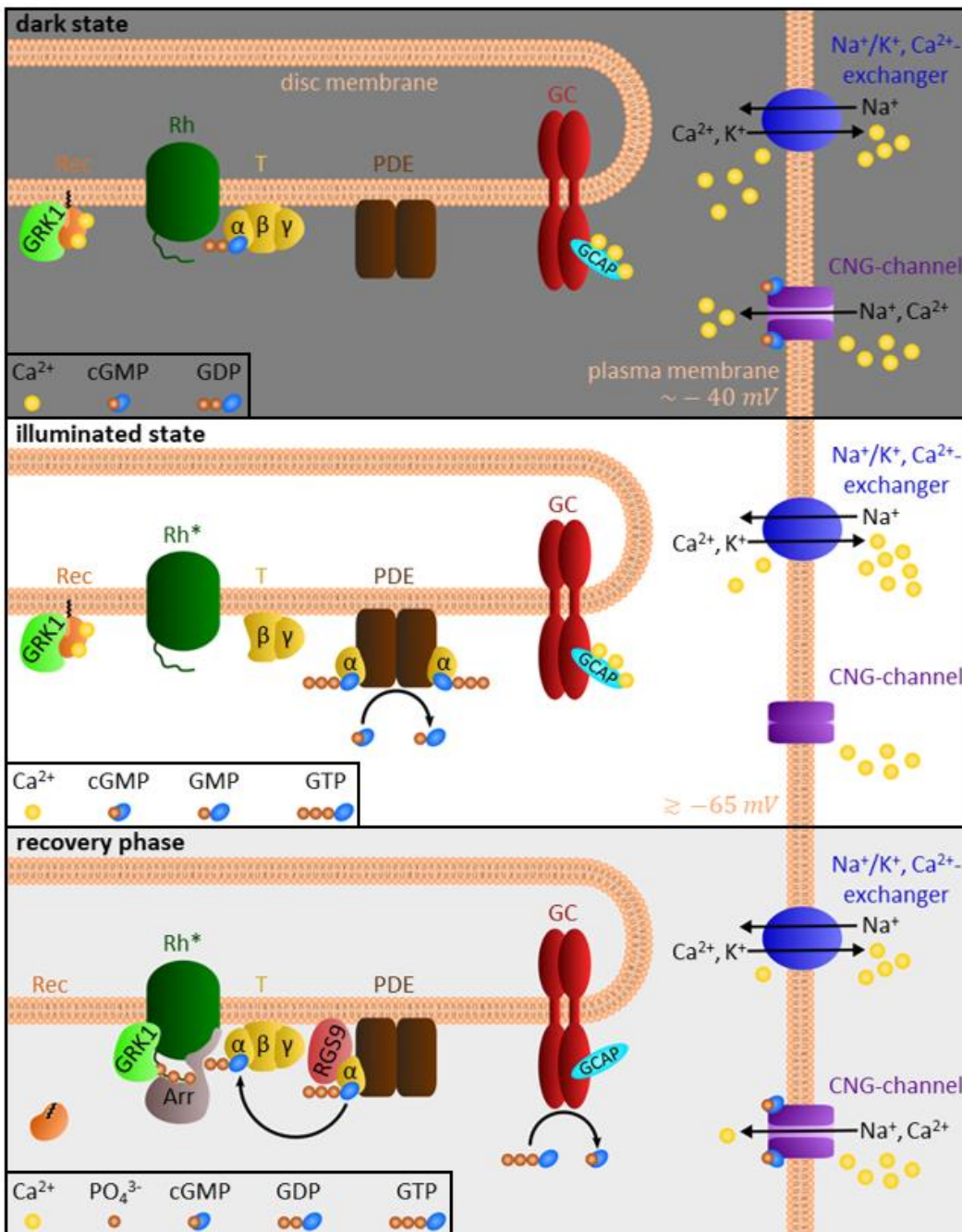


Figure 2:
Schematic overview of the phototransduction cascade in rods.

During the **dark state** of the photoreceptor, the cGMP concentration [cGMP] is relatively high. cGMP opens the cyclic nucleotide gated (CNG)-channel, allowing the influx of calcium- (Ca²⁺) and sodium-ions (Na⁺). The plasma membrane potential is around -40 mV. Ca²⁺ binds to the Ca²⁺-sensor proteins recoverin (Rec) and guanylate cyclase-activating protein (GCAP). Ca²⁺-bound recoverin is anchored to the disc membrane by its exposed myristic acid and binds the G-protein coupled receptor kinase 1 (GRK1). GCAPs inhibit the guanylate cyclase

(GC) in their Ca²⁺-bound state. The G-protein coupled receptor rhodopsin (Rh), the G-protein transducin (T) and the phosphodiesterase (PDE) are inactive. After **illumination**, the activated form of rhodopsin, meta rhodopsin II (Rh*), catalyzes the exchange of GDP to GTP at the Tα-subunit, which activates the PDE. The PDE hydrolyzes cGMP to GMP, leading to a decreased [cGMP]. The CNG-channel closes, preventing the influx of Na⁺ and Ca²⁺, and the plasma membrane hyperpolarizes. The Na⁺/K⁺, Ca²⁺-exchanger still transports Ca²⁺ out of the photoreceptor, decreasing the intracellular [Ca²⁺]. The decreasing [Ca²⁺] initiates the **recovery** of the cell to the dark state. Upon Ca²⁺-loss, recoverin undergoes a myristoyl switch, dissociates from the disc membrane, and releases the GRK1. The GRK1 now can phosphorylate Rh*, facilitating arrestin (Arr) to bind to Rh* and preventing rhodopsin from further activating T. The intrinsic GTPase activity of the Tα-subunit accelerated by RGS9 leads to the inactivation of the PDE. Further, the Ca²⁺-free GCAPs activate the GC, and the GC synthesizes cGMP out of GTP. The increasing [cGMP] leads to an opening of the CNG-channel and a Ca²⁺-influx. The dark state is recovered. Based on Pugh and Lamb (2000); Koch and Dell'Orco (2015).

1.3 Importance of the GC-GCAP system in photoreceptor outer segments

The GC-GCAP system provides an important Ca^{2+} -feedback mechanism to recover the dark state of a photoreceptor outer segment after the cell was illuminated (Figure 3). This system involves the enzyme GC (see also section 1.3.1), its regulatory protein GCAP (see also section 1.3.2), and the two second messengers cGMP and Ca^{2+} .

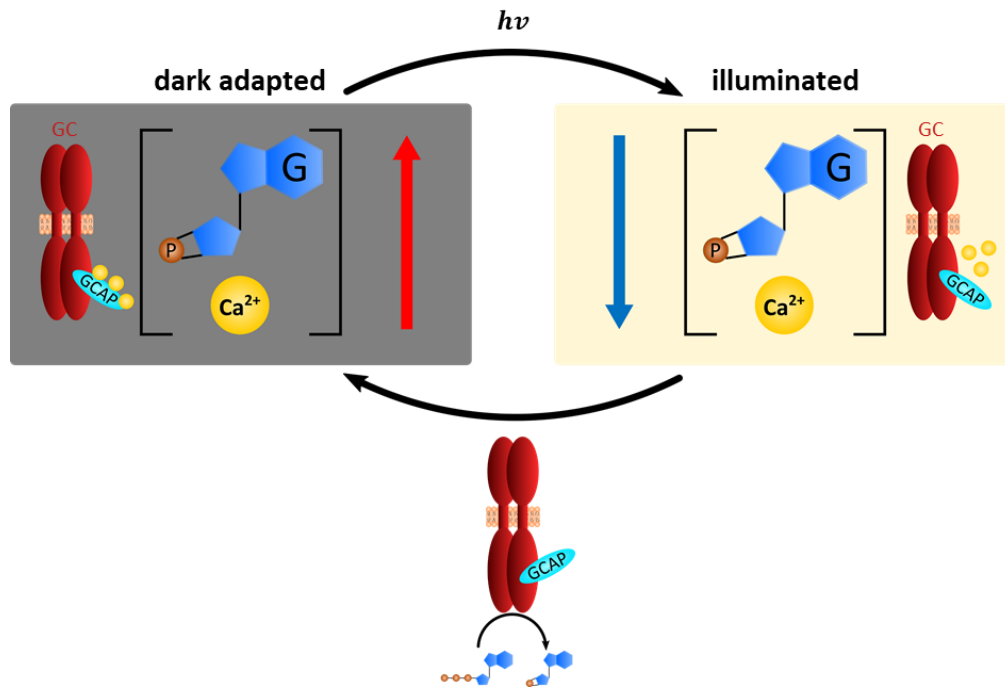


Figure 3: The GC-GCAP system as a negative feedback mechanism in phototransduction.

The GC activity is under the control of the GCAPs. The relatively high concentration of cGMP (G) during the dark state of a photoreceptor outer segment also leads to a relatively high $[\text{Ca}^{2+}]$. Ca^{2+} binds to the GCAPs, keeping them in their inhibitory conformation. A light stimulus activates the phototransduction cascade, resulting in a decrease of the $[\text{cGMP}]$ and the $[\text{Ca}^{2+}]$. The decreasing $[\text{Ca}^{2+}]$ is detected by the GCAPs, which undergo a conformational change and now enhance the GC activity. The GC synthesizes cGMP out of GTP. The increasing $[\text{cGMP}]$ also leads to an increasing $[\text{Ca}^{2+}]$. Ca^{2+} inhibits the GC via the GCAPs, and the dark state of the photoreceptor is recovered.

The importance of this system becomes particularly obvious in knockout experiments with mice. Mice possess two retinal GC and two GCAP isoforms in their photoreceptors (Cuenca et al. 1998; Howes et al. 1998; Baehr et al. 2007; Fu and Yau 2007). GC-E is present in mouse rods and cones, whereas GC-F is present only in rods. GCAP1 and GCAP2 both are present in mouse rods and cones, with GCAP1 being the predominant variant in cones. A possible relevance of expressing more than one GC or GCAP isoform in the same cell type will be addressed in section 1.5. The genes for the GCs are termed differently in different species. In mice, the genes for GC-E and GC-F are termed *Gucy2e* and *Gucy2f*, respectively. I refer to the mouse genes in this section.

In Yang et al. (1999), a homozygous *Gucy2e* knockout ($\text{GC-E}^{-/-}$) mouse line is presented. Further, a homozygous *Gucy2f* knockout ($\text{GC-F}^{-/-}$) and a homozygous *Gucy2e/Gucy2f* double knockout (GCdko) mouse line are described in Baehr et al. (2007) and Karan et al. (2010). The authors could show by suction pipette recordings that both GC isoforms are able to maintain the dark current in rods alone, and that the light

response kinetics of wildtype mouse rods and the GC single knockout mouse rods are similar. However, if both GC isoforms are missing, rods are not sensitive to light at all, and the dark current is absent. The authors further investigated the influence of GCs by full field electroretinography. The electroretinograms (ERGs) of wildtype and knockout mice (Figure 4) under scotopic conditions revealed that GC-F can barely compensate the loss of GC-E in GC-E^{-/-} mouse rods, while the scotopic ERG of GC-F^{-/-} mice is only slightly affected in comparison to wildtype mice. But again, if both GCs are knocked out, no light sensitivity is detectable. In photopic ERGs, a GC-F knockout has only little effect, whereas a GC-E knockout shows a complete loss of light sensitivity like a GCdko. This is not surprising, considering that cones are essential for photopic vision (see section 1.1), and that wildtype mouse cones only express GC-E (Baehr et al. 2007).

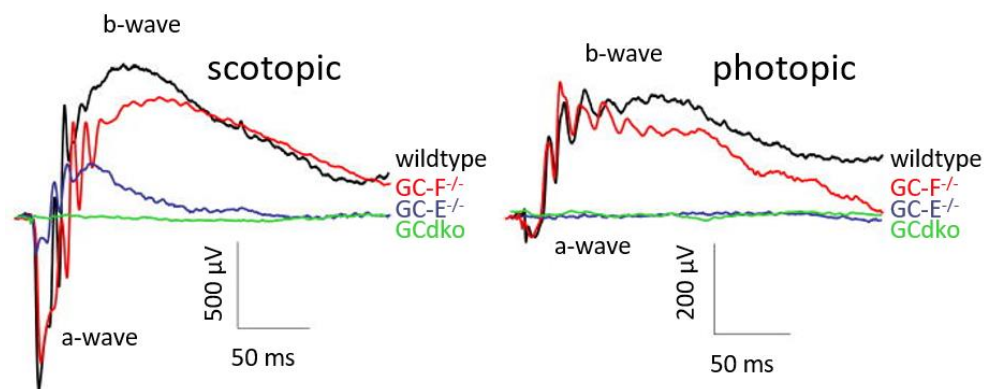


Figure 4: ERGs of wildtype and GC knockout mice.

Scotopic and photopic ERGs of wildtype mice (wildtype, black line), GC-E knockout (GC-E^{-/-}, blue line), GC-F knockout (GC-F^{-/-}, red line), and GC double knockout mice (GCdko, green line) at 2.8 log cd s m⁻². A-wave corresponds to hyperpolarization of the photoreceptors; b-wave arises from depolarization of bipolar and Müller cells, reflecting phototransduction activity (Asanad and Karanjia 2022). Modified from Karan et al. (2010).

In comparison to the knockout of GCs, knocking out GCAPs has less dramatic but still substantial effects. Mendez et al. (2001) generated a homozygous GCAP1 and GCAP2 double knockout (GCAPs^{-/-}) mouse line. The authors report that, compared to wildtype mouse rods, the knockout of GCAPs has little or no effect on the dark current and, therefore, on the basal activity of the GC in single cell recordings. The light responses, however, differ (Figure 5 A). In comparison to GCAPs^{+/+} mouse rods, GCAPs^{-/-} mouse rods generate larger and broader peaks, and the rapid phase of recovery directly after the peak of GCAPs^{+/+} mouse rods (Figure 5 A, red arrow) is missing. The time to peak is nearly three times and the total response nearly 2.5 times longer in GCAPs^{-/-} mouse rods. Due to the missing Ca²⁺-feedback of GCAPs to the GC, the recovery to the dark current in GCAPs^{-/-} mouse rods can be achieved only by the GCs' basal activity. The mean single photon response amplitude is nearly five times larger in GCAPs^{-/-} mouse rods. Further, the sensitivity of GCAPs^{-/-} mouse rods to light flashes is increased sixfold. Similar results were reported by Sakurai et al. (2011) for the cone photoresponse (Figure 5 B). The authors studied GCAPs^{-/-} mouse M-cones on a rod Tα-subunit knockout (Gnat1^{-/-}) background to ensure that the rod photoreceptor signaling is disabled. In comparison to Gnat1^{-/-} mouse M-cones, the time to peak after illumination is two times and the overall

recovery in dim light 3.3 times longer in GCAPs^{-/-} mouse M-cones, while their sensitivity increases around three-fold.

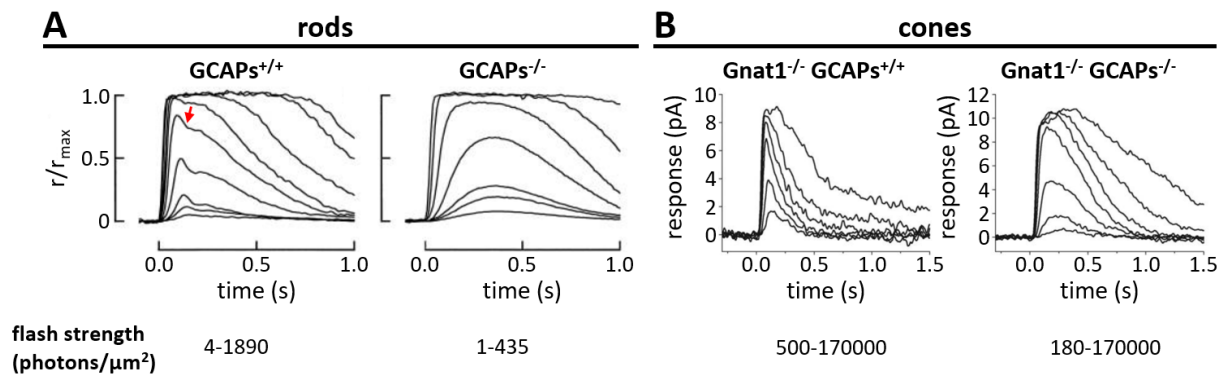


Figure 5: Light responses of mouse rods and cones with normal GCAPs expression levels or GCAPs knockout.

(A) Normalized light response families from wildtype (GCAPs^{+/+}) and homozygous GCAP1 and GCAP2 double knockout (GCAPs^{-/-}) mouse rods. The rapid phase of recovery in GCAPs^{+/+} mouse rods is marked (red arrow). Y-axis labeling and scale in GCAPs^{+/+} also applies to GCAPs^{-/-}. Modified from Mendez et al. (2001). (B) Response families in picoampere from homozygous rod T α -subunit knockout (Gnat1^{-/-}) mouse M-cones with normal GCAPs expression levels (Gnat1^{-/-} GCAPs^{+/+}) and mouse M-cones with an additional GCAPs knockout (Gnat1^{-/-} GCAPs^{-/-}). Modified from Sakurai et al. (2011). Light flashes of different strengths in photons per square micrometer were delivered at 0 s.

These experiments clearly illustrate that the GC-GCAP system is an essential mechanism to enable the photoresponse due to the GC basal activity but also to timely shut off the photoresponse, which is maintained by GCAPs. In the following two sections, molecular properties of GCs and GCAPs will be described in more detail.

1.3.1 Retinal guanylate cyclases (GCs)

Guanylate cyclases (GCs) are enzymes that produce cGMP out of GTP. They are categorized roughly into soluble GCs and particulate GCs (for review see Lucas et al. 2000). In mammals, two α - and two β -subunits of the soluble GCs have been identified. The soluble GCs contain a heme binding domain, allowing them to be activated by nitric oxide (NO) and, albeit to a much lesser extent, carbon monoxide (CO) (Stone and Marletta 1994). Particulate GCs are tyrosine kinase-like transmembrane receptors (for review see Kuhn 2016). Seven isoforms are known to be expressed in mammals, GC-A to GC-G. GC-E and GC-F are expressed in the mammalian retina. While GC-F is retina-specific, GC-E has also been detected in the pineal gland (Venkataraman et al. 2000), the olfactory bulb (Duda et al. 2001), the cochlear nerve, and the organ of Corti (Seebacher et al. 1999). In contrast to most of the other GC forms, which are regulated by binding of extracellular ligands like peptide hormones or pheromones, GC-E and GC-F are regulated by intracellular binding proteins.

The smallest functional unit of retinal GCs are homodimers (Liu et al. 1997; Yang and Garbers 1997; Ramamurthy et al. 2001). For mature retinal GCs, seven domains have been identified (Figure 6) (Lucas et al. 2000). From the N- to the C-terminal, they consist of an extracellular domain (ECD), forming the

extracellular part of the GC, a transmembrane domain (TMD), and an intracellular part, possessing a juxta membrane domain (JMD), a kinase homology domain (KHD), a dimerization domain (DD), a catalytic domain (CD, also termed cyclase-catalytic domain), and a C-terminal extension (CTE). The precursor protein additionally possesses a signal sequence at the N-terminal (Shyjan et al. 1992; Lowe et al. 1995).

The function of the ECD for retinal GCs is unknown. In *in vitro* experiments, retinal GCs with deleted or modified ECD show the same activity profile as wildtype retinal GCs (Duda et al. 1996; Laura et al. 1996; Peshenko et al. 2010). However, mutations in the ECD of GC-E are associated with Leber congenital amaurosis (Karan et al. 2010; Jacobson et al. 2013; Boye et al. 2016; Sharon et al. 2018), “the most severe retinal dystrophy causing blindness or severe visual impairment before the age of 1 year” (den Hollander et al. 2008). Therefore, the ECD must be important *in vivo*. The TMD anchors the GCs inside the membrane (Lucas et al. 2000). Parat et al. (2010) could show that GC-A (also called natriuretic peptide receptor A, NPRA) is activated by a rotation mechanism of the TMD. The authors induced a rotation by inserting alanine residues at the end of the TMD. A 40 ° rotation leads to a constitutively active GC-A, even though its activity achieves only 6 % of ligand activated GC-A. Recently, my colleagues in the Division of Biochemistry (*University of Oldenburg*) could show that this rotation mechanism does not play a role in human GC-E activation (Shahu et al. 2022). Instead, they found a different mechanism explained below. The JMDs of GC-E and GC-F are highly homologous but different from other GC JMDs like in GC-A (Lange et al. 1999; Zägel and Koch 2014). In retinal GCs, it might be part of a possible binding site for GCAP1 (Lange et al. 1999). The KHD of GC-E and GC-F binds ATP, which enhances the GC activity (Yamazaki et al. 2003). Independent of ATP-binding, it shows Mg²⁺-dependent auto phosphorylation of serine residues, which was not shown for other GC isoforms (Aparicio and Applebury 1996). This kinase activity is independent of Ca²⁺ and cyclic nucleotides. The DD is important for the dimerization of two GC molecules. Ma et al. (2010) uncovered the crystal structure of the soluble GC DD (PDB entry 3HLS), which forms a coiled-coil structure with another soluble GC DD. Further, a swinging movement of the DD might be critical for the transition of retinal GCs to the active state: The point mutation V907L in the CD of human GC-E leads to a constitutive activation, causing cone-rod dystrophy in patients (Wimberg et al. 2018a). Shahu et al. (2022) determined and compared the enzymatic catalytic parameters of wildtype human GC-E and the V907L mutant and performed molecular dynamics simulations. They conclude that GCAPs might trigger a swinging movement of the DD to stabilize the active state of the GC-E, which is stabilized by V907L mutation independent of GCAPs. The CDs of a GC dimer form the catalytic core to synthesize cGMP out of GTP (Liu et al. 1997). The primary structures of the CDs in the particulate and soluble GC are highly conserved, and the crystal structure of the latter was solved by Allerston et al. (2013) (PDB entry 3UVJ). For the coordination of GTP inside the catalytic pocket, Mg²⁺ is needed (Koch et al. 1990; Liu et al. 1997). The CTE is specific for sensory GCs, including GC-E and GC-F. Its function is still under investigation, but it is proposed that the CTE might be important for the interaction with cytoskeletal structures (discussed in Lucas et al. 2000 part II.B.3.g).

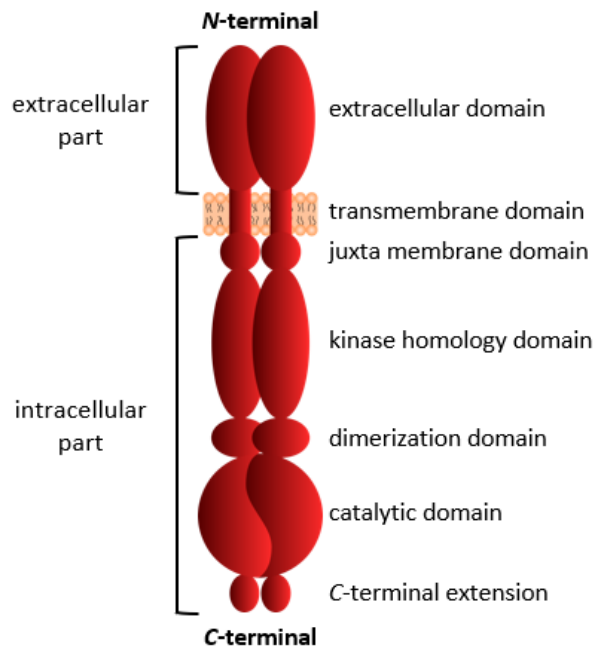


Figure 6: Domain structure of mature retinal guanylate cyclase homodimers, GC-E and GC-F.

Based on Koch and Dell'Orco (2015).

Several proteins interact with the GCs in photoreceptor outer segments (summarized in Koch and Dell'Orco 2015 Figure 4). These include the cytoskeletal proteins actin (Hallett et al. 1996) and tubulin (Schrem et al. 1999) but also the α -subunit (Rosenzweig et al. 2009). Known as GC-inhibitory proteins are RGS9-1 (Seno et al. 1998; Yu et al. 2001; Bondarenko et al. 2002) and retinal degeneration 3 (RD3) (Peshenko et al. 2011; Peshenko et al. 2016). The probably most prominent Ca^{2+} -dependent regulators of GC activity are the GCAPs (Koch and Stryer 1988; Palczewski et al. 1994; Olshevskaya et al. 1997).

The binding sites of GCAPs at the GC are still under controversial discussion. Experiments of different groups suggest either a model with a shared binding site or at least overlapping binding sites for GCAP1 and GCAP2 (Peshenko et al. 2015a; Peshenko et al. 2015b), allowing only one GCAP isoform to bind to the GC at a given time, or models with distinct GCAP binding sites (Lange et al. 1999; Sokal et al. 1999; Krylov and Hurley 2001; Duda et al. 2005; Sulmann et al. 2017) in which both GCAP isoforms can bind to the GC at the same time. Possible binding interfaces are regions within the JMD (Duda et al. 1999; Lange et al. 1999), the KHD (Krylov and Hurley 2001; Peshenko et al. 2015a; Sulmann et al. 2017), the DD (Peshenko et al. 2015b), and the CD (Sokal et al. 1999; Duda et al. 2005; Pettelkau et al. 2012; Pettelkau et al. 2013).

As key enzymes in phototransduction, GCs raised high interest in biomedical research. For example, mutations in the GC-E gene cause among others retinal diseases like Leber congenital amaurosis, cone-rod dystrophies, and Retinitis Pigmentosa (reviewed in Hunt et al. 2010).

1.3.2 Guanylate cyclase-activating proteins (GCAPs)

The family of neuronal calcium sensor (NCS) proteins is divided into several subfamilies (for reviews see Braunewell and Gundelfinger 1999; Burgoyne and Weiss 2001). One of which are the GCAPs. Like other NCS proteins, GCAPs possess four EF-hand motifs (color coded in Figure 7 A). An EF-hand consists of a loop region being flanked by two α -helices (Kretsinger and Nockolds 1973; for a review about “EF-hand calcium-binding proteins” see Lewit-Bentley and Réty 2000). In GCAPs, they are arranged in an array, with two EF-hands in the *N*-terminal semi-globule I and two EF-hands in the *C*-terminal semi-globule II (Figure 7 A). Ca^{2+} and Mg^{2+} can be coordinated in the loop region of the EF-hands. In the case of GCAPs, only EF-hands 2, 3, and 4 can bind Ca^{2+} with nanomolar affinity (Lim et al. 2009). In GCAP1, these EF-hands can also bind Mg^{2+} theoretically, but only EF-hand 2 clearly and EF-hand 3 eventually show Mg^{2+} -affinities high enough to compete with Ca^{2+} in the physiological ranges of both ions (Lim et al. 2009; Marino et al. 2015; Lim et al. 2016; see also section 1.2 for physiological ion concentrations). The non-cation binding EF-hand 1 is suggested to be involved in the interaction with the target protein, the GC (Ermilov et al. 2001; Sokal et al. 2001; Hwang et al. 2004). Further, bovine GCAP 1 is heterogeneously acylated at the *N*-terminal, and the consensus sequence for *N*-terminal acylation has been found in GCAPs of other species like human, mouse, and frog (Palczewski et al. 1994). It is assumed that this acylation is a general characteristic of all GCAPs (Palczewski et al. 2004). The most frequently found acylation of GCAPs is the myristoylation (Bereta and Palczewski 2011). For some GCAPs, the three-dimensional structure has been resolved: Ca^{2+} -bound non-myristoylated bovine GCAP2 (Figure 7 C) (Ames et al. 1999; PDB entry 1JBA), Ca^{2+} -bound non-myristoylated human GCAP3 (Stephen et al. 2006; PDB entry 2GGZ), Ca^{2+} -bound myristoylated chicken GCAP1 (Figure 7 A and B) (Stephen et al. 2007; PDB entry 2R2I), and Mg^{2+} -bound bovine GCAP1 V77E mutant (Lim et al. 2016; PDB entry 2NA0).

The Ca^{2+} - and Mg^{2+} -binding as well as the myristoyl group of the GCAPs are involved in a fine-tuned interplay for GC activity regulation. This interplay has been studied extensively for the bovine GCAPs, GCAP1 and GCAP2. They share around 40 % amino acid sequence identity (EMBOSS Needle, *EMBL-EBI*) and have similar tertiary structures (Figure 7) (Ames et al. 1999; Stephen et al. 2007). Yet, they differ in their characteristics, as I will explain in the following.

At first, it was unclear whether GCAPs undergo the so called “ Ca^{2+} -myristoyl switch”. This mechanism was proven for other myristoylated NCS proteins like recoverin (Zozulya and Stryer 1992) and neurocalcin δ (Ladant 1995). In the apo-conformation of recoverin, its myristoyl group is embedded in a hydrophobic pocket in the protein interior. Upon Ca^{2+} -binding, the myristoyl group becomes exposed to the exterior and serves as a lipid anchor for membrane association (Zozulya and Stryer 1992; Dizhoor et al. 1993; Ames and Lim 2012). Since GCAPs have a structure similar to recoverin, this Ca^{2+} -myristoyl switch seems to be plausible for GCAPs as well.

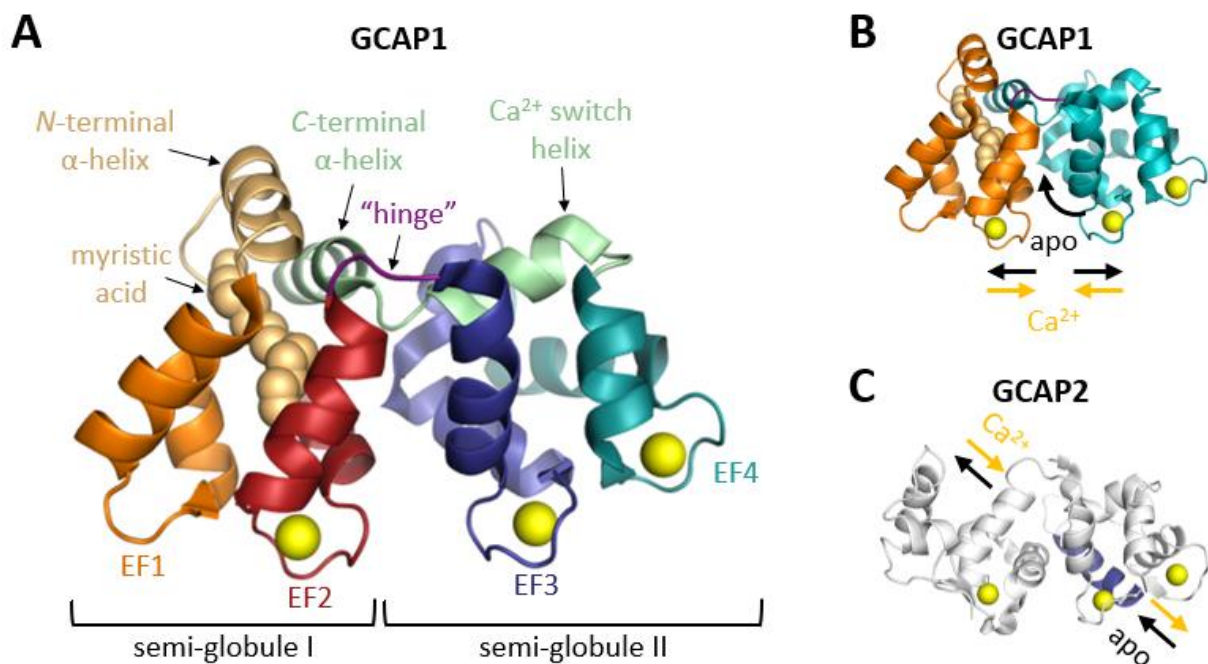


Figure 7: Structure and Ca^{2+} -dependent dynamics of myristoylated chicken GCAP1 and non-myristoylated bovine GCAP2.

The tertiary protein structures in their Ca^{2+} -bound forms are presented as cartoons. **(A)** Semi-globule I consists of the *N*-terminal (beige), EF hand (EF) 1 (orange), and EF2 (red). EF3 (dark blue), EF4 (dark cyan), and the *C*-terminal helices (light green), including the Ca^{2+} switch helix, belong to semi-globule II. Both semi-globules are connected by a hinge-region (violet). Calcium-ions (yellow spheres) are bound to EF2, EF3, and EF4. The myristic acid (beige spheres) is covalently attached to the *N*-terminal. **(B), (C)** Dynamics of the GCAP isoforms when they bind calcium-ions (Ca^{2+} , yellow arrows), and when they lose their calcium ions (apo, black arrows). **(B)** The semi-globules (orange and dark cyan, respectively) of GCAP1 connected by the hinge-region (violet) undergo a twisted accordion-like movement (Robin et al. 2015) upon Ca^{2+} -binding (Ca^{2+} , yellow arrows) or Ca^{2+} -releasing (apo, black arrows). **(C)** In GCAP2, the F-helix of EF3 (dark blue) makes a piston-like movement (Kollmann et al. 2012) upon Ca^{2+} -binding (Ca^{2+} , yellow arrows) or Ca^{2+} -releasing (apo, black arrows). GCAP1 PDB entry 2R2I (Stephen et al. 2007). GCAP2 PDB entry 1JBA (Ames et al. 1999).

Despite these similarities, the myristic acid of the Ca^{2+} -loaded GCAP1 does not leave the hydrophobic cleft (Hwang and Koch 2002; Stephen et al. 2007; Lim et al. 2009). Instead, Ca^{2+} -binding to EF-hand 4 induces a shortening of the GCAP1 " Ca^{2+} switch helix" (Figure 7 A), α -helix 10, by half a turn. Along with several intramolecular rearrangements, this causes a force on the *C*-terminal α -helix 11, which in turn alters its contact to the *N*-terminal attached myristoyl group. This proposed mechanism is termed the " Ca^{2+} myristoyl tug" (Peshenko et al. 2012; Lim et al. 2016). Comparisons between myristoylated and non-myristoylated GCAP1 also revealed that the myristoyl group significantly impacts the Ca^{2+} -dependent GC activation of GCAP1 (Hwang and Koch 2002; Hwang et al. 2003; Peshenko et al. 2012).

Myristoylation of GCAP2 does not show a significant impact on the Ca^{2+} -dependent GC activation (Hwang and Koch 2002; Hwang et al. 2003). Further, the position of the myristoyl moiety of GCAP2 is currently debated. In some studies, it seems to be solvent exposed independent of the ion-load and does not show any myristoyl switch (Olshevskaya et al. 1997; Hughes et al. 1998; Hwang and Koch 2002). The authors of a more recent study constructed and investigated a homology model of GCAP2 based on GCAP1 (Margetić et al. 2014). They propose that the myristoyl group might be buried in the protein interior in the absence of

lipophilic structures but might be exposed in the presence of lipophilic structures, which would resemble a membrane-induced myristoyl switch. This would further explain the finding that myristoylated GCAP2 associates to lipid vesicles (Vogel et al. 2007; Theisgen et al. 2011). However, this contrasts with the findings of Hwang and Koch (2002).

GCAP1 and GCAP2 also differ in their Ca^{2+} -induced molecular dynamics (Figure 7 B and C). By labelling GCAP2 with the dye Alexa Fluor®647 and measuring the fluorescence lifetime and anisotropy, Kollmann et al. (2012) could show that the α -helix between amino acids 111 and 131 moves in a piston-like way upon Ca^{2+} -binding or -releasing (Figure 7 C). Robin et al. (2015) did the same measurement with GCAP1 and further supported their results by molecular dynamics simulations. In contrast to GCAP2, GCAP1 shows a Ca^{2+} -dependent twisted accordion-like movement (Figure 7 C).

These results show that, despite two proteins sharing similar tertiary structures, the effects of ion-binding and myristoylation on the protein's dynamics and regulatory properties can differ significantly.

1.4 The GC-GCAP system and ribbon synapses

In photoreceptor outer segments, the GC-GCAP system was studied extensively. However, it is not restricted to that cell compartment within photoreceptor cells. Several groups have proven the presence of GCs and GCAPs in photoreceptor synaptic terminals (Liu et al. 1994; Cooper et al. 1995; Dizhoor et al. 1995; Gorczyca et al. 1995; Otto-Bruc et al. 1997; Duda et al. 2002; Pennesi et al. 2003; Venkataraman et al. 2003; Makino et al. 2008), the cone pedicles and the rod spherules. The synapses of photoreceptors are ribbon synapses (Figure 8 A) (Sjöstrand 1953; Sjöstrand 1958; Heidelberger et al. 2005; Sterling and Matthews 2005; tom Dieck and Brandstätter 2006). In mammals, these structurally specialized chemical synapses are also found in bipolar cells, in hair cells of the cochlea and of the vestibular system, and in pineal gland cells (Smith and Sjöstrand 1961; Hopsu and Arstila 1965; Dowling 1987; Jastrow et al. 1997; Sterling 1998; Lenzi et al. 1999). Despite being structurally different from conventional chemical synapses, they share similar protein components. The differences lie in their expressed gene isoforms and their produced protein amounts (tom Dieck and Brandstätter 2006).

The presynaptic cells of conventional chemical synapses contain ten to 100 synaptic vesicles clustering in the proximity of the active zone, and the transmitter release of the synaptic vesicles depends on the rate of action potentials generated by the nervous system cell (Heidelberger et al. 2005; tom Dieck and Brandstätter 2006). In contrast, the presynaptic cells of ribbon synapses contain at least one ribbon, anchored to the transmitter release site and extending into the cytoplasm (Figure 8 A) (Heidelberger et al. 2005; tom Dieck and Brandstätter 2006). To this ribbon, a large pool of readily releasable synaptic vesicles is tethered, and several hundreds to several thousands of synaptic vesicles release their transmitters per second (Heidelberger et al. 2005; tom Dieck and Brandstätter 2006). The rate of transmitter release is not

encoded in action potentials but in graded changes of the membrane potential. Depending on the light intensity that hits the photoreceptor, the graded change of membrane potential leads to an acceleration or a deceleration of transmitter release at the synaptic ribbon (tom Dieck and Brandstätter 2006). The high throughput of ribbon synapses enables photoreceptor cells to release transmitters tonically and over a wide range of membrane potential magnitudes.

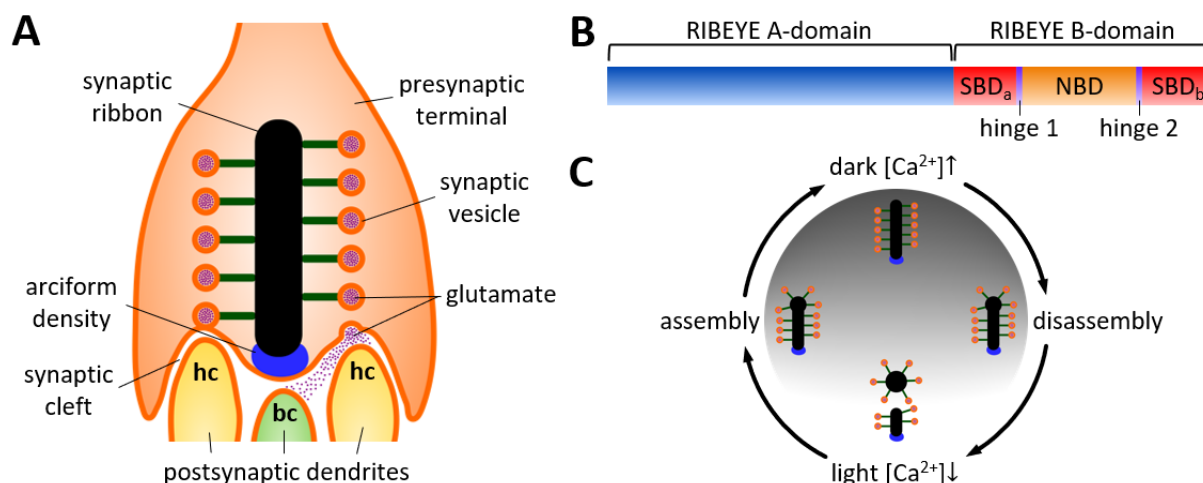


Figure 8: Photoreceptor ribbon synapse – schematic overview, RIBEYE domain structure, and Ca^{2+} - and light-dependent dynamics of ribbons.

(A) Schematic overview of photoreceptor ribbon synapses. The triad synapse comprises the photoreceptor cell (light orange) and the dendrites of bipolar cells (hc, light green) and horizontal cells (hc, yellow) invaginating into the presynaptic terminal (Wässle 2004; Nemitz et al. 2021). The presynaptic terminal contains the synaptic ribbon (black), which is anchored to the active site by the arciform density (blue). Synaptic vesicles (orange spheres), containing the neurotransmitter glutamic acid (purple dots), are tethered to the synaptic ribbon. Based on Wässle (2004); Heidelberger et al. (2005); tom Dieck and Brandstätter (2006); Schmitz et al. (2012). (B) Domain structure of RIBEYE, the major component of synaptic ribbons. The RIBEYE A-domain (blue) is unique to RIBEYE. The RIBEYE B-domain is nearly identical to CtBP2 and can be subdivided into a discontinuous substrate binding domain (SBD_a and SBD_b, red) connected to the NAD(H)-binding domain (NBD, orange) by two hinge regions (violet). Based on Venkatesan et al. (2010). (C) Ca^{2+} - and light-dependent dynamics of synaptic ribbons. The synaptic ribbon is largest in the dark at high $[\text{Ca}^{2+}]$. Upon light exposure, the $[\text{Ca}^{2+}]$ drops, and synaptic spheres disassemble from the synaptic ribbon, leaving a truncated ribbon. These synaptic spheres assemble with the truncated synaptic ribbon after shutting off light. Based on Spiwoks-Becker et al. (2004).

The major component of synaptic ribbons and the only component known to be specific for ribbon synapses is the protein RIBEYE (Schmitz et al. 2000; Zenisek et al. 2004; Wan et al. 2005; Magupalli et al. 2008). By forming multiple RIBEYE-RIBEYE interactions, it builds the synaptic ribbon (Magupalli et al. 2008). RIBEYE belongs to the C-terminal binding proteins (CtBPs), which are speculated to be involved in vesicle turnover at both ribbon synapses and conventional synapses (tom Dieck and Brandstätter 2006). The N-terminal A-domain is unique to RIBEYE, while the C-terminal B-domain is nearly identical to CtBP2 (Figure 8 B) (Schmitz et al. 2000). CtBPs in turn belong to the D-isomer-specific 2-hydroxyacid dehydrogenases (reviewed by Chinnadurai 2002). They possess a central nicotinamide adenine dinucleotide (NAD(H))-binding domain (NBD), which is connected by two flexible hinge regions to a discontinuous substrate-binding domain (SBD_a and SBD_b) (Kumar et al. 2002; Nardini et al. 2003). The N-terminal SBD_a is connected to the NBD by hinge 1. Hinge 2 connects the NBD to the C-terminal SBD_b. Binding of NAD(H) at

the NBD induces structural rearrangements between the NBD and the SBD, leading to a “closed” conformation (Lamzin et al. 1994; Nardini et al. 2003). To this closed, NAD(H)-bound conformation of RIBEYE, GCAP2 can bind at the hinge 2 region in a redox (reduction/oxidation)-insensitive manner (Venkatesan et al. 2010). However, the function of GCAP2 at the synaptic ribbon is not clear yet.

Overexpression of GCAP2 in mouse photoreceptor cells leads to a reduction of synaptic ribbon numbers (Venkatesan et al. 2010). However, this can be an effect of GCAP2 chelating intracellular Ca^{2+} (Venkatesan et al. 2010). Photoreceptor synaptic ribbons are undergoing dynamic assembly and disassembly in response to light levels (Figure 8 C) (Spiwoks-Becker et al. 2004). In the dark, synaptic ribbons are large. Upon light exposure, spherical portions, called synaptic spheres, disassemble from the synaptic ribbon and leave a smaller synaptic ribbon. This disassembly is reversible. When the illumination of the photoreceptors is cancelled, the synaptic spheres assemble with the small synaptic ribbons (Spiwoks-Becker et al. 2004). The disassembly of synaptic ribbons upon light exposure can also be mimicked by chelating extracellular Ca^{2+} with ethylene glycol-bis(β -aminoethyl ether)-*N,N,N',N'*-tetraacetic acid (EGTA) or 1,2-bis(2-Aminophenoxy)ethane-*N,N,N',N'*-tetraacetic acid (BAPTA), which in turn leads to decreasing intracellular $[Ca^{2+}]$ (Spiwoks-Becker et al. 2004). Like in the photoreceptor outer segments, the $[Ca^{2+}]$ in the photoreceptor synaptic terminals is high in the dark and drops upon illumination (Jackman et al. 2009). Therefore, Ca^{2+} seems to be important for the structural integrity of the synaptic ribbon. The exact role of GCAP2 in this interaction remains to be examined.

Some studies provide evidence that cGMP increases the number of synaptic ribbons in the pineal gland as a second messenger (Seidel et al. 1990; Spessert et al. 1992). Since GCs are present in photoreceptor synaptic terminals and GCAPs regulate GC activity in a Ca^{2+} -dependent manner in the outer segments of photoreceptors (see section 1.3), GCAPs might influence the synaptic ribbon dynamics with the GC-GCAP system as well. However, another Ca^{2+} -dependent GC activity regulating protein, S100 β , is present in photoreceptor synaptic terminals, and it regulates the GC in a way opposite to GCAPs (Duda et al. 2002; Venkataraman et al. 2003; Sharma 2010). Further, the GC-inhibiting protein retinal degeneration protein 3, which prevents activation of the GC by GCAPs, was shown to be present in the outer plexiform layer of the retina (Azadi et al. 2010; Peshenko et al. 2011; Wimberg et al. 2018b). These findings point to a complex interaction network between proteins that have been studied in photoreceptor outer segments and the synaptic ribbon.

1.5 GCs and GCAPs in photoreceptors of the zebrafish (*Danio rerio*)

The GC-GCAP system was extensively investigated in the visual systems of mice and cattle. Another model organism in retinal research is a teleost, the zebrafish (*Danio rerio*) (Bilotta and Saszik 2001). It possesses a functionally cone-dominated visual system (Fleisch and Neuhauss 2006), making it suitable for the investigation of the less well understood phototransduction in cones. Interesting for medical research, the zebrafish can regenerate many tissues, including the retina (Gemberling et al. 2013; Massoz et al. 2021).

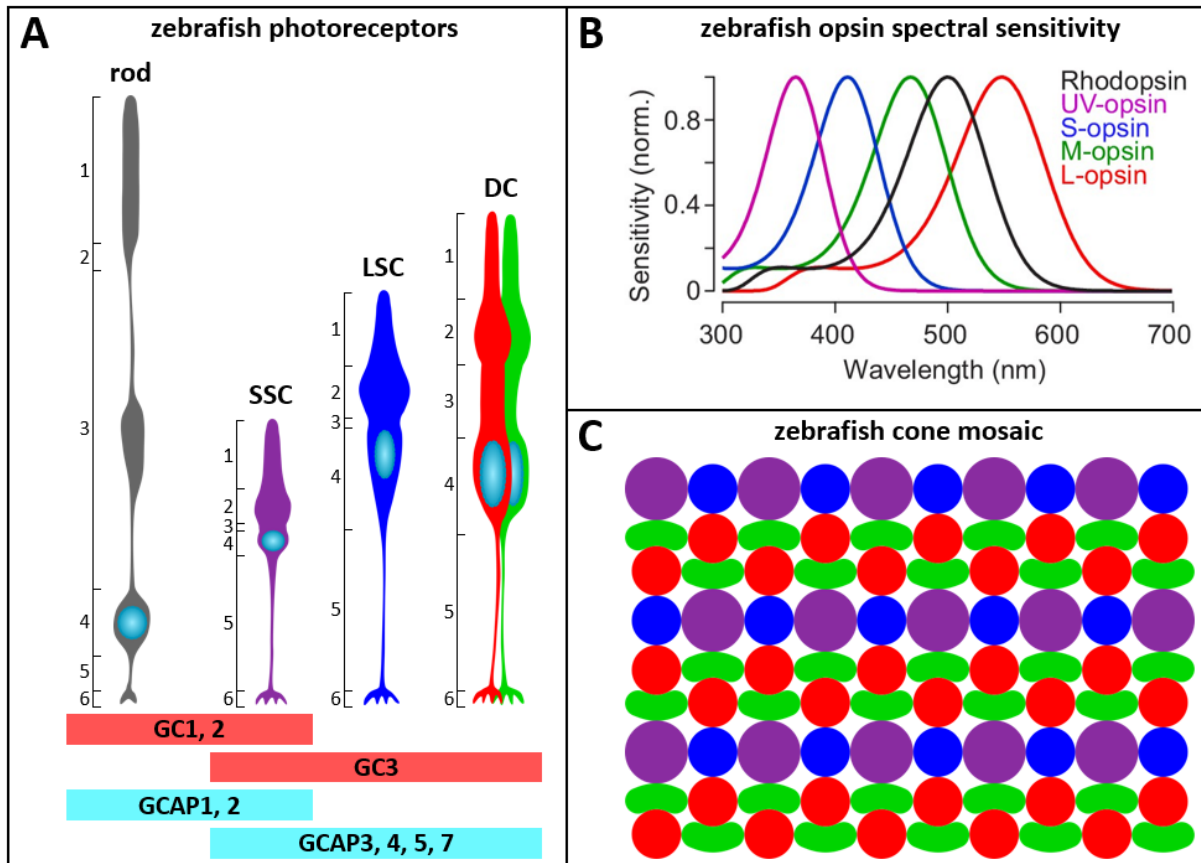


Figure 9: Photoreceptors of the zebrafish (*Danio rerio*) - schematic overview, spectral sensitivity, and mosaic.

(A) The zebrafish possesses one rod photoreceptor (grey), expressing rhodopsin, and four cone types: UV light-sensitive short single cones (SSC, violet), which express the UV-opsin, blue light-sensitive long single cones (LSC, blue), expressing the S-opsin, and green and red light-sensitive double cones (DC, green and red), which express the M- and L-opsin. Each photoreceptor type has an outer segment (1), an inner segment containing an ellipsoid (2) and a myoid (3), a nucleus (4), an axon (5), and a synaptic terminal (6) (based on Lagman et al. 2015). GC1 and 2 as well as GCAP1 and 2 are expressed in zebrafish rods and SSCs. GC3 and GCAP3, 4, 5, and 7 are expressed only in zebrafish cones (Imanishi et al. 2002; Imanishi et al. 2004; Rättscho et al. 2009; Fries et al. 2012). (B) The different opsins are sensitive to different light wavelengths (spectra taken from Franke et al. 2019). The peak sensitivities of the opsins are around 501-503 nm for rhodopsin, 360-361 nm for the UV-opsin, 407-417 nm for the S-opsin, 473-480 nm for the M-opsin, and 556-564 nm for the L-opsin (Nawrocki et al. 1985; Robinson et al. 1993; Cameron 2002; Allison et al. 2004; Fleisch and Neuhauss 2006). (C) Zebrafish cones are arranged in a specific mosaic. Based on Raymond and Barthel (2004). Color code of photoreceptor types in A also applies to B and C.

The retina of the zebrafish possesses one rod type for dim light vision and four cone types, maintaining color vision (Figure 9) (Fleisch and Neuhauss 2006). The short single cones (SSC) are sensitive to UV light, the long single cones (LSC) detect blue light, and the cones sensitive to red and green light are forming a double cone (DC) (Figure 9 B). The cone types of adult zebrafish have individual morphologies and are

arranged in a specific mosaic in the retina (Figure 9 C) (Branchek and Bremiller 1984; Larison and Bremiller 1990; Raymond et al. 1995; Raymond and Barthel 2004; Li et al. 2012), making it possible to distinguish between the cone types under a light microscope without staining them.

While two GCs (see section 1.3.1) and up to three GCAPs (Palczewski et al. 1994; Dizhoor et al. 1995; Gorczyca et al. 1995; Frins et al. 1996; Haeseleer et al. 1999; Imanishi et al. 2002) are present in mammalian photoreceptor cells, the zebrafish expresses three GC and six GCAP isoforms in its photoreceptors (Figure 9 A) (Imanishi et al. 2004; Rättscho et al. 2009). *N*-myristoyl transferase (NMT) is present in zebrafish larvae at 5 dpf (Fries et al. 2012) and enables myristoylation of zebrafish GCAPs in their native tissue, which has been proven for native GCAP3 and GCAP5 by mobility comparison after SDS-PAGE (sodium dodecyl sulfate-polyacrylamide gel electrophoresis) (Fries et al. 2012; Fries 2013). For all six zebrafish GCAPs, myristoylation *in vivo* after heterologous expression in cells of the Flp-In™-293 Cell Line (HEK293) has been shown by click chemistry (Sulmann et al. 2015). However, the amino acid sequences of zebrafish GCAPs 1, 4, and 5 were adjusted by site directed mutagenesis to enable myristoylation by yeast NMT.

A possible explanation for the high numbers of GC and GCAP isoforms in zebrafish is a gene duplication in the early evolution of teleosts (Amores et al. 1998; Meyer and Schartl 1999; Taylor et al. 2003; Christoffels et al. 2004). Due to this gene duplication, teleosts possess more isoforms of proteins in comparison to mammals, but the isoforms differ slightly in their molecular properties. In the case of zebrafish GCAPs, this can be seen in the spatial-temporal expression profiles and in the operational profiles. GC1 and 2 as well as GCAP1 and 2 are expressed in zebrafish rods and SSCs, whereas GC3 and GCAP3, 4, 5, and 7 are expressed in all zebrafish cone types but not in rods (Figure 9 A) (Imanishi et al. 2002; Imanishi et al. 2004; Rättscho et al. 2009; Fries et al. 2012). Transcripts of the zebrafish GCs and GCAP1, 2, 3, 4, and 7 can be detected between three and four days post fertilization (dpf), while transcripts of zebrafish GCAP5 are not detectable before 12-15 dpf (Rättscho et al. 2009; Rättscho et al. 2010). Further, the zebrafish GCAPs differ in their Ca²⁺-binding affinities, which are fine-tuned by Mg²⁺ and posttranslational myristoylation, and Ca²⁺-dependent target regulation (Behnen et al. 2009; Scholten and Koch 2011; Fries et al. 2012; Sulmann et al. 2015). For example, all zebrafish GCAPs heterologously expressed in *Escherichia coli* (*E. coli*) have been shown to regulate bovine GC-E extracted from bovine rod outer segments (ROS). But the IC₅₀-value, the [Ca²⁺] at which the GC activation is half-maximal, differs between the zebrafish GCAPs from 25 nM to 570 nM [Ca²⁺] (summarized in Sulmann et al. 2015 Table 1). Because of these findings, the Ca²⁺-relay model was proposed for the zebrafish GC-GCAP system (Scholten and Koch 2011; Figure 10).

The Ca²⁺-relay model was already introduced for the mammalian GC-GCAP system (Koch 2006; Koch and Dell'Orco 2013), and later, a similar mode was proposed for the zebrafish recoverin-GRK1 system (Elbers et al. 2018). Mammalian GCAP1 and GCAP2 have IC₅₀-values for the regulation of bovine GC-E between 700 nM to 1000 nM and 100 nM to 200 nM [Ca²⁺], respectively (Koch and Dell'Orco 2013). Therefore, after

a light stimulus hits the photoreceptor, leading to a decrease in intracellular $[Ca^{2+}]$ (see sections 1.2 and 1.3), mammalian GCAP1 loses its bound Ca^{2+} -ions first and enhances the GC activity. If the light stimulus is strong enough or lasts for a period long enough to reduce the intracellular $[Ca^{2+}]$ to the point that Ca^{2+} dissociates from mammalian GCAP2, GCAP2 further increases the GC activity. This Ca^{2+} -relay model provides a plausible explanation for the presence of protein variants with similar properties in the same cell compartment.

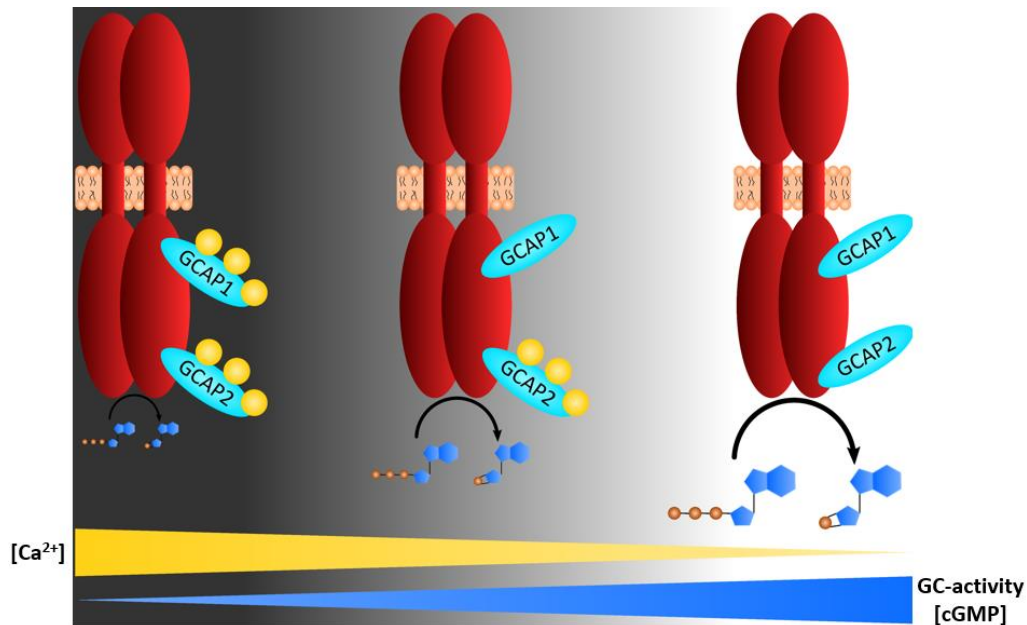


Figure 10: Ca^{2+} -relay model of the mammalian GC-GCAP system.

In the dark state of the photoreceptor (left), the $[Ca^{2+}]$ is high. Mammalian GCAP1 and GCAP2 (cyan ovals) are saturated with Ca^{2+} (yellow spheres) and inhibit the GC (red), resulting in a low to diminished GC activity and a low $[cGMP]$. When light hits the photoreceptor (middle), the $[Ca^{2+}]$ decreases. Ca^{2+} dissociates from GCAP1, which in turn enhances the catalysis of GTP (blue polygons with three brown phosphor atoms) to cGMP (blue polygons with one brown phosphor atom) by the GC, leading to an increasing $[cGMP]$. If the light stimulus is strong enough or lasts for a longer period (right), Ca^{2+} dissociates from GCAP2 as well. GCAP2 further increases the GC activity, leading to an even higher $[cGMP]$. Based on Koch and Dell'Orco (2013).

However, a complete picture of the GC-GCAP system in the zebrafish retina is missing. For example, it is unclear which GC isoform serves as a target for which specific GCAP isoform and whether these regulatory features match the expression pattern in rod and cone cells. An experimental approach in this direction would be the determination of the IC_{50} -values of each zebrafish GCAP reconstituted with each zebrafish GC. Unfortunately, a method for expressing functional zebrafish GCs in heterologous expression systems was unsuccessful so far and will be a future task. In the meantime, we can investigate the general biochemical properties of the zebrafish GCAPs and determine their regulatory effects on GCs of other species. Among the six GCAP isoforms expressed in the zebrafish retina, GCAP5 seems to be special in several aspects as described below.

1.6 Zebrafish GCAP5

At the beginning of my PhD in 2016, not much was known about zebrafish GCAP5. As to my knowledge, five publications (Imanishi et al. 2004; Rättscho et al. 2009; Scholten and Koch 2011; Koch 2013; Sulmann et al. 2015) addressed this protein before. In addition, four written theses prepared in the Division of Biochemistry (*University of Oldenburg*) investigated more or less properties of zebrafish GCAP5 (Bachelor thesis Lange 2012; Master thesis Griepenstroh 2016; and Dissertations of Fries 2013 and Sulmann 2016). In this section, I will summarize the findings about zebrafish GCAP5 by these authors.

Zebrafish GCAP5 was first cloned and expressed by Imanishi et al. in 2004. The authors detected the mRNA by reverse transcription-polymerase chain reaction (RT-PCR) only in retinal tissue, and the antisense probe in *in situ* hybridization showed a signal in the inner segments of all cone types but not in other cell types of the zebrafish retina. Their phylogenetic analysis of GCAPs resulted in teleost GCAP5 variants being closely related in sequence to GCAP1 variants of other vertebrates, e. g. Mammalia. In a developmental study, Rättscho et al. (2009) detected the first transcripts in larval zebrafish retinae around 15 dpf, which is more than ten days later than the appearance of transcripts of other zebrafish GCAPs.

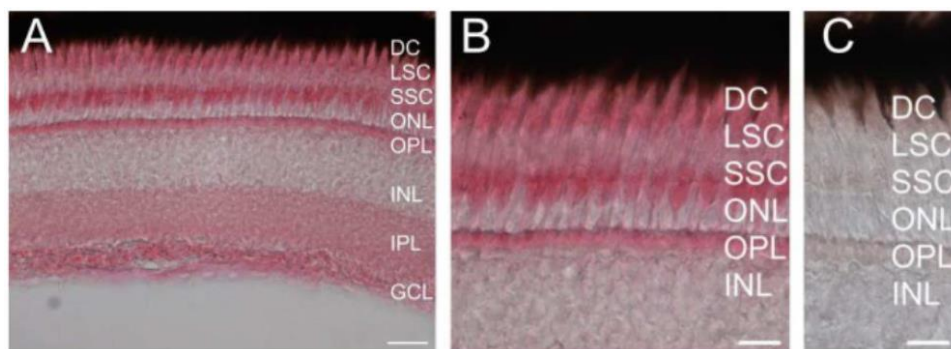


Figure 11: Immunohistochemistry against GCAP5 in cryosections of adult zebrafish retina.

(A, B) Immunoreactivity pattern of the antibody against zebrafish GCAP5 in cryosections of the zebrafish retina, stained with Fast Red. All cone types are stained from the outer segments over the inner segments in the outer nuclear layer (ONL) to the synaptic terminals in the outer plexiform layer (OPL). In addition, the inner plexiform layer (IPL) and the ganglion cell layer (GCL) are stained. No staining was observed in the inner nuclear layer (INL). (C) Pre-immune serum staining. Scale bars: A and B 20 μ m, C 10 μ m. Taken from Fries (2013).

Ramona Fries and Werner Säftel (both Division of Biochemistry, *University of Oldenburg*) purified recombinant zebrafish GCAP5 for immunization of rabbits and tested the serum supplied by the company *Pineda Antikörper-Service*. It showed high sensitivity and specificity with only little cross reactivity with zebrafish GCAP1 in preparations of adult zebrafish retinae (Fries 2013). The antibody was used for western blotting and for immunohistochemical staining of cryosections of the zebrafish retina with Fast Red, a substrate for the alkaline phosphatase (method described by Fries et al. 2012). Surprisingly, on the protein level, zebrafish GCAP5 was detected at four dpf at the latest (Fries 2013). Immunohistochemical staining of adult zebrafish retinae revealed that zebrafish GCAP5 is present in all cone types (Figure 11), which agrees with the findings of Imanishi et al. (2004). The strongest staining was found in the SSCs, followed by DCs and LSCs. On the subcellular level, the staining was especially strong in the inner segments and in the

synaptic terminals of cones, the latter resulted in a staining of the outer plexiform layer. Further, the inner plexiform layer and the ganglion cell layer were stained. Comparisons of the mobility in SDS-polyacrylamide gels of recombinant non-myristoylated and myristoylated zebrafish GCAP5 with native GCAP5, detected with the anti-GCAP5 antibody after western blotting, revealed that native zebrafish GCAP5 is posttranslational modified at five dpf (Fries 2013). Since this coincides with the detection of the zebrafish NMT at five dpf (Fries et al. 2012), a myristoylation of zebrafish GCAP5 in its native tissue is quite likely. Another possible modification is *N*-acetylation. Zebrafish GCAP5 possesses an aspartic acid at position three, which would favor *N*-acetylation over *N*-myristoylation at least by the yeast NMT (Utsumi et al. 2001). However, posttranslational acetylation, which adds only 42 Da to a protein and reduces its net charge by just one, is mostly not detectable by SDS-PAGE (Buehl et al. 2014). Thus, the findings of Fries (2013) strongly point to native GCAP5 being myristoylated.

Comparative analyses of the zebrafish GCAPs revealed that recombinant zebrafish GCAP5 binds Ca^{2+} and is sensitive to changes in $[\text{Ca}^{2+}]$ (Scholten and Koch 2011; Sulmann et al. 2015; Sulmann 2016). The Ca^{2+} -sensitivity is fine-tuned by myristoylation and influenced by Mg^{2+} . However, the x-fold activation when GCAP5 was reconstituted with the bovine GC-E from ROS (Scholten and Koch 2011) or with zebrafish GCs from membranes of the zebrafish retina (Fries 2013) was rather low in comparison to the other zebrafish GCAPs. This raises the question whether zebrafish GCAP5 is a real regulator of a GC or inhabits other functions and targets.

We further have hints that zebrafish GCAP5 might possess characteristics unique in comparison to all GCAP isoforms across different species investigated so far: binding of iron-ions and redox-sensitivity (Lange 2012; Griepenstroh 2016). If ferrous iron (Fe^{2+}) was added to the LB medium used for expression of non-myristoylated zebrafish GCAP5 in *E. coli* cells, the GCAP5 solution after purification was reddish (Lange 2012). The presence of Fe^{2+} was confirmed by absorbance spectroscopy, showing an increased absorbance around 420 nm which was not bleached by adding sodium borohydride (Lange 2012). Therefore, pyridoxal 5'-phosphate as a source for the reddish color can be excluded (Huang et al. 2008). Quantification of Fe^{2+} with 2,2'-Bipyridine revealed that the percentage of Fe^{2+} -bound GCAP5 increased with increasing iron(II)-sulfate (FeSO_4) concentration in the LB medium during expression in *E. coli* (Lange 2012). While 100 μM FeSO_4 in the LB medium resulted in 0.625 μM Fe^{2+} bound to 50 μM of purified GCAP5, 2 mM FeSO_4 in the LB medium led to 8.8 μM Fe^{2+} bound to 50 μM of purified GCAP5. Higher $[\text{FeSO}_4]$ in the LB medium were either cytotoxic or led to problems during purification of GCAP5. The loading of GCAP5 with Fe^{2+} further diminished the cysteine accessibility (Lange 2012). Zebrafish GCAP5 possesses five cysteines. For the non-myristoylated GCAP5 that was not loaded with Fe^{2+} , one cysteine was accessible. In the case of Fe^{2+} -loaded non-myristoylated GCAP5, less than one cysteine was accessible. Additionally, the author investigated the cysteine accessibility of non-myristoylated GCAP5 that was not loaded with Fe^{2+} but purified under reducing conditions, using 2 mM 2-Mercaptoethanol for all buffers after lysing of *E. coli* cells.

In this reduced purified GCAP5, two to three cysteines were accessible. Reduction of zebrafish GCAP5 also influenced the regulation of the bovine GC-E from ROS (Lange 2012). While normally purified non-myristoylated GCAP5 in its Fe²⁺-loaded and non-loaded form did not differ in their bovine GC-E regulatory profiles, the reduced purified GCAP5 showed a stronger enhancement of bovine GC-E activation under Ca²⁺-free conditions. Further, reduction seemed to favor a monomeric state of zebrafish GCAP5, while non-reduced as well as Fe²⁺-loaded GCAP5 were mainly present as dimers and oligomers as detected by analytical SEC (Lange 2012).

Zebrafish GCAP5 possesses five cysteines with a clustering of three cysteines at its *N*-terminal: Cys15, Cys17, and Cys28. While the position of Cys28 corresponds to cysteines in zebrafish GCAPs 1, 2, and 7 as well as bovine GCAPs 1 and 2, and positioning of Cys17 corresponds to a cysteine in bovine GCAP1, Cys15 is not conserved (Figure A1). Since this clustering is unique among the GCAPs, and cysteines are known to be involved in Fe²⁺-binding of iron-sulfur proteins (deMaré et al. 1996; Min et al. 2001; Emerson et al. 2003) but also can mediate redox-sensitivity (Barford 2004), we assumed that the cysteines might be responsible for the postulated Fe²⁺-binding and the redox-sensitivity of GCAP5. The focus of Griepenstroh (2016) was more on the cysteines of zebrafish GCAP5. Griepenstroh showed that substitution of Cys15 and Cys17 by alanine decreases the cysteine accessibility of non-myristoylated zebrafish GCAP5 by one in the single cysteine mutants and by two in the double cysteine mutant. Reduction of the non-myristoylated wildtype GCAP5 uncovered all five cysteines, which contrasts with the results of Lange (2012). Mutation of the cysteines seemed to reduce the GCAP5-regulated bovine GC-E activity in comparison to the wildtype, while reduction seemed to enhance the activity of bovine GC-E reconstituted with wildtype GCAP5 in the presence and absence of Ca²⁺. Lange (2012) observed this effect of reduction on the GCAP5-regulated GC-E activity only in the absence of Ca²⁺.

1.7 Aims of the thesis

Since I investigated only zebrafish GCAP5, I will refer to this protein as GCAP5 in the following for simplicity.

The results of Fries (2013) suggest that GCAP5 is myristoylated in the zebrafish retina (see section 1.6). In our lab (Division of Biochemistry, *University of Oldenburg*), we use the yeast NMT for co-expression in *E. coli* to allow posttranslational addition of a myristoyl group. However, GCAP5 harbors an aspartic acid residue at position three, which favors acetylation (Utsumi et al. 2001). Therefore, I used a GCAP5 mutant with the aspartic acid substituted by asparagine (D3N) to favor acylation by yeast NMT. The D3N mutation was present in all GCAP5 variants investigated in this thesis. I will refer to GCAP5-D3N as the wildtype GCAP5 for simplicity.

The focus of this thesis was on the effects of myristoylation on GCAP5, the influence of Cys15 and Cys17, its possible redox-sensitivity, and Fe²⁺-dependency with respect to Ca²⁺-dependent properties. Another goal was to establish a protocol for immunohistochemical staining of GCAP5 in cryosections of the zebrafish retina using fluorescence markers for co-localization analysis.

Purification protocol: The first important step was to optimize the purification protocol for GCAP5 heterologously expressed in *E. coli*. The existing protocol in our group (Division of Biochemistry, *University of Oldenburg*) resulted in a sufficient yield of GCAP5 but insufficient purity for some of my planned experiments. With the protocol of our cooperation partners of the Department of Chemistry (*UC Davis*), I received pure protein but at a very low yield. The goal was to obtain GCAP5 with a minimum purity of 90 % and a yield of at least 1 mg protein out of 500 mL *E. coli*-culture. With the resulting protocol, I purified the following GCAP5 variants and mutants: non-myristoylated wildtype (non-myr WT), myristoylated wildtype (WT), reduced purified myristoylated wildtype (reduced WT), myristoylated C15A-C17A mutant (C15A-C17A), myristoylated H18E-Y21E mutant (H18E-Y21E), and myristoylated V76E mutant (V76E).

Effects of myristoylation: Myristoylation can have a large impact on GCAP's dynamics and interactions (Hwang and Koch 2002; Hwang et al. 2003; Peshenko et al. 2012). To see what impact *N*-myristoylation has on GCAP5, I performed my experiments with non-myr WT in comparison to the myristoylated WT. The myristoylation rate of myristoylated GCAP5 variants was checked by reversed phase-HPLC.

Ca²⁺-sensitivity: GCAPs are known to be Ca²⁺-sensors that undergo conformational changes upon Ca²⁺-binding and -releasing (see section 1.3.2) and regulate retinal GCs in a Ca²⁺-dependent manner (see section 1.3). Even though GCAP5 is only a weak activator of bovine GC-E from ROS preparations (Scholten and Koch 2011), it still shows Ca²⁺-dependent properties (Scholten and Koch 2011; Lange 2012; Sulmann et al. 2015; Griepenstroh 2016). Thus, I performed most of my experiments in the presence and in the absence of Ca²⁺ (cysteine accessibility measurements, Fe²⁺-dependent GC assay) or under Ca²⁺-titrations (tryptophan fluorescence spectroscopy, GC assay).

Fe²⁺-dependent target regulation: GCAP5 possesses a cysteine cluster at its *N*-terminal (see section 1.6 and Figure A1). Cysteines can function as Fe²⁺-binding sites (deMaré et al. 1996; Min et al. 2001; Emerson et al. 2003), and we have hints that GCAP5 might bind Fe²⁺, possibly with Cys15 and Cys17 (see section 1.6). Whether this putative Fe²⁺-binding affects the target regulation of GCAP5 remained unclear. We addressed these topics together with our cooperation partners of the Department of Chemistry (*UC Davis*), who performed nuclear magnetic resonance (NMR) structural studies of the wildtype GCAP5 and the C15A-C17A mutant implying Fe²⁺. I tested the effect of Fe²⁺ on GCAP5 target regulation by preloading GCAP5 with Fe²⁺ and reconstituting it with the recombinant human GC-E in the presence of low [Fe²⁺] and in the presence and absence of Ca²⁺ for GC assay analysis. Our results are published in Lim et al. (2017).

Redox-sensitivity: Cysteines are not only able to coordinate Fe²⁺, but they can also function as redox-sensory sites (Barford 2004). The results of Lange (2012) and Griepenstroh (2016) suggest that GCAP5 might be redox-sensitive, possibly due to Cys15 and Cys17. To test this hypothesis, I purified WT GCAP5 under reducing conditions and compared it to WT purified under normal conditions and to the C15A-C17A mutant. Except for the cysteine accessibility measurements that were performed in the absence of dithiothreitol (DTT), reduced WT was always kept at 5 mM DTT instead of 1 mM DTT for reduction. In addition to the experiments on the background of Ca²⁺-dependency, I tested a redox-dependent dimerization of all GCAP5 variants by analytical SEC measurements in the absence and presence of 5 mM DTT. Therefore, I also included the GCAP5 mutants H18E-Y21E and V76E, which might prevent dimerization. In GCAP1, the corresponding amino acid positions have been shown to be crucial parts of the dimerization interface (Lim et al. 2018).

Immunohistochemistry with fluorescence markers: The localization of GCAP5 within the zebrafish retina was already shown by Fries (2013), who used Fast Red for immunohistochemistry staining. Together with apl. Prof. Dr. Ulrike Janssen-Bienhold (Division of Visual Neuroscience, *University of Oldenburg*), I established a protocol for immunohistochemistry staining against GCAP5 with fluorescence markers for future co-localization studies.

2 Material and methods

Unless otherwise stated, all methods were performed according to Sambrook et al. (1989), eventually with modifications.

2.1 Devices and consumables

2.1.1 Devices

Autoclave

V-150 (*Systec*)

Centrifuges

Avanti J-E Centrifuge (*Beckmann Coulter*)

rotor JA-25.50

rotor JLA-10.500

Centrifuge 5415 D (*Eppendorf*)

Centrifuge 5415 R (*Eppendorf*)

Heraeus Biofuge Primo R (*Thermo Fisher Scientific*)

rotor #7588

Heraeus Labofuge 400 (*Thermo Fisher Scientific*)

rotor #8179

Microcentrifuge 1-16 (*Sigma Laborzentrifugen*)

Sorvall Discovery M120 SE Micro-Ultracentrifuge (*Thermo Fisher Scientific*)

rotor S100AT4

Ultracentrifuge Sorvall WX90 (*Thermo Fisher Scientific*)

rotor SureSpin 630

rotor Type 70 Ti

Clean bench

HERASafe (*Heraeus*)

Cryostat

LeicaCM1860 (*Leica Biosystems*)

Cuvettes

Quartz cuvettes (*Helma Analytics*)

Block thermostats

Mixingblock MB 102 (*BIOER*)

Thermomixer Comfort (*Eppendorf*)

Digital 2 Block Heater 120 (*VWR*)

Fluorescence spectroscopy

Fluorescence spectrometer (*Photon Technology International*)

Software: FeliX32

FPLC

Äkta start (*GE Healthcare*)

software: UNICORN start 1.0

AZURA Bio Lab (*KNAUER*)

software: PurityChrom® Bio 5

FPLC columns

HiLoad 26/60 Superdex 75 (*GE Healthcare*)

HiLoad 26/60 Superdex 200 (*GE Healthcare*)

HiPrep Butyl FF 16/10 (*Cytiva*)

HiTrap Q HP 5 mL (*Cytiva*)

Mono Q 5/50 GL (*Cytiva*)

RESOURCE Q (*GE Healthcare*)

Gel electrophoresis

Mini-Protean 3 (*Bio-Rad*)

HPLC

Primaide (*VWR Hitachi*)

software: Primaide

LaChrom Elite (*VWR Hitachi*)

software: EZChrom Elite

HPLC columns

BioSep-SEC-S2000 (*Phenomenex*)

LiChrospher® 100 RP-18 (5 µm) LiChroCART®
250-4 (*Merck*)

Imager

AlphaImager (*AlphaInnotech/Biozym*)

ECL ChemoCam Imager (*INTAS*)

Incubators

Incubator (*Memmert*)

Rotating incubator: Rotator SB3 (*Stuart*)

Shaking incubator: Multitron (*Infors HT*)

Cell culture: HERA cell 150 (*Heraeus Instruments*)

Lyophilizer

Alpha 1-2 LDplus (*Christ*)

Magnetic stirrer

MR3001 (*Heidolph*)

Microscope

Leica TCS SP2 (*Leica Microsystems*)

software: Leica Confocal Software

pH-meter

InoLab 720 (*WTW*)

Elektrode: Sentix 41 (*WTW*)

Photometer

FoodALYT (*Omnilab*)

Scales

Acculab ALC-210.4 (*Sartorius*)

ENTRIS323-1S (*Sartorius Lab Instruments*)

Sonification bath

Sonorex RK-100 (*BANDELIN electronic*)

Sonorex Digiplus DL 102 H (*BANDELIN electronic*)

Ultrasonic homogenizer

transducer: UW 2200 (*BANDELIN electronic*)

generator: HD 2200 (*BANDELIN electronic*)

Vacuum concentrator

Concentrator 5301 (*Eppendorf*)

Vacuum pump

PIZ 100 (*Saskia Hochvakuum*)

Diaphragm Vacuum Pump MZ 2C (*VACUUBRAND*)

Voltage source

E835 (*Consort*)

Vortex mixer

Vortex Genie 2 (*Scientific Industries*)

Water bath

WNB14 (*Memmert*)

Western blot

Mini-Protean Tetra System (*Bio-Rad*)

2.1.2 Chemicals

All chemicals used had a quality of at least analytical grade. Unless otherwise stated, the chemicals were purchased from *Carl Roth, Fluka, Merck, ONMI Life Science, SERVA, Sigma-Aldrich, VWR*, or the chemical storage of the *University of Oldenburg*. All solutions were prepared with double distilled water produced of fully desalted water of the *University of Oldenburg*. Buffers and solvents used for HPLC analytic had at least a quality of HPLC grade and were degassed prior to use.

(NH ₄) ₂ SO ₄ , ammonium sulfate	GTP, guanosine 5'-triphosphate
2-mercaptoethanol	guanidine hydrochloride
2-propanol	HCl, hydrochloric acid (37 %)
acetic acid	HEPES, <i>N</i> -2-Hydroxyethylpiperazine- <i>N'</i> -2-ethane sulphonic acid
ammonium persulfate	
ATP, adenosine 5'-triphosphate	IPTG, Isopropyl β-d-1-thiogalactopyranoside
bromophenol blue	K ₂ HPO ₄ , dipotassium hydrogen phosphate
CaCl ₂ , calcium chloride	KCl, potassium chloride
Coomassie Brilliant Blue R-250	KH ₂ PO ₄ , potassium dihydrogen phosphate
dithioerythritol	KOH, potassium hydroxide
DTNB, Ellmann's Reagent, 5,5'-dithio- <i>bis</i> -(2-nitrobenzoic acid)	L-cysteine
DTT, dithiothreitol	Mes, 2-(<i>N</i> -Morpholino)-ethane sulphonic acid
EDTA, ethylenediaminetetraacetic acid	methanol
EGTA, ethylene glycol- <i>bis</i> (β-aminoethyl ether)- <i>N,N,N',N'</i> -tetraacetic acid	methanol HPLC grade
ethanol	MgCl ₂ , magnesium chloride
ethanol (denatured with toluene)	Mops, 3-(<i>N</i> -Morpholino)propane sulfonic acid
FeSO ₄ , iron(II) sulfate	MS-222
fura-2 (<i>Invitrogen</i>)	myristic acid
glycerol	NaCl, sodium chloride
glycine	NH ₄ HCO ₃ , ammonium hydrogen carbonate
	nitrogen, liquid
	OGP, octyl β-D-glucoopyranoside

PBS, phosphate buffered saline (<i>Gibco</i>)	TEMED, N,N,N',N'-tetramethylethylenediamine
PFA, paraformaldehyde	TFA, trifluoroacetic acid
PMSF, phenylmethylsulfonyl fluoride	Tris, tris(hydroxymethyl)aminomethane
SDS, sodium dodecyl sulfate pellets	Triton X-100
sodium orthovanadate	Tween-20
sucrose	Zaprinast

2.1.3 Consumables, media, sera, enzymes, antibiotics

ampicillin	<i>Carl Roth</i>
Bradford reagent: Protein Assay Dye Reagent Concentrate	<i>Bio-Rad</i>
BSA, bovine serum albumin	<i>Sigma-Aldrich</i>
cell scraper	<i>TPP</i>
ChemiBLOCKER	<i>Sigma-Aldrich</i>
cOmplete, Mini, EDTA-free Protease Inhibitor Cocktail	<i>Roche</i>
cryomatrix: Tissue Tek O.C.T. compound	<i>Sakura Finete Europe</i>
disposable needles: Sterican® 0.9 × 70 mm, 20 G × 2 ¾''	<i>B. Braun</i>
DMEM, Dulbecco's Modified Eagle Medium, high glucose, GlutaMAX™ Supplement	<i>Gibco</i>
DNase	<i>AppliChem</i>
FBS, fetal bovine serum	<i>Gibco</i>
kanamycin	<i>Carl Roth</i>
L-15 medium	<i>Sigma-Aldrich</i>
LB agar (Lennox)	<i>Carl Roth</i>
LB medium: LB broth (Lennox)	<i>Carl Roth</i>
Lysozyme	<i>Sigma-Aldrich</i>
Macrosep® Advance Centrifugal Devices, 20 mL, 10K	<i>PALL Corporation</i>
mammalian protease inhibitor cocktail	<i>Sigma-Aldrich</i>
NDS, normal donkey serum	<i>Santa Cruz Biotechnology</i>

Poly/Mount	<i>Polysciences</i>
powdered milk	<i>Carl Roth</i>
Precision Plus Protein™ Unstained Protein Standard	<i>Bio-Rad</i>
ROTIPHORESE®Gel 40 (37.5:1)	<i>Carl Roth</i>
tissue culture dishes, 10 cm	<i>TPP</i>
transfer membrane ROTI®NC	<i>Carl Roth</i>
transfer membrane ROTI®PVDF	<i>Carl Roth</i>
Trypsin/EDTA	<i>Gibco</i>
VectaShield	<i>Vector Laboratories</i>
VISKING dialysis tubing (MWCO 12,000-14,000)	<i>SERVA</i>
WesternBright ECL	<i>Advanta</i>
WesternBright Peroxide	<i>Advanta</i>
Whatman®-blotting paper, 3MM	<i>Carl Roth</i>
dialysis capsule: Slide-A-Lyzer™ MINI Dialysis Devices, 3.5 K MWCO, 0.1 mL	<i>Thermo Fisher Scientific</i>

2.1.4 Antibodies

Table 1: Antibodies used for immunohistochemistry or immunodetecting after western blotting.

Specifications of primary and secondary antibodies used for immunohistochemistry (histo) or immunodetection after western blotting (w. b.) with recommended dilutions are listed.

	antibody	immunogen	host, type	dilution histo	dilution w. b.	source
primary	anti-GCAP5	zebrafish GCAP5	rabbit, polyclonal	1:2000	1:250	<i>Pineda, Fries 2013</i>
	zpr1	zebrafish arrestin 3a	mouse, monoclonal	1:1000	-	<i>ZIRC</i>
secondary	anti-rabbit POD	rabbit IgG	goat, polyclonal	-	1:5000	<i>Jackson Dianova</i>
	anti-rabbit Alexa Fluor®488	rabbit IgG	donkey, polyclonal	1:1000	-	<i>Invitrogen</i>
	F(ab') ₂ anti-rabbit Alexa Fluor®488	rabbit IgG	donkey, polyclonal	1:1000	-	<i>Jackson ImmunoResearch</i>
	anti-mouse Alexa Fluor®568	mouse IgG	donkey, polyclonal	1:1000	-	<i>Invitrogen</i>

2.1.5 Bacterial strain

***E. coli* BL21 CodonPlus (DE3)-RP:** *E. coli* B F⁻ *ompT hsdS*(r_Bm_B⁻) *dcm*⁺ *Tet*^r *gal* λ(DE3) *endA endA* Hte [*argU proL* Cam^r]

2.1.6 Vectors and plasmids

pET21a(+) (*Novagen*): expression of GCAP5 in *E. coli*

pBB131: co-expression of yeast NMT in *E. coli* (Duronio et al. 1990), kindly provided by Prof. Dr. J. I. Gordon (Center for Genome Sciences & Systems Biology, *Washington University*)

pIRES2-EGFP (*Clontech*): expression of human GC-E in HEK293 cells

2.1.7 Mammalian cell line

HEK293 cell line stably expressing human GC-E: HEK293 cell line (Flp-InTM-293 Cell Line, *Invitrogen*), kindly provided by Prof. Dr. H. G. Nothwang (Division of Neurogenetics, *University of Oldenburg*); stable expression of human GC-E generated and described by Wimberg et al. (2018)

2.2 Heterologous expression and purification of GCAPs

All GCAP variants were expressed heterologously in *E. coli* and purified by chromatography. The purification protocol for GCAP5 had to be optimized. Therefore, two protocols of the Division of Biochemistry (*University of Oldenburg*) and of the Department of Chemistry (*UC Davis*) and some variations were tested (Table 2, Table 3).

Table 2: Purification protocols for GCAP5 of the Division of Biochemistry (*University of Oldenburg*) and variations.

Numbers are the sections in this thesis. Underlined parts indicate variations in comparison to protocol 1a.

protocol 1a (Division of Biochemistry)	protocol 1b	protocol 1c
2.2.1 (Inoculation of an overnight culture)	2.2.1 (Inoculation of an overnight culture)	2.2.1 (Inoculation of an overnight culture)
2.2.2 (Expression in <i>E. coli</i>)	2.2.2 (Expression in <i>E. coli</i>)	2.2.2 (Expression in <i>E. coli</i>)
2.2.3, 2.2.3.1 (Cell lysis with lysozyme, ultracentrifugation, denaturation)	2.2.3, 2.2.3.1 (Cell lysis with lysozyme, ultracentrifugation, denaturation)	2.2.3, 2.2.3.1 (Cell lysis with lysozyme, ultracentrifugation, denaturation)
2.2.4 (Dialysis and ultracentrifugation)	2.2.4 (Dialysis and ultracentrifugation)	2.2.4 (Dialysis and ultracentrifugation)
2.2.5.1 (Ammonium sulfate precipitation)	2.2.5.1 (Ammonium sulfate precipitation)	2.2.5.1 (Ammonium sulfate precipitation)
2.2.6.1 (SEC) with HiLoad 26/60 Superdex 75	2.2.6.1 (SEC) with HiLoad 26/60 Superdex 75	2.2.6.1 (SEC) with HiLoad 26/60 Superdex 75
2.2.6.2 (AEC) with column RESOURCE Q (<i>GE Healthcare</i>)	2.2.6.2 (AEC) with <u>Mono Q 5/50 GL</u> (<i>Cytiva</i>)	2.2.6.2 (AEC) with <u>Hi Trap Q HP</u> (<i>Cytiva</i>)
2.2.7 (Buffer exchange and lyophilization)	2.2.7 (Buffer exchange and lyophilization)	2.2.7 (Buffer exchange and lyophilization)

Table 3: Purification protocols for GCAP5 of the Department of Chemistry (*UC Davis*) and variation.

Numbers are the sections in this thesis. Underlined parts indicate variations in comparison to protocol 2a.

protocol 2a (Department of Chemistry)	protocol 2b
2.2.1 (Inoculation of an overnight culture)	2.2.1 (Inoculation of an overnight culture)
2.2.2 (Expression in <i>E. coli</i>)	2.2.2 (Expression in <i>E. coli</i>)
2.2.3, 2.2.3.2 (Cell lysis by ultrasonication, ultracentrifugation)	2.2.3, 2.2.3.2 (Cell lysis by ultrasonication, ultracentrifugation, <u>denaturation</u>)
2.2.6.3 (HIC)	<u>2.2.4 (Dialysis and ultracentrifugation)</u>
2.2.6.2 (AEC)	2.2.6.3 (HIC) with combined supernatants from 2.2.3, and 2.2.4
2.2.5.2 (Concentrating with a spin concentrator)	2.2.6.2 (AEC)
2.2.6.1 (SEC) with HiLoad 26/60 Superdex 200	2.2.5.2 (Concentrating with a spin concentrator)
2.2.7 (Buffer exchange and lyophilization)	2.2.6.1 (SEC) with HiLoad 26/60 Superdex 200
	2.2.7 (Buffer exchange and lyophilization)

2.2.1 Retransformation, preparation of glycerol stocks, inoculation of overnight cultures

The DNA of GCAP5 variants was cloned by Dr. Alexander Scholten (Division of Biochemistry, *University of Oldenburg*). To express the DNA in *E. coli* cells, it was retransformed into BL21-CodonPlus cells or into BL21-CodonPlus cells containing the plasmid pBB131 for non-myristoylated or for myristoylated GCAP5, respectively. The plasmid pBB131 contains the gene for the *N*-myristoyltransferase (NMT). This enables the *E. coli* cells to myristoylate the co-expressed GCAPs.

One μL of the GCAP5 DNA was added to 50 μL of competent *E. coli* cells and incubated (10 min, ice-cold). Afterwards, the bacterial cells were heat shocked (1 min, 42 °C) and incubated (10 min, ice-cold). Two hundred μL of LB medium were added to the bacterial cells, incubated (20 min, 37 °C), and afterwards applied on a LB agar dish supplied with ampicillin (end concentration 100 $\mu\text{g}/\text{mL}$) for non-myristoylated variants. For myristoylated variants, kanamycin (end concentration 30 $\mu\text{g}/\text{mL}$) was added as well. The dish was incubated (overnight, 37 °C). The next day, some colonies of the dish were picked and transferred to 5 mL of LB medium supplied with the respective antibiotics. The 5 mL culture was incubated (overnight, 37 °C, in a rotating incubator). The culture was used to prepare glycerol stocks (50 % culture, 50 % glycerol).

For inoculating an overnight culture, 5 μL of a glycerol stock were added to 5 mL of LB medium supplied with the respective antibiotics and incubated (overnight, 37 °C, in a rotating incubator). The overnight culture was now ready for inoculating a 500 mL culture for expression (see section 2.2.2).

2.2.2 Expression in *E. coli*

For non-myristoylated GCAP5 variants, 500 mL of LB medium supplied with ampicillin (end concentration 100 $\mu\text{g}/\text{mL}$) were inoculated with a 5 mL overnight culture (see section 2.2.1) and incubated (37 °C, in a shaking incubator). After the 500 mL culture reached an OD_{600} of approximately 0.6, expression was induced by adding IPTG (end concentration 1 mM). For expression, the culture was incubated (4 h, 37 °C, 180 rpm, in a shaking incubator). Afterwards, the culture was centrifuged (10 min, 5 000 $\times g$, 4 °C). The pellet was resuspended in 10 mL of 50 mM Tris/HCl pH 8.0 or of *E. coli* resuspension buffer (see section 2.2.3.2), depending on the cell lysis protocol, and then stored at -80 °C.

For myristoylated GCAP5 variants, the 500 mL of LB medium were supplied with kanamycin (end concentration 30 $\mu\text{g}/\text{mL}$) additionally, and after reaching an OD_{600} of approximately 0.4, myristic acid (end concentration 50 $\mu\text{g}/\text{mL}$) was added to the culture.

2.2.3 Cell lysis, ultracentrifugation, denaturation

After the cells were harvested (see section 2.2.2), they had to be lysed prior to purification of the GCAP. The cell lysis was performed either with lysozyme or by ultrasonication. If GCAP5 was to be purified from the cytosolic fraction (purification protocol 2a, Table 3), I proceeded with the supernatant after ultracentrifugation for the hydrophobic interaction chromatography (see section 2.2.6.3). If I had to purify GCAP5 from inclusion bodies, the pellet after ultracentrifugation was resuspended in 6 M guanidine hydrochloride for denaturation and incubated (overnight, 4 °C), and the next step was the renaturation by dialysis (see section 2.2.4).

2.2.3.1 Lysozyme

The cell suspension (see section 2.2.2) was filled up to 20 mL with 50 mM Tris/HCl pH 8.0 and supplied with lysozyme (end concentration 100 µg/mL) and DNase (end concentration 5 U/mL). After the lysis (30 min, 30 °C, in a water bath), DTT (end concentration 1 mM) and PMSF (end concentration 0.1 mM) were added, and the suspension was ultracentrifuged (30 min, 35 000 rpm, Beckmann Type 70 Ti rotor, 4 °C).

2.2.3.2 Ultrasonication

The cell suspension (see section 2.2.2) was filled up to 20 mL with *E. coli* resuspension buffer, supplied with DTT (end concentration 1 mM) and PMSF (end concentration 0.1 mM), and ultrasonicated (50 % cycle, 30 % power; 30 sec pulse and 30 sec pause, 8 times). Afterwards, the suspension was ultracentrifuged (30 min, 35 000 rpm, Beckmann Type 70 Ti rotor, 4 °C).

E. coli resuspension buffer:

20 mM Tris/HCl pH 7.5

0.1 M KCl

1 mM EGTA

10 % (v/v) glycerol

2.2.4 Dialysis and ultracentrifugation

If I purified GCAP5 from inclusion bodies, the denatured GCAP5 was renatured by dialysis. The suspension after denaturation (see section 2.2.3) was transferred to a dialysis tube (MWCO: 12 000 - 14 000 Da), and the dialysis tube was incubated in 3 L of dialysis buffer (5 h, 4 °C, slowly stirring). After exchanging the dialysis buffer, the dialysis tube was incubated again (overnight, 4 °C, slowly stirring). The next day, the suspension out of the dialysis tube was ultracentrifuged (30 min, 35 000 rpm, Beckmann Type 70 Ti rotor, 4 °C), and the supernatant was saved for purification of GCAP5.

Dialysis buffer:

20 mM Tris/HCl pH 7.5

150 mM NaCl

1 mM DTT

2.2.5 Concentrating of protein

Depending on the purification protocol, either the supernatant after ultracentrifugation (see section 2.2.4) was precipitated with ammonium sulfate, or the eluate after anion exchange chromatography (AEC) (see section 2.2.6.2) was concentrated in a spin concentrator in order to achieve a smaller volume appropriate to be loaded onto a size exclusion chromatography (SEC) column (see section 2.2.6.1).

2.2.5.1 Ammonium sulfate precipitation

According to the purification protocol of the Division of Biochemistry (*University of Oldenburg*), the ammonium sulfate precipitation was used for concentrating the renatured proteins after dialysis (see section 2.2.4). The precipitation was performed in two steps. First, the ammonium sulfate concentration was increased from 0 to 30 % (w/v), followed by the second step from 30 % to 80 % (w/v) ammonium sulfate.

The required amount of ammonium sulfate (determined with Equation 1) was stirred into the ice-cold protein solution in small portions, incubated (20 min, ice-cold, stirring slowly), and then centrifuged (20 min, 20 000 rpm, Beckmann rotor JA25.5, 4 °C). After the first step to 30 % (w/v) ammonium sulfate, the supernatant after centrifugation was used for the second step to 80 % (w/v) ammonium sulfate. After the second step, the pellet after centrifugation was resuspended in 2 mL of SEC buffer (see section 2.2.6.1).

$$m = \frac{1.77 \cdot (x - x_0)}{3.54 - x} \cdot V$$

Equation 1: Calculation of the required mass of ammonium sulfate for a certain percentage of saturation.

m is the required mass of ammonium sulfate in g, x and x_0 are the wanted and the initial relative concentration of ammonium sulfate, respectively, and V is the initial volume of the renatured fraction.

2.2.5.2 Spin concentrator

According to the purification protocol of the Department of Chemistry (*UC Davis*), the spin concentrator was used to concentrate the AEC fractions (see section 2.2.6.2) that needed to be purified further by SEC (see section 2.2.6.1). The AEC fractions containing the GCAP were pooled in a spin concentrator (20 mL, 10k, *PALL Life Sciences*) and concentrated by centrifugation to a volume around 2 mL (4 000 xg, 12 °C).

2.2.6 Fast-performance liquid chromatography (FPLC)

In our lab, we use the ÄKTA start (*GE Healthcare*) or the AZURA lab Bio LC (*KNAUER*) fast-performance liquid chromatography (FPLC) system. Most of the FPLC columns following were used with the ÄKTA start. The AEC column Mono Q 5/50 GL (*Cytiva*) was used with the AZURA lab Bio LC due to the high pressure on the column during chromatography.

2.2.6.1 Size exclusion chromatography (SEC)

To separate proteins by their sizes, a SEC was performed. The SEC column was equilibrated with at least two column volumes of SEC buffer. The resuspended pellet after the ammonium sulfate precipitation (see section 2.2.5.1) or the concentrated AEC fractions (see section 2.2.5.2) were ultracentrifuged (15 min, 100 000 xg, 4 °C), and the supernatant was loaded onto the column (flow rate: 1 mL/min, fraction size: 10 mL). The eluted fractions were frozen in liquid nitrogen and stored at -80 °C. The presence of GCAP5 in the SEC fractions was checked by SDS-PAGE (see section 2.5.1). GCAP5 containing fractions were either purified further by AEC (Koch lab purification protocol 1a-c, Table 2; see section 2.2.6.2) or prepared for lyophilization (purification protocol 2a and 2b, Table 3; see section 2.2.7).

The SEC buffer of the Division of Biochemistry (*University of Oldenburg*) was used for the SEC column HiLoad 26/60 Superdex 75 (*GE Healthcare*), the SEC buffer of the Department of Chemistry (*UC Davis*) for the SEC column HiLoad 26/60 Superdex 200 (*GE Healthcare*).

SEC buffer (Division of Biochemistry):

20 mM Tris/HCl pH 7.5
150 mM NaCl
2 mM CaCl₂
1 mM DTT

SEC buffer (Department of Chemistry):

20 mM Tris/HCl pH 7.5
100 mM NaCl
1 mM DTT

2.2.6.2 Anion exchange chromatography (AEC)

Proteins can be separated by their charge with ion exchange chromatography methods. I used an AEC for GCAP5. For the purification according to protocol 2a and 2b (Table 3), I used the RESOURCE Q column (*GE Healthcare*) and the AEC buffers A and B (Department of Chemistry). With purification protocol 1a-c (Table 2), I also tested the Mono Q 5/50 GL column (*Cytiva*) and the HiTrap Q HP 5 mL column (*Cytiva*) with the AEC buffers A and B (Division of Biochemistry).

The column was equilibrated with AEC buffer A. If I followed the Department of Chemistry protocol (Table 3), the ionic strength of the GCAP5 containing HIC fractions (see section 2.2.6.3) was lowered by diluting the fractions fivefold with double distilled water (H₂O). If I followed the Division of Biochemistry protocol (Table 2), the GCAP5 containing SEC fractions (see section 2.2.6.1) were supplied with EDTA (end

concentration 4 mM). The prepared sample solution was loaded onto the equilibrated AEC column. The unbound was washed out of the column with five column volumes (CV) of AEC buffer A. Afterwards, the proteins were eluted with a linear gradient from 0 % to 100 % AEC Buffer B within 20 CV. The flow rate and the fraction size depended on the column used (Table 4). The eluted fractions were frozen in liquid nitrogen and stored at -80 °C. The presence of GCAP5 in the AEC fractions was checked by SDS-PAGE (see section 2.5.1). GCAP5 containing fractions were either purified further by SEC (purification protocol 2a and 2b, Table 3; see section 2.2.6.1) or prepared for lyophilization (purification protocol 1a-c, Table 2; see section 2.2.7).

Table 4: AEC columns with flow rates and fraction sizes.

AEC column	flow rate (mL/min)	fraction size (mL)
RESOURCE Q (<i>GE Healthcare</i>)	2	6
Mono Q 5/50 GL (<i>Cytiva</i>)	0.75	2
HiTrap Q HP 5 mL (<i>Cytiva</i>)	2	5

AEC buffer A (Division of biochemistry):

20 mM Tris/HCl pH 7.5
2 mM EGTA
1 mM DTT

AEC buffer B (Division of biochemistry):

20 mM Tris/HCl pH 7.5
1 M NaCl
2 mM EGTA
1 mM DTT

AEC buffer A (Department of Chemistry):

20 mM Tris/HCl pH 7.5
1 mM DTT

AEC buffer B (Department of Chemistry):

20 mM Tris/HCl pH 7.5
0.5 M NaCl
1 mM DTT

2.2.6.3 Hydrophobic interaction chromatography (HIC)

With the HIC, proteins can be separated by their hydrophobicity. In this case, the salting-out effect of $(\text{NH}_4)_2\text{SO}_4$ and the HIC column HiPrep Butyl FF 16/10 (*Cytiva*) were used. The column was equilibrated with HIC buffer A (flow rate 2 mL/min). The supernatant after the ultrasonication (see section 2.2.3.2) was supplied with $(\text{NH}_4)_2\text{SO}_4$ (end concentration 0.35 M) and then loaded onto the equilibrated HIC column. Afterwards, the column was washed with 5 CV of buffer A. The protein was eluted with 100 % buffer B (fraction size 5 mL/min). The eluted fractions were frozen in liquid nitrogen and stored at -80 °C. The presence of GCAP5 in the HIC fractions was checked by SDS-PAGE (see section 2.5.1). GCAP5 containing fractions were purified further by AEC (purification protocol 2a and 2b, Table 3; see section 2.2.6.2).

HIC buffer A:

20 mM Tris/HCl pH 7.5

0.35 M $(\text{NH}_4)_2\text{SO}_4$

1 mM DTT

HIC buffer B:

20 mM Tris/HCl pH 7.5

2 mM EGTA

1 mM DTT

2.2.7 Buffer exchange and lyophilization

If the purity of the protein of interest was sufficient after chromatography (see section 2.2.6), the corresponding fractions were pooled in a spin concentrator (20 mL, 10k, *PALL Life Sciences*). Afterwards, the buffer was exchanged six times by 5 mM NH_4HCO_3 and concentrated to around 500 μL . The protein concentration of the solution was determined by a Bradford Assay (see section 2.4.2). After dividing the protein solution to 100 μg , 200 μg , or 500 μg aliquots, the protein was lyophilized. The lyophilized protein was stored at $-80\text{ }^\circ\text{C}$ until use.

2.3 Purification of reduced protein

To purify reduced GCAP5, the protein was expressed in *E. coli* and purified from inclusion bodies after purification protocol 1c (Table 2) with the following modifications. The AEC (see section 2.2.6.2) was performed in the presence of 5 mM DTT. Prior to buffer exchange (see section 2.2.7), the NH_4HCO_3 solution was degassed. The lyophilization took place directly after the buffer exchange.

2.4 Determination of protein concentration

The protein concentration in a solution was determined either by a Bradford Assay (see section 2.4.2) or by measuring the UV-absorbance of purified proteins at 280 nm (see section 2.4.1). The latter was only used for protein solutions that contained one pure soluble protein. For suspensions of insoluble proteins, a modified Bradford Assay with octyl β -D-glucopyranoside (OGP) was used (see section 2.4.2.1).

2.4.1 UV-absorbance at 280 nm

The protein concentration of solutions with purified protein can be determined by measuring the extinction at 280 nm. The solution in which the protein is dissolved served as a blank. The molar protein concentration can be calculated with the Lambert-Beer law (Equation 2). With the given molar concentration of the protein, the mass of the protein in the sample solution can be calculated (Equation 3, Table 5).

$$\Delta E_{280} = \varepsilon_{280} \cdot c \cdot d$$

Equation 2: Lambert-Beer law.

ΔE_{280} is the extinction of the sample solution at 280 nm subtracted by the extinction of the blank. ε_{280} is the molar extinction coefficient of the protein of interest at 280 nm in $\text{L} \cdot \text{mol}^{-1} \cdot \text{cm}^{-1}$ (Table 5). c is the molar concentration of the protein of interest in the sample solution in $\text{mol} \cdot \text{L}^{-1}$. d is the optical path of the cuvette in cm.

$$m = c \cdot V \cdot M$$

Equation 3: Calculation of the mass of a protein in a solution.

m is the mass, in this case of the protein in g. c is the molar concentration of the protein of interest in the sample solution in $\text{mol} \cdot \text{L}^{-1}$. V is the volume of the sample solution in L. M is the molar mass of the protein of interest in $\text{g} \cdot \text{mol}^{-1}$ (Table 5).

Table 5: Molar extinction coefficients and molar masses of GCAP3 and GCAP5.

The experimentally determined molar extinction coefficients (ε_{280}) and the molar masses (M) of myristoylated (myr) bovine GCAP1, myr zebrafish GCAP3, and non-myristoylated (non-myr) and myr zebrafish GCAP5 are listed (Division of Biochemistry, *University of Oldenburg*).

	ε_{280} in $\text{L} \cdot \text{mol}^{-1} \cdot \text{cm}^{-1}$	M in Da
myr bovine GCAP3	27 580	23 510
myr zebrafish GCAP3	23 500	21 850
non-myr zebrafish GCAP5	21 990	22 420
myr zebrafish GCAP5	21 990	22 420

2.4.2 Bradford Assay

To determine the protein concentration in a solution according to Bradford (Bradford 1976, Compton and Jones 1985), the sample solution was diluted tenfold in double distilled H_2O . Ten μL of the diluted sample solution were filled up to 800 μL with double distilled H_2O and then mixed with 200 μL of Protein Assay Dye Reagent Concentrate (Bio-Rad). As a blank, 800 μL of double distilled H_2O were treated analogically. Exactly 15 min after adding the Protein Assay Dye Reagent Concentrate, the absorbance at 595 nm was measured. With the measured absorbance, the mass concentration of the protein could be calculated using the BSA calibration line in our lab (Equation 4). If the sample solution contains only one purified protein, the molar concentration can be calculated using the mass concentration (Equation 3, Table 5).

$$\beta = \frac{10 \mu\text{g}}{0.535} \cdot \Delta E_{595 \text{ nm}} \cdot \frac{10}{10 \mu\text{L}}$$

Equation 4: Calculation of the mass concentration of the protein with the BSA calibration line.

β is the mass concentration of proteins in the sample solution in $\mu\text{g} \cdot \mu\text{L}^{-1}$. The quotient is given by the BSA calibration line. Ten μg of BSA correspond to an extinction of 0.535. ΔE_{595} is the extinction of the sample solution at 595 nm subtracted by the extinction of the blank. The dilution of the sample solution (1:10) and the used volume of the diluted sample solution (10 μL) are included in the equation.

2.4.2.1 Modified Bradford Assay with OGP

The protein concentration in a suspension can be determined according to Bradford as well, if the suspension is treated with octyl β -D-glucopyranoside (OGP) first (Fanger 1987). Therefore, 5 μ L of the sample suspension diluted ten-fold were mixed with OGP (end concentration 10 % (w/v)) and incubated (10 min, RT). The mixture was filled up to 800 μ L with double distilled H₂O. Afterwards, the protein concentration was determined as explained in section 2.4.2. As a blank, 5 μ L of double distilled H₂O were treated analogically.

2.5 Specific proof of proteins

To proof the presence of specific proteins in my *in-vitro* samples, I used either the sodium dodecyl sulfate-polyacrylamide gel electrophoresis (SDS-PAGE) or the western blot with subsequent immunoassay and enhanced chemiluminescence (ECL) technique. The SDS-PAGE was primarily used to monitor the progress in protein purification.

2.5.1 SDS-PAGE

A discontinuous SDS-PAGE according to Laemmli with modifications was performed (Laemmli 1970). For pouring SDS-polyacrylamide gels (SDS-gels), the gel chamber Mini-Protean 3 (*Bio-Rad*) was assembled according to manufacturer instructions. Subsequently, a 15 % separating gel and a 5 % stacking gel were poured (pipetting scheme see Table A2), and a comb was used for pocket formation.

The samples were filled up to equal volumes with the buffer in which they were dissolved. After adding 4x SDS-sample buffer, the samples were incubated (5 min, 95 °C). The gel running chamber with the SDS-gels was filled with running buffer, and the samples were pipetted into the pockets in the stacking gel. For analysis, the Precision Plus Protein™ Unstained Protein Standard (*Bio-Rad*) was pipetted in a separate pocket. Afterwards, the electrophoresis was started (40 min, 200 V (const.), 15 W). The voltage source E835 (*Consort*) was used.

After the electrophoresis, the gel was detached from the glass plates, shortly rinsed with water, and then fixed in gel destaining solution (5 min, RT, on a shaking incubator). The fixed gel was stained in gel staining solution (overnight, RT, on a shaking incubator). The next day, the gel was destained in gel destaining solution (30 min, RT, on a shaking incubator, three times), then placed in water for letting it increase in size, and finally analyzed with the Alphamager (*AlphaInnotech/Biozym*).

4x SDS-sample buffer:

125 mM Tris/HCl pH 6.8
50 % (v/v) glycerol
4 % (w/v) SDS
0.025 % bromophenol blue
10 % (v/v) 2-mercaptoethanol

gel running buffer:

25 mM Tris
192 mM glycine
1 % (w/v) SDS

gel staining solution:

0.25 % (w/v) Coomassie Brilliant Blue R-250
10 % (v/v) acetic acid
40 % (v/v) ethanol (denatured with toluene)

gel destaining solution:

10 % (v/v) acetic acid
40 % (v/v) ethanol (denatured with toluene)

2.5.2 Western blot (“blue method”)

Zebrafish GCAPs are relatively hydrophobic and acidic. Therefore, our standard western blotting does not work for GCAP5, since it does not adhere to the blot membrane. To overcome this problem, Werner Säftel (Division of Biochemistry, *University of Oldenburg*) developed the “blue method” on the basis of a protocol used by Thompson and Larson (1992) (Fries et al. 2012; Fries et al. 2013).

For the blue method, both the separating gel and the stacking gel (see section 2.5.1) contain 1 mM CaCl₂. After the electrophoresis, the gel was fixed in fixing solution (5 min, RT, on a shaking incubator) and then stained in blue method staining solution (2 h, RT, on a shaking incubator). The destaining procedure in 10 % acetic acid followed in several steps (3x 20 min, then overnight, RT, on a shaking incubator). The next day, the gel was rinsed in double distilled H₂O and then incubated in detergent solution (1 h, RT, on a shaking incubator).

Based on McKeon and Lyman (1991), the gel was equilibrated in Towbin buffer with 0.5 mM CaCl₂ (1x 1 min, 3x 10 min, 4 °C, on a shaking incubator). Two Whatman®-blotting papers (*Carl Roth*) and the transfer membrane (ROTI®NC or ROTI®PVDF, both *Carl Roth*) were equilibrated as well (30 min, 4 °C). If a ROTI®PVDF-membrane was used, it was activated in Methanol prior to equilibration in Towbin buffer (1 min, RT, on a shaking incubator). The tank blot (Mini Protean Tetra System, *Bio-Rad*) was assembled according to manufacturer instructions, and the transfer was started (100 V (const.), 15 W, 45 min). After a successful transfer, I continued with the immunoassay (see section 2.5.3).

fixing solution:

25 % (v/v) 2-propanol
10 % (v/v) acetic acid

blue method staining solution:

0.25 % (w/v) Coomassie Brilliant Blue R-250
25 % (v/v) 2-propanol
10 % (v/v) acetic acid

detergent solution:

50 mM Tris/HCl pH 7.4

1 % (w/v) SDS

Towbin buffer with CaCl₂:

25 mM Tris

192 mM glycine

20 % (v/v) methanol

0.5 mM CaCl₂

2.5.3 Immunoassay and antigen detection with ECL technique

After the western blot (see section 2.5.2), the membrane with the transferred proteins was washed in TBS (5 min, RT, on a shaking incubator) and then blocked in blocking solution (30 min, RT, on a shaking incubator). The blocked membrane was incubated with the primary antibody rabbit anti-GCAP5 diluted between 1:250 and 1:5000 in blocking solution (1 h, RT, on a shaking incubator). Afterwards, the membrane was washed in TBST (3x 5 min, RT, on a shaking incubator) and then incubated with the peroxidase (POD) coupled secondary antibody goat anti-rabbit POD diluted 1:5000 in blocking solution (1 h, RT, on a shaking incubator). After the incubation, the membrane was washed in TBST (4x 5 min, RT, on a shaking incubator). For a last washing step, TBS was used (5 min, RT, on a shaking incubator).

The antigen detection was done using the ECL technique. The secondary antibody coupled POD can use luminol as a substrate. Under alkaline conditions and in the presence of hydrogen peroxide (H₂O₂), luminol is oxidized by the POD, resulting in chemiluminescence.

To detect GCAP5 on the membrane after the immunoassay, the WesternBright Peroxide solution and the WesternBright ECL solution (both *Advansta*) were mixed at a ratio of 1:1. The mixture was applied onto the membrane. The membrane with the WesternBright solutions was placed between two transparent sheets, and the chemiluminescence was detected by the ECL ChemoCam Imager (*INTAS*).

TBS:

20 mM Tris/HCl pH 7.4

154 mM NaCl

TBST:

20 mM Tris/HCl pH 7.4

154 mM NaCl

0.05 % (v/v) Tween-20

blocking solution:

TBS

2 % (w/v) BSA or powdered milk

2.6 Determination of the Cysteine accessibility with the Ellman's Reagent

Wildtype GCAP5 contains five (Figure A1), the C15A-C17A mutant three cysteines with unknown accessibility. The cysteine accessibility of a protein can be determined with Ellman's Reagent, 5,5'-dithio-bis-(2-nitrobenzoic acid) (DTNB) (Riddles et al. 1983; Ellman 1959). DTNB reacts with the thiol group of a cysteine to the yellow colored 2-nitro-5-thiobenzoic acid (TNB) and a mixed disulfide (Figure 12). By measuring the extinction of the reaction product TNB at 412 nm, the number of accessible cysteines of a protein can be estimated.

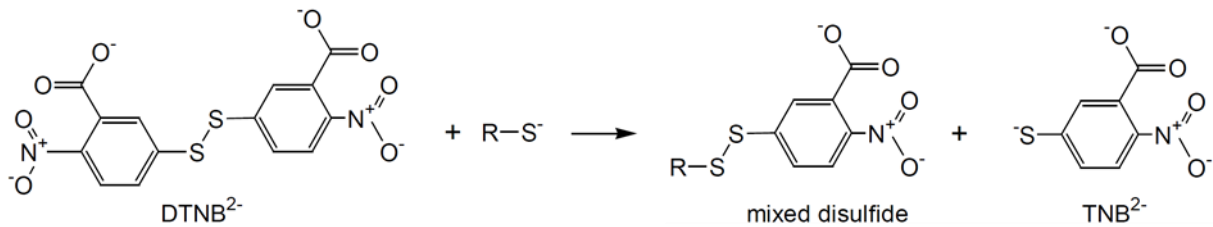


Figure 12: Color-forming reaction of Ellman's reagent with sulfhydryl groups.

Modified from: <https://www.thermofisher.com/order/catalog/product/22582#/22582> (access: 11.06.2020).

To determine the cysteine accessibility of GCAP5 variants, lyophilized GCAP was resuspended in PBS (Gibco) and sonicated (5 min, ice-cold, in an ultrasonic bath). The protein concentration was determined by a Bradford Assay (see section 2.4.2). Five μM GCAP with either 100 μM EGTA or 1 mM CaCl_2 were prepared in PBS. After adding DTNB (end concentration 60 μM), the sample was incubated (at least 10 min, RT). The extinction of the sample at 412 nm was measured in a 500 μL quartz glass cuvette. As negative control, zebrafish GCAP3, which contains no cysteines, was used. Double distilled H_2O served as a blank.

The number of accessible cysteines was determined by using a calibration line with L-cysteine. The DTNB solution was always prepared freshly, and a new calibration line was made for each DTNB solution. Therefore, a calibration spanning the range from 0 to 30 μM of L-cysteine was created by increasing the cysteine concentration in increments of 5 μM . The measuring procedure was the same as the one described for GCAP samples (s. above). The number of accessible cysteines was calculated with Equation 5.

$$cysteines_{accessible} = \frac{\Delta E_{412 \text{ nm}}}{\frac{slope_{calibration \ line}}{5 \mu\text{M}}}$$

Equation 5: Calculation of the number of accessible cysteines.

The number of accessible cysteines ($cysteines_{accessible}$) was calculated with the measured extinction at 412 nm ($\Delta E_{412 \text{ nm}}$), the slope of the calibration line for the respective DTNB solution ($slope_{calibration \ line}$), and the concentration of the GCAP solution (5 μM).

DTNB solution:

15 mM DTNB in 100 mM Tris/HCl pH 8.0

2.7 Tryptophan fluorescence spectroscopy

The fluorescence of tryptophan can change depending on its environment (Hellmann and Schneider 2019). The environment can be the solvent in which the protein is present but also surrounding amino acids in the protein. GCAPs are known to change their conformation in a calcium dependent manner, which can be monitored by tryptophan fluorescence spectroscopy (Peshenko and Dizhoor 2004), and GCAP5 contains two tryptophans, W20 and W93. Therefore, I tested the GCAP5 variants for calcium dependent conformational changes by tryptophan fluorescence spectroscopy. The $[\text{Ca}^{2+}]_{free}$ was adjusted with a Ca^{2+} -EGTA buffer system using $\text{K}_2\text{CaEGTA}^{2+}$ and $\text{K}_2\text{H}_2\text{EGTA}$ (Klabusay and Blinks 1996). Fluorescence spectra

were recorded with a fluorescence spectrometer (*Photon Technology International*) and the software FeliX32.

2.7.1 Determination of $[Ca^{2+}]_{free}$ with fura-2

To determine the exact $[Ca^{2+}]_{free}$ of my samples, I used the calcium indicator fura-2 (pentapotassium salt, *Invitrogen*). The $[Ca^{2+}]_{free}$ in a solution can be calculated with Equation 6 by measuring the excitation spectrum of fura-2.

$$[Ca^{2+}]_{free} = K_D \cdot Q \cdot \frac{R - R_{min}}{R_{max} - R}$$

Equation 6: Calculation of the $[Ca^{2+}]_{free}$ with the fura-2 excitation spectrum.

$[Ca^{2+}]_{free}$ is the free calcium concentration. The dissociation constant K_D of fura-2 and Ca^{2+} is 224 nM. Q is the quotient of the fluorescence intensities (F) F_{min} to F_{max} at 380 nm. *min* and *max* always refer to the minimum and the maximum $[Ca^{2+}]_{free}$, respectively. R is the F at 340 nm divided by the F at 380 nm. (www.thermofisher.com; accession date: 16.02.2020)

Samples were prepared with 1 μ M fura-2 and certain quantities of K_2H_2EGTA and $K_2CaEGTA$ (pipetting scheme see Table A8) filled up to 500 μ L with fluorescence buffer. The excitation spectrum from 300 nm to 450 nm was measured in a fluorescence quartz glass cuvette. The emission wavelength was 510 nm. With Equation 6, the $[Ca^{2+}]_{free}$ for specific compositions of the Ca^{2+} -EGTA buffers was determined (Figure A8, Table A8).

By solving the equation of the regression (Figure A8) for $\mu M_{[Ca^{2+}]_{free}}$, the $[Ca^{2+}]_{free}$ for the composition of the Ca^{2+} -EGTA buffer system in the samples used for the tryptophan fluorescence was calculated (Equation 7).

$$\mu L_{K_2CaEGTA} = \frac{-0.0141 + 20.3026 \cdot (\mu M_{[Ca^{2+}]_{free}})^{1.0043}}{0.1233^{1.0043} + (\mu M_{[Ca^{2+}]_{free}})^{1.0043}}$$

$$\Rightarrow \mu M_{[Ca^{2+}]_{free}} = \sqrt[1.0043]{\frac{\mu L_{K_2CaEGTA} \cdot 0.1233^{1.0043} + 0.0141}{20.3026 - \mu L_{K_2CaEGTA}}}$$

Equation 7: Calculation of the $[Ca^{2+}]_{free}$ for the tryptophan fluorescence with the Ca^{2+} -EGTA buffer system.

The free calcium-ion concentration ($[Ca^{2+}]_{free}$) in μ M can be calculated for any composition of the Ca^{2+} -EGTA buffer system within the range of more than 0 μ L to 20 μ L of $K_2CaEGTA$ filled up to 500 μ L with fluorescence buffer.

fluorescence buffer:

80 mM HEPES/KOH pH 7.5

40 mM KCl

1 mM DTT

2.7.2 Tryptophan fluorescence spectroscopy with GCAP5

Five hundred µg of lyophilized GCAP5 were suspended in 500 µL of fluorescence buffer and sonicated (5 min, ice-cold, in an ultrasonic bath) to avoid aggregates. Possible remaining aggregates were pelleted by centrifugation (13 000 rpm, 10 min, RT). The supernatant was transferred to a fresh Eppendorf tube and filled up to 17 mL with fluorescence buffer.

For the Ca²⁺ titration, the Ca²⁺-EGTA buffer system components and CaCl₂ solutions filled up to 20 µL with fluorescence buffer were prepared in Eppendorf tubes (free calcium concentrations used for each GCAP5 variant see Table A9 and Table A10). The [Ca²⁺]_{free} for the samples prepared with the Ca²⁺-EGTA buffer system were calculated with Equation 7.

Each Ca²⁺ solution was mixed with 480 µL of the protein solution, and the tryptophan fluorescence was measured in a fluorescence quartz glass cuvette. The excitation wavelength was 280 nm. The emission spectrum from 300 nm to 420 nm was recorded with a resolution of 2 nm. The fluorescence intensity maxima were plotted against the [Ca²⁺]_{free}.

fluorescence buffer:

80 mM HEPES/KOH pH 7.5

40 mM KCl

1 mM DTT (5mM DTT for reduced GCAP5)

2.8 Cell culture conditions of HEK293-human GC-E cell line and cell harvesting

For testing the GC regulation of the GCAP5 variants, I needed a GC source. In our lab, we have a HEK293 cell line in which the human GC-E is stably transfected. The advantages over the bovine GC-E from ROS preparations are independence of the schedule of the slaughterhouse as well as of their method, which can affect the quality of the cattle's eyes. Further, HEK293 cells do not express the phototransduction machinery, which would start the phototransduction cascade upon light exposure and thus change the [cGMP] that we need to control during the GC assay. This allows us to perform the GC assay not under low red light but under day light conditions.

The cells were cultivated on 10 cm tissue culture dishes (*TPP*) in 10 mL of Dulbecco's Modified Eagle Medium (DMEM, high glucose, GlutaMAX™ Supplement, *Gibco*) supplied with fetal bovine serum (FBS, *Gibco*) and Antibiotic-Antimycotic (100X, *Gibco*) and kept at 37 °C, 37 % humidity and 5 % CO₂. If the cells were 80-90 % confluent, they were either passaged or harvested.

For passaging, the DMEM was removed first. The cells were washed with PBS (*Gibco*). After removing the PBS, the cells were incubated in 1 mL of Trypsin/EDTA (*Gibco*) (2-5 min, 37 °C) to detach them from the plate surface. To the cell suspension, 9 mL of DMEM including supplements were added, and the cells were

separated by pipetting. Between 30 μ L and 1 mL of the cell suspension was transferred to a new tissue culture dish with fresh DMEM including supplements.

For cell harvesting, the cells were scraped in DMEM with a cell scraper. The DMEM with the cells was transferred to a tube and centrifuged (5 min, 300-500 xg, 4 °C). The supernatant was removed, and the cell pellet was washed in two steps with 2 mL and 1 mL of PBS, respectively, and centrifuged again after each washing step (5 min, 300-500 xg, 4 °C). Prior to the second centrifugation step during washing, the cell suspension was transferred to a 1.5 mL Eppendorf tube. After centrifugation, the PBS was removed, and the cell pellet was stored at -80 °C until use.

2.9 GC assay

To investigate the influence of the myristoylation, of the redox state, and of C15 and C17 on the GC regulation of GCAP5, GC assays were performed according to Hwang et al. (2003) and Scholten and Koch (2011). GCAP5 was incubated with the human GC-E in the presence of GTP. Afterwards, the amount of produced cGMP was measured by reversed phase-HPLC.

2.9.1 Preparation of the GC

A harvested cell pellet of the HEK293-human GC-E cell line (see section 2.8) was resuspended in 1 mL of HEK293 lysis buffer supplied with a mammalian protease inhibitor cocktail (end dilution 1:500) and then incubated (30 min, ice-cold). Afterwards, the cells were disrupted by pipetting them with a syringe through a disposable needle (Sterican® 0.9 \times 70 mm, 20 G \times 2 $\frac{3}{4}$ ", *B. Braun*) up and down ten to twenty times. The cell membranes were pelleted by centrifugation (4 min, 13 000 xg, 4 °C), and the pellet was resuspended in 100 μ L of membrane resuspension buffer. The suspension was used for the enzymatic assay (see section 2.9.3) and to determine the protein concentration with the modified Bradford Assay with OGP (see section 2.4.2.1).

HEK293 lysis buffer:

10 mM HEPES/KOH pH 7.4

1 mM DTT

membrane resuspension buffer:

50 mM HEPES/KOH pH 7.4

50 mM KCl

20 mM NaCl

1 mM DTT

2.9.2 Preparation of GCAPs

As a positive control for the GC assay, I used either myristoylated zebrafish GCAP3 or myristoylated bovine GCAP1. Both were purified by chromatography methods after heterologous expression in *E. coli* according to the protocol of the Division of Biochemistry (*University of Oldenburg*) and stored at -80 °C for further use in the Division of Biochemistry (*University of Oldenburg*).

Lyophilized GCAP was dissolved in 10 mM sodium phosphate buffer (end concentration 4 µg/µL) and supplied with DTT (end concentration 1 mM, end concentration for reduced GCAP5 5 mM). The GCAP solution was sonicated in an ultrasonic bath (5 min, ice-cold). Afterwards, the protein concentration was determined by a Bradford Assay (see section 2.4.2).

The IC₅₀-value, the inhibitory [Ca²⁺] at which the GC activity is half maximal, was determined with a Ca²⁺ titration. Therefore, 10 µL of a 50 µM GCAP solution were mixed with the Ca²⁺-EGTA buffer system components K₂H₂EGTA and K₂CaEGTA (Klabusay and Blinks 1996; pipetting scheme see Table A11). As a positive control, I used either zebrafish GCAP3 or bovine GCAP1. Double distilled H₂O served as a negative control. The controls were analyzed only at the lowest and at the highest [Ca²⁺] but not used for Ca²⁺-titrations.

2.9.3 Enzymatic assay

Twenty µL of the GCAP solution (see section 2.9.2) were mixed with 10 µL of the GC solution (see section 2.9.1), vortexed, and then incubated (5 min, RT). The enzymatic reaction was started by adding 20 µL of 2.5x GC buffer. The mixture was vortexed again and then incubated (5 min, 30 °C). By adding 50 µL of 0.1 M EDTA (ice-cold), the reaction was stopped. The mixture was vortexed and then denatured by heating (5 min, 95 °C).

The samples after the GC assay were either shock frozen in liquid nitrogen and stored at -20 °C until analysis or analyzed directly by reversed phase-HPLC (see section 2.10.2.1).

2.5x GC buffer:

75 mM Mops/KOH pH 7.2	2.5 mM DTT
150 mM KCl	2.5 mM GTP
10 mM NaCl	0.75 mM ATP
8.75 mM MgCl ₂	0.4 mM Zaprinast

2.9.4 GC assay with FeSO₄

To investigate the influence of Fe²⁺ on the GC regulation of GCAP5, a GC assay with FeSO₄ was performed with WT and C15A-C17A as described (Lim et al. 2017).

Lyophilized GCAP was resuspended in 30 mM Mes pH 6.6, and DTT (end concentration 1 mM) was added. For iron-loading, FeSO₄ (end concentration 100 μM) was added as well. The concentration of FeSO₄ was reduced by dialysis to 100 nM. Therefore, the GCAP solution was transferred to a dialysis capsule (Slide-A-Lyzer™ MINI Dialysis Devices, 3.5 K MWCO, 0.1 mL, *Thermo Fisher Scientific*) and incubated in dialysis buffer (at least 5 h, 4 °C, slowly stirring). After exchanging the dialysis buffer, the GCAP in the dialysis capsule was incubated again (overnight, 4 °C, slowly stirring). After dialysis, the GCAP solution was sonicated (5 min, ice-cold, in an ultrasonic bath), and the protein concentration of the sample was determined by a Bradford Assay (see section 2.4.2). The controls with iron were treated analogically. For the controls without iron, iron-loading with FeSO₄ was skipped, and the dialysis buffer did not contain FeSO₄.

The DTT concentration of the 2.5x GC buffer was increased to 12.5 mM DTT. In addition, FeSO₄ (end concentration 250 nM) was added for the GC assay with the iron loaded GCAPs.

dialysis buffer:

30 mM Mops/KOH pH 7.2

60 mM KCl

3.5 mM MgCl₂

1 mM DTT

100 nM FeSO₄ (only for iron-loaded GCAPs and controls)

2.9.5 GC assay under reducing conditions

The GC assay under reducing conditions was only performed with reduced purified myristoylated GCAP5 and the corresponding controls. Therefore, the sodium phosphate buffer used to resuspend lyophilized GCAP was supplied with DTT (end concentration 5 mM), and the 2.5x GC buffer contained 12.5 mM DTT. The controls were treated analogically.

2.10 High performance liquid chromatography (HPLC)

While the FPLC, which I used for protein purification, works under atmospheric pressure, the high-performance liquid chromatography (HPLC) can operate under higher pressures. The advantages of the HPLC are higher speed, better resolution, and more options for automatic processing (Lottspeich and Zorbas 2012). I used the analytical SEC (see section 2.10.1) to determine the dimerization and aggregation rate of GCAP5 as well as the reversed phase-HPLC (see section 2.10.2) for GC assay analysis (see

section 2.10.2.1) and for myristoylation rate analysis (see section 2.10.2.2). All aqueous buffers were filtered and degassed prior to use. Hydrophobic solvents used always were HPLC grade and only degassed.

2.10.1 Analytical SEC

With the analytical SEC, proteins can be separated on a porous stationary phase by their hydrodynamic volume (Lottspeich and Zorbas 2012). The hydrodynamic size of a protein and its dynamic equilibria between monomers and oligomers can be determined if compared to standard proteins. I tested GCAP5 for dimerization since GCAPs are known to form dimers (Olshevskaya et al. 1999; Ermilov et al. 2001; Boni et al. 2020). I also investigated whether the GCAP5 mutants V76E and H18E-Y21E prevent a dimerization of the GCAP. To detect possible redox effects, the analytical SEC was performed under non-reducing (no DTT) and under reducing conditions (5 mM DTT), respectively. DTT has no influence on the retention times of the standard substances (not shown).

For the analytical SEC, the HPLC system Primaide (*VWR Hitachi*) was used with the column BioSep-SEC-S2000 (*Phenomenex*) at a flow rate of 0.35 mL/min. The soluble phase was either analytical SEC buffer or reducing analytical SEC buffer. To assign the peaks of the chromatograms to specific protein sizes, the column BioSep-SEC-S2000 (*Phenomenex*) was calibrated with the Low Molecular Weight Gel Filtration Calibration Kit (*GE Healthcare*). Acetone was used as a reference for the total elution time of the column. Lyophilized GCAP5 was resuspended in analytical SEC buffer or reducing analytical SEC buffer and sonicated (5 min, ice-cold, in an ultrasonic bath) to avoid aggregates. Possible remaining aggregates were pelleted by centrifugation (13 000 rpm, 10 min, RT). The protein concentration of the supernatant was determined by a Bradford Assay (see section 2.4.2). For the HPLC-analysis, 20 μ L of GCAP5 solution containing 50 μ g of protein were injected onto the preequilibrated column. The hydrodynamic sizes of the proteins were calculated with Equation 8.

$$k_r = \frac{t_e - t_0}{t_t - t_0}$$

Equation 8: Calculation of the retention factor k_r .

k_r is the retention factor. t_e is the elution time of the analyte. t_0 is the void time for the column and equal to t_e of Blue Dextran 2000, amounting to 5.96 min. t_t is the total elution time and equal to t_e of acetone, amounting to 12.593 min. t_e of each standard substance is listed in Table A3. In the manual of the Low Molecular Weight Gel Filtration Calibration Kit (*GE Healthcare*), this formula is given with retention volumes instead of retention times. However, since the relation between t_e and t_0 to the elution volume (V_e) and the flow rate (F) of a chromatographic system are defined as $V_e = t_e \cdot F$ and $V_0 = t_0 \cdot F$, k_r can be defined by using the retention time as well (Lottspeich and Zorbas 2012).

<u>analytical SEC buffer:</u>	<u>reducing analytical SEC buffer:</u>
30 mM Mops/KOH pH 7.2	30 mM Mops/KOH pH 7.2
50 mM KCl	50 mM KCl
4 mM NaCl	4 mM NaCl
	5 mM DTT

2.10.2 Reversed phase-HPLC

With the reversed phase-HPLC, molecules can be separated by their relative hydrophobicity (Lottspeich and Zorbas 2012). The analyte is loaded onto the hydrophobic stationary phase under aqueous conditions. When applying a gradient from the aqueous solvent to a hydrophobic solvent, molecules containing a less hydrophobic surface elute earlier than molecules with more hydrophobic surfaces. I used the reversed phase-HPLC for the analysis of the GC assay (see section 2.10.2.1) and for the myristoylation rate analysis (see section 2.10.2.2).

2.10.2.1 GC assay analysis

The amount of produced cGMP during the GC assay (see section 2.9) was quantified by a reversed phase-HPLC according to Koch (1991). Therefore, the HPLC system LaChrom Elite (*VWR Hitachi*) was used with the column LiChrospher® 100 RP-18 (5 µm) LiChroCART® 250-4 (*Merck*) at a flow rate of 1 mL/min. After incubation for GC activity, the samples were centrifuged (10 min, 15000 xg, 18 °C). The supernatant was used for the HPLC analysis. The HPLC column was equilibrated with 5 mM of KH₂PO₄ pH 5.0. After the injection of 80 µL sample solution, a staggered gradient from 0 % to 15 % methanol in six minutes and from 15 % to 70 % methanol in 7.5 min was applied. The absorbance at 260 nm in AU was recorded over time. The integral of the cGMP peak in a chromatogram was determined with the software EZChrom Elite and a predefined calibration line. The base line was always below the whole peak, and the start and end time were always set to certain times before and after the peak maximum, respectively.

2.10.2.2 Myristoylation rate analysis

The *E. coli* cells are used to heterologously express myristoylated GCAP5 co-express the NMT (see section 2.2.1). However, this does not guarantee the myristoylation of GCAPs. Since I wanted to investigate differences between myristoylated and non-myristoylated GCAP5, I needed to determine the myristoylation rate of the purified GCAPs. Myristoylation enhances the hydrophobicity of a protein. Therefore, the non-myristoylated part and the myristoylated part of GCAP5 can be separated by reversed phase-HPLC.

For the myristoylation rate analysis, the HPLC system Primaide (VWR Hitachi) was used with the column Luna® 5 µm C18(2) (Phenomenex) at a flow rate of 1 mL/min. Lyophilized GCAP5 was resuspended in double distilled H₂O (end concentration 2 µg/µL) and sonicated (5 min, ice-cold, in an ultrasonic bath) to avoid aggregates. Possible remaining aggregates were pelleted by centrifugation (13 000 rpm, 10 min, RT). The supernatant was used for the HPLC-analysis. The HPLC column was equilibrated with double distilled H₂O/0.1 % TFA. After injecting 80 µL of GCAP5 solution, a gradient from 0 % to 100 % acetonitrile/0.1 % TFA was applied. The absorbance at 280 nm in AU was recorded over time. The start time, end time, retention time, base line, and integrals of the peaks in a chromatogram were detected and calculated by the software Primaide (Figure A7, Table A6).

2.11 Preparation of adult zebrafish retinae

For localizing GCAP5 in the retina of adult zebrafishes, the retina had to be isolated first. Adult zebrafish (*Danio rerio*, n = 16) were provided by the breeding facility of Prof. Dr. Gabriele Gerlach (Institute of Biology and Environmental Sciences, *University of Oldenburg*). The zebrafish were kept in 3 L aquaria at 26 °C under a 13 h/11 h light/dark cycle and at an alternating diet of flake food (*Artemia salina*) and white mosquito larvae on a daily basis. All experiments were approved by the local animal welfare committee (LAVES, *Niedersächsisches Landesamt für Verbraucherschutz und Lebensmittelsicherheit*) and followed the guidelines of the German Animal Welfare Act (Tierschutzgesetz; BGBl. I S. 1206, 1313 and BGBl. I S. 1934). All preparations were done between 9 and 12 am with light adapted zebrafish.

The preparation of the eye cups was done in ice-cold L-15 medium pH 7.4. The zebrafish were deeply anesthetized with MS-222 and then decapitated. Afterwards, the eyes were removed with a dissecting set and transferred to fresh L-15 medium. The cornea, the sclera, and the lens were removed with micro spring scissors. If the eye cup was used for immunohistochemistry staining, the eye cup was transferred to an Eppendorf tube, and the tissue was fixed (see section 2.11.2). If the retina was used for a western blot (see section 2.5.2), the pigment epithelium was removed with fine brushes, and the retina was transferred to an Eppendorf tube for subcellular fractionation (see section 2.11.1).

L-15 medium:

1.38 % (w/v) L-15 medium pH 7.4

2.11.1 Subcellular fractionation

To analyze the localization of GCAP5 in subcellular fractions of the retina by western blot, I did a subcellular fractionation with the isolated zebrafish retinae (n=13) (see section 2.11). Isolated retinae were pooled and homogenized in ice-cold homogenization buffer (25 µL per retina). Three hundred µL of the total homogenate were transferred to an Eppendorf tube and centrifuged (10 min, 1 000 rpm, 4 °C). The

supernatant (SN1) was transferred to a fresh Eppendorf tube. The pellet was washed in 50 μ L of homogenization buffer and centrifuged again (10 min, 1 000 rpm, 4 °C). The supernatant was pooled with SN1. The pellet (P1, nuclear cell fraction) was resuspended in 50 μ L of homogenization buffer. SN1 was centrifuged (1 h, 14 000 rpm, 4 °C). The supernatant (SN2, cytosolic cell fraction) was transferred to a fresh Eppendorf tube. The pellet (P2, membrane cell fraction) was resuspended in 30 μ L of homogenization buffer.

After the fractionation, the protein concentrations of the total homogenate, P1, P2, and SN2 were determined with a modified Bradford Assay (see section 2.4.2.1), and the fractions were used for a western blot (see section 2.5.2) and a subsequent immunoassay (see section 2.5.3) against GCAP5.

Centrifuge 5417R (*Eppendorf*)

homogenization buffer (10 mL):

50 mM Tris/HCl pH 7.4	0.1 mM sodium orthovanadate
2 mM EDTA	5 μ g/mL aprotinin
2 mM EGTA	2 μ g/mL leupeptin
1 mM PMSF	1 tablet cOmplete, Mini, EDTA-free Protease Inhibitor Cocktail (<i>Roche</i>)
1 mM dithioerythritol	

2.11.2 Tissue fixation

The isolated zebrafish eye cups (see section 2.11) were fixed in fixing solution (20 min, RT), and the fixed eye cups were washed in PB (3x 10 min, RT). Afterwards, the eye cups were incubated in 30 % (w/v) sucrose in PB as a cryoprotectant (overnight, 4 °C) until cryosectioning (see section 2.11.3).

fixing solution:

0.1 M sodium phosphate buffer pH 7.4
2% (w/v) PFA
3 % (w/v) sucrose

PB:

0.1 M sodium phosphate buffer pH 7.4

2.11.3 Preparation of cryosections

The fixed eye cups (see section 2.11.2) were incubated in cryomatrix (Tissue Tek O.C.T. compound, *Sakura Finete Europe*) (30 min, RT) and then frozen in fresh cryomatrix by using liquid nitrogen. The frozen eye cups were either stored at -20 °C or cryosectioned directly.

Cryosectioning was done in a cryostat (LeicaCM1860, *Leica Biosystems*) at -21 °C. Vertical sections of 20 µm were made and dried on a microscope slide (at least 1 h, 37 °C, on a heating plate). The slides with the dried slices were stored at -20 °C until immunohistochemical staining (see section 2.11.4).

2.11.4 Immunohistochemistry on cryosections

The cryosections (see section 2.11.3) were thawed (15 min, 37 °C, on a heating plate), edged with a liquid blocker, and washed in PB (3x 10 min, RT). Afterwards, the cryosections were blocked in blocking solution (1 h, RT, in a moist chamber) and then incubated with the primary antibody (overnight, 4 °C, in a moist chamber). The next day, after washing the cryosections in PB (3x 10 min, RT), they were incubated with the secondary antibody (1 h, RT, in a moist chamber). The stained cryosections were washed in PB (3x 10 min, RT, dark), then mounted either in Aqua Poly/Mount (*Polysciences*) or in VectaShield (*Vector Laboratories*), and hardened (1 h, RT, dark). The mounted cryosections were stored at -20 °C or analyzed directly with a confocal laser scanning microscope (see section 2.11.5).

PB:

0.1 M sodium phosphate pH 7.4

blocking solution:

0.1 M sodium phosphate pH 7.4

0.3 % (v/v) Triton X-100

10 % (v/v) normal donkey serum

2.11.5 Image acquisition by confocal microscopy

For image acquisition, a confocal laser scanning microscope (Leica TCS SP2, *Leica Microsystems*) was used according to a previous description (Hilgen et al. 2011). Stacks were scanned with a 63x/1.32 plan apochromatic oil-immersion objective (16 slices, z-distance 300 nm, resolution: 1024 × 1024 pixels). Crosstalk between the channels was ruled out by performing scans of different wavelengths sequentially. Using Fiji (Schindelin et al. 2012), single scans were superimposed for co-localization analysis, and images presented as average projections of 4, 8 or 16/16 single scans were adjusted for brightness and contrast for presentation.

3 Results

3.1 Purification of recombinant GCAP5

To investigate the GCAP5 variants, I first had to heterologously express them in *E. coli* and then purify by chromatography methods. The variants to be purified were non-myristoylated wildtype (non-myr WT), myristoylated wildtype (WT), reduced purified myristoylated wildtype (reduced WT), myristoylated C15A-C17A mutant (C15A-C17A), which might prevent a putative iron-binding, and the possibly dimerization preventing mutants myristoylated H18E-Y21E (H18E-Y21E) and myristoylated V76E (V76E) of GCAP5. All variants possessed a D3N mutation to enable myristoylation in *E. coli* (see section 1.7).

I tried two purification protocols of the Division of Biochemistry (*University of Oldenburg*) and the Department of Chemistry (*UC Davis*) and some variations (Table 2, Table 3). The protocol of the Division of Biochemistry was termed protocol 1a and its variations protocol 1b and 1c. The variations comprise other AEC columns. Analogically, the Department of Chemistry protocol was termed protocol 2a and its variation protocol 2b. In protocol 2a, the proteins are purified from the cytosolic fraction after cell lysis, while they are purified from inclusion bodies by denaturation and subsequent renaturation in protocol 2b.

Using protocol 1a, the purity of the protein was not sufficient in the end (Figure A2 A). Using protocol 2a, the protein was more than 90 % pure after purification. However, the yield was below 1 mg per 500 mL *E. coli*-culture. If I tried to purify GCAP5 according to protocol 2b (Figure A3), the purity of most fractions after the SEC was insufficient, comparable with the AEC fractions using protocol 1a. A few fractions showed more than 90 % purity, but the yield per 500 mL *E. coli*-culture was below 1 mg. I then tried the Division of Biochemistry protocol with two other AEC columns (Jennifer Richter, Bachelor thesis, Division of Biochemistry, 2019). Before, I used the AEC column RESOURCE Q (*GE Healthcare*), but even after cleaning with pepsin, the protein purification result remained the same. We tried the AEC columns Mono Q 5/50 GL and HiTrap Q HP 5mL (both *Cytiva*). When using the Mono Q column (protocol 1b, Figure A2 B), the yield of the protein seemed much higher than after using the Resource Q column (protocol 1a), but the protein was still not pure in most of the fractions. By using the HiTrap Q HP column (protocol 1c), most of the impurities after the SEC could be removed while achieving a purity of more than 90 % (Figure 13).

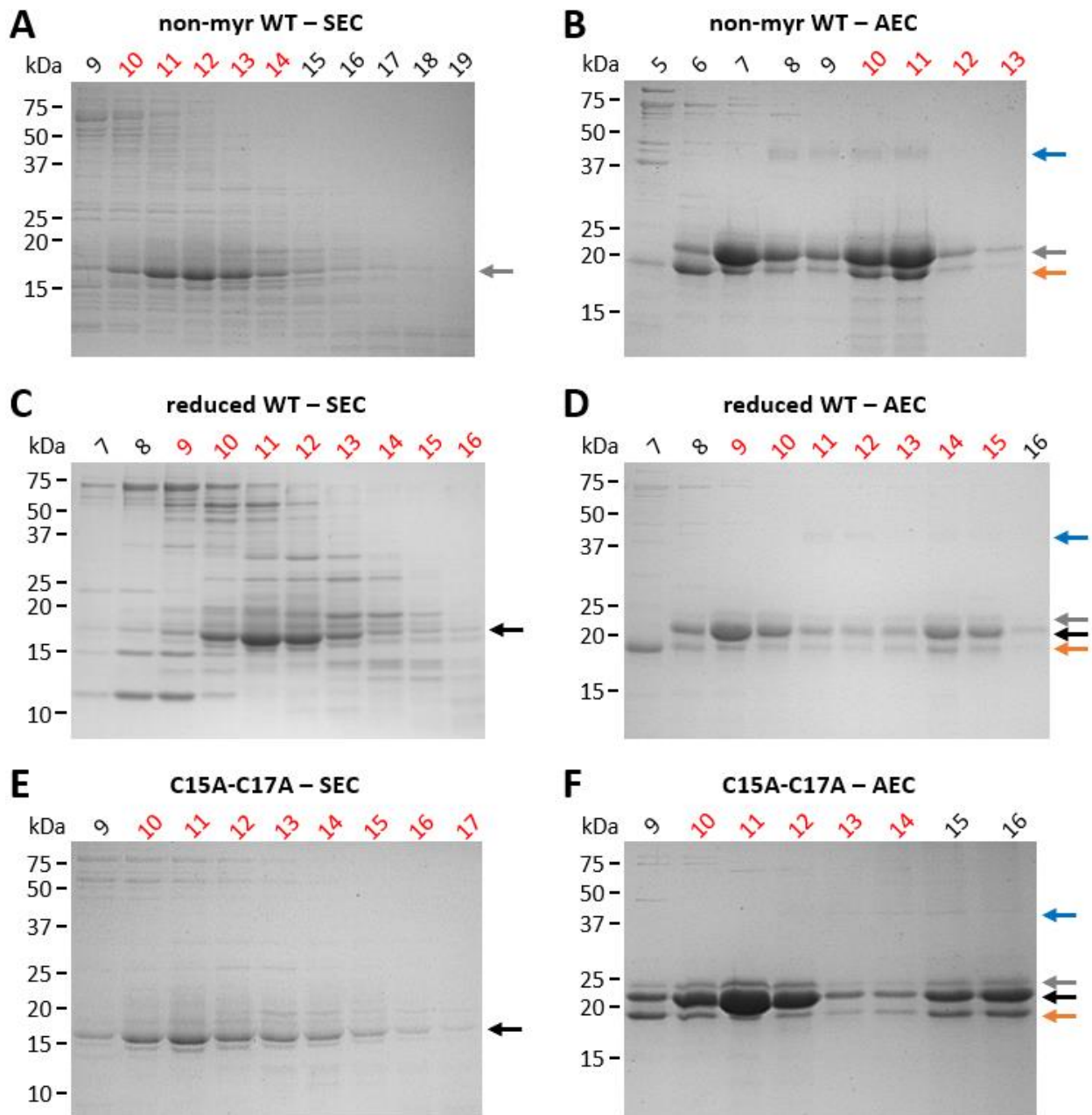


Figure 13: Coomassie-stained SDS-gels after SEC and AEC of successful GCAP5 purification.

Purification progress of recombinant GCAP5 (A, B) non-myristoylated WT, (C, D) reduced WT, and (E, F) C15A-C17A. Nine μL of selected fractions after size exclusion chromatography (SEC) or after anion exchange chromatography (AEC), each mixed with 4x SDS-sample buffer, were applied onto a 15 % SDS-polyacrylamide gel. Mobilities and sizes of the standard proteins (kDa) are shown to the left of each gel, fraction numbers above. Ten mL SEC fractions were collected 100 mL after injection of the protein sample, 5 mL AEC fractions directly after starting the gradient for elution. Red written SEC fractions were used for the following AEC, red marked AEC fractions for buffer exchange and subsequent lyophilization. Monomeric GCAP5 has a mobility of around 18 kDa in SDS-polyacrylamide gels, appearing as a double (non-myristoylated WT) or triple band (all myristoylated variants) possibly consisting of the apo-state of non-myristoylated GCAP5 (grey arrows), the apo-state of myristoylated GCAP5 (black arrows), and the calcium-bound state (orange arrows). Dimeric GCAP5 has a mobility of around 37 kDa (blue arrows).

The different mobilities of the monomeric GCAP5 bands in SDS-polyacrylamide gels after the SEC and after the AEC (Figure 13, black arrows) can be explained with the Ca^{2+} -shift (Scholten and Koch 2011; Lange 2012; Griepentstroh 2016; see also Figure A10). The SEC buffer contained 2 mM CaCl_2 . Prior to the AEC, the sample solution was adjusted to 4 mM EGTA, and the AEC buffers contained 2 mM EGTA. The double band

of non-myr WT GCAP5 after the AEC (Figure 13 B) might represent the apo state (black arrow) and the Ca²⁺-bound state (orange arrow), respectively. However, the latter could as well be degraded GCAP5. If GCAP5 was myristoylated, an additional band could be seen in the gel after the AEC (grey arrows). Since myristoylation of GCAP5 was reported to be not very efficient (Sulmann et al. 2015), this might be the non-myristoylated part of purified recombinant GCAP5. A similar result was already described by Fries (2013) and for bovine GCAP1 and bovine GCAP2 by Hwang and Koch (2002) and Olshevskaya et al. (1997). A dimeric form of GCAP5 was observed for all variants after the AEC (blue arrows, see also Figure 21). The purification progresses of WT and the mutants V76E and H18E-Y21E were similar to the purification progress of reduced WT (Figure 13 C and D), with a lower intensity of the GCAP5 bands for both of the mutants (not shown). The yields of the variants were different but at least higher than 1 mg per 500 mL *E. coli* culture, with the highest yield achieved by far for non-myr WT (Table 6).

Table 6: Yields achieved for GCAP5 variants.

The approximate yields in mg per 500 mL *E. coli* culture of purified GCAP5 non-myr WT, WT, reduced WT, C15A-C17A, H18E-Y21E, and V76E are listed.

GCAP5 variant	mg per 500 mL <i>E. coli</i> culture
non-myr WT	25
WT	5
reduced WT	5
C15A-C17A	6
H18E-Y21E	3
V76E	2

3.2 Analytical SEC

A possible dimerization of GCAP5 was studied by analytical SEC. First, a calibration line was created with standard substances (Figure A4 and Table A3). With the calibration line, the elution times of the GCAP5 analytical SEC chromatogram peaks were associated to the hydrodynamic size and protein state (Table 7).

Table 7: GCAP5 protein states observed on the BioSep-SEC-S2000 column.

By comparing the elution times (t_e) in minutes (min) of recombinant GCAP5 peaks on the BioSep-SEC-S2000 column (Phenomenex) with the calibration line, the associated protein sizes in kDa and protein states were determined. States observed are aggregates, dimers, monomers, and an unclear state between the elution times of the monomeric and the dimeric state.

t_e (min)	size (kDa)	protein state
5.9	> 45	aggregate
7.5	42	dimer
8	36	unclear
9.3	20	monomer

The analytical SEC chromatograms of GCAP5 were recorded in three triple measurements under reducing and under non-reducing conditions, respectively (Figure 14, dotted and solid lines, respectively), and the relative integrals of the peaks were determined by the HPLC software Primaide (Figure 15, grey and black bars, respectively; see also Table A4). Each GCAP5 variant showed aggregation under both redox conditions (Figure 14, ~5.9 min). With up to 98 % of aggregates, V76E showed the highest aggregation rate (Figure 15 F). Reducing conditions significantly decreased aggregation (Figure 15, $p \leq 0.001$) and enhanced dimerization ($p \leq 0.001$, for non-myr WT $p = 0.002$) for all GCAP5 variants except for C15A-C17A (Figure 15 D; $p = 0.672$ and $p = 0.204$, respectively). With more than 50 % dimers, C15A-C17A showed the highest dimerization rate and the lowest tendency to form aggregates.

A small proportion of monomers was detected in two measurements of non-myr WT without DTT and in three measurements of non-myr WT with DTT (Figure 14 A, grey, ~9.3 min) and reduced WT under both conditions (Figure 14 B, black), respectively. The Mann-Whitney rank sum test did not show a significant difference between the redox conditions (Figure 15 A and C). However, the sample size n of detected monomer peaks was too low to assure reliable results.

The non-myr WT chromatogram clearly showed a peak next to the dimer peak (Figure 14 A, grey, ~8 min), indicating either a more spherical conformation of the non-myr WT dimer or a more loose conformation to denatured form of the non-myr WT monomer. Yet, the proximity of both peaks was too close and their amplitudes too low for the HPLC program Primaide to reliably detect the peaks as two single peaks. The elongated shoulder of the reduced WT chromatogram (Figure 14 B, black, ~8 min) might have the same reason as the peak next to the dimer peak observed for non-myr WT.

C15A-C17A was the only GCAP5 variant not responding to changes in the tested redox conditions. For all other variants, reducing conditions diminished the aggregation rate and increased the dimerization rate. The mutants H18E-Y21E and V76E, which we expected to prevent dimerization of GCAP5 (see section 1.7), either behaved similar to WT or tended to aggregate nearly completely. Therefore, both mutants were not included in the following experiments.

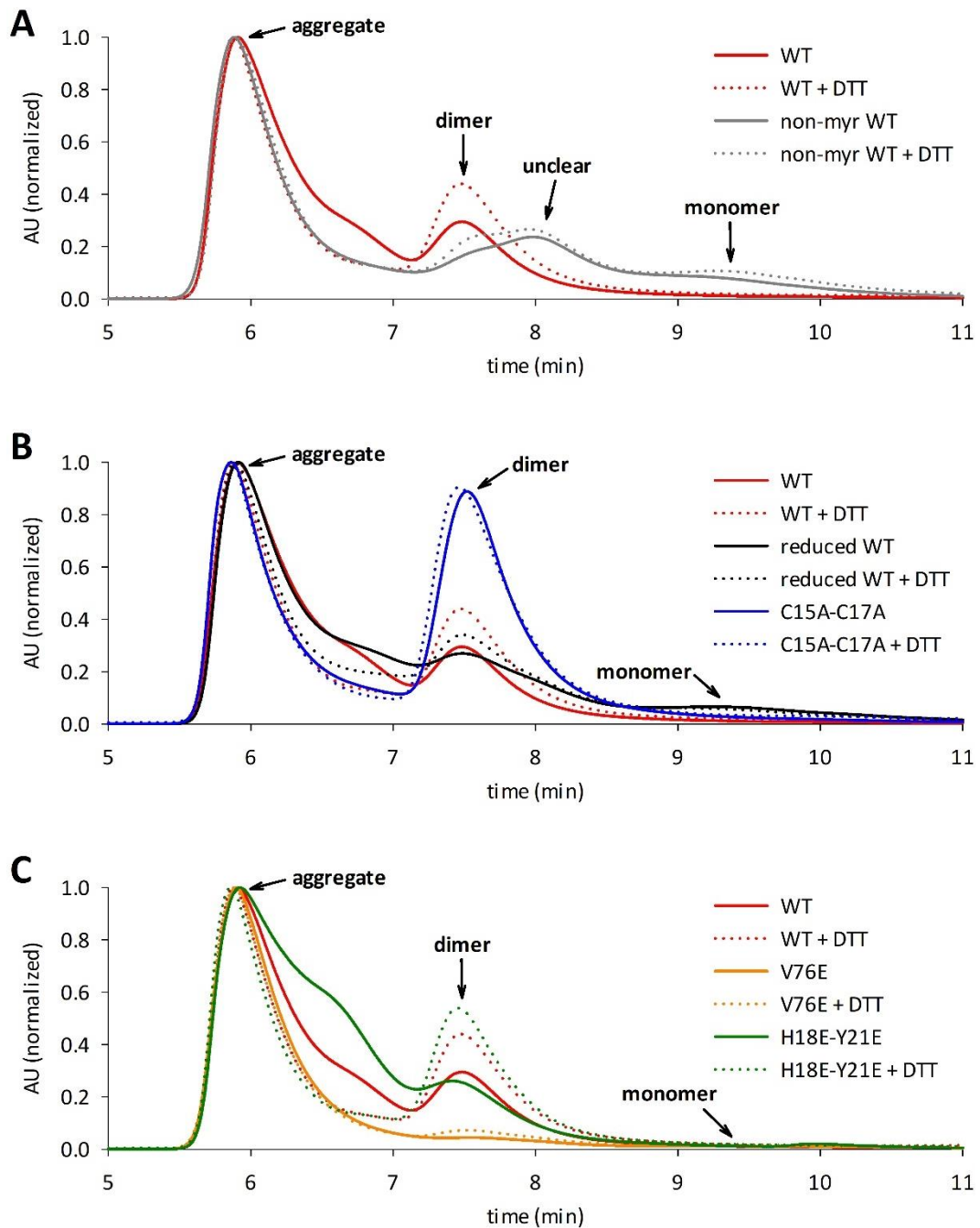


Figure 14: Analytical SEC chromatograms of GCAP5.

Representative analytical SEC chromatograms of recombinant GCAP5 from five to eleven min after GCAP5 injection, normalized to the maximum of the peak at around 5.9 min (aggregate) for comparison. GCAP5 (30 or 50 μ g) was analyzed in the absence (solid lines) and in the presence of DTT (5 mM, dotted lines). WT (red) is compared to (A) non-myr WT (grey), (B) reduced WT (black) and C15A-C17A (blue), and (C) V76E (orange) and H18E-Y21E (dark green). The absorbance in AU at 280 nm was recorded over time in minutes. Arrows indicate the peak positions of aggregated (~5.9 min), dimeric (~7.5 min, ~42 kDa), monomeric GCAP5 (~9.3 min, ~20 kDa), and an unclear state of GCAP5 between the peaks of a monomeric and a dimeric state (~8 min, ~36 kDa). Data listed in Table A4.

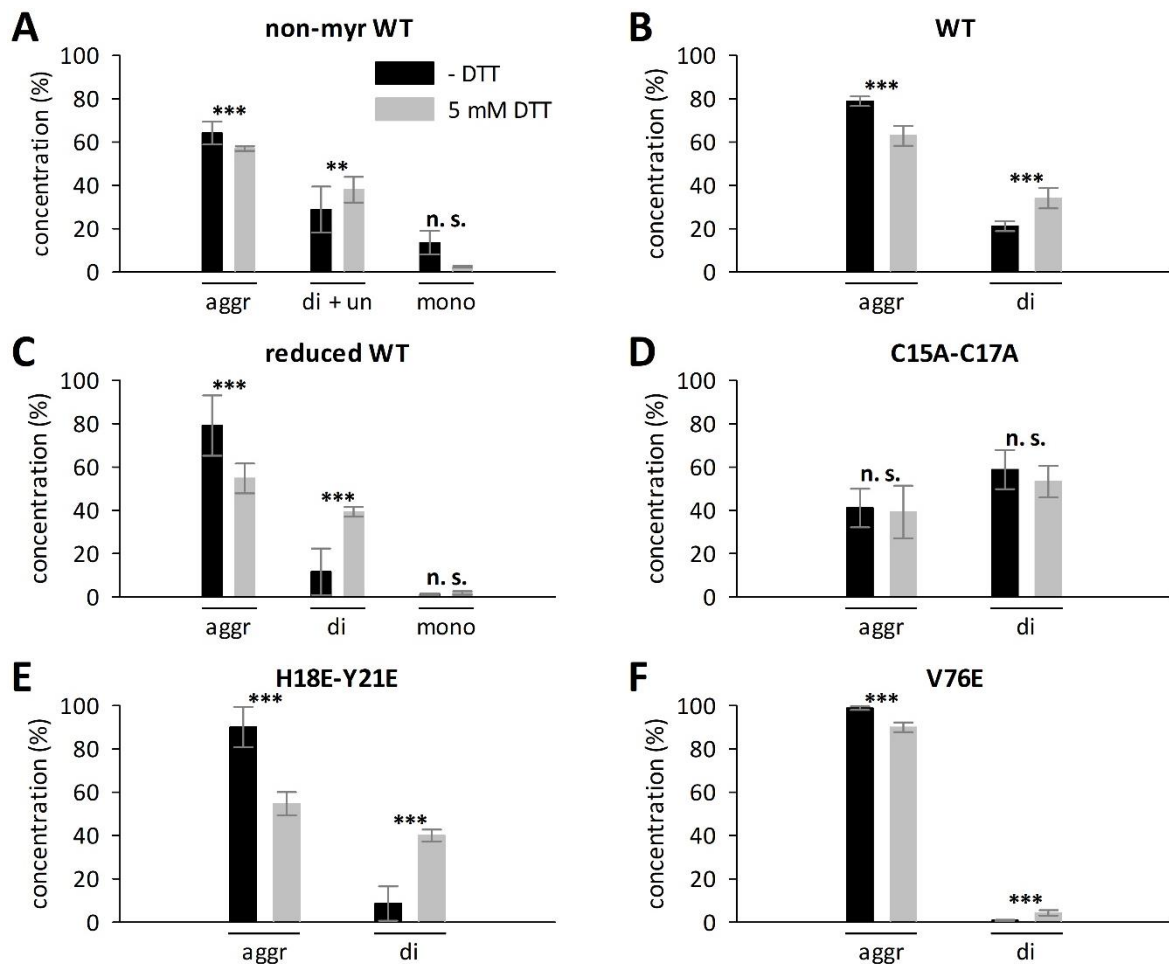


Figure 15: Relative integrals of the analytical SEC chromatogram peaks.

Relative integrals of the analytical SEC chromatogram peaks (Figure 14), determined by the HPLC program Primaide. Recombinant GCAP5 (30 or 50 μ g) (A) non-myr WT, (B) WT, (C) reduced WT, (D) C15A-C17A, (E) H18E-Y21E, and (F) V76E were analyzed under non-reducing (- DTT, grey bars) and reducing conditions (5 mM DTT, black bars), respectively. Bars indicate the mean, error bars the standard deviation. The peaks are categorized in aggregated protein (aggr), dimeric (di) or dimeric protein together with an unclear state (di + un), and monomeric protein (mono). The sample size n of detected peaks of three triple measurements (one single measurement and two triple measurements for C15A-C17A - DTT) is (A) two for non-myr WT mono - DTT, three for non-myr WT mono 5 mM DTT and (C) reduced WT mono under both redox conditions, (D) seven for C15A-C17A - DTT aggr and di, (F) eight for V76E di, and nine for all other categories. Significance of differences between the redox conditions were tested with the Mann-Whitney rank sum test. For reduced WT, the conditions for the t-test were given, resulting in the same significance level. Significance levels are highly significant (***: $p \leq 0.001$), moderately significant (**: $p \leq 0.01$), significant (*: $p \leq 0.05$) and non-significant (n. s.: $p > 0.05$). Data listed in Table A4.

3.3 Myristoylation rate

To obtain myristoylated protein, GCAP5 was co-expressed with the NMT in *E. coli*, and myristic acid was supplied prior to expression. The myristoylation rate of GCAP5 was determined by reversed phase-HPLC. Because of the covalently bound hydrophobic myristoyl group, the myristoylated part of the purified protein elutes later than the non-myristoylated part. Myristoylation rates were calculated with the integrals below the peaks of the chromatograms.

The conditions for the reversed phase-HPLC were tested with non-myristoylated WT and WT GCAP5 purified according to protocol 2a first (Figure 16, grey and dark red, respectively; see Table 3 for purification protocol). Non-myristoylated WT eluted around 31 min after injection (Figure 16 A, grey, peak 1). A peak with the same retention time was observed in the chromatogram of WT (Figure 16 A, dark red, peak 1). This peak, therefore, was assigned as the non-myristoylated part of WT GCAP5. The chromatogram also showed a second peak around 32.1 min (Figure 16 A, dark red, peak 2), which must be the myristoylated part. The resulting myristoylation rate of WT purified according to protocol 2a was approximately 69 % (Table 8, scenario 1). These runs were initially meant to be test runs to determine a sufficient method to analyze the myristoylation rate of GCAP5.

Recombinant GCAP5 used for all experiments except for the Fe²⁺-dependent GC assay (see section 3.6) was purified using protocol 1c (Table 2). After the positive test runs with GCAP5 purified according to protocol 2a (Table 3), the myristoylation rates of GCAP5 WT and reduced WT purified according to protocol 1c (Table 2) were analyzed analogically. However, the chromatograms of WT (Figure 16 A, red) and of reduced WT (Figure 16 B, black) both showed four peaks. Since peak 1 of both variants had a retention time of around 31 min, this represents, at least partially, the non-myristoylated part of the variants. The three peaks thereafter in both chromatograms were hard to interpret. Since peak 2 of WT and reduced WT purified according to protocol 1c eluted at retention times shortly before 32.1 min, this peak could represent the non-myristoylated part together with peak 1, but it could also at least partially represent the myristoylated part of GCAP5. Peak 3 of WT and reduced WT purified according to protocol 1c eluted shortly after 32.1 min. Therefore, this peak could either belong to the myristoylated part of GCAP5, to dimeric or aggregated GCAP5, which might partially be myristoylated, or it might not be GCAP5 at all. Keeping these possibilities in mind, the following scenarios are plausible (Table 8):

scenario 1: Peak 2 is the myristoylated part of GCAP5, the following peaks are not GCAP5 $\Rightarrow \frac{p_2}{p_1+p_2}$

scenario 2: Peak 2 is the monomeric myristoylated part of GCAP5, peak 3 is dimeric or aggregated GCAP5 which might be partially myristoylated, peak 4 is not GCAP5 $\Rightarrow \frac{p_2}{p_1+p_2+p_3}$

scenario 3: Peak 2 is the monomeric myristoylated part of GCAP5, the following peaks are dimeric or aggregated GCAP5 which might be partially myristoylated $\Rightarrow \frac{p_2}{p_1+p_2+p_3+p_4}$

scenario 4: Peak 2 and 3 are the myristoylated part of GCAP5, peak 4 is not GCAP5 $\Rightarrow \frac{p_2+p_3}{p_1+p_2+p_3}$

scenario 5: Peak 2 and 3 are the monomeric myristoylated part of GCAP5, peak 4 is dimeric or aggregated GCAP5 which might be partially myristoylated $\Rightarrow \frac{p_2+p_3}{p_1+p_2+p_3+p_4}$

scenario 6: Peak 1 and 2 are the non-myristoylated part, peak 3 is the myristoylated part of GCAP5, peak 4 is not GCAP5 $\Rightarrow \frac{p_3}{p_1+p_2+p_3}$

scenario 7: Peak 1 and 2 are the non-myristoylated part, peak 3 is the monomeric myristoylated part of GCAP5, peak 4 is dimeric or aggregated GCAP5 which might be partially myristoylated $\Rightarrow \frac{p_3}{p_1+p_2+p_3+p_4}$

scenario 8: Peak 2, 3, and 4 are the myristoylated part of GCAP5 $\Rightarrow \frac{p_2+p_3+p_4}{p_1+p_2+p_3+p_4}$

The resulting myristoylation rates for WT purified according to protocol 1c range between 32 % and 92 %, for reduced WT between 25 % and 96 % (Table 8).

For the myristoylation rate analysis of C15A-C17A, only the protein purified according to protocol 2a (Table 3) was available. The chromatogram (Figure 16 C, blue) showed one peak with a retention time around 32.2 min (peak 2), a shoulder prior to peak 2 (peak 1), and a second peak around 33.3 min. Peak 2 and peak 3 are shifted by additional 1.2 min in comparison to peak 1 and peak 2 of WT GCAP5 purified according to protocol 2a. This retention time shift might occur due to the replacement of the first two cysteines by more hydrophobic alanine. Due to the time shift, a ninth scenario is plausible for C15A-C17A (Table 8):

Scenario 9: Peak 1 is not GCAP5, peak 2 is the non-myristoylated part, peak 3 the myristoylated part of GCAP5 $\Rightarrow \frac{p_3}{p_2+p_3}$

Due to the time shift mentioned above, scenario 6 and scenario 9 are the most likely possibilities for C15A-C17A, resulting in a myristoylation rate between 62 % and 68 %. For clarification, the analysis of the non-myristoylated purified C15A-C17A mutant would be necessary.

In summary, these results show that the purification protocol might affect biochemical properties of GCAP5.

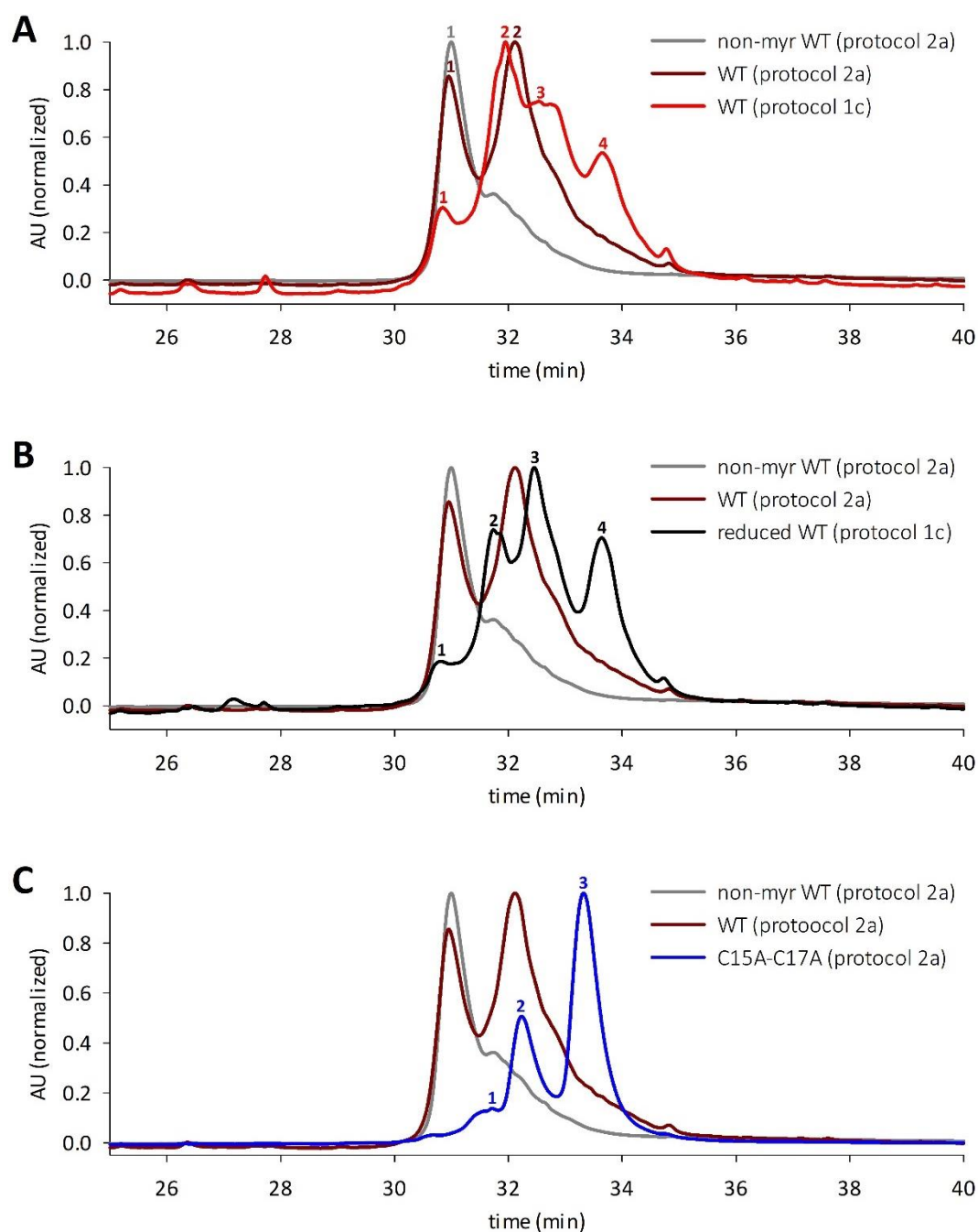


Figure 16: Reversed phase-HPLC chromatograms of GCAP5.

Reversed phase-HPLC chromatograms of recombinant GCAP5 from 25 to 40 min after GCAP5 injection, each normalized to the maximum of the highest peak within this time range for comparison. GCAP5 (160 μ g) was analyzed using a gradient from 100 % double distilled H₂O/0.1 % TFA to 100 % Acetonitrile/0.1 % TFA in 55 min. (A-C) Non-myr WT (grey) and WT (dark red) were purified according to purification protocol 2a (Table 3) from the soluble fraction after expression. These runs, which originally were meant to be test runs to determine a sufficient method to analyze the myristoylation rate of GCAP5, are compared with recombinant GCAP5 (A) WT (red), and (B) reduced WT (black), both purified from inclusion bodies according to protocol 1c (Table 2, see also section 3.1), and (C) C15A-C17A (blue) purified according to protocol 2a due to availability issues. The absorbance in AU at 280 nm was recorded over time in minutes. The peaks of each chromatogram are numbered. Grey and dark red colored numbers in A also apply to B and C. Retention times and areas of the peaks are listed in Table A6.

Table 8: Possible myristoylation rates of GCAP5.

The possible myristoylation rates of GCAP5 non-myristoylated WT, WT, reduced WT, and C15A-C17A purified either according to protocol 1c (Table 2) or protocol 2a (Table 3) were calculated using the following equations: $s_1 = \frac{p_2}{p_1+p_2}$ | $s_2 = \frac{p_2}{p_1+p_2+p_3}$ | $s_3 = \frac{p_2}{p_1+p_2+p_3+p_4}$ | $s_4 = \frac{p_2+p_3}{p_1+p_2+p_3}$ | $s_5 = \frac{p_2+p_3}{p_1+p_2+p_3+p_4}$ | $s_6 = \frac{p_3}{p_1+p_2+p_3}$ | $s_7 = \frac{p_3}{p_1+p_2+p_3+p_4}$ | $s_8 = \frac{p_2+p_3+p_4}{p_1+p_2+p_3+p_4}$ | $s_9 = \frac{p_3}{p_2+p_3}$, with s standing for scenario and p standing for the integral of the numbered peak of the chromatogram (Figure 16). Scenario 9 was only calculated for C15A-C17A due to the time shift of 1.2 min of peak 2 and peak 3 in comparison to peak 1 and peak 3 of WT purified according to protocol 2a. The most likely possible scenarios for C15A-C17A are underlined.

	myristoylation rate (%)								
	S ₁	S ₂	S ₃	S ₄	S ₅	S ₆	S ₇	S ₈	S ₉
non-myristoylated WT (protocol 2a)	-	-	-	-	-	-	-	-	-
WT (protocol 2a)	69	-	-	-	-	-	-	-	-
WT (protocol 1c)	82	≥ 49	≥ 39	89	≥ 71	41	≥ 32	92	-
reduced WT (protocol 1c)	87	≥ 35	≥ 25	95	≥ 68	60	≥ 43	96	-
C15A-C17A (protocol 2a)	76	≥ 29	-	91	-	<u>62</u>	-	91	<u>68</u>

3.4 Cysteine accessibility

GCAP5 WT possesses five (Figure A1), the C15A-C17A mutant three cysteines. When switching between conformations, the cysteine accessibility of a protein can change. The calcium dependent cysteine accessibility of GCAP5 was determined with DTNB (Figure 17) by comparing the extinction at 412 nm with an L-cysteine calibration line. For each DTNB solution, a new calibration line was made. The significance of differences in the cysteine accessibility was tested statistically with the student t-test and with the Mann-Whitney rank sum test using the software SigmaPlot. If no test is stated in the following text, the t-test failed and the p-value was determined with the Mann-Whitney rank sum test.

Myristoylated zebrafish GCAP3 does not contain cysteines (Figure A1) and, therefore, served as a negative control (Figure 17, myristoylated GCAP3). Independent of the [Ca²⁺] (Mann-Whitney rank sum test: $p = 0.965$, t-test: $p = 0.985$), no cysteine was detected. All GCAP5 variants possess accessible cysteines. In comparison to the Ca²⁺-free protein, around one less cysteine was detected in the presence of Ca²⁺ for WT ($p = 0.002$) and for reduced WT (Mann-Whitney rank sum test: $p = 0.005$, t-test: $p = 0.001$), respectively. In the case of C15A-C17A, up to two less cysteines were accessible ($p < 0.001$). Non-myristoylated WT did not show a statistically significant decrease in the cysteine accessibility. However, with a p-value of 0.052, I would not exclude the possibility that there is a difference.

Up to three cysteines of non-myristoylated WT were accessible. In comparison, myristoylation diminished the accessibility by one to two cysteines (EGTA: $p < 0.001$, CaCl₂: $p = 0.002$), whereas reduction uncovered up to three cysteines in the absence of Ca²⁺ ($p = 0.014$), even though reduced WT was myristoylated. In the presence of Ca²⁺, this difference between non-myristoylated WT and reduced WT was not statistically significant (Mann-Whitney rank sum test: $p = 0.092$, t-test: $p = 0.056$). Here, the p-value, especially of the t-test, was too small to exclude a redox-dependency. C15A-C17A was the only GCAP5 variant whose cysteines were all

accessible in the absence of Ca^{2+} . With three cysteines, it was the same amount as for non-myr WT ($p = 0.479$).

Generally, the presence of Ca^{2+} lowered the cysteine accessibility. The same goes for myristoylation, whereas reduction showed the opposite effect. The largest Ca^{2+} -dependency was seen for C15A-C17A.

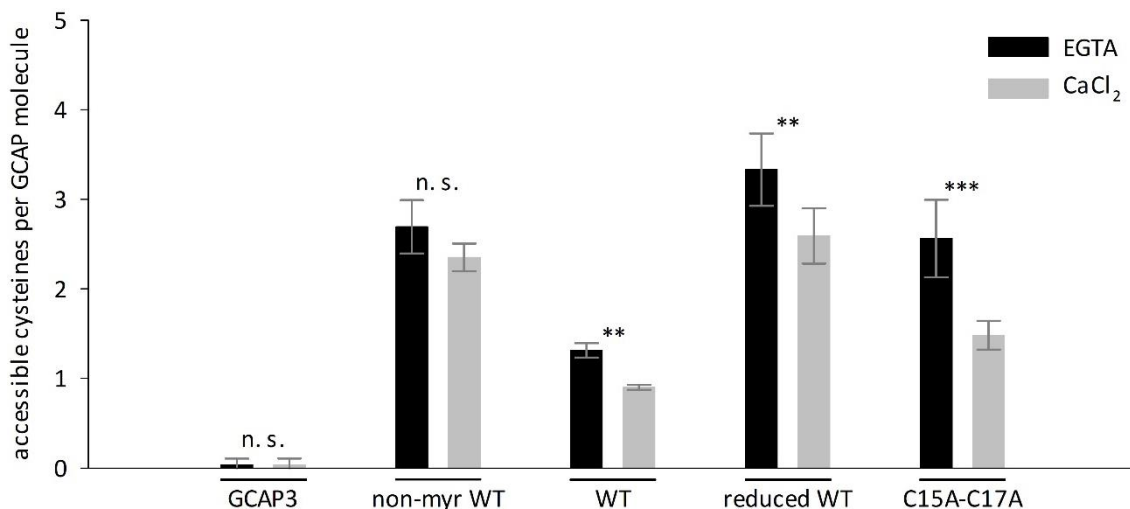


Figure 17: Cysteine accessibility of GCAP5.

Cysteine accessibilities of recombinant GCAP5 (5 μM) non-myr WT, WT, reduced WT, and C15A-C17A were determined in the absence of free calcium (100 μM EGTA, black bars) and in the presence of calcium (1 mM CaCl_2 , grey bars), respectively. Myristoylated zebrafish GCAP3 (GCAP3) does not contain any cysteine and served as a negative control. Protein samples were mixed with DTNB (end concentration 60 μM), and after 10 min of incubation, the extinction at 412 nm was measured. Bars indicate the mean, error bars the standard deviation. Sample size n is six for WT with CaCl_2 , eight for reduced WT under both conditions, and nine for all other categories. Significance of differences between the Ca^{2+} conditions were tested with the Mann-Whitney rank sum test. For reduced WT, the conditions for the t-test were given, resulting in a highly significant difference. Significance levels are highly significant (***: $p \leq 0.001$), moderately significant (**: $p \leq 0.01$), significant (*: $p \leq 0.05$) and non-significant (n. s.: $p > 0.05$). Data listed in Table A7.

3.5 Tryptophan fluorescence

GCAP5 possesses two intrinsic tryptophans, W20 and W93. This allows to investigate Ca^{2+} -dependent conformational changes of GCAP5 by tryptophan fluorescence spectroscopy. The $[\text{Ca}^{2+}]_{\text{free}}$ of the sample solutions were determined with fura-2 previously.

For each $[\text{Ca}^{2+}]_{\text{free}}$, the AU of the fluorescence intensity maximum (F_{max}) and the wavelength of the F_{max} (λ_{max}) were determined. Independent of the $[\text{Ca}^{2+}]_{\text{free}}$ and of the GCAP5 variant, the λ_{max} was always around 335 nm, ranging from 328 to 341 nm (Figure A9, Table A10). The Ca^{2+} -dependent course of F_{max} differed between the GCAP5 variants (Figure 18, Table A9). The clearest change was observed for C15A-C17A (J-L, blue). Up to around 100 nM $[\text{Ca}^{2+}]_{\text{free}}$, F_{max} was decreasing. At higher $[\text{Ca}^{2+}]_{\text{free}}$, until around 10 μM , it increased, whereas F_{max} dropped down again at even further increasing $[\text{Ca}^{2+}]_{\text{free}}$.

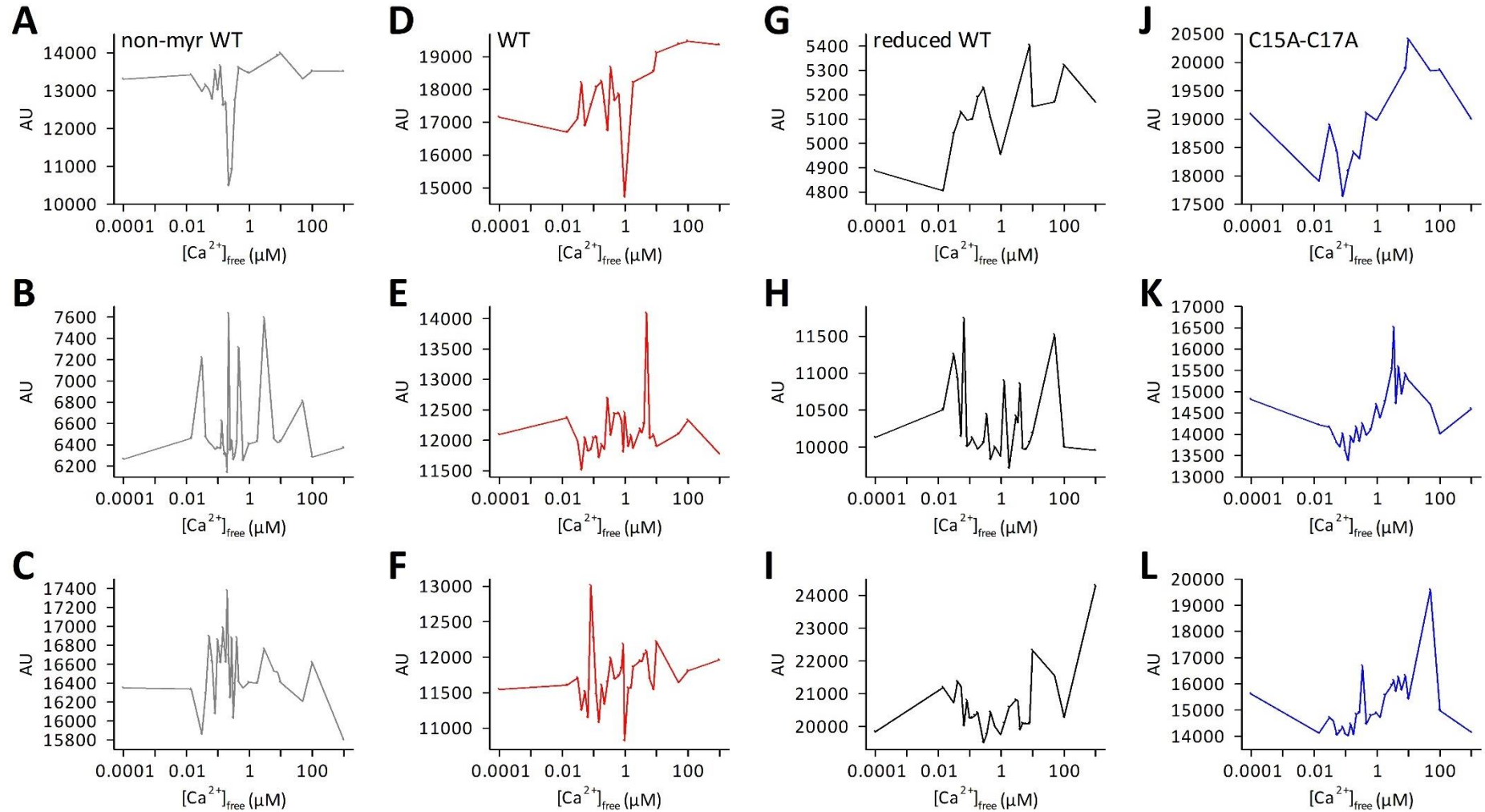


Figure 18: Ca^{2+} -dependent tryptophan fluorescence of GCAP5.

Three independent Ca^{2+} -titrations of GCAP5 (A-C) non-myristoylated WT (grey), (D-F) WT (red), (G-I) reduced WT (black), and (J-L) C15A-C17A (blue), respectively. Single $[\text{Ca}^{2+}]_{\text{free}}$ differ between the measurements, but all are in the range of 1 nM to 1 M $[\text{Ca}^{2+}]_{\text{free}}$. Lyophilized recombinant GCAP5 (500 μg) was resuspended in fluorescence buffer. Potential aggregates were pelleted, and the supernatant was filled up to 15-17 mL. Tryptophans were excited at 280 nm. The emission spectrum was recorded from 300 to 420 nm in 2 nm steps and smoothed (FeliX32). The fluorescence intensity maximum of each smoothed spectrum is plotted against the $[\text{Ca}^{2+}]_{\text{free}}$ in μM . Note that the y-scales vary due to differing solubilities of the GCAP5 variants. Data listed in Table A9.

A similar yet small tendency could be seen for WT (D-F, red). However, the changes were by far not as steep as for C15A-C17A. The results of non-myr WT (A-C, grey) and reduced WT (G-I, black) are hard to interpret due to large outliers. Non-myr WT did not seem to change its F_{\max} in a Ca^{2+} -dependent manner. Reduced WT showed an increase in the fluorescence intensity in one measurement (G). In the other two measurements, the F_{\max} was increasing until around 50 nM and then decreasing until around 8 μM free Ca^{2+} . If there really were differences, probably they were very small, though.

λ_{\max} indicated that the two tryptophans of GCAP5 were partially buried in the interior of the protein, independent of the $[\text{Ca}^{2+}]_{\text{free}}$. Non-myr WT and reduced WT did not show a clear Ca^{2+} -dependent conformational change with the tryptophan fluorescence spectroscopy. WT might change its conformation in a Ca^{2+} -dependent manner, but the change seemed to be very small. The C15A-C17A mutant showed a biphasic fluorescence change.

3.6 GC assay

GCAPs are known to regulate GCs in a Ca^{2+} -dependent manner, showing high activity at low $[\text{Ca}^{2+}]_{\text{free}}$ followed by a sigmoidal decrease of the GC activity with increasing $[\text{Ca}^{2+}]_{\text{free}}$ and low activity at high $[\text{Ca}^{2+}]_{\text{free}}$ (Hwang and Koch 2002; Hwang et al. 2003; Scholten and Koch 2011). So far, zebrafish GCs could not be expressed functionally in heterologous expression systems. Therefore, we use GCs of other species. Non-myristoylated GCAP5 was a rather weak activator of the bovine GC-E in former studies (Scholten and Koch 2011). The authors used a GC-E obtained from bovine rod outer segments. Today, we have access to a HEK293 cell line stably expressing the human GC-E, which provides several advantages (see section 2.8). Thus, I tested the activation profile of GCAP5 with this recombinant human GC-E with a calcium titration (Figure 19).

Since the Ca^{2+} -dependent differences were rather small for some variants, the results for each GCAP5 variant normalized to the value of the lowest $[\text{Ca}^{2+}]_{\text{free}}$ are shown separately (Figure 19 A-D). To compare the magnitude of GC-E activation between the GCCAP5 variants, representative measurements of each variant are shown (Figure 19 E). These were normalized to the value of the lowest $[\text{Ca}^{2+}]_{\text{free}}$ of non-myr WT incubated with the same GC-E solution as the respective other GCAP5 variant.

Non-myr WT showed a surprising GC-E activation profile (Figure 19 A). Instead of inhibiting the GC-E with increasing $[\text{Ca}^{2+}]_{\text{free}}$ as shown for the bovine GC-E (Scholten and Koch 2011), non-myr WT activated the human GC-E with increasing $[\text{Ca}^{2+}]_{\text{free}}$. At around 1 μM $[\text{Ca}^{2+}]_{\text{free}}$, an intermediate plateau was reached until 10 μM . At higher $[\text{Ca}^{2+}]_{\text{free}}$ until 100 μM , the GC-E activity increased further.

The activation profile of WT was a little more like one would expect with respect to the physiological range of $[\text{Ca}^{2+}]_{\text{free}}$ (Figure 19 B). After a slight increase in the GC-E activity from 1.77 nM to 29 nM $[\text{Ca}^{2+}]_{\text{free}}$, the GC-E activity decreased until around 1 μM $[\text{Ca}^{2+}]_{\text{free}}$. Unexpectedly, the GC-E activity increased again with

further increasing $[Ca^{2+}]_{free}$. However, this $[Ca^{2+}]$ range is out of the physiological range. In comparison to non-myr WT, the human GC-E activation of WT was around two to four times higher within the physiological range of $[Ca^{2+}]_{free}$ (Figure 19 E). The ratio decreased with increasing $[Ca^{2+}]_{free}$. Thus, myristoylation of GCAP5 seems to enhance the GC activation.

Reduced WT did not show a clear Ca^{2+} -dependent human GC-E activation (Figure 19 C). Reducing conditions during the GC assay were achieved by using 5 mM DTT in the reaction solution instead of 1 mM. From 1.77 nM to 29 nM $[Ca^{2+}]_{free}$, the GC-E activity slightly increased. At higher $[Ca^{2+}]_{free}$, the activity stayed more or less the same, maybe slightly decreasing at $[Ca^{2+}]_{free}$ higher than 1 μ M. The very high standard deviations were also present in the triple measurements of one experiment, indicating that reduction renders GCAP5 nearly insensitive to $[Ca^{2+}]$ changes. Within the physiological range, reduced WT activated the human GC-E between 13 and 19 times stronger than non-myr WT and around six times stronger than WT (Figure 19 E). The human GC-E activity was not altered by the higher DTT concentration (see Figure 20 C). Thus, redox processes may play a role in the GC activity regulation in zebrafish photoreceptors.

The C15A-C17A mutant showed a GC activation profile as known from other GCAP isoforms (Figure 19 D). GC-E activity was highest at the lowest $[Ca^{2+}]_{free}$ and decreased in a sigmoidal manner with increasing $[Ca^{2+}]_{free}$. The half maximal activation (IC_{50}) was at $0.124 \pm 0.006 \mu$ M $[Ca^{2+}]_{free}$ ($p < 0.001$). The x-fold activation was 8.9 ± 0.7 . In relation to non-myr WT, the human GC-E activation of C15A-C17A was around eight times higher at high $[Ca^{2+}]_{free}$ and 36 times higher at low $[Ca^{2+}]_{free}$ (Figure 19 E) concerning the physiological range of $[Ca^{2+}]_{free}$. If compared to WT, the GC-E activity was four to ten times higher when regulated by C15A-C17A. These results suggest that C15 and/or C17 are critical amino acid positions controlling the activation profile of GCAP5, and cysteines in this position can significantly impair the activating properties.

WT and C15A-C17A were also tested in the presence and absence of Ca^{2+} and/or Fe^{2+} (Figure 20; results already published in Lim et al. 2017). WT neither showed a calcium dependent human GC-E activation in the presence nor in the absence of Fe^{2+} (Figure 20 A). Addition of Fe^{2+} inhibited the GCAP5 mediated GC-E activity. This was not an effect of Fe^{2+} or the higher DTT concentration on the human GC-E itself (Figure 20 C): Control incubations of human GC-E without GCAPs showed no effect of Fe^{2+} on the basal activity. Also, the GC-E activity was not influenced by the Mes buffer used for loading GCAPs with Fe^{2+} (Figure 20 B). In the absence of Fe^{2+} , no difference was observed between the human GCAP1 mediated GC-E activity in established sodium phosphate buffer and in the tested Mes buffer. However, in the absence of Ca^{2+} , the human GCAP1 mediated GC-E activity went down to the level of Ca^{2+} -induced inhibition of the GC-E when incubated with Fe^{2+} .

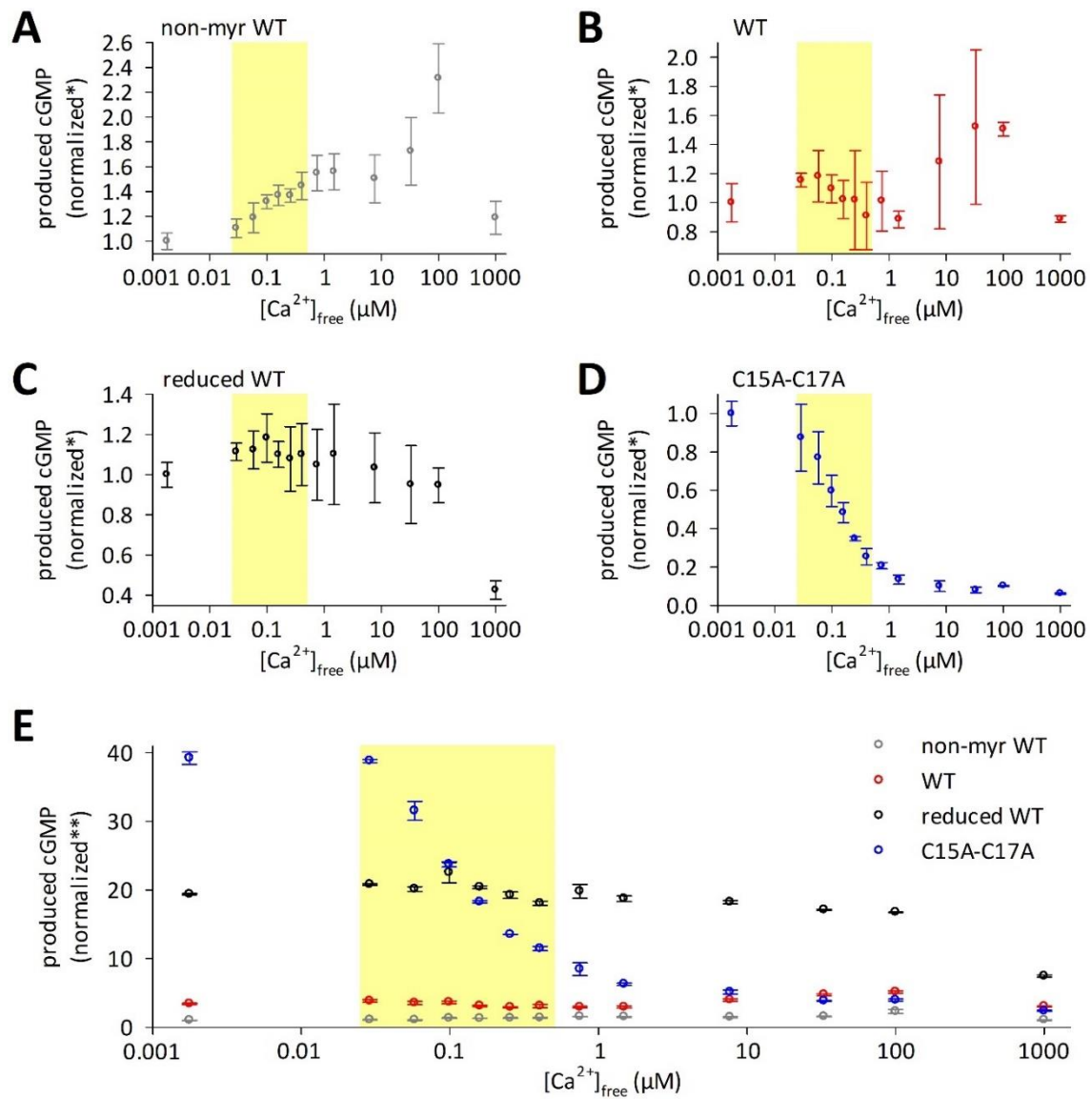


Figure 19: Ca²⁺-dependent human GC-E activation profile by GCAP5.

Recombinant human GC-E was incubated with recombinant GCAP5 (10 μM) (A) non-myristoylated WT (1 mM DTT), (B) WT (1 mM DTT), (C) reduced WT (5 mM DTT), and (D) C15A-C17A (1 mM DTT). Circles indicate the mean, error bars the standard deviation of three sets normalized to the mean at 1.77 nM [Ca²⁺]_{free} (normalized*). One set consists of three measurements. (E) Representative set of all four GCAP5 variants normalized to the mean of non-myristoylated WT at 1.77 nM [Ca²⁺]_{free} (normalized**). X-scales are logarithmic. The physiological [Ca²⁺]_{free} is highlighted in yellow. Data of A-D listed in Table A12. Data of E listed in Table A13.

In contrast to WT, the C15A-C17A mutant showed a Ca²⁺-dependent human GC-E activation in the absence of Fe²⁺ as known from other GCAPs (Figure 20 A). Adding of Fe²⁺ decreased the GC-E activity in the absence of Ca²⁺, but a Ca²⁺-dependency remained. Since C15A-C17A does not bind Fe²⁺ in the nanomolar range (Lim et al. 2017), and the [Fe²⁺] was set to 100 nM, the effect of Fe²⁺ on the GC-E activity mediated by C15A-C17A as well as human GCAP1 might have occurred due to the equilibrium between the applied chelator EGTA with both Ca²⁺ and Fe²⁺.

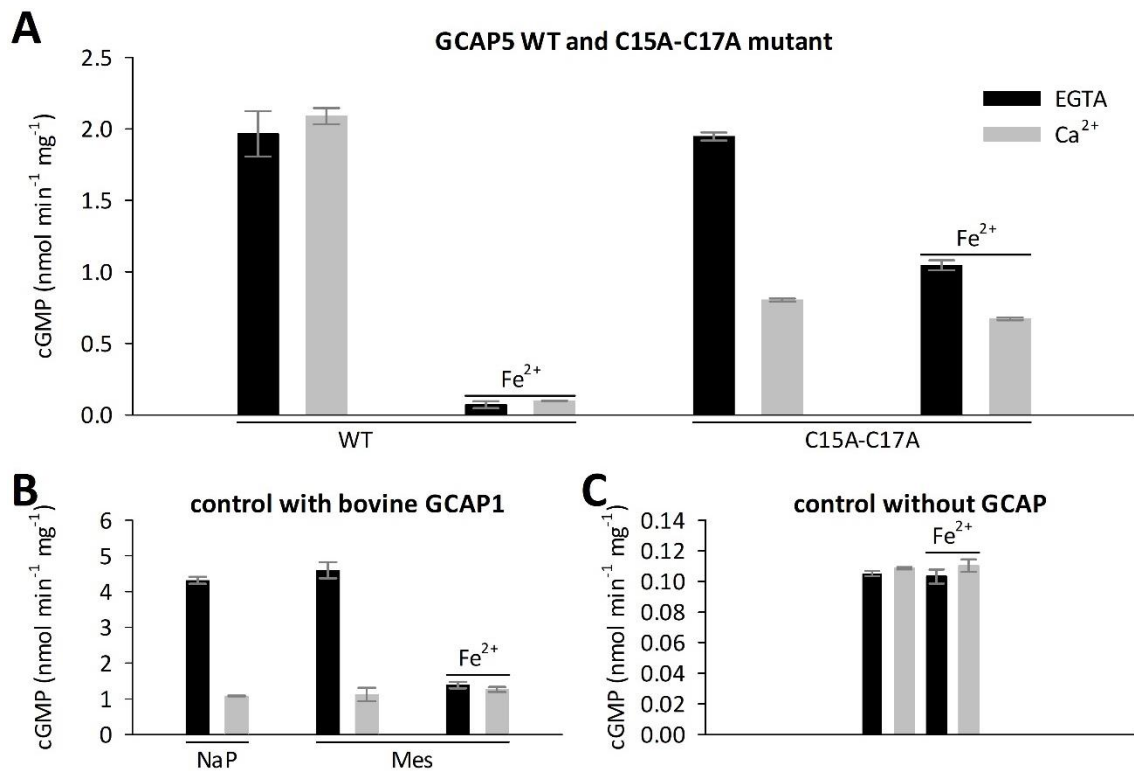


Figure 20: Fe²⁺-dependent human GC-E activation by GCAP5 WT and C15A-C17A mutant.

(A) Recombinant human GC-E was incubated with recombinant GCAP5 (10 μ M) WT or C15A-C17A in the presence of EGTA (< 10 nM, black bars) or in the presence of Ca²⁺ (1.5 μ M [Ca²⁺]_{free}, grey bars) and/or in the presence of Fe²⁺ (100 nM) combined with a higher DTT concentration (5 mM instead of 1 mM). (B) Control incubations of recombinant human GC-E with recombinant myristoylated bovine GCAP1 (10 μ M) in the absence and presence of Fe²⁺, respectively. Lyophilized bovine GCAP1 was either resuspended in sodium phosphate buffer (NaP) or in Mes buffer like GCAP5. (C) Control incubation of recombinant human GC-E without GCAPs in the presence and absence, respectively, of Ca²⁺ and/or Fe²⁺ in Mes buffer. Black and grey bars in B and C are as indicated in A. Error bars indicate the standard deviation. Modified from Lim et al. 2017. Data listed in Table A14.

3.7 Localization of GCAP5 in photoreceptors of the zebrafish retina

In addition to the *in vitro* experiments, GCAP5 should be localized in photoreceptors of the adult zebrafish retina *in situ*. This was already done using fast red by Fries (2013). For co-localization studies, the antibody against GCAP5 (anti-GCAP5, previously described by Fries 2013) was tested with fluorescence markers.

To assure that the antibody was still working, it was tested on subcellular fractions of the zebrafish retina by western blotting and subsequent immunodetection first (Figure 21 A). Myristoylated GCAP5 has a mobility of around 18 kDa in SDS-polyacrylamide gels (Figure 21 A, black arrow; Fries 2013; see also section 3.1). The cytosolic fraction (c) showed a band at this mobility. The membrane fraction (m) also showed this band but with weaker intensity. This indicates that GCAP5 is a cytosolic protein that might also form complexes with membrane bound proteins in the zebrafish retina. The positive control (+) showed a triple band between 15 kDa and 20 kDa. The most intense band of the positive control (black arrow), which probably is myristoylated GCAP5 (Fries 2013, see also 3.1 and Figure 13), had the same mobility as GCAP5 in the cytosolic fraction. Therefore, the native GCAP5 might be myristoylated in the zebrafish retina. This is

consistent with previous results (Fries 2013). Recombinant GCAP5 formed dimers with a mobility of around 37 kDa (blue arrow). This band was not visible in the subcellular fractions. However, the amount of GCAP5 in the retinal fractions applied onto the gel might have been too low to detect a non-myristoylated GCAP5 and a dimer in the native tissue after 3 min of illumination. Longer illumination also revealed two bands around the mobility of putative non-myristoylated GCAP5 and of dimeric GCAP5 (Figure A11 A). This indicates that GCAP5 is only partially myristoylated in the native tissue. The negative control recombinant myristoylated zebrafish GCAP3 (-) showed no signal.

Further, dilutions of 1:250, 1:1000, 1:2000, and 1:5000 of the antibody rabbit anti-GCAP5 were tested for western blotting and subsequent immunodetection. A dilution of 1:1000 was still sufficient for detecting 2 ng of purified recombinant GCAP5 (Figure A11 B). However, for detecting GCAP5 in subcellular fractions of the retina, I would suggest the 1:250 dilution, if 5 µg of total protein are used for western blotting.

After reconfirming the specificity and sensitivity of the anti-GCAP5 antibody, it was tested for fluorescent immunohistochemistry staining on cryosections of the zebrafish retina. Therefore, different conditions were tested. The optimized conditions are described in section 2.11.4. Less well working conditions (not shown) were washing with TBS instead of with PB, using TBST for blocking solution and antibody solutions instead of PB/Triton X-100, and using the ChemiBLOCKER (Sigma-Aldrich) instead of NDS (*Santa Cruz Biotechnology*). Mounting in VectaShield (*Vector Laboratories*) resulted in better fluorescence signals than mounting in Aqua Poly/Mount (*Polysciences*). Dilutions of the rabbit anti-GCAP5 antibody tested are 1:500, 1:1000, 1:2000, 1:3000, and 1:4000. The 1:2000 dilution resulted in sufficient fluorescence signals, whereas the fluorescence intensity decreased with higher dilutions (not shown). The secondary antibody donkey-F(ab')₂ anti-rabbit Alexa Fluor®488 (*Jackson ImmunoResearch*) seemed to penetrate deeper into the tissue section than the antibody donkey anti-rabbit Alexa Fluor®488 (*Invitrogen*), resulting in better spatial evaluation of the staining. Using the donkey antibody led to a somehow punctuated pattern (Figure A12), whereas the donkey-F(ab')₂ antibody generated a much smoother staining (Figure 21, Figure 22).

The stained cryosections showed anti-GCAP5 immunoreactivity in the outer plexiform layer (OPL) as well as in the inner segments and outer segments of zebrafish cones (Figure 21 C, D, G). Categorizations of cone types in the following were made based on their morphology (see section 1.5). A SSC showed immunoreactivity in the inner segment and in the cone pedicle (Figure 21 C, two violet arrowheads). The inner segment and the outer segment of another SSC were stained as well (Figure 21 C white box, and D violet arrowhead). A strong fluorescence signal was observed in the outer segment of either a LSC or a DC (Figure 21 C, white arrowhead). The control (Figure 21 E) showed low background of the secondary antibody in cone outer segments, in the ellipsoid of the inner segments, and very low background in the OPL. On another stained cryosection (Figure 21 G), several SSCs (violet arrowheads) showed immunoreactivity of the anti-GCAP5 antibody. One SSC (violet circle in the myoid) was stained from the

outer segment over the inner segment to the cone pedicle, indicating that GCAP5 is present in the whole SSCs except for the unstained nuclei and mitochondria in the myoid of inner segments. In addition, inner segments of LSCs (blue arrowheads) and DCs (orange arrowheads) were stained on this cryosection. These results indicate that GCAP5 expression is especially strong in SSCs but also present in LSCs and DCs, which is consistent with previous findings received with fast red by Fries (2013).

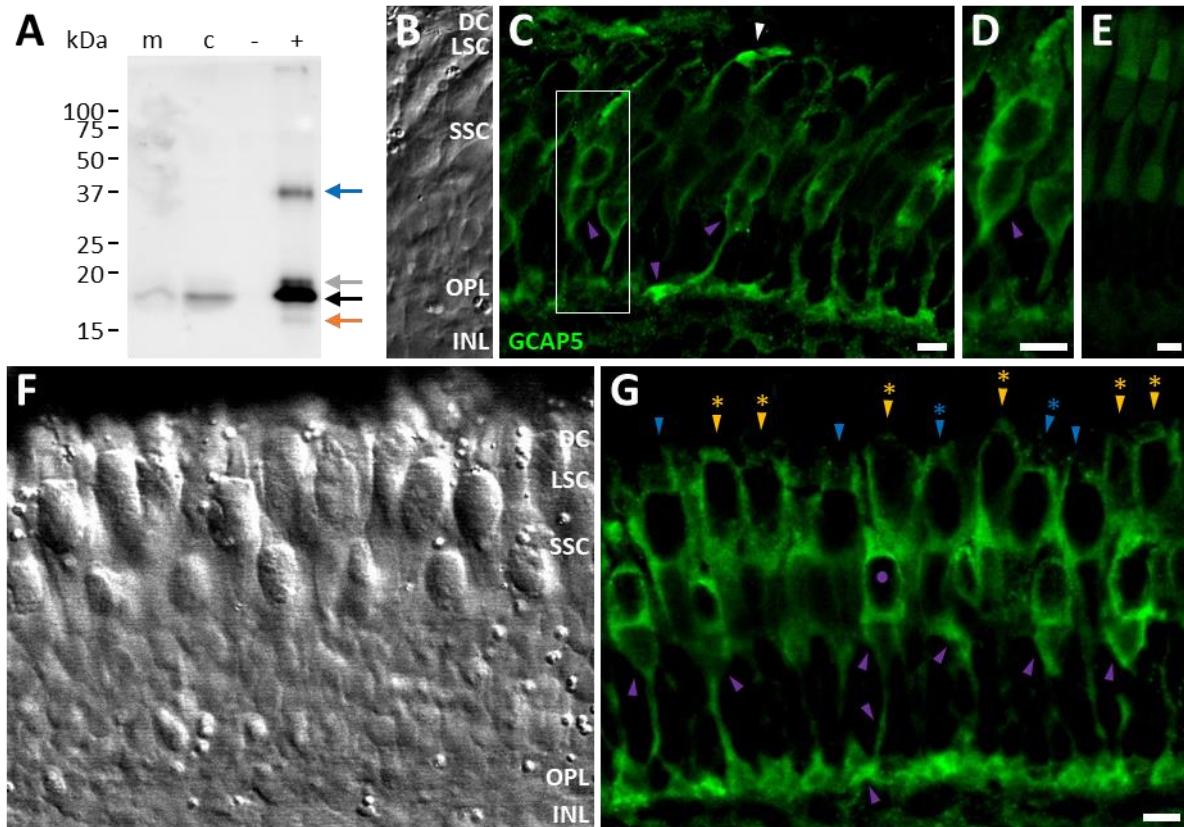


Figure 21: GCAP5 immunoreactivity in the zebrafish retina and in photoreceptors.

(A) Western blot after 3 min of illumination showing GCAP5 immunoreactivity (primary antibody rabbit anti-GCAP5, 1:250, secondary antibody goat anti-rabbit POD, 1:5000) in subcellular fractions of the zebrafish retina (5 μg of total protein; m: membrane fraction, c: cytosolic fraction). Monomeric myristoylated GCAP5 has a mobility of around 18 kDa in SDS-polyacrylamide gels appearing as a triple band. These three bands possibly represent the apo-state of myristoylated GCAP5 (black arrow), the calcium-bound state (orange arrow), which, however, could also be a degraded GCAP5, and the non-myristoylated part of recombinant purified GCAP5 (grey arrow). Dimeric GCAP5 has a mobility of around 37 kDa (blue arrow). The positive control is purified recombinant myristoylated GCAP5 (+, 2 ng), the negative control purified recombinant myristoylated zebrafish GCAP3 (-, 2 ng). (C, D, G) Immunoreactivity pattern of anti-GCAP5 (primary antibody rabbit anti-GCAP5, 1:2000, secondary antibody donkey-F(ab')₂ anti-rabbit Alexa Fluor®488, 1:1000) in sections of the zebrafish retina. Images present projections of 7 x 0.3 μm (C) and of 15 x 0.3 μm (D, G). The white Box in C marks the area of D. Arrowheads point to parts of short single cones (SSC) (violet arrowheads; C, D, G), the outer segment of a long single cone (LSC) or double cone (DC) (white arrowhead; C), LSCs (blue arrowheads; G) and DCs (yellow arrowheads; G), respectively. Stars indicate assumptions of cone classifications. The violet point indicates a SSC with stained outer segment, inner segment, axon, and cone pedicle. (B, G) Layers of the retina are indicated in the transmissions (DC: double cone, LSC: long single cone, SSC: short single cone, OPL: outer plexiform layer, INL: inner nuclear layer). (E) The control without the primary antibody shows background in the photoreceptors (projection of 7 x 0.3 μm). Scale bars: 5 μm. Scale bar in C also applies to B, scale bar in G also applies to F.

In addition to the single staining, I tested a co-localization of GCAP5 and *zpr1*, a marker for arrestin 3a (Larison and Bremiller 1990; Zou et al. 2008; Nadolski et al. 2020), which is expressed in DCs specifically (Figure 22). The overlay revealed expression of GCAP5 in the inner segments, axons, and cone pedicles of DCs (white arrows). However, not all DCs were stained by the anti-GCAP5 antibody (orange arrowheads). This might be a hint that only the green-sensitive or the red-sensitive cone type expresses GCAP5 or that the expression level in one of these cone types is very low. The outer segments were not covered well in this section, prohibiting a sound conclusion. The control staining of both secondary antibodies showed low background in the inner and outer segments of photoreceptors and very low background in the OPL.

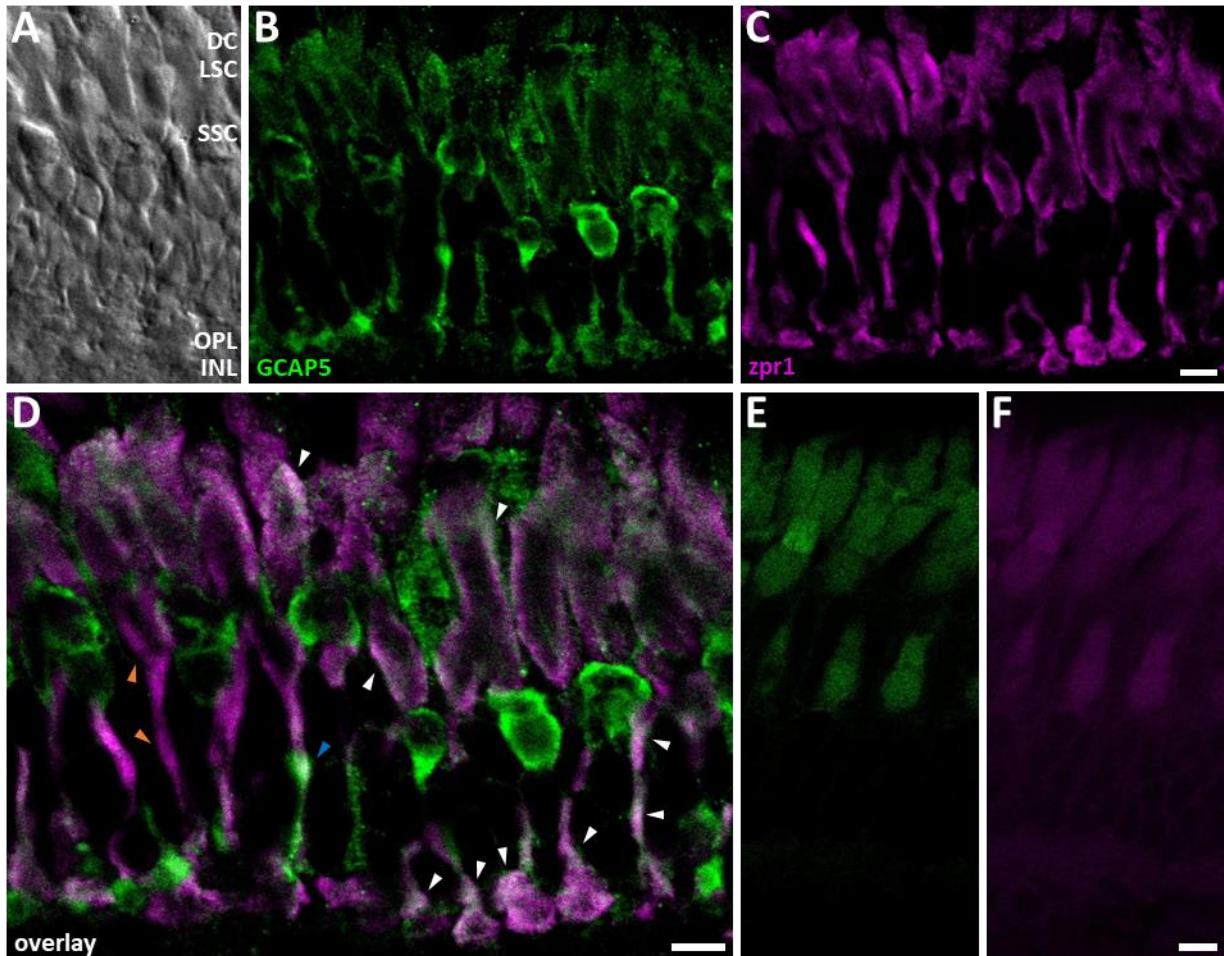


Figure 22: Localization of GCAP5 in double cones of the zebrafish retina.

(B) Immunoreactivity pattern of anti-GCAP5 (primary antibody rabbit anti-GCAP5, 1:2000; secondary antibody donkey-F(ab')₂ anti-rabbit Alexa Fluor®488, 1:1000, green). (C) Immunoreactivity pattern of the monoclonal antibody *zpr1* (Zebrafish International Research Center, 1:1000; secondary antibody donkey anti-mouse-Alexa Fluor®568, 1:1000, magenta). *zpr1* detects cone arrestin 3a, which is expressed in double cones specifically. (D) Immunohistochemical co-staining against GCAP5 and with the monoclonal antibody *zpr1* (projection of 3 x 0.3 μm). The staining against GCAP5 and the *zpr1* staining partially overlap in the merged picture (white arrowheads pointing to white spots). Orange arrowheads point to the inner segment and the axon of a double cone not showing GCAP5 staining. The blue arrowhead points to a structure that seems to show an overlapping signal in the projection but is not overlapping in single scans. (A) Layers of the Retina are indicated in the transmission (DC: double cone, LSC: long single cone, SSC: short single cone, OPL: outer plexiform layer, INL: inner nuclear layer). (E, F) The controls for the secondary antibodies both show background in the photoreceptors (projection of 3 x 0.3 μm). Scale bars: 5μm. Scale bar in D also applies to A-C, scale bar in F also applies to E.

4 Discussion

4.1 Purification of GCAP5

The first goal was to establish a purification protocol of recombinant GCAP5 with a minimum purity of 90 % and a yield of at least 1 mg protein out of 500 mL *E. coli* culture. For this purpose, I tried the standard protocol of the Division of Biochemistry (*University of Oldenburg*) (Table 2, protocol 1a) and the purification protocol of the Department of Chemistry (*UC Davis*) (Table 3, protocol 2a), which resulted either in a sufficient yield with insufficient purity or in a high purity but very low yield, respectively (Figure A2, Figure A3). The main differences between these purification protocols were purification from inclusion bodies (protocol 1a) or the cytosolic fraction (protocol 2a) after cell lysis, enzymatic cell lysis with lysozyme (protocol 1a) or physical lysis by ultrasonication (protocol 2a), and different FPLC columns. Due to the following reasons, it seemed reasonable to optimize the purification of GCAP5 from inclusion bodies: First, GCAP5 tends to accumulate in inclusion bodies rather than being soluble during expression in *E. coli* (Scholten and Koch 2011). Second, comparative experiments with non-myristoylated GCAP5 purified from inclusion bodies and from the cytosolic fraction, respectively, led to similar results (Scholten and Koch 2011). I achieved GCAP5 of desired purity and yield by exchanging the AEC column RESOURCE Q (*GE Healthcare*) by the AEC column Hi Trap Q HP (*Cytiva*) in the purification protocol of the Division of Biochemistry (*University of Oldenburg*) (protocol 1c; see section 3.1).

Using this protocol 1c, I purified all GCAP5 variants to analyze their dimerization rate by analytical SEC (see section 3.2), their cysteine accessibility using DTNB (see section 3.4), their conformational changes by intrinsic tryptophan fluorescence measurements (see section 3.5), and their Ca^{2+} -dependent target regulation by GC assay measurements with Ca^{2+} -titrations (see section 3.6). Moreover, I used GCAP5 purified using protocol 2a for the Fe^{2+} -dependent GC assay (see section 3.6) to exclude with complete certainty differences between GCAP5 used for target regulation analysis by me and GCAP5 used for NMR structural studies by our cooperation partners of the Department of Chemistry (*UC Davis*) for our publication (Lim et al. 2017). The only analysis in which I included both GCAP5 purified according to protocol 1c and GCAP5 purified according to protocol 2a is the myristoylation rate analysis by reversed phase-HPLC (see section 3.3).

With this method, we expect only one peak in the reversed phase-HPLC chromatogram of non-myristoylated GCAP5 and two peaks in the chromatogram of myristoylated GCAP5. In the latter, the first peak, representing the non-myristoylated part of purified GCAP5, would have the same retention time as the peak in the chromatogram of non-myristoylated GCAP5, whereas the second peak, representing the myristoylated part of purified GCAP5, would have a higher retention time due to higher hydrophobicity, given by the covalently attached myristoyl group. While the reversed phase-HPLC chromatogram of GCAP5 WT purified using protocol 2a met these expectations, the chromatogram of GCAP5 WT purified according

to protocol 1c showed four peaks. This proves that the purification of GCAP5 from inclusion bodies by denaturing and subsequently renaturing the protein affects the biochemical properties of GCAP5. The additional peaks could result from aggregated GCAP5 since GCAP5 purified using protocol 1c showed high aggregation rates, even though I precipitated possible aggregates by centrifugation and used only the supernatant for analytical SEC measurements (see section 3.2). Unfortunately, this result means that all following interpretations must be read with caution, and the experiments with recombinant GCAP5 should be repeated with GCAP5 purified from the cytosolic fraction after cell lysis.

For future experiments with recombinant GCAP5, I suggest purifying the protein from the soluble fraction after cell lysis. One possibility is to perform batch purifications according to protocol 2a despite the low yield. With each batch, each experiment would be performed once. To reproduce the results of one batch, a new batch of GCAP5 would be purified and analyzed. A second possibility is using another vector and adjusting the parameters for expression in *E. coli* accordingly. I used the vector pET21a(+) (*Novagen*), which contains the T7 promoter for fast expression of high amounts of protein (Studier and Moffatt 1986; Tabor 2001; Kaur et al. 2018). However, if the expression is too fast, the protein might misfold, leading to inclusion bodies (Kaur et al. 2018), which is the case for GCAP5 (Scholten and Koch 2011). Therefore, it could be advantageous to clone the GCAP5 DNA into another vector that increases the solubility of the protein in comparison to the T7 promoter. For example, the pCold vector (*Takara Bio*), which includes the cold-shock Protein A promoter, meets this criterion.

4.2 Fine-tuning of GCAP5 by myristoylation

Myristoylation has substantial effects on the stability and regulatory properties of mammalian GCAP1 (Hwang and Koch 2002; Hwang et al. 2003; Peshenko et al. 2012). That myristoylation also affects target regulatory properties of GCAP5 was shown by Sulmann et al. (2015), who compared their data of myristoylated GCAP5 with previously published data of non-myristoylated GCAP5 (Scholten and Koch 2011). Because of this, I included non-myristoylated and myristoylated GCAP5 in my studies to further examine the effects of myristoylation on the biochemical characteristics of GCAP5. Since we use the yeast NMT for co-expression in *E. coli*, and the native GCAP5 harbors an aspartate residue at position three favoring acetylation, I used GCAP5 with a D3N mutation for all of my experiments.

Unfortunately, the myristoylation rate analysis of purified recombinant GCAP5 by reversed phase-HPLC (see section 3.3) was inconclusive and raised questions regarding the conditions of heterologous expression in *E. coli* and the purification protocol (discussed in section 4.1). While the reversed phase-HPLC chromatograms (Figure 16) of GCAP5 purified from the cytosolic fraction (purification protocol 2a, Table 3) were reasonable, resulting in a myristoylation rate of GCAP5 WT around 69 %, the chromatograms of GCAP5 purified from inclusion bodies (purification protocol 1c, Table 2) led to several possible

interpretations with potential myristoylation rates between 25 % and 96 % (Table 8). It was already shown that preparations of purified recombinant myristoylated GCAP often include trace amounts of non-myristoylated GCAP (Olshevskaya et al. 1997). Surprisingly, non-myristoylated GCAP, in comparison to myristoylated GCAP, shows a lower mobility of 1 kDa in SDS-polyacrylamide gels, even though myristoylation adds around 210 Da to the protein mass (Olshevskaya et al. 1997; Hwang and Koch 2002). This characteristic was also utilized by Fries (2013) to show that GCAP5 is most likely myristoylated in its native tissue, which is consistent with my result of the western blotting regarding the specificity of the anti-GCAP5 antibody (Figure 21; discussed in section 4.6). Trace amounts of non-myristoylated GCAP5 could also be seen in the SDS-polyacrylamide gels used to monitor the purification progress after the AEC (Figure 13 D and F, grey arrows). The triple band most likely comprised non-myristoylated GCAP5 (grey arrow), myristoylated GCAP5 in its apo-form (black arrow), and myristoylated GCAP5 in its Ca²⁺-bound form (orange arrow). Even if assuming that both the band for putative non-myristoylated and the band for putative Ca²⁺-bound myristoylated GCAP5 were non-myristoylated GCAP5, the intensity of the band for myristoylated GCAP5 was still high enough to amount to more than 60 % of the total intensity of all three bands. Thus, I assume that the myristoylation rate of the recombinant myristoylated GCAP5 variants was at least 60 %. That recombinant GCAP5 does not have a high myristoylation rate is consistent with previous results (Sulmann et al. 2015). Despite the relatively low myristoylation rate and the questions regarding the correct conformation (see section 4.1), myristoylation significantly affects the biochemical properties of GCAP5 that was purified according to protocol 1c (summarized in Table 9).

Table 9: Effect of myristoylation on GCAP5.

Results of analytical SEC (dimer concentration in %, unclear state, monomers, see section 3.2), DTNB measurement (accessible cysteines, see section 3.4), tryptophan fluorescence (conformational change, see section 3.5), and GC assay analysis (target regulation, see section 3.6) of non-myr WT and WT GCAP5 are listed for comparison. Light red background indicates higher values or, in the case of unclear state and monomers, higher observation rates. ¹ The program Primaide could not reliably detect the peak representing dimers and the peak representing the unclear state (Figure 14) as two independent peaks. Therefore, the dimer concentration might be lower than stated.

	dimer concentration (%)	unclear state	monomers	accessible cysteines	conformational change	target regulation
non-myr WT	29 - 38 ¹ redox-dependency	always visible, not always detectable	not always visible/ detectable	2 - 3 no Ca ²⁺ -dependency	no Ca ²⁺ -dependency	very low activity, low Ca ²⁺ -dependency
WT	21 - 34 redox-dependency	-	-	1 - 2 Ca ²⁺ -dependency	very low Ca ²⁺ -dependency	low activity, low Ca ²⁺ -dependency

While myristoylated GCAP5 tends to form dimers (see also Lim et al. 2017) and aggregates, monomers and an unclear state with a hydrodynamic radius between that of monomeric and dimeric GCAP5 were observed for non-myristoylated GCAP5 by analytical SEC additionally (see section 3.2). The retention time of a protein on the analytical SEC column depends notably on the hydrodynamic radius of the protein (Hagel 1989; Irvine 2001). Thus, the correlation between the retention time and the protein size in kDa is

most accurate for spherical proteins, and the accuracy decreases the more the protein's shape differs from a sphere. For example, of several proteins with the same weight, the experimentally determined apparent mass of a spherical protein will be relatively small, around the actual mass of the protein. Higher apparent masses will be determined for oval or non-spherical proteins, and the apparent masses of denatured proteins will be even larger (Yau and Bly 1980; Hagel 1989). Monomeric GCAP5 weighs around 22 kDa (Table 5). The apparent masses associated to the peaks representing the monomeric, the unclear, and the dimeric state were 20 kDa, 36 kDa, and 42 kDa, respectively. Therefore, the unclear state could either be another dimeric form of GCAP5, or it could be denatured GCAP5. Either way, myristoylation seems to stabilize a specific dimeric conformation and prevents the formation of monomeric GCAP5. However, to clearly distinguish between the dimeric and the unclear state, and to reliably detect the monomeric state, the analytical SEC should be repeated with a higher protein load (between 100 μ g and 200 μ g), preferably with GCAP5 purified from the cytosolic fraction after expression in *E. coli* (discussed in section 4.1).

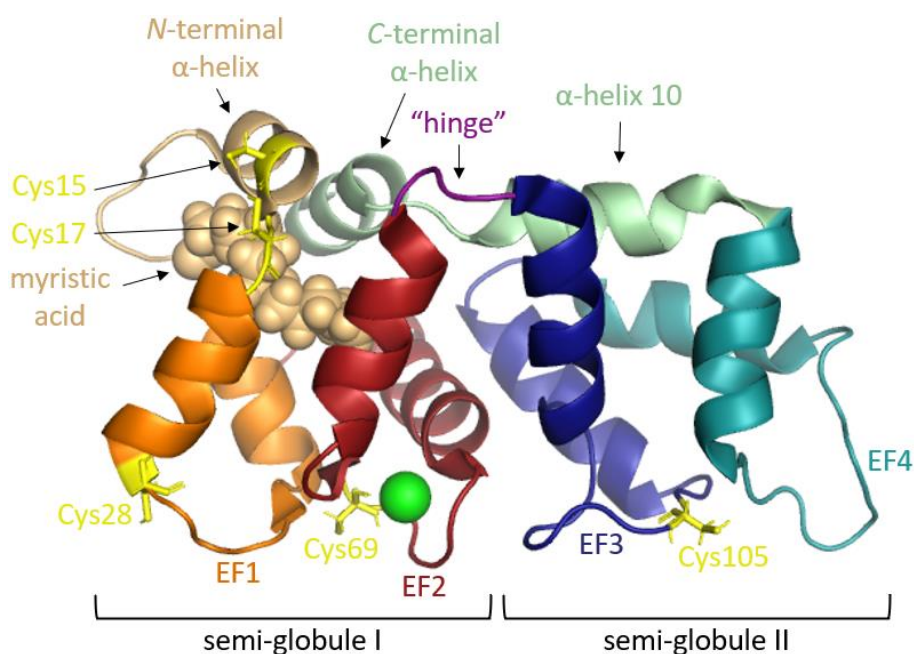


Figure 23: NMR-derived structure of Mg^{2+} -bound, Ca^{2+} -free, and Fe^{2+} -free myristoylated GCAP5.

The tertiary protein structure is presented as a cartoon. Semi-globule I consists of the *N*-terminal (beige), EF hand (EF) 1 (orange), and EF2 (red). EF3 (dark blue), EF4 (dark cyan), and the *C*-terminal helices (light green), including α -helix 10, belong to semi-globule II. Both semi-globules are connected by a hinge-region (violet). A magnesium-ion (green sphere) is bound to EF2. The myristic acid (beige spheres) is covalently attached to the *N*-terminus. Cysteines (Cys15, Cys17, Cys28, Cys69, and Cys105) are depicted as yellow sticks. Color code is identical to the color code of Ca^{2+} -bound chicken GCAP1 (Figure 7 A) for comparison. PDB entry 7M2M (Cudia et al. 2021).

Myristoylation of GCAP5 further shields one to two cysteines (see section 3.4). This is consistent with the results of Hwang and Koch (2002), who observed a shielding effect for one cysteine by myristoylation in bovine GCAP1 and 2. Like in bovine GCAPs, the shielding of cysteines by the myristoyl moiety in GCAP5 might not arise from a direct interaction of cysteines and the myristic acid. Instead, the myristoyl moiety might act as an allosteric regulator and influence a Ca^{2+} -dependent conformational change. This conclusion would be in agreement with the Ca^{2+} -myristoyl tug mechanism (Peshenko et al. 2012; Lim et al. 2016).

Recently, our cooperation partners of the Department of Chemistry (*UC Davis*) presented the NMR-derived structure of Mg²⁺-bound, Ca²⁺-free, and Fe²⁺-free myristoylated GCAP5 (Cudia et al. 2021; Figure 23). The structure is similar to the crystal structure of Ca²⁺-bound chicken GCAP1 (Stephen et al. 2007; Figure 7 A). Comparisons of Ca²⁺-bound and Ca²⁺-free/Mg²⁺-bound GCAP5 revealed that the α -helix 10 and the C-terminal α -helix 11 react similar to the corresponding α -helices in chicken GCAP1 upon Ca²⁺-binding (Cudia et al. 2021). This strongly reinforces the hypothesis of a Ca²⁺-myristoyl tug mechanism for GCAP5. That myristoylation influences a Ca²⁺-dependent conformational change of GCAP5 is further supported by tryptophan fluorescence measurements of non-myr WT and WT (see section 3.5). While no Ca²⁺-dependent differences were observed for non-myr WT, WT showed at least a small tendency of increasing fluorescence emission with increasing [Ca²⁺]_{free}. However, this change was very small, and the data of three measurements varied. Therefore, it should be verified by further tryptophan fluorescence measurements as performed by Peshenko et al. (2019) (discussed in section 4.3). If the tryptophan fluorescence increases with increasing [Ca²⁺]_{free}, this would be consistent with the results of Peshenko et al. (2019), who measured the Ca²⁺-dependent tryptophan fluorescence of bovine GCAP1. An increased Ca²⁺-sensitivity by myristoylation was not seen in GC assay analysis (see section 3.6). Both non-myr WT and WT showed only a very low Ca²⁺-dependency regarding the GC activation. Instead, myristoylation of GCAP5 enhanced the general GC activity by the factor two to four.

The comparison of non-myr WT and WT GCAP5 reveals that myristoylation might stabilize a specific conformation of GCAP5 and eventually renders GCAP5 slightly sensitive to changes in [Ca²⁺]_{free}. The latter is nearly irrelevant for GC activation, but independent of Ca²⁺, the overall GC activity is increased by myristoylation of GCAP5.

4.3 Ca²⁺-sensitivity of GCAP5 is influenced by myristoylation, reduction, and cysteines

Mammalian GCAPs react to Ca²⁺-binding by changing their conformation (see section 1.3.2) and by regulating the activity of retinal GCs (see section 1.3). Their Ca²⁺-sensitivity is fine-tuned among others by myristoylation (see section 1.3.2). Results of previous experiments suggest that the unique N-terminal cysteine cluster of GCAP5, namely Cys15 and Cys17, influence the Ca²⁺-dependent properties of GCAP5 (Gripenstroh 2016). Further, reduction of GCAP5 affected its target regulatory properties, but the results of different authors are inconclusive (Lange 2012; Gripenstroh 2016). My studies confirm that the Ca²⁺-sensitivity of GCAP5 is influenced by myristoylation, by reduction, and by mutation of Cys15 and Cys17 (summarized in Table 10). The effects of myristoylation on GCAP5's Ca²⁺-sensitivity are discussed in section 4.2.

Except for non-myr WT that showed no significant Ca²⁺-dependent cysteine accessibility, Ca²⁺-binding shields at least one cysteine of GCAP5 (see section 3.4). In the case of C15A-C17A, two cysteines became

accessible in the absence of Ca^{2+} , resulting in an exposure of all cysteines present in this mutant. A similar result was reported for bovine GCAP1, which exposes Cys106 located in EF3 only upon chelating of Ca^{2+} with EGTA (Hwang et al. 2001). This cysteine position of bovine GCAP1 corresponds to Cys105 of GCAP5 (Figure A1). The second cysteine that is exposed in C15A-C17A in the absence of free Ca^{2+} might be Cys69 in EF2. This cysteine is not conserved in bovine and zebrafish GCAPs (Figure A1). Since it is located in the loop region of an EF hand similar to Cys105 (Figure 23), both cysteines might be shielded when Ca^{2+} is coordinated in the respective EF hand. Even though myristoylation shields one cysteine of wildtype GCAP5 (discussed in section 4.2), all cysteines of the also myristoylated mutant C15A-C17A were exposed under Ca^{2+} -free conditions. This resulted in the same number of accessible cysteines as for non-myr WT. It is tempting to conclude that Cys15 and Cys17 of non-myr WT and WT are forming disulfide bonds, for example by dimerization. However, the dimer interface of Fe^{2+} -free GCAP5 does not include Cys15 and Cys17 (Cudia et al. 2021), and I measured the cysteine accessibility in the absence of Fe^{2+} . Further, the sulfhydryl groups of the two cysteines should be solvent exposed because the *N*-terminal helix of GCAP5 is elongated by two amino acids in comparison to GCAP1 (Cudia et al. 2021) and the distance of 24 Å between Cys15 residues of Fe^{2+} -free dimeric GCAP5 (Cudia et al. 2021) is too large to be involved in dimerization by forming disulfide bonds. Yet, reduction uncovers two cysteines of WT GCAP5. It cannot be excluded that mutation of Cys15 and Cys17 modifies the way GCAP5 changes its conformation upon binding of Ca^{2+} . This prohibits to assign accessible cysteine residues of C15A-C17A to wildtype GCAP5. To solve this puzzle, further investigation is needed including cysteine mutants as described by Hwang et al. (2001). These investigations should include GCAP5 mutants purified under normal and under reducing conditions as well as testing for disulfide bonds by using iodoacetate derivatives (Hirose et al. 1988; Hollecker 1997; Hwang et al. 2001).

Table 10: Ca^{2+} -dependency of GCAP5.

Results of DTNB measurement (cysteine accessible with Ca^{2+} , see section 3.4), tryptophan fluorescence (conformational change, see section 3.5), and GC assay analysis (target regulation, see section 3.6) of non-myr WT, WT, reduced WT, and C15A-C17A are listed for comparison. Light blue background indicates no/no significant change, light violet background slight, significant changes, light red background big, significant changes.

	maximum cysteine accessibility	cysteine accessibility change with Ca^{2+}	conformational change	target regulation
non-myr WT	≤ 3	n. s.	not visible	very low Ca^{2+} -dependency
WT	≤ 2	** up to 1 less	very low	very low Ca^{2+} -dependency
reduced WT	≤ 4	** ≈ 1 less	not visible	no Ca^{2+} -dependency
C15A-C17A	≤ 3	*** up to 2 less	biphasic	high Ca^{2+} -dependency x-fold activation ≈ 9 $\text{IC}_{50} \approx 0.124 \mu\text{M} [\text{Ca}^{2+}]_{\text{free}}$

The tryptophan fluorescence measurements confirmed that non-myr WT is not and that WT might be slightly Ca^{2+} -sensitive (see section 3.5). The significant Ca^{2+} -dependency of reduced WT in DTNB

measurements could not be seen with this method. However, tryptophan fluorescence is very sensitive to small influences during the experimental procedure. I used the Ca^{2+} -EGTA buffer system with K_2CaEGTA and $\text{K}_2\text{H}_2\text{EGTA}$ (Klabusay and Blinks 1996). Many protein samples with $[\text{Ca}^{2+}]_{\text{free}}$ adjusted using the Ca^{2+} -EGTA buffer system were prepared. After measuring one sample, the cuvette had to be washed and dried before measuring the next sample. If the cuvette is not dried completely, this can falsify the results and lead to large outliers, especially if the conformational change of the studied protein is rather small. A better method might be to prepare one protein sample with EGTA and adding a defined amount of Ca^{2+} before each measurement (Peshenko et al. 2019). The $[\text{Ca}^{2+}]_{\text{free}}$ can be calculated using algorithms as described by Peshenko et al. (2019). It would also be possible to verify the calculated $[\text{Ca}^{2+}]_{\text{free}}$ with fura-2. Despite the concerns regarding the used method, C15A-C17A clearly showed a biphasic conformational change in a Ca^{2+} -dependent manner, similar to bovine GCAP1 (Peshenko et al. 2019). Thus, Cys15 and/or Cys17 strongly influence the Ca^{2+} -dependent conformational change of GCAP5. This does not necessarily mean that GCAP5 completely lost its ability to reorganize its structure upon Ca^{2+} -binding. It could as well mean that the rearrangement of the tryptophans of GCAP5 or the residues surrounding the tryptophans in the tertiary structure of GCAP5 might be smaller and/or different compared to C15A-C17A or bovine GCAP1.

C15A-C17A also resembled bovine GCAP1 in Ca^{2+} -dependent target regulation of human GC-E (see section 3.6). The Ca^{2+} -dependent behavior was not seen for the GCAP5 variants without mutation of Cys15 and Cys17. While non-myr WT and WT showed only very little Ca^{2+} -dependent changes, reduced WT showed no Ca^{2+} -dependency when reconstituted with human GC-E at all. Instead, the analysis of these variants revealed that myristoylation enhances GCAP5 regulated human GC-E activity, and that this effect is largely increased by reduction of GCAP5. Cys15 and Cys17 are not the only residues that prevent a Ca^{2+} -sensitive GC-E regulation by GCAP5. In a recent study, we could show that mutation of Arg22 restores human GC-E regulation in a Ca^{2+} -dependent manner as well, despite the presence of Cys15 and Cys17 (Cudia et al. 2021). It would be interesting whether this mutant also shows redox-dependent properties like wildtype GCAP5.

In summary, the presence of Cys15 and Cys17 does not completely abolish Ca^{2+} -sensitivity of GCAP5. However, the transmission of Ca^{2+} -sensing to target regulation is largely impaired, at least when reconstituted with human GC-E. In exchange, the *N*-terminal cysteine cluster enables GCAP5 to be a redox-sensitive regulator of GC-E activity (discussed in section 4.4).

4.4 GCAP5 is a redox-sensor

Cysteine residues can enable proteins to sense changes in the redox-potential, which might be linked to the protein's activity or regulatory properties (Gilbert 1990). Lange (2012) and Griepenstroh (2016) reported that reduced purified GCAP5 showed different characteristics and regulatory properties than wildtype

GCAP5. I could confirm that GCAP5 is sensitive to reduction, and that Cys15 and Cys17 are probably involved in redox-sensing (summarized in Table 11).

All GCAP5 variants harboring Cys15 and Cys17 showed a significant increase in their dimerization rate under stronger reducing conditions (5 mM DTT) compared to standard *in vitro* reducing conditions (1 mM DTT) (see section 3.2). C15A-C17A was the only variant that did not react to the higher reducing potential, emphasizing that Cys15 and Cys17 are essential for the redox-sensitivity of GCAP5.

Table 11: Redox-dependency of GCAP5.

Results of analytical SEC (difference of dimer concentration when reduced and concentration of monomers when reduced in percent points, see section 3.2), DTNB measurement (accessible cysteines, see section 3.4), tryptophan fluorescence (conformational change, see section 3.5), and GC assay analysis (target regulation, see section 3.6) of non-myr WT, WT, reduced WT, C15A-C17A, H18E-Y21E, and V76E are listed for comparison. Light blue background indicates no significant change, light red background higher values. Dark grey background indicates that this variant was not studied with the respective method under higher reducing conditions. ¹ The program Primaide could not reliably detect the peak representing dimers and the peak representing the unclear state (Figure 14) as two independent peaks. Therefore, the difference of dimer concentration might be misleading.

	difference of dimer concentration when reduced (%-points)	concentration of monomers when reduced (%-points)	accessible cysteines	conformational change	target regulation
non-myr WT	** +9.2 ¹	n. s. not always detectable	-	-	-
WT	*** +12.8	not visible	1 - 2	very low	low activity, low Ca ²⁺ - dependency
reduced WT	*** +27.6	n. s. not always detectable	2 - 4	not visible	moderate activity, no Ca ²⁺ - dependency
C15A-C17A	n. s.	not visible	-	-	-
H18E-Y21E	*** +31.4	not visible	-	-	-
V76E	*** +3.5	not visible	-	-	-

With this method, I also analyzed whether the residues H18, Y21, and V76 are important for the dimer formation of GCAP5. These residues are conserved in GCAP1 (Figure A1). Exchanging them by site-directed mutagenesis with glutamic acid reduces GCAP1 dimerization and prevents GC activation by GCAP1 (Lim et al. 2018). Here, I could see that only mutation of V76 reduced the dimerization rate of GCAP5. However, this did not lead to the formation of monomers. Instead, this mutant aggregated nearly completely (Figure 15). This contrasts with the findings of our cooperation partners from the Department of Chemistry (UC Davis) (Cudia et al. 2021). They performed analytical SEC measurements with GCAP5 purified from the cytosolic fraction after expression in *E. coli*. Even though we used different solvents for analytical SEC buffers, I suppose that our different results are a consequence of me purifying recombinant GCAP5 from inclusion bodies. This further emphasizes that recombinant GCAP5 should not be purified from inclusion bodies by denaturation and subsequent renaturation but rather from the cytosolic fraction (discussed in section 4.1).

Reduced WT GCAP5 showed different properties from WT in all other experiments. Two to three additional cysteines were accessible in reduced WT (see section 3.4). The very small tendency of WT to change its conformation in a Ca^{2+} -dependent manner in tryptophan fluorescence measurements was missing for reduced WT (see section 3.5). Further, when reconstituted with recombinant human GC-E, reduced WT was also missing the very low Ca^{2+} -dependent target regulation that was observed for WT (see section 3.6). Surprisingly, reduced WT enhanced the human GC-E activity in comparison to WT by the factor six in a Ca^{2+} -independent manner. This was not reported for any other GCAP so far. It would be interesting to compare the GC-E regulation of WT and reduced WT to C15A-C17A and C15A-C17A purified under reducing conditions (reduced C15A-C17A). If C15A-C17A does not show redox-sensitive target regulatory properties, Cys15 and Cys17 are definitely essential for the redox-sensitivity of GCAP5. Also, the effect of myristoylation on redox-sensitive target regulation of GCAP5 was not investigated so far. But what are the biological consequences of GCAP5 losing Ca^{2+} -dependent for gaining redox-dependent regulation of cGMP synthesis?

Redox-sensitive processes are not mentioned in the classical phototransduction cascade of vertebrate photoreceptors (see section 1.2). However, light can cause oxidative stress, and photoreceptors are constantly exposed to light (Demontis et al. 2002; Athanasiou et al. 2013). Additionally, photoreceptors need to reproduce the proteins needed in the outer segments continuously since the retinal pigment epithelium phagocytoses the apical parts of the photoreceptor outer segments on a daily basis (Athanasiou et al. 2013; Molday and Moritz 2015). During protein folding in the endoplasmic reticulum (ER), reactive oxygen species are produced as a by-product (Chong et al. 2017). In combination, this makes photoreceptors susceptible for oxidative stress (Usui et al. 2009; Campochiaro et al. 2015), which in turn leads to ER stress (Chong et al. 2017). Several hereditary diseases leading to photoreceptor degeneration are linked to high cGMP concentrations (for review see Power et al. 2020). While cGMP functions as a second messenger in the phototransduction cascade together with Ca^{2+} (see sections 1.2 and 1.3), high cGMP concentrations over a longer period of time are cytotoxic (Olshevskaya et al. 2002; Paquet-Durand et al. 2011). On the one hand, cGMP opens the CNG-channels in photoreceptor cells (see section 1.2). If the CNG-channels are constantly opened, Ca^{2+} can freely enter the photoreceptor cell, leading to a disturbed Ca^{2+} equilibrium and ultimately to cell death (Power et al. 2020). On the other hand, another prominent effector protein is activated by cGMP, the cGMP-dependent protein kinase (PKG). This kinase is better known in the $\text{NO} \rightarrow \text{soluble GC} \rightarrow \text{cGMP} \rightarrow \text{PKG}$ signaling pathway (Hofmann et al. 2006). In contrast to the inner retina where stimulation of soluble GC by the gasotransmitter NO leads to increased cGMP concentrations, photoreceptors do not express a soluble GC, and NO stimulation in photoreceptors leads to decreasing cGMP concentrations (Gotzes et al. 1998; Wei et al. 2012). Further, overstimulation of the PKG causes photoreceptor degeneration, whereas inhibition of the PKG in several retinitis pigmentosa models as well as knockdown or ablation of PKG2 in an achromatopsia model protect photoreceptors from

degenerating (Paquet-Durand et al. 2009; Vighi et al. 2018; Koch et al. 2020). Yet, controlled activation of PKG1 was reported to have neuroprotective effects under oxidative stress conditions (Pilz and Broderick 2005 part 5.5.2).

Interestingly, NO is not only an activator of soluble GCs. Several proteins are regulated by S-nitrosylation, a reversible posttranslational modification of the cysteine's thiol group by NO, involved in redox-homeostasis (Hess et al. 2005; Hess and Stamler 2012; Fernando et al. 2019; Nasuno et al. 2021). Since GCAP5 harbors two solvent exposed cysteines (Cudia et al. 2021) which seem to be responsible for the redox-dependent target regulation and partial loss of Ca²⁺-sensitivity of GCAP5 (this thesis), NO is a promising candidate for GCAP5 regulation. It is possible to induce S-nitrosylation of recombinant proteins *in vitro* (Lai et al. 2001). Whether the modification was successful can be detected by several methods (Stamler et al. 1992; Lai et al. 2001; Forrester et al. 2009; Liu et al. 2018). If GCAP5 will be tested positive for S-nitrosylation, the next step would be comparative target regulation by S-nitrosylated GCAP5, reduced WT, and WT, respectively, measured by GC assay. If GCAP5 can be S-nitrosylated, and if this modification affects retinal GC activity, NO might trigger a conformational change of GCAP5 necessary for target regulation in zebrafish photoreceptors. This would further point to GCAP5 being involved in cell protection under oxidative stress conditions, which might also explain why GCAP5 expression seems to be especially high in SSCs as discovered by immunohistochemistry (Fries 2013; see section 3.7). Since the opsin of SSCs senses UV light (see section 1.5), SSCs need to be receptive for this relatively low wavelength light. Light with lower wavelength is more potent at inducing oxidative stress, though, at least in rod photoreceptor cells (Demontis et al. 2002). This is not surprising given that the energy of light is inversely proportional to the wavelength. However, this putative involvement of GCAP5 is just speculation based on initial research, and the role of GCAP5 in the zebrafish retina needs to be investigated further.

4.5 Fe²⁺-bound GCAP5 inhibits GC-E activity despite reduction

Cysteine residues can coordinate metal ions by forming iron-sulfur (Fe-S) clusters, which can be involved in redox-sensing of proteins (Crack et al. 2012; Crack et al. 2014; Maio and Rouault 2015). GCAP5 contains two non-conserved cysteines (Figure A1), and we have hints that GCAP5 might bind Fe²⁺ (Lange 2012; Griepenstroh 2016). Thus, we tested target regulatory properties of Fe²⁺-loaded GCAP5 in comparison to C15A-C17A by performing GC assays (see section 3.6). In parallel, the Department of Chemistry (*UC Davis*) tested structure and binding properties of Fe²⁺-binding to GCAP5. Our results are published in Lim et al. (2017).

We could show that two GCAP5-molecules bind one Fe²⁺ with nanomolar affinity ($K_d < 100$ nM). A second Fe²⁺ binds to EF2 of GCAP5 with micromolar affinity ($K_d = 3 \pm 1$ μ M). Even though this would be in the physiological range of total intracellular [Fe²⁺] of around 500 to 700 μ M in neurons of the central nervous

system (Reinert et al. 2019), intracellular Fe^{2+} is almost always kept bound, for example to ferritin (Frazer and Anderson 2014). Therefore, the low affinity Fe^{2+} -binding of GCAP5 is unlikely to be physiologically relevant (Lim et al. 2017). C15A-C17A lacked the high affinity binding site for Fe^{2+} , emphasizing that GCAP5 forms an Fe-S cluster. A structural model based on NMR structural analysis revealed that GCAP5 forms a $[\text{Fe}(\text{SCys})_4]$ complex (Lim et al. 2017; Figure 24). One Fe^{2+} is coordinated by Cys15 and Cys17 of two GCAP5-molecules, which form a dimer. This complex formation was also reported for rubredoxin (Min et al. 2001) and a two-iron superoxide reductase (deMaré et al. 1996; Emerson et al. 2003). Dimerization of GCAP5 was observed in the presence as well as in the absence of Fe^{2+} , consistent with the analytical SEC results in this thesis (see section 3.2).

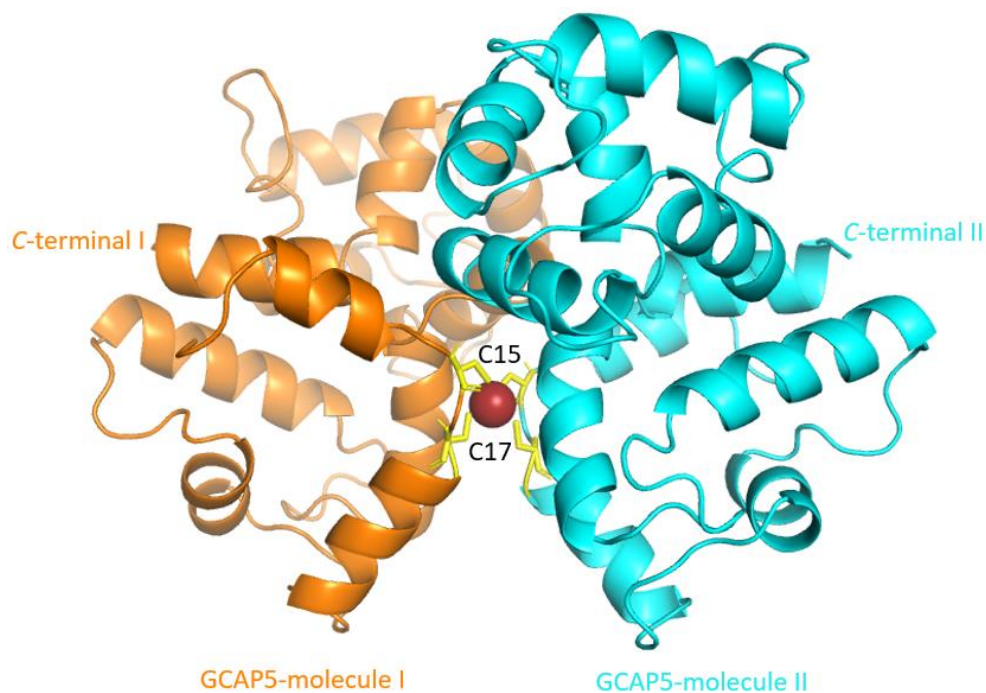


Figure 24: Modeled structure of the Fe^{2+} -bound GCAP5 dimer.

The quaternary protein structure in its Fe^{2+} -bound form is presented as a cartoon. Two GCAP5-molecules (orange and cyan, respectively) form a dimer. Cysteines C15 and C17 (yellow sticks) of both GCAP5-molecules coordinate one Fe^{2+} (red sphere), forming a $[\text{Fe}(\text{SCys})_4]$ complex. C-terminal of each GCAP5-molecule is labelled for orientation. PDB structure kindly provided by Prof. Dr. J. B. Ames (Department of Chemistry, *UC Davis*).

Fe^{2+} further affects target regulation of GCAP5 (see section 3.6). WT showed no Ca^{2+} -dependent regulation of recombinant human GC-E in the presence and absence of Fe^{2+} , respectively, (Figure 20), which is consistent with the results of the GC assay with Ca^{2+} -titration (Figure 19). However, when GCAP5 was loaded with Fe^{2+} , the human GC-E activity dropped down to the level of basal activity (Figure 20 C). This is particularly interesting, considering that WT was reconstituted with the GC-E under higher reducing conditions. Instead of using the standard *in vitro* DTT concentration of 1 mM, I used 5 mM DTT for the incubation of GCAP5 with the GC-E. Reduced WT, however, showed an increased activation of recombinant human GC-E in comparison to WT (Figure 19 E). This raises the question whether GCAP5 actually binds to GCs in its Fe^{2+} -loaded form. Binding of GCAP5 to non-purified GCs can be investigated by backscattering

interferometry. This technique is highly sensitive and allows to analyze protein-protein interactions in solution without labelling or immobilizing the putative interaction partners, and it is possible to use cell lysates without purifying the protein of interest (Markov et al. 2004; Bornhop et al. 2007; Kussrow et al. 2009; Baksh et al. 2011; Bornhop et al. 2016; Sulmann et al. 2017; Wimberg et al. 2018b). Even though Fe^{2+} did not have the same effect on target regulation of C15A-C17A, the x-fold activation of human GC-E reconstituted with C15A-C17A decreased (Figure 20 A). A similar effect was observed for human GC-E reconstituted with human GCAP1 (Figure 20 B). C15A-C17A does not bind Fe^{2+} in the nanomolar range (Lim et al. 2017), and the $[\text{Fe}^{2+}]$ was set to 100 nM. I used the Ca^{2+} -EGTA buffer system (Klabusay and Blinks 1996) to adjust the $[\text{Ca}^{2+}]_{\text{free}}$ in the reaction solution. However, the absolute stability constants of EGTA with Ca^{2+} and Fe^{2+} are 11.00 and 11.92, respectively (stability constants taken from <https://www.sigmaaldrich.com/DE/en/technical-documents/technical-article/protein-biology/protein-purification/chelators>; access: 10.12.2022). Thus, the complex formation of EGTA with Fe^{2+} is slightly favored. It is likely that Fe^{2+} disturbed Ca^{2+} -buffering by the Ca^{2+} -EGTA buffer system, leading to a higher $[\text{Ca}^{2+}]_{\text{free}}$ concentration in the reaction solution than intended and, therefore, to lower activation of human GC-E by C15A-C17A and human GCAP1, respectively.

The Fe^{2+} -dependent inhibition of GC activation by GCAP5 is consistent with the hypotheses that GCAP5 might be involved in cell protection under oxidative stress conditions, and that NO might trigger a conformational change of GCAP5 necessary for target regulation in zebrafish photoreceptors (see section 4.4). Free intracellular iron can generate reactive oxygen species in the Fenton/Haber-Weiss reaction, causing oxidative stress (for review see Picard et al. 2020). A recent mathematical model of iron-induced oxidative stress in photoreceptors showed how iron-ions might lead to reactive oxygen species and increased Ca^{2+} -influx, resulting in a reduced visual signal (Pattanaik et al. 2021). Further, increasing $[\text{Ca}^{2+}]$ can lead to photoreceptor degeneration (Power et al. 2020). Taking the hypotheses made above into consideration, in zebrafish cones, excess free iron might be bound by GCAP5. If Fe^{2+} -bound GCAP5 still binds to retinal GCs and prevents their activation, this would lead to decreasing $[\text{cGMP}]$ due to PDE activity and thus limit Ca^{2+} -influx through CNG-channels (see section 1.2). Consequently, iron-binding by GCAP5 might be important to ensure that visual stimuli are transmitted accurately under oxidative stress conditions. Of all retinal cell types, cones are especially sensitive to iron (Lucius and Sievers 1996; Rogers et al. 2007; Picard et al. 2008; Kurz et al. 2009). On a subcellular level of rat cones, the highest iron level was observed in the inner segments (Yefimova et al. 2000). This could explain why GCAP5 was found most abundant in inner segments of zebrafish cones by immunohistochemistry (Fries 2013; see section 3.7). It is possible that Fe^{2+} -bound GCAP5 is further influenced by NO since Fe-S clusters are susceptible for this gasotransmitter (Crack et al. 2014). However, Fe^{2+} -binding might not be necessary for a possible nitrosylation of GCAP5 (discussed in section 4.4).

Again, a difference was observed between GCAP5 purified from inclusion bodies and from the cytosolic fraction, respectively, after expression in *E. coli* (discussed in section 4.1). In the absence of Ca^{2+} , human GC-E activity levels regulated by WT and C15A-C17A, respectively, differed largely, if GCAP5 was purified from inclusion bodies (Figure 19). If GCAP5 was purified from the cytosolic fraction, this difference was not observed (Figure 20).

4.6 GCAP5 in the adult zebrafish retina

GCAP5 is expressed in all cone types of the zebrafish retina as shown on RNA (Imanishi et al. 2004; Rättscho et al. 2009) and on protein level (Fries 2013). Fries (2013) localized GCAP5 already on immunohistochemically stained sections of the zebrafish retina using fast red. For future co-localization experiments, I established a protocol for immunohistochemical staining with fluorescent markers together with apl. Prof. Dr. Ulrike Janssen-Bienhold (Division of Visual Neuroscience, *University of Oldenburg*) (see section 3.7). Therefore, I reconfirmed the specificity and sensitivity of the primary antibody rabbit anti-GCAP5. In subcellular fractions of the retina, only a band with the size of monomeric myristoylated GCAP5 was detected in the cytosolic fraction and to a lesser extent in the membrane fraction (Figure 21 A). Since recombinant GCAP5 tends to form dimers *in vitro* (Lim et al. 2017; Cudia et al. 2021; see section 3.1 and 3.2), I extended the illumination time of the blot membrane, revealing a band with low intensity around the size of dimeric GCAP5 and also a band of monomeric non-myristoylated GCAP5 (Figure A11). To verify a dimerization of native GCAP5 and an incomplete myristoylation in subcellular fraction of the retina by western blotting with subsequent immunodetection, I suggest using a higher protein load for the SDS-PAGE and to use the anti-GCAP5 antibody in a 1:250 dilution. However, other methods, like affinity chromatography with the cytosolic fraction of the zebrafish retina and the anti-GCAP5 antibody, might be more reasonable to prevent overloading of the polyacrylamide gel. The problem here is that we would need huge amounts of zebrafish eyes to achieve sufficient yields of native GCAP5. For comparison, 10-15 μg of GCAP is the yield out of 100 bovine retinae (Gorczyca et al. 1994), and the cattle's eye is much larger than the zebrafish' eye. To detect 2 ng of purified recombinant GCAP5, a 1:2000 dilution is still sufficient as revealed by dilution series of the anti-GCAP5 antibody (Figure A11).

Immunohistochemical staining of the photoreceptor layer in sections of the zebrafish retina with the primary antibody rabbit anti-GCAP5 (*Pineda*) detected by the secondary antibody donkey-F(ab')₂ anti-rabbit Alexa Fluor®488 (*Jackson ImmunoResearch*) revealed similar results as described by Fries (2013) (summarized in section 1.6). GCAP5 was localized in all cone types, with especially strong staining in SSCs (Figure 21). This could hint to a higher expression level of GCAP5 in SSCs in comparison to the other cone types, which would be consistent with the hypothesis that GCAP5 is important for photoreceptor cell protection from light induced oxidative stress (discussed in section 4.4). However, the anti-GCAP5 antibody cross reacts to a low extend with zebrafish GCAP1 (Fries 2013), which is expressed in SSCs as well (Imanishi

et al. 2004). Therefore, the higher intensity staining of SSCs could be the sum intensity of GCAP5 and GCAP1 reactivity. Contrary to this hypothesis is the finding that no inner segments of rod photoreceptors were stained by the anti-GCAP5 antibody (Figure 21 and Figure 22). If the antibody stained GCAP1 to a visible extend, the inner segments of rods should have been visible in between the axons of the cone photoreceptors, which was not the case. Outer segments of rod photoreceptors were most likely embedded by the pigment epithelium since the zebrafishes used for preparation of the retinae were light adapted (Hodel et al. 2006).

On a subcellular level, the staining against GCAP5 was most intense in cone inner segments and cone pedicles. The high reactivity in cone pedicles might hint to an interaction of GCAP5 with RIBEYE as shown for mammalian GCAPs (see section 1.4). This hypothesis can be challenged by co-localization studies of GCAP5 and RIBEYE in sections of the zebrafish retina, by heterologous expression of RIBEYE, which could be reconstituted with GCAP5, including co-localization studies and backscattering interferometry, and by pull down assay. The latter, however, is problematic due to the high amount of protein and, therefore, zebrafish eyes needed (see above).

Co-staining of GCAP5 and arrestin 3a, a marker for DCs, confirmed that GCAP5 is expressed in DCs (Figure 22). Before, this conclusion was made based on the morphology of zebrafish cones and the zebrafish cone mosaic (see section 1.5). However, not all DCs were stained by the anti-GCAP5 antibody. This raises the hypothesis that only the red-sensitive cones or the green sensitive cones express GCAP5. I used vertical sections of the zebrafish retina for co-localization analysis. To verify the expression of GCAP5 in all double cones, co-staining of GCAP5 and arrestin 3a in horizontal sections of the zebrafish retina would be preferable. In addition, isolated zebrafish DCs (Aquila et al. 2015; Aquila et al. 2019) could be stained against zebrafish GCAP5.

In summary, the primary antibody rabbit anti-GCAP5 (*Pineda*) detected by the secondary antibody donkey-F(ab')₂ anti-rabbit Alexa Fluor®488 (*Jackson ImmunoResearch*) generates a specific staining of GCAP5 in zebrafish photoreceptors with sufficient sensitivity and can be used for co-localization studies with fluorescent markers.

4.7 Conclusion

GCAP5 from the zebrafish retina is a photoreceptor GC-activating protein that largely lost Ca²⁺-dependent properties but inhabits redox-sensitive properties instead. This sensitivity exchange is mediated by a unique cysteine cluster at its N-terminal, namely Cys15 and Cys17 (discussed in section 4.3). Mutation of both cysteines by alanine restored Ca²⁺-dependent characteristics and target regulation as known from other GCAP isoforms. Redox-sensitivity of GCAP5 also influenced regulation of recombinant human GC-E (discussed in section 4.4). While myristoylation had only a minor effect on target regulation of GCAP5

(discussed in section 4.2), purifying GCAP5 under higher reducing conditions led to enhanced GC activation in comparison to GCAP5 purified under standard reducing conditions. Cys15 and Cys17 don't only render GCAP5 sensitive to the reduction potential: Two GCAP5-molecules coordinate Fe^{2+} with nanomolar affinity, forming an Fe-S cluster (discussed in section 4.5).

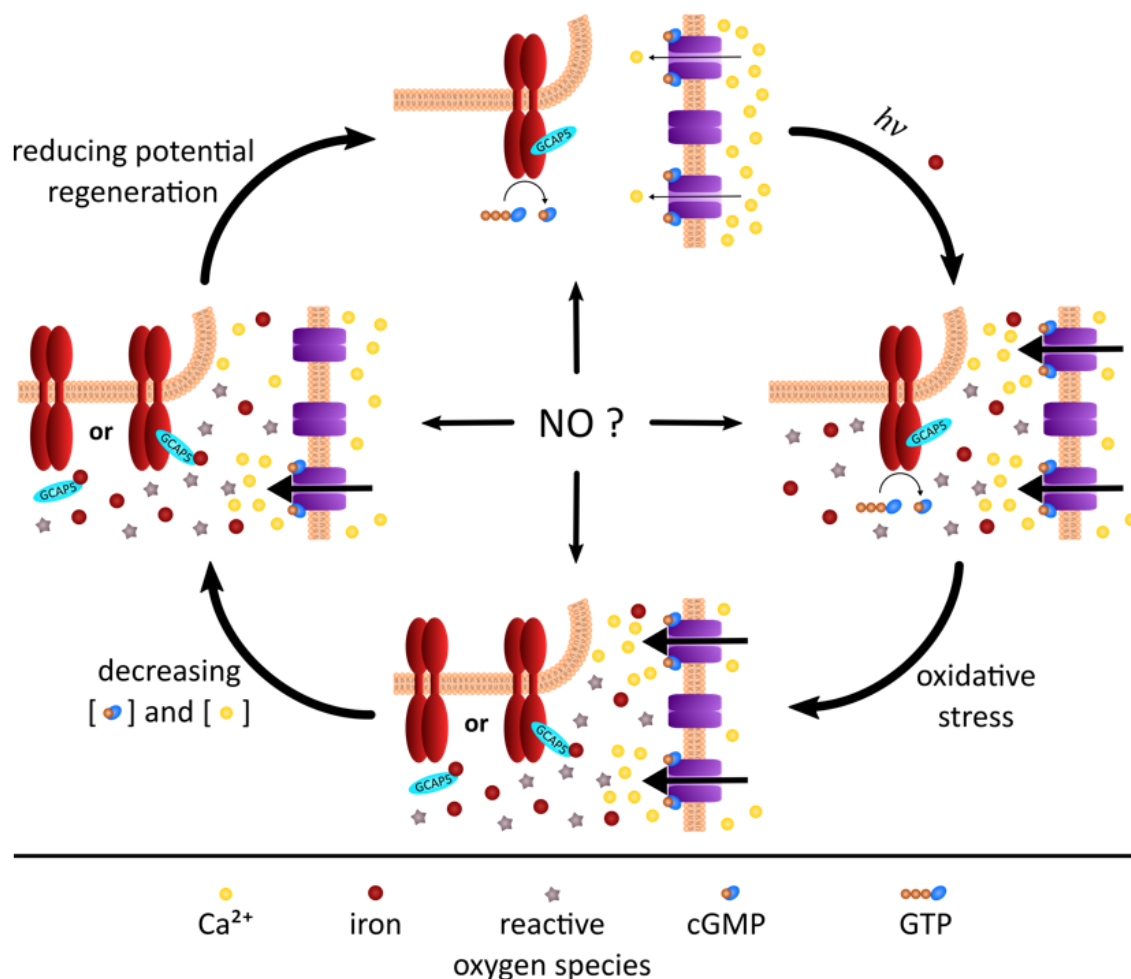


Figure 25: Putative involvement of GCAP5 in cell protection against light/iron-induced oxidative stress.

Under normal reducing conditions (**top**), GCAP5 (cyan ellipsoid) activates the GC (red dimer), which produces cGMP out of GTP. A fraction of the CNG-channels (violet) is kept open by cGMP, allowing a small influx (thin arrows through CNG-channels) of Ca^{2+} . Light and excess iron can induce oxidative stress (**right**), leading to the production of reactive oxygen species. This causes an increased inward flow (thick arrows through CNG-channels) of Ca^{2+} . GCAP5 now binds iron or senses the disturbance of the reduction potential by Cys15 and Cys17 and inhibits the GC or dissociates from it (**bottom**). Due to the activities of the PDE and the Na^+/K^+ , Ca^{2+} -exchanger (both not depicted), intracellular [cGMP] and [Ca^{2+}] decrease (**left**). A small fraction of CNG-channels might be kept open by cGMP provided by GC basal activity. The lowered [cGMP] and [Ca^{2+}] might induce cell protective measures, maybe involving the inhibition of PKG, to return the cone cell to its normal reducing conditions (**top**). It is unclear whether the gasotransmitter NO is involved in this process.

The biological consequences can only be speculated so far (Figure 25). GCAP5 is a cytosolic protein, and most thiols of cysteine residues in the cytosol are kept in their reduced form (Gilbert 1990). Reduced GCAP5 showed an enhanced GC activation *in vitro*. This was completely abolished when GCAP5 was loaded with iron, despite keeping the protein at higher reducing conditions prior to and during reconstitution with human GC-E. Excess iron can cause oxidative stress and lead to photoreceptor degeneration (Picard et al.

2020). This process might include a higher influx of Ca^{2+} into the photoreceptor cell (Pattanaik et al. 2021). If GCAP5 binds iron, or the reduction potential of the cytosol drops due to reactivity of reactive oxygen species with glutathione (Gilbert 1990), zebrafish retinal GCs might be inhibited by GCAP5, or GCAP5 might dissociate from the GC, both leading to lower [cGMP]. The CNG-channels would close, limiting Ca^{2+} -induced damage (Power et al. 2020). Further, the PKG would be prevented from activation, which was shown to have positive effects in retinal degeneration models (Paquet-Durand et al. 2009; Vighi et al. 2018; Koch et al. 2020). Photoreceptors are prone to oxidative stress for several reasons (see sections 4.4 and 4.5), and light of lower wavelength was shown to be more potent in inducing oxidative stress in rod photoreceptors (Demontis et al. 2002). Thus, the putative cell protective role of GCAP5 might be especially important in SSCs, which showed a higher GCAP5 expression level than the other zebrafish cone types (discussed in sections 4.4 and 4.6). The UV-light absorbing SSCs have the most basal location of cones in the zebrafish retina under daylight conditions (Hodel et al. 2006) and, therefore, might at least in part protect the other, more apical located cone types from UV-light induced damage. GCAP5 might further be influenced by NO, a gasotransmitter involved in redox-homeostasis and reacting with cysteine thiols and Fe-S clusters (discussed in sections 4.4 and 4.5).

However, the target regulatory properties of GCAP5 were tested with the human GC-E because recombinant expression of functional zebrafish GCs failed so far. Further, I performed most of my experiments with recombinant GCAP5 purified from inclusion bodies after expression in *E. coli*. A few experiments carried out with GCAP5 purified from inclusion bodies and from the cytosolic fraction, respectively, revealed that they differ in their biochemical characteristics (discussed in section 4.1). Thus, the results of this thesis should be treated with caution and challenged in future experiments.

References

- Abbas, S., Marino, V., Dell'Orco, D. and Koch, K.-W. (2019). "Molecular Recognition of Rhodopsin Kinase GRK1 and Recoverin Is Tuned by Switching Intra- and Intermolecular Electrostatic Interactions." Biochemistry **58**(43): 4374-4385.
- Allerston, C. K., von Delft, F. and Gileadi, O. (2013). "Crystal Structures of the Catalytic Domain of Human Soluble Guanylate Cyclase." PLoS ONE **8**(3): e57644.
- Allison, W. T., Haimberger, T. J., Hawryshyn, C. W. and Temple, S. E. (2004). "Visual pigment composition in zebrafish: Evidence for a rhodopsin-porphyrpsin interchange system." Vis Neurosci **21**(6): 945-952.
- Ames, J. B., Dizhoor, A. M., Ikura, M., Palczewski, K. and Stryer, L. (1999). "Three-dimensional structure of guanylyl cyclase activating protein-2, a calcium-sensitive modulator of photoreceptor guanylyl cyclases." The Journal of biological chemistry **274**(27): 19329-19337.
- Ames, J. B., Levay, K., Wingard, J. N., Lusin, J. D. and Slepak, V. Z. (2006). "Structural basis for calcium-induced inhibition of rhodopsin kinase by recoverin." The Journal of biological chemistry **281**(48): 37237-37245.
- Ames, J. B. and Lim, S. (2012). "Molecular structure and target recognition of neuronal calcium sensor proteins." Biochimica et biophysica acta **1820**(8): 1205-1213.
- Amores, A., Force, A., Yan, Y. L., Joly, L., Amemiya, C., Fritz, A., Ho, R. K., Langeland, J., Prince, V., Wang, Y. L., Westerfield, M., Ekker, M. and Postlethwait, J. H. (1998). "Zebrafish hox clusters and vertebrate genome evolution." Science **282**(5394): 1711-1714.
- Anderson, G. R., Posokhova, E. and Martemyanov, K. A. (2009). "The R7 RGS protein family: multi-subunit regulators of neuronal G protein signaling." Cell biochemistry and biophysics **54**(1-3): 33-46.
- Aparicio, J. G. and Applebury, M. L. (1996). "The photoreceptor guanylate cyclase is an autophosphorylating protein kinase." The Journal of biological chemistry **271**(43): 27083-27089.
- Aquila, M., Benedusi, M., Fasoli, A. and Rispoli, G. (2015). "Characterization of Zebrafish Green Cone Photoresponse Recorded with Pressure-Polished Patch Pipettes, Yielding Efficient Intracellular Dialysis." PLoS ONE **10**(10): e0141727.
- Aquila, M., Dell'Orco, D., Fries, R., Koch, K.-W. and Rispoli, G. (2019). "Incorporating phototransduction proteins in zebrafish green cone with pressure-polished patch pipettes." Biophys Chem **253**: 106230.
- Arshavsky, V. Y. and Burns, M. E. (2012). "Photoreceptor signaling: supporting vision across a wide range of light intensities." The Journal of biological chemistry **287**(3): 1620-1626.
- Arshavsky, V. Y. and Wensel, T. G. (2013). "Timing is everything: GTPase regulation in phototransduction." Invest Ophthalmol Vis Sci **54**(12): 7725-7733.

Asanad, S. and Karanjia, R. (2022). Full-Field Electroretinogram. StatPearls. Treasure Island (FL), StatPearls Publishing

Copyright © 2022, StatPearls Publishing LLC.

Athanasίου, D., Aguilà, M., Bevilacqua, D., Novoselov, S. S., Parfitt, D. A. and Cheetham, M. E. (2013). "The cell stress machinery and retinal degeneration." FEBS Lett **587**(13): 2008-2017.

Azadi, S., Molday, L. L. and Molday, R. S. (2010). "RD3, the protein associated with Leber congenital amaurosis type 12, is required for guanylate cyclase trafficking in photoreceptor cells." Proceedings of the National Academy of Sciences of the United States of America **107**(49): 21158-21163.

Baden, T., Euler, T. and Berens, P. (2020). "Understanding the retinal basis of vision across species." Nature Reviews Neuroscience **21**(1): 5-20.

Baehr, W., Karan, S., Maeda, T., Luo, D.-G., Li, S., Bronson, J. D., Watt, C. B., Yau, K.-W., Frederick, J. M. and Palczewski, K. (2007). "The function of guanylate cyclase 1 and guanylate cyclase 2 in rod and cone photoreceptors." The Journal of biological chemistry **282**(12): 8837-8847.

Baksh, M. M., Kussrow, A. K., Mileni, M., Finn, M. G. and Bornhop, D. J. (2011). "Label-free quantification of membrane-ligand interactions using backscattering interferometry." Nat Biotechnol **29**(4): 357-360.

Barford, D. (2004). "The role of cysteine residues as redox-sensitive regulatory switches." Curr Opin Struct Biol **14**(6): 679-686.

Baylor, D. A. (1987). "Photoreceptor signals and vision. Proctor lecture." Investigative Ophthalmology & Visual Science **28**(1): 34-49.

Baylor, D. A. and Nunn, B. J. (1986). "Electrical properties of the light-sensitive conductance of rods of the salamander *Ambystoma tigrinum*." The Journal of physiology **371**: 115-145.

Behnen, P., Scholten, A., Räscho, N. and Koch, K.-W. (2009). "The cone-specific calcium sensor guanylate cyclase activating protein 4 from the zebrafish retina." J Biol Inorg Chem **14**(1): 89-99.

Bereta, G. and Palczewski, K. (2011). "Heterogeneous N-terminal acylation of retinal proteins results from the retina's unusual lipid metabolism." Biochemistry **50**(18): 3764-3776.

Bilotta, J. and Saszik, S. (2001). "The zebrafish as a model visual system." Int J Dev Neurosci **19**(7): 621-629.

Bondarenko, V. A., Yu, H., Yamazaki, R. K. and Yamazaki, A. (2002). "A novel role of RGS9: inhibition of retinal guanylyl cyclase." Molecular and cellular biochemistry **230**(1-2): 125-128.

Bonì, F., Marino, V., Bidoia, C., Mastrangelo, E., Barbiroli, A., Dell'Orco, D. and Milani, M. (2020). "Modulation of Guanylate Cyclase Activating Protein 1 (GCAP1) Dimeric Assembly by Ca²⁺ or Mg²⁺: Hints to Understand Protein Activity." Biomolecules **10**(10).

- Bornhop, D. J., Kammer, M. N., Kussrow, A., Flowers, R. A., 2nd and Meiler, J. (2016). "Origin and prediction of free-solution interaction studies performed label-free." Proceedings of the National Academy of Sciences of the United States of America **113**(12): E1595-1604.
- Bornhop, D. J., Latham, J. C., Kussrow, A., Markov, D. A., Jones, R. D. and Sørensen, H. S. (2007). "Free-solution, label-free molecular interactions studied by back-scattering interferometry." Science **317**(5845): 1732-1736.
- Boye, S. L., Olshevskaya, E. V., Peshenko, I. V., McCullough, K. T., Boye, S. E. and Dizhoor, A. M. (2016). "Functional study of two biochemically unusual mutations in GUCY2D Leber congenital amaurosis expressed via adenoassociated virus vector in mouse retinas." Mol Vis **22**: 1342-1351.
- Bradford, M. M. (1976). "A rapid and sensitive method for the quantitation of microgram quantities of protein utilizing the principle of protein-dye binding." Anal Biochem **72**: 248-254.
- Branchek, T. and Bremiller, R. (1984). "The development of photoreceptors in the zebrafish, *Brachydanio rerio*. I. Structure." J Comp Neurol **224**(1): 107-115.
- Braunewell, K. H. and Gundelfinger, E. D. (1999). "Intracellular neuronal calcium sensor proteins: a family of EF-hand calcium-binding proteins in search of a function." Cell Tissue Res **295**(1): 1-12.
- Buehl, C. J., Deng, X., Liu, M., McAndrew, M. J., Hovde, S., Xu, X. and Kuo, M. H. (2014). "Resolving acetylated and phosphorylated proteins by neutral urea Triton-polyacrylamide gel electrophoresis: NUT-PAGE." BioTechniques **57**(2): 72-80.
- Burgoyne, R. D. and Weiss, J. L. (2001). "The neuronal calcium sensor family of Ca²⁺-binding proteins." The Biochemical journal **353**(Pt 1): 1-12.
- Burns, M. E. and Pugh, E. N., Jr. (2010). "Lessons from photoreceptors: turning off g-protein signaling in living cells." Physiology (Bethesda, Md.) **25**(2): 72-84.
- Cameron, D. A. (2002). "Mapping absorbance spectra, cone fractions, and neuronal mechanisms to photopic spectral sensitivity in the zebrafish." Vis Neurosci **19**(3): 365-372.
- Campochiaro, P. A., Strauss, R. W., Lu, L., Hafiz, G., Wolfson, Y., Shah, S. M., Sophie, R., Mir, T. A. and Scholl, H. P. (2015). "Is There Excess Oxidative Stress and Damage in Eyes of Patients with Retinitis Pigmentosa?" Antioxid Redox Signal **23**(7): 643-648.
- Chen, C., Nakatani, K. and Koutalos, Y. (2003). "Free magnesium concentration in salamander photoreceptor outer segments." The Journal of physiology **553**(Pt 1): 125-135.
- Chen, C. K., Inglese, J., Lefkowitz, R. J. and Hurley, J. B. (1995). "Ca²⁺-dependent interaction of recoverin with rhodopsin kinase." The Journal of biological chemistry **270**(30): 18060-18066.
- Chinnadurai, G. (2002). "CtBP, an unconventional transcriptional corepressor in development and oncogenesis." Mol Cell **9**(2): 213-224.

- Chong, W. C., Shastri, M. D. and Eri, R. (2017). "Endoplasmic Reticulum Stress and Oxidative Stress: A Vicious Nexus Implicated in Bowel Disease Pathophysiology." Int J Mol Sci **18**(4).
- Christoffels, A., Koh, E. G., Chia, J. M., Brenner, S., Aparicio, S. and Venkatesh, B. (2004). "Fugu genome analysis provides evidence for a whole-genome duplication early during the evolution of ray-finned fishes." Mol Biol Evol **21**(6): 1146-1151.
- Compton, S. J. and Jones, C. G. (1985). "Mechanism of dye response and interference in the Bradford protein assay." Analytical biochemistry **151**(2): 369-374.
- Cooper, N., Liu, L., Yoshida, A., Pozdnyakov, N., Margulis, A. and Sitaramayya, A. (1995). "The bovine rod outer segment guanylate cyclase, ROS-GC, is present in both outer segment and synaptic layers of the retina." J Mol Neurosci **6**(3): 211-222.
- Crack, J. C., Green, J., Thomson, A. J. and Le Brun, N. E. (2012). "Iron-sulfur cluster sensor-regulators." Curr Opin Chem Biol **16**(1-2): 35-44.
- Crack, J. C., Green, J., Thomson, A. J. and Le Brun, N. E. (2014). "Iron-sulfur clusters as biological sensors: the chemistry of reactions with molecular oxygen and nitric oxide." Acc Chem Res **47**(10): 3196-3205.
- Cudia, D., Roseman, G. P., Assafa, T. E., Shahu, M. K., Scholten, A., Menke-Sell, S.-K., Yamada, H., Koch, K.-W., Milhauser, G. and Ames, J. B. (2021). "NMR and EPR-DEER Structure of a Dimeric Guanylate Cyclase Activator Protein-5 from Zebrafish Photoreceptors." Biochemistry **60**(41): 3058-3070.
- Cuenca, N., Lopez, S., Howes, K. and Kolb, H. (1998). "The localization of guanylyl cyclase-activating proteins in the mammalian retina." Invest Ophthalmol Vis Sci **39**(7): 1243-1250.
- deMaré, F., Kurtz, D. M., Jr. and Nordlund, P. (1996). "The structure of *Desulfovibrio vulgaris* rubrerythrin reveals a unique combination of rubredoxin-like FeS₄ and ferritin-like diiron domains." Nat Struct Biol **3**(6): 539-546.
- Demontis, G. C., Longoni, B. and Marchiafava, P. L. (2002). "Molecular steps involved in light-induced oxidative damage to retinal rods." Invest Ophthalmol Vis Sci **43**(7): 2421-2427.
- den Hollander, A. I., Roepman, R., Koenekoop, R. K. and Cremers, F. P. (2008). "Leber congenital amaurosis: genes, proteins and disease mechanisms." Prog Retin Eye Res **27**(4): 391-419.
- Dizhoor, A. M., Chen, C. K., Olshevskaya, E., Sinelnikova, V. V., Phillipov, P. and Hurley, J. B. (1993). "Role of the acylated amino terminus of recoverin in Ca²⁺-dependent membrane interaction." Science **259**(5096): 829-832.
- Dizhoor, A. M., Ericsson, L. H., Johnson, R. S., Kumar, S., Olshevskaya, E., Zozulya, S., Neubert, T. A., Stryer, L., Hurley, J. B. and Walsh, K. A. (1992). "The NH₂ terminus of retinal recoverin is acylated by a small family of fatty acids." The Journal of biological chemistry **267**(23): 16033-16036.
- Dizhoor, A. M. and Hurley, J. B. (1996). "Inactivation of EF-hands makes GCAP-2 (p24) a constitutive activator of photoreceptor guanylyl cyclase by preventing a Ca²⁺-induced "activator-to-inhibitor" transition." The Journal of biological chemistry **271**(32): 19346-19350.

Dizhoor, A. M., Olshevskaya, E. V., Henzel, W. J., Wong, S. C., Stults, J. T., Ankoudinova, I. and Hurley, J. B. (1995). "Cloning, sequencing, and expression of a 24-kDa Ca(2+)-binding protein activating photoreceptor guanylyl cyclase." The Journal of biological chemistry **270**(42): 25200-25206.

Dowling, J. E. (1987). The retina: an approachable part of the brain. Cambridge, MA, Harvard University Press.

Duda, T., Fik-Rymarkiewicz, E., Venkataraman, V., Krishnan, R., Koch, K.-W. and Sharma, R. K. (2005). "The calcium-sensor guanylate cyclase activating protein type 2 specific site in rod outer segment membrane guanylate cyclase type 1." Biochemistry **44**(19): 7336-7345.

Duda, T., Goraczniak, R., Surgucheva, I., Rudnicka-Nawrot, M., Gorczyca, W. A., Palczewski, K., Sitaramayya, A., Baehr, W. and Sharma, R. K. (1996). "Calcium modulation of bovine photoreceptor guanylate cyclase." Biochemistry **35**(26): 8478-8482.

Duda, T., Koch, K.-W., Venkataraman, V., Lange, C., Beyermann, M. and Sharma, R. K. (2002). "Ca(2+) sensor S100beta-modulated sites of membrane guanylate cyclase in the photoreceptor-bipolar synapse." Embo j **21**(11): 2547-2556.

Duda, T., Krishnan, A., Venkataraman, V., Lange, C., Koch, K.-W. and Sharma, R. K. (1999). "Mutations in the Rod Outer Segment Membrane Guanylate Cyclase in a Cone-Rod Dystrophy Cause Defects in Calcium Signaling." Biochemistry **38**(42): 13912-13919.

Duda, T., Venkataraman, V., Krishnan, A., Nagele, R. G. and Sharma, R. K. (2001). "Negatively calcium-modulated membrane guanylate cyclase signaling system in the rat olfactory bulb." Biochemistry **40**(15): 4654-4662.

Duronio, R. J., Jackson-Machelski, E., Heuckeroth, R. O., Olins, P. O., Devine, C. S., Yonemoto, W., Slice, L. W., Taylor, S. S. and Gordon, J. I. (1990). "Protein N-myristoylation in Escherichia coli: reconstitution of a eukaryotic protein modification in bacteria." Proceedings of the National Academy of Sciences of the United States of America **87**(4): 1506-1510.

Elbers, D., Scholten, A. and Koch, K.-W. (2018). "Zebrafish Recoverin Isoforms Display Differences in Calcium Switch Mechanisms." Front Mol Neurosci **11**: 355.

Ellman, G. L. (1959). "Tissue sulfhydryl groups." Archives of Biochemistry and Biophysics **82**(1): 70-77.

Emerson, J. P., Cabelli, D. E. and Kurtz, D. M., Jr. (2003). "An engineered two-iron superoxide reductase lacking the [Fe(SCys)₄] site retains its catalytic properties in vitro and in vivo." Proceedings of the National Academy of Sciences of the United States of America **100**(7): 3802-3807.

Ermilov, A. N., Olshevskaya, E. V. and Dizhoor, A. M. (2001). "Instead of binding calcium, one of the EF-hand structures in guanylyl cyclase activating protein-2 is required for targeting photoreceptor guanylyl cyclase." The Journal of biological chemistry **276**(51): 48143-48148.

Fanger, B. O. (1987). "Adaptation of the Bradford protein assay to membrane-bound proteins by solubilizing in glucopyranoside detergents." Analytical biochemistry **162**(1): 11-17.

- Fernando, V., Zheng, X., Walia, Y., Sharma, V., Letson, J. and Furuta, S. (2019). "S-Nitrosylation: An Emerging Paradigm of Redox Signaling." Antioxidants (Basel) **8**(9).
- Fleisch, V. C. and Neuhaus, S. C. (2006). "Visual behavior in zebrafish." Zebrafish **3**(2): 191-201.
- Forrester, M. T., Foster, M. W., Benhar, M. and Stamler, J. S. (2009). "Detection of protein S-nitrosylation with the biotin-switch technique." Free Radic Biol Med **46**(2): 119-126.
- Franke, K., Maia Chagas, A. A.-O., Zhao, Z. A.-O., Zimmermann, M. A.-O., Bartel, P. A.-O., Qiu, Y., Szatko, K. P., Baden, T. A.-O. and Euler, T. A.-O. (2019). "An arbitrary-spectrum spatial visual stimulator for vision research. LID - 10.7554/eLife.48779 [doi] LID - e48779." (2050-084X (Electronic)).
- Frazer, D. M. and Anderson, G. J. (2014). "The regulation of iron transport." Biofactors **40**(2): 206-214.
- Fries, R. (2013). Das retinale Guanylatcyclase-System des Zebrafisches (*Danio rerio*). School of Mathematics and Science, Carl von Ossietzky University Oldenburg.
- Fries, R., Scholten, A., Säftel, W. and Koch, K.-W. (2012). "Operation profile of zebrafish guanylate cyclase-activating protein 3." Journal of Neurochemistry **121**(1): 54-65.
- Fries, R., Scholten, A., Säftel, W. and Koch, K.-W. (2013). "Zebrafish guanylate cyclase type 3 signaling in cone photoreceptors." PLoS ONE **8**(8): e69656.
- Frins, S., Bönigk, W., Müller, F., Kellner, R. and Koch, K.-W. (1996). "Functional characterization of a guanylyl cyclase-activating protein from vertebrate rods. Cloning, heterologous expression, and localization." The Journal of biological chemistry **271**(14): 8022-8027.
- Fu, Y. and Yau, K.-W. (2007). "Phototransduction in mouse rods and cones." Pflugers Archiv : European journal of physiology **454**(5): 805-819.
- Gemberling, M., Bailey, T. J., Hyde, D. R. and Poss, K. D. (2013). "The zebrafish as a model for complex tissue regeneration." Trends Genet **29**(11): 611-620.
- Gilbert, H. F. (1990). "Molecular and cellular aspects of thiol-disulfide exchange." Adv Enzymol Relat Areas Mol Biol **63**: 69-172.
- Gorczyca, W. A., Gray-Keller, M. P., Detwiler, P. B. and Palczewski, K. (1994). "Purification and physiological evaluation of a guanylate cyclase activating protein from retinal rods." Proceedings of the National Academy of Sciences of the United States of America **91**(9): 4014-4018.
- Gorczyca, W. A., Polans, A. S., Surgucheva, I. G., Subbaraya, I., Baehr, W. and Palczewski, K. (1995). "Guanylyl cyclase activating protein. A calcium-sensitive regulator of phototransduction." The Journal of biological chemistry **270**(37): 22029-22036.
- Gotzes, S., de Vente, J. and Müller, F. (1998). "Nitric oxide modulates cGMP levels in neurons of the inner and outer retina in opposite ways." Vis Neurosci **15**(5): 945-955.

Gray-Keller, M. P. and Detwiler, P. B. (1994). "The calcium feedback signal in the phototransduction cascade of vertebrate rods." Neuron **13**(4): 849-861.

Griepenstroh, N. (2016). Redoxeigenschaften des neuronalen Calciumsensors GCAP5 aus der Zebrafischnetzhaute, Carl von Ossietzky University Oldenburg.

Haeseleer, F., Sokal, I., Li, N., Pettenati, M., Rao, N., Bronson, D., Wechter, R., Baehr, W. and Palczewski, K. (1999). "Molecular characterization of a third member of the guanylyl cyclase-activating protein subfamily." The Journal of biological chemistry **274**(10): 6526-6535.

Hagel, L. (1989). Gel Filtration. Protein Purification: principles, high resolution methods, and applications. J.-C. Janson and L. Rydén. New York, VCH Publishers, Inc. **1**: 63-106.

Hallett, M. A., Delaat, J. L., Arikawa, K., Schlamp, C. L., Kong, F. and Williams, D. S. (1996). "Distribution of guanylate cyclase within photoreceptor outer segments." Journal of Cell Science **109**(7): 1803-1812.

Heidelberger, R., Thoreson, W. B. and Witkovsky, P. (2005). "Synaptic transmission at retinal ribbon synapses." Prog Retin Eye Res **24**(6): 682-720.

Hellmann, N. and Schneider, D. (2019). "Hands On: Using Tryptophan Fluorescence Spectroscopy to Study Protein Structure." Methods Mol Biol **1958**: 379-401.

Hess, D. T., Matsumoto, A., Kim, S. O., Marshall, H. E. and Stamler, J. S. (2005). "Protein S-nitrosylation: purview and parameters." Nat Rev Mol Cell Biol **6**(2): 150-166.

Hess, D. T. and Stamler, J. S. (2012). "Regulation by S-nitrosylation of protein post-translational modification." The Journal of biological chemistry **287**(7): 4411-4418.

Hilgen, G., von Maltzahn, J., Willecke, K., Weiler, R. and Dedek, K. (2011). "Subcellular distribution of connexin45 in OFF bipolar cells of the mouse retina." J Comp Neurol **519**(3): 433-450.

Hirose, M., Takahashi, N., Oe, H. and Doi, E. (1988). "Analyses of intramolecular disulfide bonds in proteins by polyacrylamide gel electrophoresis following two-step alkylation." Anal Biochem **168**(1): 193-201.

Hodel, C., Neuhauss, S. C. and Biehlmaier, O. (2006). "Time course and development of light adaptation processes in the outer zebrafish retina." Anat Rec A Discov Mol Cell Evol Biol **288**(6): 653-662.

Hofmann, F., Feil, R., Kleppisch, T. and Schlossmann, J. (2006). "Function of cGMP-dependent protein kinases as revealed by gene deletion." Physiol Rev **86**(1): 1-23.

Hollecker, M. (1997). Protein Structure: A Practical Approach. Oxford, IRL Press at Oxford University Press.

Hopsu, V. K. and Arstila, A. U. (1965). "AN APPARENT SOMATO-SOMATIC SYNAPTIC STRUCTURE IN THE PINEAL GLAND OF THE RAT." Exp Cell Res **37**: 484-487.

- Howes, K., Bronson, J. D., Dang, Y. L., Li, N., Zhang, K., Ruiz, C., Helekar, B., Lee, M., Subbaraya, I., Kolb, H., Chen, J. and Baehr, W. (1998). "Gene array and expression of mouse retina guanylate cyclase activating proteins 1 and 2." Invest Ophthalmol Vis Sci **39**(6): 867-875.
- Huang, Q., Hong, X. and Hao, Q. (2008). "SNAP-25 is also an iron-sulfur protein." FEBS Lett **582**(10): 1431-1436.
- Hughes, R. E., Brzovic, P. S., Dizhoor, A. M., Klevit, R. E. and Hurley, J. B. (1998). "Ca²⁺-dependent conformational changes in bovine GCAP-2." Protein Sci **7**(12): 2675-2680.
- Hughes, R. E., Brzovic, P. S., Klevit, R. E. and Hurley, J. B. (1995). "Calcium-dependent solvation of the myristoyl group of recoverin." Biochemistry **34**(36): 11410-11416.
- Hunt, D. M., Buch, P. and Michaelides, M. (2010). "Guanylate cyclases and associated activator proteins in retinal disease." Molecular and cellular biochemistry **334**(1-2): 157-168.
- Hurley, J. B. and Stryer, L. (1982). "Purification and characterization of the gamma regulatory subunit of the cyclic GMP phosphodiesterase from retinal rod outer segments." (0021-9258 (Print)).
- Hwang, J. Y. and Koch, K.-W. (2002). "Calcium- and myristoyl-dependent properties of guanylate cyclase-activating protein-1 and protein-2." Biochemistry **41**(43): 13021-13028.
- Hwang, J. Y., Lange, C., Helten, A., Höppner-Heitmann, D., Duda, T., Sharma, R. K. and Koch, K.-W. (2003). "Regulatory modes of rod outer segment membrane guanylate cyclase differ in catalytic efficiency and Ca(2+)-sensitivity." Eur J Biochem **270**(18): 3814-3821.
- Hwang, J. Y., Schlesinger, R. and Koch, K. W. (2001). "Calcium-dependent cysteine reactivities in the neuronal calcium sensor guanylate cyclase-activating protein 1." FEBS Lett **508**(3): 355-359.
- Hwang, J. Y., Schlesinger, R. and Koch, K. W. (2004). "Irregular dimerization of guanylate cyclase-activating protein 1 mutants causes loss of target activation." Eur J Biochem **271**(18): 3785-3793.
- Imamoto, Y. and Shichida, Y. (2014). "Cone visual pigments." Biochimica et Biophysica Acta (BBA) - Bioenergetics **1837**(5): 664-673.
- Imanishi, Y., Li, N., Sokal, I., Sowa, M. E., Lichtarge, O., Wensel, T. G., Saperstein, D. A., Baehr, W. and Palczewski, K. (2002). "Characterization of retinal guanylate cyclase-activating protein 3 (GCAP3) from zebrafish to man." Eur J Neurosci **15**(1): 63-78.
- Imanishi, Y., Yang, L., Sokal, I., Filipek, S., Palczewski, K. and Baehr, W. (2004). "Diversity of guanylate cyclase-activating proteins (GCAPs) in teleost fish: characterization of three novel GCAPs (GCAP4, GCAP5, GCAP7) from zebrafish (*Danio rerio*) and prediction of eight GCAPs (GCAP1-8) in pufferfish (*Fugu rubripes*)." J Mol Evol **59**(2): 204-217.
- Irvine, G. B. (2001). "Determination of molecular size by size-exclusion chromatography (gel filtration)." Curr Protoc Cell Biol **Chapter 5**: Unit 5.5.

- Jackman, S. L., Choi, S. Y., Thoreson, W. B., Rabl, K., Bartoletti, T. M. and Kramer, R. H. (2009). "Role of the synaptic ribbon in transmitting the cone light response." Nat Neurosci **12**(3): 303-310.
- Jacobson, S. G., Cideciyan, A. V., Peshenko, I. V., Sumaroka, A., Olshevskaya, E. V., Cao, L., Schwartz, S. B., Roman, A. J., Olivares, M. B., Sadigh, S., Yau, K.-W., Heon, E., Stone, E. M. and Dizhoor, A. M. (2013). "Determining consequences of retinal membrane guanylyl cyclase (RetGC1) deficiency in human Leber congenital amaurosis en route to therapy: residual cone-photoreceptor vision correlates with biochemical properties of the mutants." Human molecular genetics **22**(1): 168-183.
- Jastrow, H., von Mach, M. A. and Vollrath, L. (1997). "The shape of synaptic ribbons in the rat pineal gland." Cell Tissue Res **287**(2): 255-261.
- Karan, S., Frederick, J. M. and Baehr, W. (2010). "Novel functions of photoreceptor guanylate cyclases revealed by targeted deletion." Molecular and cellular biochemistry **334**(1-2): 141-155.
- Kaup, U. B. and Koch, K.-W. (1992). "Role of cGMP and Ca²⁺ in vertebrate photoreceptor excitation and adaptation." Annu Rev Physiol **54**: 153-175.
- Kaur, J., Kumar, A. and Kaur, J. (2018). "Strategies for optimization of heterologous protein expression in E. coli: Roadblocks and reinforcements." Int J Biol Macromol **106**: 803-822.
- Kawamura, S. and Tachibanaki, S. (2012). "Explaining the functional differences of rods versus cones." Wiley Interdisciplinary Reviews: Membrane Transport and Signaling **1**(5): 675-683.
- Klabusay, M. and Blinks, J. R. (1996). "Some commonly overlooked properties of calcium buffer systems: a simple method for detecting and correcting stoichiometric imbalance in CaEGTA stock solutions." Cell Calcium **20**(3): 227-234.
- Koch, K.-W. (1991). "Purification and identification of photoreceptor guanylate cyclase." The Journal of biological chemistry **266**(13): 8634-8637.
- Koch, K.-W. (2006). "GCAPs, the classical neuronal calcium sensors in the retina - a Ca²⁺-relay model of guanylate cyclase activation." Calcium Binding Proteins **1**(3-6).
- Koch, K.-W. (2013). "The guanylate cyclase signaling system in zebrafish photoreceptors." FEBS Lett **587**(13): 2055-2059.
- Koch, K.-W. and Dell'Orco, D. (2013). "A calcium-relay mechanism in vertebrate phototransduction." ACS Chem Neurosci **4**(6): 909-917.
- Koch, K.-W. and Dell'Orco, D. (2015). "Protein and Signaling Networks in Vertebrate Photoreceptor Cells." Frontiers in Molecular Neuroscience **8**(67).
- Koch, K.-W., Eckstein, F. and Stryer, L. (1990). "Stereochemical course of the reaction catalyzed by guanylate cyclase from bovine retinal rod outer segments." The Journal of biological chemistry **265**(17): 9659-9663.

- Koch, K.-W. and Stryer, L. (1988). "Highly cooperative feedback control of retinal rod guanylate cyclase by calcium ions." Nature **334**(6177): 64-66.
- Koch, M., Scheel, C., Ma, H., Yang, F., Stadlmeier, M., Glück, A. F., Murenu, E., Traube, F. R., Carell, T., Biel, M., Ding, X. Q. and Michalakis, S. (2020). "The cGMP-Dependent Protein Kinase 2 Contributes to Cone Photoreceptor Degeneration in the Cnga3-Deficient Mouse Model of Achromatopsia." Int J Mol Sci **22**(1).
- Kollmann, H., Becker, S. F., Shirdel, J., Scholten, A., Ostendorp, A., Lienau, C. and Koch, K.-W. (2012). "Probing the Ca(2+) switch of the neuronal Ca(2+) sensor GCAP2 by time-resolved fluorescence spectroscopy." ACS Chem Biol **7**(6): 1006-1014.
- Korenbrodt, J. I. (2012). "Speed, sensitivity, and stability of the light response in rod and cone photoreceptors: facts and models." Prog Retin Eye Res **31**(5): 442-466.
- Kretsinger, R. H. and Nockolds, C. E. (1973). "Carp muscle calcium-binding protein. II. Structure determination and general description." The Journal of biological chemistry **248**(9): 3313-3326.
- Krylov, D. M. and Hurley, J. B. (2001). "Identification of proximate regions in a complex of retinal guanylyl cyclase 1 and guanylyl cyclase-activating protein-1 by a novel mass spectrometry-based method." The Journal of biological chemistry **276**(33): 30648-30654.
- Kuhn, M. (2016). "Molecular Physiology of Membrane Guanylyl Cyclase Receptors." Physiological Reviews **96**(2): 751-804.
- Kumar, V., Carlson, J. E., Ohgi, K. A., Edwards, T. A., Rose, D. W., Escalante, C. R., Rosenfeld, M. G. and Aggarwal, A. K. (2002). "Transcription corepressor CtBP is an NAD(+)-regulated dehydrogenase." Mol Cell **10**(4): 857-869.
- Kurz, T., Karlsson, M., Brunk, U. T., Nilsson, S. E. and Frennesson, C. (2009). "ARPE-19 retinal pigment epithelial cells are highly resistant to oxidative stress and exercise strict control over their lysosomal redox-active iron." Autophagy **5**(4): 494-501.
- Kussrow, A., Kaltgrad, E., Wolfenden, M. L., Cloninger, M. J., Finn, M. G. and Bornhop, D. J. (2009). "Measurement of monovalent and polyvalent carbohydrate-lectin binding by back-scattering interferometry." Anal Chem **81**(12): 4889-4897.
- Ladant, D. (1995). "Calcium and membrane binding properties of bovine neurocalcin delta expressed in Escherichia coli." The Journal of biological chemistry **270**(7): 3179-3185.
- Laemmli, U. K. (1970). "Cleavage of structural proteins during the assembly of the head of bacteriophage T4." Nature **227**(5259): 680-685.
- Lagman, D., Callado-Pérez, A., Franzén, I. E., Larhammar, D. and Abalo, X. M. (2015). "Transducin duplicates in the zebrafish retina and pineal complex: differential specialisation after the teleost tetraploidisation." (1932-6203 (Electronic)).

- Lai, T. S., Hausladen, A., Slaughter, T. F., Eu, J. P., Stamler, J. S. and Greenberg, C. S. (2001). "Calcium regulates S-nitrosylation, denitrosylation, and activity of tissue transglutaminase." Biochemistry **40**(16): 4904-4910.
- Lamb, T. D. (2016). "Why rods and cones?" Eye **30**(2): 179-185.
- Lamzin, V. S., Dauter, Z., Popov, V. O., Harutyunyan, E. H. and Wilson, K. S. (1994). "High resolution structures of holo and apo formate dehydrogenase." J Mol Biol **236**(3): 759-785.
- Lange, C., Duda, T., Beyermann, M., Sharma, R. K. and Koch, K.-W. (1999). "Regions in vertebrate photoreceptor guanylyl cyclase ROS-GC1 involved in Ca²⁺-dependent regulation by guanylyl cyclase-activating protein GCAP-1." FEBS Letters **460**(1): 27-31.
- Lange, C. and Koch, K.-W. (1997). "Calcium-dependent binding of recoverin to membranes monitored by surface plasmon resonance spectroscopy in real time." Biochemistry **36**(40): 12019-12026.
- Lange, L. (2012). Die Bindung von Eisen an den Calciumsensor zGCAP5, Carl von Ossietzky University Oldenburg.
- Larison, K. D. and Bremiller, R. (1990). "Early onset of phenotype and cell patterning in the embryonic zebrafish retina." Development **109**(3): 567-576.
- Laura, R. P., Dizhoor, A. M. and Hurley, J. B. (1996). "The Membrane Guanylyl Cyclase, Retinal Guanylyl Cyclase-1, Is Activated through Its Intracellular Domain (∗)." Journal of Biological Chemistry **271**(20): 11646-11651.
- Lenzi, D., Runyeon, J. W., Crum, J., Ellisman, M. H. and Roberts, W. M. (1999). "Synaptic vesicle populations in saccular hair cells reconstructed by electron tomography." J Neurosci **19**(1): 119-132.
- Lewit-Bentley, A. and Réty, S. (2000). "EF-hand calcium-binding proteins." Curr Opin Struct Biol **10**(6): 637-643.
- Li, Y. N., Tsujimura, T., Kawamura, S. and Dowling, J. E. (2012). "Bipolar cell-photoreceptor connectivity in the zebrafish (*Danio rerio*) retina." J Comp Neurol **520**(16): 3786-3802.
- Lim, S., Peshenko, I., Dizhoor, A. and Ames, J. B. (2009). "Effects of Ca²⁺, Mg²⁺, and myristoylation on guanylyl cyclase activating protein 1 structure and stability." Biochemistry **48**(5): 850-862.
- Lim, S., Peshenko, I. V., Olshevskaya, E. V., Dizhoor, A. M. and Ames, J. B. (2016). "Structure of Guanylyl Cyclase Activator Protein 1 (GCAP1) Mutant V77E in a Ca²⁺-free/Mg²⁺-bound Activator State." The Journal of biological chemistry **291**(9): 4429-4441.
- Lim, S., Roseman, G., Peshenko, I., Manchala, G., Cudia, D., Dizhoor, A. M., Millhauser, G. and Ames, J. B. (2018). "Retinal guanylyl cyclase activating protein 1 forms a functional dimer." PLoS ONE **13**(3): e0193947.

Lim, S., Scholten, A., Manchala, G., Cudia, D., Zlomke-Sell, S.-K., Koch, K.-W. and Ames, J. B. (2017). "Structural characterization of ferrous ion binding to retinal guanylate cyclase activator protein 5 from zebrafish photoreceptors." Biochemistry **56**(51): 6652-6661.

Liu, C., Zhang, C. W., Lo, S. Q., Ang, S. T., Chew, K. C. M., Yu, D., Chai, B. H., Tan, B., Tsang, F., Tai, Y. K., Tan, B. W. Q., Liang, M. C., Tan, H. T., Tang, J. Y., Lai, M. K. P., Chua, J. J. E., Chung, M. C. M., Khanna, S., Lim, K. L. and Soong, T. W. (2018). "S-Nitrosylation of Divalent Metal Transporter 1 Enhances Iron Uptake to Mediate Loss of Dopaminergic Neurons and Motoric Deficit." J Neurosci **38**(39): 8364-8377.

Liu, X., Seno, K., Nishizawa, Y., Hayashi, F., Yamazaki, A., Matsumoto, H., Wakabayashi, T. and Usukura, J. (1994). "Ultrastructural localization of retinal guanylate cyclase in human and monkey retinas." Exp Eye Res **59**(6): 761-768.

Liu, Y., Ruoho, A. E., Rao, V. D. and Hurley, J. H. (1997). "Catalytic mechanism of the adenylyl and guanylyl cyclases: modeling and mutational analysis." Proceedings of the National Academy of Sciences of the United States of America **94**(25): 13414-13419.

Lottspeich, F. and Zorbach, H. (2012). Bioanalytik, Springer-Verlag.

Lowe, D. G., Dizhoor, A. M., Liu, K., Gu, Q., Spencer, M., Laura, R., Lu, L. and Hurley, J. B. (1995). "Cloning and expression of a second photoreceptor-specific membrane retina guanylyl cyclase (RetGC), RetGC-2." Proceedings of the National Academy of Sciences of the United States of America **92**(12): 5535-5539.

Lucas, K. A., Pitari, G. M., Kazerounian, S., Ruiz-Stewart, I., Park, J., Schulz, S., Chepenik, K. P. and Waldman, S. A. (2000). "Guanylyl cyclases and signaling by cyclic GMP." Pharmacol Rev **52**(3): 375-414.

Lucius, R. and Sievers, J. (1996). "Postnatal retinal ganglion cells in vitro: protection against reactive oxygen species (ROS)-induced axonal degeneration by cocultured astrocytes." Brain Res **743**(1-2): 56-62.

Luo, D.-G., Xue, T. and Yau, K.-W. (2008). "How vision begins: an odyssey." (1091-6490 (Electronic)).

Ma, X., Beuve, A. and van den Akker, F. (2010). "Crystal structure of the signaling helix coiled-coil domain of the beta1 subunit of the soluble guanylyl cyclase." BMC structural biology **10**: 2-2.

Maeda, T., Imanishi, Y. and Palczewski, K. (2003). "Rhodopsin phosphorylation: 30 years later." Prog Retin Eye Res **22**(4): 417-434.

Magupalli, V. G., Schwarz, K., Alpadi, K., Natarajan, S., Seigel, G. M. and Schmitz, F. (2008). "Multiple RIBEYE-RIBEYE interactions create a dynamic scaffold for the formation of synaptic ribbons." J Neurosci **28**(32): 7954-7967.

Maio, N. and Rouault, T. A. (2015). "Iron-sulfur cluster biogenesis in mammalian cells: New insights into the molecular mechanisms of cluster delivery." Biochimica et biophysica acta **1853**(6): 1493-1512.

Makino, C. L., Peshenko, I. V., Wen, X. H., Olshevskaya, E. V., Barrett, R. and Dizhoor, A. M. (2008). "A role for GCAP2 in regulating the photoresponse. Guanylyl cyclase activation and rod electrophysiology in GUCY1B knock-out mice." The Journal of biological chemistry **283**(43): 29135-29143.

- Margetić, A., Nannemann, D., Meiler, J., Huster, D. and Theisgen, S. (2014). "Guanylate Cyclase-Activating Protein-2 Undergoes Structural Changes upon Binding to Detergent Micelles and Bicelles." Biochimica et biophysica acta **1838**(11): 2767-2777.
- Marino, V., Sulmann, S., Koch, K.-W. and Dell'Orco, D. (2015). "Structural effects of Mg²⁺ on the regulatory states of three neuronal calcium sensors operating in vertebrate phototransduction." Biochimica et biophysica acta **1853**(9): 2055-2065.
- Markov, D. A., Swinney, K. and Bornhop, D. J. (2004). "Label-free molecular interaction determinations with nanoscale interferometry." J Am Chem Soc **126**(50): 16659-16664.
- Masland, R. H. (2012). "The neuronal organization of the retina." Neuron **76**(2): 266-280.
- Massoz, L., Dupont, M. A. and Manfroid, I. (2021). "Zebra-Fishing for Regenerative Awakening in Mammals." Biomedicines **9**(1).
- Mavlyutov, T. A., Cai, Y. and Ferreira, P. A. (2002). "Identification of RanBP2- and kinesin-mediated transport pathways with restricted neuronal and subcellular localization." Traffic **3**(9): 630-640.
- McKeon, T. A. and Lyman, M. L. (1991). "Calcium ion improves electrophoretic transfer of calmodulin and other small proteins." Analytical biochemistry **193**(1): 125-130.
- Mendez, A., Burns, M. E., Sokal, I., Dizhoor, A. M., Baehr, W., Palczewski, K., Baylor, D. A. and Chen, J. (2001). "Role of guanylate cyclase-activating proteins (GCAPs) in setting the flash sensitivity of rod photoreceptors." Proceedings of the National Academy of Sciences of the United States of America **98**(17): 9948-9953.
- Meyer, A. and Scharf, M. (1999). "Gene and genome duplications in vertebrates: the one-to-four (-to-eight in fish) rule and the evolution of novel gene functions." Curr Opin Cell Biol **11**(6): 699-704.
- Min, T., Ergenekan, C. E., Eidsness, M. K., Ichiye, T. and Kang, C. (2001). "Leucine 41 is a gate for water entry in the reduction of Clostridium pasteurianum rubredoxin." Protein Sci **10**(3): 613-621.
- Molday, R. S. and Moritz, O. L. (2015). "Photoreceptors at a glance." J Cell Sci **128**(22): 4039-4045.
- Nadolski, N. J., Balay, S. D., Wong, C. X. L., Waskiewicz, A. J. and Hocking, J. C. (2020). "Abnormal Cone and Rod Photoreceptor Morphogenesis in gdf6a Mutant Zebrafish." Invest Ophthalmol Vis Sci **61**(4): 9.
- Nakatani, K., Chen, C., Yau, K. W. and Koutalos, Y. (2002). "Calcium and phototransduction." Adv Exp Med Biol **514**: 1-20.
- Nakatani, K. and Yau, K. W. (1988). "Guanosine 3',5'-cyclic monophosphate-activated conductance studied in a truncated rod outer segment of the toad." The Journal of physiology **395**: 731-753.

Nardini, M., Spanò, S., Cericola, C., Pesce, A., Massaro, A., Millo, E., Luini, A., Corda, D. and Bolognesi, M. (2003). "CtBP/BARS: a dual-function protein involved in transcription co-repression and Golgi membrane fission." Embo j **22**(12): 3122-3130.

Nasuno, R., Yoshioka, N., Yoshikawa, Y. and Takagi, H. (2021). "Cysteine residues in the fourth zinc finger are important for activation of the nitric oxide-inducible transcription factor Fzf1 in the yeast *Saccharomyces cerevisiae*." Genes Cells **26**(10): 823-829.

Nawrocki, L., BreMiller, R., Streisinger, G. and Kaplan, M. (1985). "Larval and adult visual pigments of the zebrafish, *Brachydanio rerio*." Vision Res **25**(11): 1569-1576.

Nemitz, L., Dedek, K. and Janssen-Bienhold, U. (2021). "Synaptic Remodeling in the Cone Pathway After Early Postnatal Horizontal Cell Ablation." Front Cell Neurosci **15**: 657594.

Olshevskaya, E. V., Ermilov, A. N. and Dizhoor, A. M. (1999). "Dimerization of guanylyl cyclase-activating protein and a mechanism of photoreceptor guanylyl cyclase activation." The Journal of biological chemistry **274**(36): 25583-25587.

Olshevskaya, E. V., Ermilov, A. N. and Dizhoor, A. M. (2002). "Factors that affect regulation of cGMP synthesis in vertebrate photoreceptors and their genetic link to human retinal degeneration." Molecular and cellular biochemistry **230**(1-2): 139-147.

Olshevskaya, E. V., Hughes, R. E., Hurley, J. B. and Dizhoor, A. M. (1997). "Calcium binding, but not a calcium-myristoyl switch, controls the ability of guanylyl cyclase-activating protein GCAP-2 to regulate photoreceptor guanylyl cyclase." The Journal of biological chemistry **272**(22): 14327-14333.

Otto-Bruc, A., Fariss, R. N., Haeseleer, F., Huang, J., Buczyłko, J., Surgucheva, I., Baehr, W., Milam, A. H. and Palczewski, K. (1997). "Localization of guanylate cyclase-activating protein 2 in mammalian retinas." Proceedings of the National Academy of Sciences of the United States of America **94**(9): 4727-4732.

Palczewski, K., Sokal, I. and Baehr, W. (2004). "Guanylate cyclase-activating proteins: structure, function, and diversity." Biochem Biophys Res Commun **322**(4): 1123-1130.

Palczewski, K., Subbaraya, I., Gorczyca, W. A., Helekar, B. S., Ruiz, C. C., Ohguro, H., Huang, J., Zhao, X., Crabb, J. W., Johnson, R. S. and et al. (1994). "Molecular cloning and characterization of retinal photoreceptor guanylyl cyclase-activating protein." Neuron **13**(2): 395-404.

Paquet-Durand, F., Beck, S., Michalakis, S., Goldmann, T., Huber, G., Mühlfriedel, R., Trifunović, D., Fischer, M. D., Fahl, E., Duetsch, G., Becirovic, E., Wolfrum, U., van Veen, T., Biel, M., Tanimoto, N. and Seeliger, M. W. (2011). "A key role for cyclic nucleotide gated (CNG) channels in cGMP-related retinitis pigmentosa." Human molecular genetics **20**(5): 941-947.

Paquet-Durand, F., Hauck, S. M., van Veen, T., Ueffing, M. and Ekström, P. (2009). "PKG activity causes photoreceptor cell death in two retinitis pigmentosa models." J Neurochem **108**(3): 796-810.

Parat, M., Blanchet, J. and De Léan, A. (2010). "Role of juxtamembrane and transmembrane domains in the mechanism of natriuretic peptide receptor A activation." Biochemistry **49**(22): 4601-4610.

- Pattanaik, D. K., Sahu, A. P., Lakshminarayanan, V. and Sharma, N. K. (2021). "The alpha-Wave of the Electroretinogram and Iron-Induced Oxidative Stress: A Model." Acta Biotheor **70**(1): 2.
- Pennesi, M. E., Howes, K. A., Baehr, W. and Wu, S. M. (2003). "Guanylate cyclase-activating protein (GCAP) 1 rescues cone recovery kinetics in GCAP1/GCAP2 knockout mice." Proceedings of the National Academy of Sciences of the United States of America **100**(11): 6783-6788.
- Peshenko, I. V., Cideciyan, A. V., Sumaroka, A., Olshevskaya, E. V., Scholten, A., Abbas, S., Koch, K.-W., Jacobson, S. G. and Dizhoor, A. M. (2019). "A G86R mutation in the calcium-sensor protein GCAP1 alters regulation of retinal guanylyl cyclase and causes dominant cone-rod degeneration." The Journal of biological chemistry **294**(10): 3476-3488.
- Peshenko, I. V. and Dizhoor, A. M. (2004). "Guanylyl cyclase-activating proteins (GCAPs) are Ca²⁺/Mg²⁺ sensors: implications for photoreceptor guanylyl cyclase (RetGC) regulation in mammalian photoreceptors." (0021-9258 (Print)).
- Peshenko, I. V. and Dizhoor, A. M. (2006). "Ca²⁺ and Mg²⁺ binding properties of GCAP-1. Evidence that Mg²⁺-bound form is the physiological activator of photoreceptor guanylyl cyclase." The Journal of biological chemistry **281**(33): 23830-23841.
- Peshenko, I. V. and Dizhoor, A. M. (2007). "Activation and inhibition of photoreceptor guanylyl cyclase by guanylyl cyclase activating protein 1 (GCAP-1): the functional role of Mg²⁺/Ca²⁺ exchange in EF-hand domains." The Journal of biological chemistry **282**(30): 21645-21652.
- Peshenko, I. V., Olshevskaya, E. V., Azadi, S., Molday, L. L., Molday, R. S. and Dizhoor, A. M. (2011). "Retinal degeneration 3 (RD3) protein inhibits catalytic activity of retinal membrane guanylyl cyclase (RetGC) and its stimulation by activating proteins." Biochemistry **50**(44): 9511-9519.
- Peshenko, I. V., Olshevskaya, E. V. and Dizhoor, A. M. (2008). "Binding of guanylyl cyclase activating protein 1 (GCAP1) to retinal guanylyl cyclase (RetGC1). The role of individual EF-hands." The Journal of biological chemistry **283**(31): 21747-21757.
- Peshenko, I. V., Olshevskaya, E. V. and Dizhoor, A. M. (2015a). "Evaluating the role of retinal membrane guanylyl cyclase 1 (RetGC1) domains in binding guanylyl cyclase-activating proteins (GCAPs)." The Journal of biological chemistry **290**(11): 6913-6924.
- Peshenko, I. V., Olshevskaya, E. V. and Dizhoor, A. M. (2015b). "Dimerization Domain of Retinal Membrane Guanylyl Cyclase 1 (RetGC1) Is an Essential Part of Guanylyl Cyclase-activating Protein (GCAP) Binding Interface." The Journal of biological chemistry **290**(32): 19584-19596.
- Peshenko, I. V., Olshevskaya, E. V. and Dizhoor, A. M. (2016). "Functional Study and Mapping Sites for Interaction with the Target Enzyme in Retinal Degeneration 3 (RD3) Protein." The Journal of biological chemistry **291**(37): 19713-19723.
- Peshenko, I. V., Olshevskaya, E. V., Lim, S., Ames, J. B. and Dizhoor, A. M. (2012). "Calcium-myristoyl Tug is a new mechanism for intramolecular tuning of calcium sensitivity and target enzyme interaction for guanylyl cyclase-activating protein 1: dynamic connection between N-fatty acyl group and EF-hand controls calcium sensitivity." The Journal of biological chemistry **287**(17): 13972-13984.

- Peshenko, I. V., Olshevskaya, E. V., Yao, S., Ezzeldin, H. H., Pittler, S. J. and Dizhoor, A. M. (2010). "Activation of retinal guanylyl cyclase RetGC1 by GCAP1: stoichiometry of binding and effect of new LCA-related mutations." Biochemistry **49**(4): 709-717.
- Pettelkau, J., Schröder, T., Ihling, C. H., Olausson, B. E., Kölbl, K., Lange, C. and Sinz, A. (2012). "Structural Insights into retinal guanylylcyclase-GCAP-2 interaction determined by cross-linking and mass spectrometry." Biochemistry **51**(24): 4932-4949.
- Pettelkau, J., Thondorf, I., Theisgen, S., Lilie, H., Schröder, T., Arlt, C., Ihling, C. H. and Sinz, A. (2013). "Structural analysis of guanylyl cyclase-activating protein-2 (GCAP-2) homodimer by stable isotope-labeling, chemical cross-linking, and mass spectrometry." J Am Soc Mass Spectrom **24**(12): 1969-1979.
- Picard, E., Daruich, A., Youale, J., Courtois, Y. and Behar-Cohen, F. (2020). "From Rust to Quantum Biology: The Role of Iron in Retina Physiopathology." Cells **9**(3).
- Picard, E., Fontaine, I., Jonet, L., Guillou, F., Behar-Cohen, F., Courtois, Y. and Jeanny, J. C. (2008). "The protective role of transferrin in Müller glial cells after iron-induced toxicity." Mol Vis **14**: 928-941.
- Pilz, R. B. and Broderick, K. E. (2005). "Role of cyclic GMP in gene regulation." Front Biosci **10**: 1239-1268.
- Power, M., Das, S., Schütze, K., Marigo, V., Ekström, P. and Paquet-Durand, F. (2020). "Cellular mechanisms of hereditary photoreceptor degeneration - Focus on cGMP." Prog Retin Eye Res **74**: 100772.
- Pugh, E. N. and Lamb, T. D. (2000). Chapter 5 Phototransduction in vertebrate rods and cones: Molecular mechanisms of amplification, recovery and light adaptation. Handbook of Biological Physics. D. G. Stavenga, W. J. DeGrip and E. N. Pugh, North-Holland. **3**: 183-255.
- Ramamurthy, V., Tucker, C., Wilkie, S. E., Daggett, V., Hunt, D. M. and Hurley, J. B. (2001). "Interactions within the coiled-coil domain of RetGC-1 guanylyl cyclase are optimized for regulation rather than for high affinity." The Journal of biological chemistry **276**(28): 26218-26229.
- Rätscho, N., Scholten, A. and Koch, K.-W. (2009). "Expression profiles of three novel sensory guanylate cyclases and guanylate cyclase-activating proteins in the zebrafish retina." Biochimica et biophysica acta **1793**(6): 1110-1114.
- Rätscho, N., Scholten, A. and Koch, K.-W. (2010). "Diversity of sensory guanylate cyclases in teleost fishes." Molecular and cellular biochemistry **334**(1-2): 207-214.
- Raymond, P. A. and Barthel, L. K. (2004). "A moving wave patterns the cone photoreceptor mosaic array in the zebrafish retina." Int J Dev Biol **48**(8-9): 935-945.
- Raymond, P. A., Barthel, L. K. and Curran, G. A. (1995). "Developmental patterning of rod and cone photoreceptors in embryonic zebrafish." J Comp Neurol **359**(4): 537-550.
- Reinert, A., Morawski, M., Seeger, J., Arendt, T. and Reinert, T. (2019). "Iron concentrations in neurons and glial cells with estimates on ferritin concentrations." BMC Neurosci **20**(1): 25.

Riddles, P. W., Blakeley, R. L. and Zerner, B. (1983). "Reassessment of Ellman's reagent." Methods in enzymology **91**: 49-60.

Rieke, F. and Baylor, D. A. (1998). "Single-photon detection by rod cells of the retina." Reviews of Modern Physics **70**(3): 1027-1036.

Robin, J., Brauer, J., Sulmann, S., Marino, V., Dell'Orco, D., Lienau, C. and Koch, K.-W. (2015). "Differential Nanosecond Protein Dynamics in Homologous Calcium Sensors." ACS Chem Biol **10**(10): 2344-2352.

Robinson, J., Schmitt, E. A., Hárosi, F. I., Reece, R. J. and Dowling, J. E. (1993). "Zebrafish ultraviolet visual pigment: absorption spectrum, sequence, and localization." Proceedings of the National Academy of Sciences of the United States of America **90**(13): 6009-6012.

Rogers, B. S., Symons, R. C., Komeima, K., Shen, J., Xiao, W., Swaim, M. E., Gong, Y. Y., Kachi, S. and Campochiaro, P. A. (2007). "Differential sensitivity of cones to iron-mediated oxidative damage." Invest Ophthalmol Vis Sci **48**(1): 438-445.

Rosenzweig, D. H., Nair, K. S., Levay, K., Peshenko, I. V., Crabb, J. W., Dizhoor, A. M. and Slepak, V. Z. (2009). "Interaction of retinal guanylate cyclase with the alpha subunit of transducin: potential role in transducin localization." The Biochemical journal **417**(3): 803-812.

Sakurai, K., Chen, J. and Kefalov, V. J. (2011). "Role of Guanylyl Cyclase Modulation in Mouse Cone Phototransduction." The Journal of Neuroscience **31**(22): 7991.

Sambrook, J., Fritsch, E. F. and Maniatis, T. (1989). Molecular cloning: a laboratory manual. Cold Spring Harbor, NY, Cold Spring Harbor Laboratory Press.

Schindelin, J., Arganda-Carreras, I., Frise, E., Kaynig, V., Longair, M., Pietzsch, T., Preibisch, S., Rueden, C., Saalfeld, S., Schmid, B., Tinevez, J. Y., White, D. J., Hartenstein, V., Eliceiri, K., Tomancak, P. and Cardona, A. (2012). "Fiji: an open-source platform for biological-image analysis." Nat Methods **9**(7): 676-682.

Schmitz, F. (2009). "The making of synaptic ribbons: how they are built and what they do." Neuroscientist **15**(6): 611-624.

Schmitz, F., Königstorfer, A. and Südhof, T. C. (2000). "RIBEYE, a component of synaptic ribbons: a protein's journey through evolution provides insight into synaptic ribbon function." Neuron **28**(3): 857-872.

Scholten, A. and Koch, K. W. (2011). "Differential calcium signaling by cone specific guanylate cyclase-activating proteins from the zebrafish retina." PLoS ONE **6**(8): e23117.

Schrem, A., Lange, C., Beyermann, M. and Koch, K.-W. (1999). "Identification of a domain in guanylyl cyclase-activating protein 1 that interacts with a complex of guanylyl cyclase and tubulin in photoreceptors." The Journal of biological chemistry **274**(10): 6244-6249.

Seebacher, T., Beitz, E., Kumagami, H., Wild, K., Ruppertsberg, J. P. and Schultz, J. E. (1999). "Expression of membrane-bound and cytosolic guanylyl cyclases in the rat inner ear." Hear Res **127**(1-2): 95-102.

Seidel, A., Kantarjian, A. and Vollrath, L. (1990). "A possible role for cyclic guanosine monophosphate in the rat pineal gland." Neurosci Lett **110**(1-2): 227-231.

Seno, K., Kishigami, A., Ihara, S., Maeda, T., Bondarenko, V. A., Nishizawa, Y., Usukura, J., Yamazaki, A. and Hayashi, F. (1998). "A possible role of RGS9 in phototransduction. A bridge between the cGMP-phosphodiesterase system and the guanylyl cyclase system." The Journal of biological chemistry **273**(35): 22169-22172.

Shahu, M. K., Schuhmann, F., Scholten, A., Solov'yov, I. A. and Koch, K.-W. (2022). "The Transition of Photoreceptor Guanylate Cyclase Type 1 to the Active State." Int J Mol Sci **23**(7).

Sharma, R. K. (2010). "Membrane guanylate cyclase is a beautiful signal transduction machine: overview." Molecular and cellular biochemistry **334**(1-2): 3-36.

Sharon, D., Wimberg, H., Kinary, Y. and Koch, K.-W. (2018). "Genotype-functional-phenotype correlations in photoreceptor guanylate cyclase (GC-E) encoded by GUCY2D." Prog Retin Eye Res **63**: 69-91.

Shyjan, A. W., de Sauvage, F. J., Gillett, N. A., Goeddel, D. V. and Lowe, D. G. (1992). "Molecular cloning of a retina-specific membrane guanylyl cyclase." Neuron **9**(4): 727-737.

Sjöstrand, F. S. (1953). "The Ultrastructure of the Retinal Rod Synapses of the Guinea Pig Eye." J Appl Physics **24**(11): 1422-1422.

Sjöstrand, F. S. (1958). "Ultrastructure of retinal rod synapses of the guinea pig eye as revealed by three-dimensional reconstructions from serial sections." Journal of Ultrastructure Research **2**(1): 122-170.

Smith, C. A. and Sjöstrand, F. S. (1961). "A synaptic structure in the hair cells of the guinea pig cochlea." Journal of Ultrastructure Research **5**(2): 184-192.

Sokal, I., Haeseleer, F., Arendt, A., Adman, E. T., Hargrave, P. A. and Palczewski, K. (1999). "Identification of a guanylyl cyclase-activating protein-binding site within the catalytic domain of retinal guanylyl cyclase 1." Biochemistry **38**(5): 1387-1393.

Sokal, I., Li, N., Klug, C. S., Filipek, S., Hubbell, W. L., Baehr, W. and Palczewski, K. (2001). "Calcium-sensitive regions of GCAP1 as observed by chemical modifications, fluorescence, and EPR spectroscopies." The Journal of biological chemistry **276**(46): 43361-43373.

Spessert, R., Gupta, B. B., Seidel, A., Maitra, S. K. and Vollrath, L. (1992). "Involvement of cyclic guanosine monophosphate (cGMP) and cytosolic guanylate cyclase in the regulation of synaptic ribbon numbers in rat pineal gland." Brain Res **570**(1-2): 231-236.

Spiwox-Becker, I., Glas, M., Lasarzik, I. and Vollrath, L. (2004). "Mouse photoreceptor synaptic ribbons lose and regain material in response to illumination changes." Eur J Neurosci **19**(6): 1559-1571.

Stamler, J. S., Jaraki, O., Osborne, J., Simon, D. I., Keaney, J., Vita, J., Singel, D., Valeri, C. R. and Loscalzo, J. (1992). "Nitric oxide circulates in mammalian plasma primarily as an S-nitroso adduct of serum albumin." Proceedings of the National Academy of Sciences of the United States of America **89**(16): 7674-7677.

- Stephen, R., Bereta, G., Golczak, M., Palczewski, K. and Sousa, M. C. (2007). "Stabilizing function for myristoyl group revealed by the crystal structure of a neuronal calcium sensor, guanylate cyclase-activating protein 1." Structure (London, England : 1993) **15**(11): 1392-1402.
- Stephen, R., Palczewski, K. and Sousa, M. C. (2006). "The crystal structure of GCAP3 suggests molecular mechanism of GCAP-linked cone dystrophies." J Mol Biol **359**(2): 266-275.
- Sterling, P. (1998). The Retina. The synaptic organization of the brain. New York, Oxford University Press: 205-253.
- Sterling, P. and Matthews, G. (2005). "Structure and function of ribbon synapses." Trends Neurosci **28**(1): 20-29.
- Stone, J. R. and Marletta, M. A. (1994). "Soluble guanylate cyclase from bovine lung: activation with nitric oxide and carbon monoxide and spectral characterization of the ferrous and ferric states." Biochemistry **33**(18): 5636-5640.
- Stryer, L. (1991). "Visual excitation and recovery." The Journal of biological chemistry **266**(17): 10711-10714.
- Studier, F. W. and Moffatt, B. A. (1986). "Use of bacteriophage T7 RNA polymerase to direct selective high-level expression of cloned genes." J Mol Biol **189**(1): 113-130.
- Sulmann, S. (2016). The Guanylate Cyclase-GCAP System - a multi protein complex in phototransduction. School of Mathematics and Science, Carl von Ossietzky University Oldenburg.
- Sulmann, S., Kussrow, A., Bornhop, D. J. and Koch, K.-W. (2017). "Label-free quantification of calcium-sensor targeting to photoreceptor guanylate cyclase and rhodopsin kinase by backscattering interferometry." Scientific Reports **7**(1): 45515.
- Sulmann, S., Vocke, F., Scholten, A. and Koch, K.-W. (2015). "Retina specific GCAPs in zebrafish acquire functional selectivity in Ca²⁺-sensing by myristoylation and Mg²⁺-binding." Scientific Reports **5**(1): 11228.
- SurrIDGE, A. K., Osorio, D. and Mundy, N. I. (2003). "Evolution and selection of trichromatic vision in primates." Trends in Ecology & Evolution **18**(4): 198-205.
- Tabor, S. (2001). "Expression using the T7 RNA polymerase/promoter system." Curr Protoc Mol Biol **Chapter 16**: Unit16.12.
- Tanaka, T., Ames, J. B., Harvey, T. S., Stryer, L. and Ikura, M. (1995). "Sequestration of the membrane-targeting myristoyl group of recoverin in the calcium-free state." Nature **376**(6539): 444-447.
- Taylor, J. S., Braasch, I., Frickey, T., Meyer, A. and Van de Peer, Y. (2003). "Genome duplication, a trait shared by 22000 species of ray-finned fish." Genome Res **13**(3): 382-390.

Theisgen, S., Thomas, L., Schröder, T., Lange, C., Kovermann, M., Balbach, J. and Huster, D. (2011). "The presence of membranes or micelles induces structural changes of the myristoylated guanylate-cyclase activating protein-2." European Biophysics Journal **40**(4): 565-576.

Thompson, D. and Larson, G. (1992). "Western blots using stained protein gels." BioTechniques **12**(5): 656-658.

tom Dieck, S. and Brandstätter, J. H. (2006). "Ribbon synapses of the retina." Cell Tissue Res **326**(2): 339-346.

Usui, S., Oveson, B. C., Lee, S. Y., Jo, Y. J., Yoshida, T., Miki, A., Miki, K., Iwase, T., Lu, L. and Campochiaro, P. A. (2009). "NADPH oxidase plays a central role in cone cell death in retinitis pigmentosa." J Neurochem **110**(3): 1028-1037.

Utsumi, T., Sato, M., Nakano, K., Takemura, D., Iwata, H. and Ishisaka, R. (2001). "Amino acid residue penultimate to the amino-terminal gly residue strongly affects two cotranslational protein modifications, N-myristoylation and N-acetylation." The Journal of biological chemistry **276**(13): 10505-10513.

Venkataraman, V., Duda, T., Vardi, N., Koch, K.-W. and Sharma, R. K. (2003). "Calcium-modulated guanylate cyclase transduction machinery in the photoreceptor--bipolar synaptic region." Biochemistry **42**(19): 5640-5648.

Venkataraman, V., Nagele, R., Duda, T. and Sharma, R. K. (2000). "Rod Outer Segment Membrane Guanylate Cyclase Type 1-Linked Stimulatory and Inhibitory Calcium Signaling Systems in the Pineal Gland: Biochemical, Molecular, and Immunohistochemical Evidence." Biochemistry **39**(20): 6042-6052.

Venkatesan, J. K., Natarajan, S., Schwarz, K., Mayer, S. I., Alpadi, K., Magupalli, V. G., Sung, C. H. and Schmitz, F. (2010). "Nicotinamide adenine dinucleotide-dependent binding of the neuronal Ca²⁺ sensor protein GCAP2 to photoreceptor synaptic ribbons." J Neurosci **30**(19): 6559-6576.

Vighi, E., Trifunović, D., Veiga-Crespo, P., Rentsch, A., Hoffmann, D., Sahaboglu, A., Strasser, T., Kulkarni, M., Bertolotti, E., van den Heuvel, A., Peters, T., Reijerkerk, A., Euler, T., Ueffing, M., Schwede, F., Genieser, H. G., Gaillard, P., Marigo, V., Ekström, P. and Paquet-Durand, F. (2018). "Combination of cGMP analogue and drug delivery system provides functional protection in hereditary retinal degeneration." Proceedings of the National Academy of Sciences of the United States of America **115**(13): E2997-e3006.

Vogel, A., Schröder, T., Lange, C. and Huster, D. (2007). "Characterization of the myristoyl lipid modification of membrane-bound GCAP-2 by 2H solid-state NMR spectroscopy." Biochimica et Biophysica Acta (BBA) - Biomembranes **1768**(12): 3171-3181.

Wan, L., Almers, W. and Chen, W. (2005). "Two ribeye genes in teleosts: the role of Ribeye in ribbon formation and bipolar cell development." J Neurosci **25**(4): 941-949.

Wässle, H. (2004). "Parallel processing in the mammalian retina." Nat Rev Neurosci **5**(10): 747-757.

Wej, T., Schubert, T., Paquet-Durand, F., Tanimoto, N., Chang, L., Koeppen, K., Ott, T., Griesbeck, O., Seeliger, M. W., Euler, T. and Wissinger, B. (2012). "Light-driven calcium signals in mouse cone photoreceptors." J Neurosci **32**(20): 6981-6994.

Weiergräber, O. H., Senin, I., Zernii, E. Y., Churumova, V. A., Kovaleva, N. A., Nazipova, A. A., Permyakov, S. E., Permyakov, E. A., Philippov, P. P., Granzin, J. and Koch, K.-W. (2006). "Tuning of a neuronal calcium sensor." The Journal of biological chemistry **281**(49): 37594-37602.

Wensel, T. G. and Stryer, L. (1986). "Reciprocal control of retinal rod cyclic GMP phosphodiesterase by its gamma subunit and transducin." (0887-3585 (Print)).

Wimberg, H., Janssen-Bienhold, U. and Koch, K.-W. (2018b). "Control of the Nucleotide Cycle in Photoreceptor Cell Extracts by Retinal Degeneration Protein 3." Front Mol Neurosci **11**: 52.

Wimberg, H., Lev, D., Yosovich, K., Namburi, P., Banin, E., Sharon, D. and Koch, K.-W. (2018a). "Photoreceptor Guanylate Cyclase (GUCY2D) Mutations Cause Retinal Dystrophies by Severe Malfunction of Ca(2+)-Dependent Cyclic GMP Synthesis." Front Mol Neurosci **11**: 348.

Woodruff, M. L., Sampath, A. P., Matthews, H. R., Krasnoperova, N. V., Lem, J. and Fain, G. L. (2002). "Measurement of cytoplasmic calcium concentration in the rods of wild-type and transducin knock-out mice." The Journal of physiology **542**(Pt 3): 843-854.

Yamazaki, A., Yu, H., Yamazaki, M., Honkawa, H., Matsuura, I., Usukura, J. and Yamazaki, R. K. (2003). "A critical role for ATP in the stimulation of retinal guanylyl cyclase by guanylyl cyclase-activating proteins." The Journal of biological chemistry **278**(35): 33150-33160.

Yang, R. B. and Garbers, D. L. (1997). "Two eye guanylyl cyclases are expressed in the same photoreceptor cells and form homomers in preference to heteromers." The Journal of biological chemistry **272**(21): 13738-13742.

Yang, R. B., Robinson, S. W., Xiong, W. H., Yau, K. W., Birch, D. G. and Garbers, D. L. (1999). "Disruption of a retinal guanylyl cyclase gene leads to cone-specific dystrophy and paradoxical rod behavior." J Neurosci **19**(14): 5889-5897.

Yau, W. W. and Bly, D. D. (1980). Size Exclusion Chromatography (GPC). Washington, D. C., American Chemical Society.

Yefimova, M. G., Jeanny, J. C., Guillonau, X., Keller, N., Nguyen-Legros, J., Sergeant, C., Guillou, F. and Courtois, Y. (2000). "Iron, ferritin, transferrin, and transferrin receptor in the adult rat retina." Invest Ophthalmol Vis Sci **41**(8): 2343-2351.

Yu, H., Bondarenko, V. A. and Yamazaki, A. (2001). "Inhibition of retinal guanylyl cyclase by the RGS9-1 N-terminus." Biochem Biophys Res Commun **286**(1): 12-19.

Zägel, P. and Koch, K.-W. (2014). "Dysfunction of outer segment guanylate cyclase caused by retinal disease related mutations." Frontiers in Molecular Neuroscience **7**(4).

Zenisek, D., Horst, N. K., Merrifield, C., Sterling, P. and Matthews, G. (2004). "Visualizing synaptic ribbons in the living cell." J Neurosci **24**(44): 9752-9759.

Zou, J., Lathrop, K. L., Sun, M. and Wei, X. (2008). "Intact retinal pigment epithelium maintained by Nok is essential for retinal epithelial polarity and cellular patterning in zebrafish." J Neurosci **28**(50): 13684-13695.

Zozulya, S. and Stryer, L. (1992). "Calcium-myristoyl protein switch." Proceedings of the National Academy of Sciences **89**(23): 11569.

Appendix

Amino acid codes

Table A1: Three letter and one letter codes of 20 proteinogenic amino acids.

name	three letter code	one letter code
alanine	Ala	A
arginine	Arg	R
asparagine	Asn	N
aspartic acid	Asp	D
cysteine	Cys	C
glutamic acid	Glu	E
glutamine	Gln	Q
glycine	Gly	G
histidine	His	H
isoleucine	Ile	I
leucine	Leu	L
lysine	Lys	K
methionine	Met	M
phenylalanine	Phe	F
proline	Pro	P
serine	Ser	S
threonine	Thr	T
tryptophan	Trp	W
tyrosine	Tyr	Y
valine	Val	V

Amino acid sequences of bovine and zebrafish GCAPs

bGCAP1	MGNIMD----	--GKSVEELS	ST E CHQWYKK	FMTECP S GQL	TLYEFRQFFG	LKNLSPWASQ	54
bGCAP2	MGQQFSWEEA	EENGAVGAAD	AAQLQEWYKK	FLEECPSGTL	FMHEFKRFFK	VPDN-EEATQ	59
zGCAP5	MGD-SS----	--SMSATELS	ACKCHQWYRK	FMTECPSGQL	TFYEFKKFFG	LKNLSEKSNA	53
zGCAP1	MGN-ST----	--GSTVDDLQ	AVEMHLWYKK	FMTECP S GQL	TLHEFKQFFG	LRGLDPKANA	53
zGCAP2	MGQRLSDD--	---SDEKEID	VAELQEWYKK	FVIECP S GTL	FMHDFKSFFG	VTEN-PEAAD	54
zGCAP3	MGA--H----	--ASNLDEVL	AEDMHYWY N K	FMRES P SGLI	TLFELKNMLE	MQGMTEEASS	52
zGCAP4	MGN--N----	--HASLDDIL	AEDMHHWY N K	FMRES P SGLI	TLFELKSILG	LQGMNEDANS	52
zGCAP7	MGQNQSDEE-	-----EEEVE	L T EIQPLYTR	FMKVC P SGAL	HLHEFRIRIFG	VQSSSEEEAL	54
bGCAP1	YVEQM F ETFD	FNKDG I IDFM	EYVAALS L VL	KGK V EQKLRW	YFKLYD V DGN	GCIDR D ELLT	114
bGCAP2	YVEAM F RAFD	TNGD N TIDFL	EYVAAL N LVL	RGTLE H KLKW	TFKIYD K DRN	GCIDR Q ELLD	119
zGCAP5	YVNTMFKTFD	IDDDGCIDFM	EYVAALSLVL	KGGVQQKLRW	YFKLFDMDGS	GCIDKDELLL	113
zGCAP1	YIEQM F RTFD	MNKDG I IDFM	EYVAALS L VM	RGKME H KLRW	YFKLYD V DGN	GCIDR Y ELLN	113
zGCAP2	YIENM F RAFD	KNGD N TIDFL	EYVAAL N LVL	RGKLE H KLKW	TFKMYD K DGS	GCID K TELKE	114
zGCAP3	YVDQ V FFTFD	MDGD G YIDFV	EYIAAV S LLL	KGEIN Q KLKW	YFKL F DQDGN	GKIDR D EMET	112
zGCAP4	YVDQ V FCTFD	MDRD G YIDFV	EYIAA I SMLL	KGEIN Q KLKW	YFKL F DQDGN	GKID K DELET	112
zGCAP7	YMET I FKSFD	TNRD N VIDFM	EFVA A VHLVL	RGNLE D RLLKW	SFKVY D RDEN	GKLD R QEVIH	114
bGCAP1	IIRAI R AINP	CS-----	-D S TMTAEEF	TDTV F SKIDV	NGDG E LSLEE	FMEGV Q KDQM	165
bGCAP2	IVESI Y KLKK	ACS V EVEAEQ	Q G KLLTPEEV	VDRIF L LVDE	NGDG Q LSLNE	FVEG A RRDKW	179
zGCAP5	IFKAVQAING	AE-----	-P-EISAEDL	ADIVFNKIDV	NGDGELSLEE	FMEGISADEK	163
zGCAP1	I I KAIRA I NG	SE-----	-T Q ESSAEEF	TNRV F ERIDI	NGDG E LSLDE	FVAG A RSDEE	164
zGCAP2	IVESI Y RLKK	ACH G ELDAE-	-CN L LLTPDQV	VDRIF E LVDE	NGDG E LSLDE	FIDG A RRDKW	172
zGCAP3	IFKAI Q DITR	SY-----	---E I PPDDI	VSLI Y ERIDV	N N EGELTLEE	FITG A KEHPD	161
zGCAP4	IFTAI Q DITR	NR-----	---D I VPEEI	VALIF E KIDV	N G EGELTLEE	FIEG A KEHPE	161
zGCAP7	VIRIL C LKK	N-----	-R I NMTPVEI	CDRIF E LLDE	N N DG Q ISLSE	FLEGA E KDAW	164
bGCAP1	LLDTL T RS L D	LTRIV R RLQ N	GEQDE E GASG	RETEA A EADG	205		
bGCAP2	VMKML Q MDL-	-NPSS W ISQ Q	RRKS A MF---	-----	204		
zGCAP5	ISEMLTQSLD	LTRIVSNIYN	DSYIEQEAEI	IEDQA-----	198		
zGCAP1	FMEV M MK S LD	LTHIV A MI H N	RR H SV----	-----	189		
zGCAP2	VMKML Q MDV-	-N P GD W INE Q	RRR S ANF---	-----	197		
zGCAP3	IM E ML T K M MD	LTHV L E I I V N	G Q KK K KE---	-----	188		
zGCAP4	IM D ML K IL M D	LTPV L L I I V E	GR Q K-----	-----	185		
zGCAP7	IM D LL K L D T-	-N A R V W F R D N	LG K K T -----	-----	187		

Figure A1: Sequence alignment of bovine and zebrafish GCAPs.

Amino acid sequence alignment of bovine GCAPs (bGCAP) and zebrafish GCAPs (zGCAP). In the zGCAP5 sequence (bold), D3 (light blue), which is mutated to N in all GCAP5 variants investigated in this thesis, cysteines (red letters), positions of C15 and C17 (yellow background), H18 and Y21 (green letters), and V76 (orange letter) are marked. Bars above the sequences mark the EF hands 1 (orange), 2 (dark red), 3 (dark blue), and 4 (dark cyan). Numbers on the right are the numbers of the last amino acid of the sequence in the respective line. NCBI Reference Sequences: NP_776971.1 (bGCAP1), NP_777211.1 (bGCAP2), AAW23331.1 (zGCAP5), NP_571945.1 (zGCAP1), NP_571946.1 (zGCAP2), NP_919374.1 (zGCAP3), AAW23330.1 (zGCAP4), AAW23332.1 (zGCAP7).

SDS-PAGE

Table A2: Pipetting scheme for SDS-gels.

	15 % separating gel (μL)	5 % stacking gel (μL)
double distilled H ₂ O	1475	610
1.5 M Tris/HCl pH8.8	1000	-
0.5 M Tris/HCl pH 6.8	-	250
ROTIPHORESE® Gel 40 (37.5:1)	1500	125
TEMED	2.5	1.2
10 % (w/v) ammonium persulfate	21.5	12

Purification of GCAP5

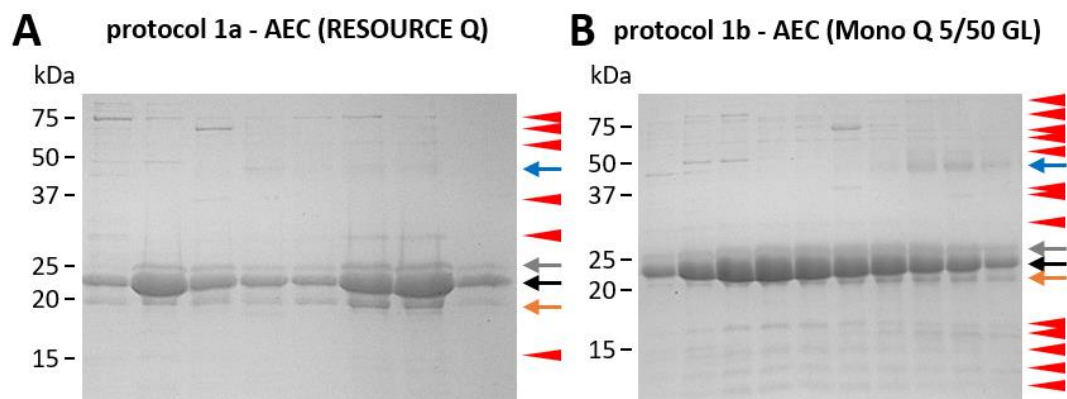


Figure A2: Purity control of myristoylated zebrafish GCAP5-D3N-C28A purified using protocol 1a and 1b.

Purification progress of recombinant myristoylated GCAP5-D3N-C28A after (A) purification protocol 1a and (B) purification protocol 1b. Nine μL of selected fractions after anion exchange chromatography (AEC), each mixed with 4x SDS-sample buffer, were applied onto a 15 % SDS-polyacrylamide gel. Mobilities and sizes of the standard proteins (kDa) are shown to the left of each gel. (A) Six or (B) 2 mL AEC fractions were collected directly after starting the gradient for elution. Monomeric myristoylated GCAP5 has a mobility of around 18 kDa in SDS-polyacrylamide gels appearing as a triple band, possibly consisting of the apo-state of non-myristoylated GCAP5 (grey arrows), the apo-state of myristoylated GCAP5 (black arrows), and the calcium-bound state (orange arrows). Dimeric GCAP5 has a mobility of around 37 kDa (blue arrows). Bands with other mobilities probably are impurities (red arrowheads).

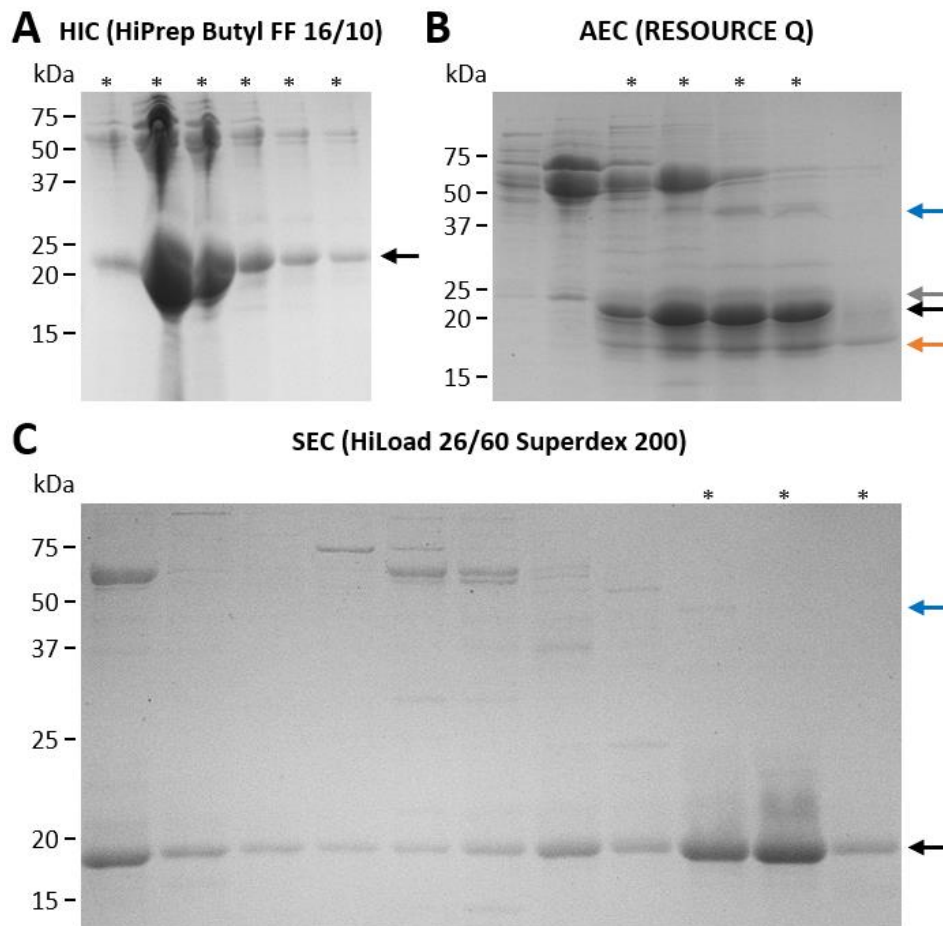


Figure A3: Purity control of myristoylated zebrafish GCAP5-D3N-C28A purified using protocol 2b.

Purification progress of recombinant myristoylated GCAP5-D3N-C28A after purification protocol 2b. Nine μL of selected fractions after (A) hydrophobic interaction chromatography (HIC), (B) anion exchange chromatography (AEC), and (C) size exclusion chromatography (SEC), each mixed with 4x SDS-sample buffer, were applied onto 15 % SDS-polyacrylamide gels. Mobilities and sizes of the standard proteins (kDa) are shown to the left of each gel. Five mL HIC fractions and 6 mL AEC fractions were collected directly after starting the gradients, 10 mL SEC fractions were collected 100 mL after injection of the protein sample. Starred HIC fractions were used for the AEC, starred AEC fractions for the SEC. Starred SEC fractions were used for buffer exchange and subsequent lyophilization. Monomeric myristoylated GCAP5 has a mobility of around 18 kDa in SDS-polyacrylamide gels (black arrow). Dimeric GCAP5 has a mobility of around 37 kDa (blue arrow).

Analytical SEC

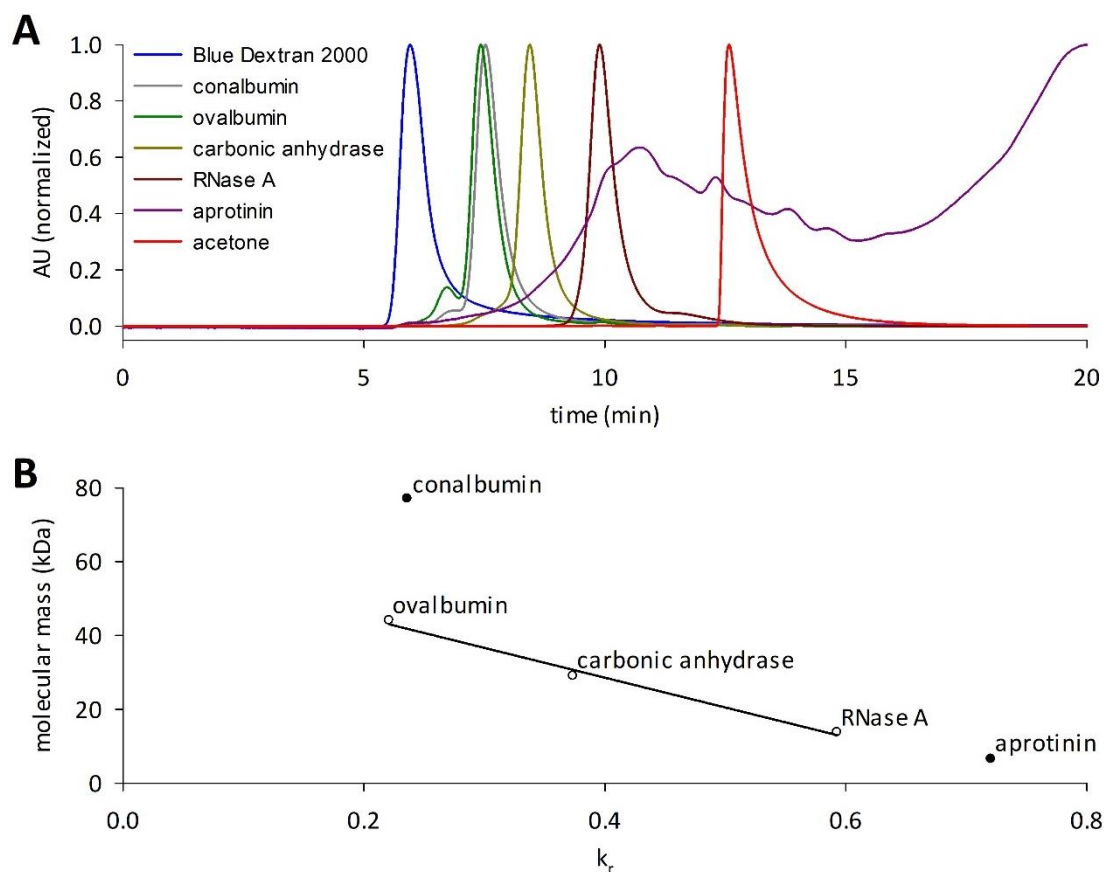


Figure A4: Calibration of the analytical SEC column BioSep-SEC-S2000 - chromatograms and calibration line.

The analytical SEC column BioSep-SEC-S2000 (*Phenomenex*) was calibrated with the Low Molecular Weight Gel Filtration Calibration Kit (*GE Healthcare*) and acetone. (A) Chromatograms of the calibration substances normalized to the highest absorbance. The absorbance in AU at 280 nm was recorded over time in minutes. (B) For each standard substance, the molecular mass in kDa is plotted against the retention factor k_r calculated with Equation 8. The best calibration line was achieved without conalbumin and aprotinin (black circles). The equation for the calibration line is: $molecular\ mass\ [kDa] = -80.696 \cdot k_r + 60.854$

Table A3: Calibration of the analytical SEC column BioSep-SEC-S2000 - specifications of standard substances.

The analytical SEC column BioSep-SEC-S2000 (*Phenomenex*) was calibrated with the Low Molecular Weight Gel Filtration Calibration Kit (*GE Healthcare*) and acetone. For each standard substance, the molecular mass in kDa, the elution time (t_e) in minutes, and the retention factor (k_r) calculated with Equation 8 are listed.

	kDa	t_e (min)	k_r
acetone	0.05808	12.593	1
aprotinin	6.5	10.740	0.720603
RNase A	13.7	9.893	0.592914573
carbonic Anhydrase	29	8.440	0.373869347
ovalbumin	44	7.427	0.221155779
conalbumin	75	7.527	0.236231
Blue Dextran 2000	2 000	5.960	0

Table A4: Analytical SEC of GCAP5.

GCAP5 non-myr WT, WT, reduced WT, C15A-C17A, H18E-Y21E, and V76E were analyzed by analytical SEC. The protein states observed are the monomer, the dimer, an unclear state (un), and aggregates. The mean and the standard deviation of the elution time, the apparent size in kDa, and the concentration (relative integral) of the peaks are listed. The p-value of the concentration (c) was determined with the Mann-Whitney Rank Sum Test and, if possible, with the t-test by the software SigmaPlot. n is the number of detected peaks, the minimum n for consideration was two. Each variant was analyzed nine times in the presence (+ DTT) and in the absence of DTT (- DTT), respectively. Data of Figure 14 and Figure 15.

		elution time (min)		apparent size (kDa)		concentration (%)		p-value of c		n	
		- DTT	+ DTT	- DTT	+ DTT	- DTT	+ DTT	M-W test	t-test	- DTT	+ DTT
non-myr WT	monomer	9.3710 ± 0.2028	9.3268 ± 0.0961	19.4 ± 2.5	19.9 ± 1.2	13.5 ± 5.4	2.3 ± 0.5	0.2	-	2	3
	dimer + un	7.9736 ± 0.0242	7.9637 ± 0.0147	36.5 ± 0.3	36.5 ± 0.2	28.8 ± 10.6	38.0 ± 5.9	0.002	-	9	9
	aggregate	5.8781 ± 0.0244	5.8872 ± 0.0257	> 45	> 45	64.1 ± 5.3	57.0 ± 1.0	< 0.001	-	9	9
WT	dimer	7.4512 ± 0.0770	7.4798 ± 0.0089	42.7 ± 0.9	42.4 ± 0.1	21.2 ± 2.2	34.0 ± 4.7	< 0.001	< 0.001	9	9
	aggregate	5.8912 ± 0.0205	5.8707 ± 0.0246	> 45	> 45	78.8 ± 2.2	62.8 ± 4.6	< 0.001	< 0.001	9	9
reduced WT	monomer	9.2220 ± 0.0377	9.3423 ± 0.0886	21.2 ± 0.5	19.7 ± 1.1	1.2 ± 0.4	1.9 ± 0.8	0.4	0.288	3	3
	dimer	7.5028 ± 0.0120	7.4882 ± 0.0042	42.1 ± 0.1	42.3 ± 0.1	11.7 ± 10.7	39.3 ± 2.2	< 0.001	-	9	9
	aggregate	5.8847 ± 0.0264	5.8770 ± 0.0182	> 45	> 45	79.2 ± 13.9	54.8 ± 6.9	0.001	-	9	9
C15A-C17A	dimer	7.5040 ± 0.0260	7.4777 ± 0.0130	42.1 ± 0.3	42.4 ± 0.2	58.8 ± 9.0	53.3 ± 7.3	0.204	-	7	9
	aggregate	5.8554 ± 0.0216	5.8518 ± 0.0130	> 45	> 45	41.1 ± 9.0	39.2 ± 12.1	0.672	-	7	9
H18E-Y21E	dimer	7.4459 ± 0.0281	7.4443 ± 0.0087	42.8 ± 0.3	42.8 ± 0.1	8.6 ± 7.9	40.0 ± 2.7	< 0.001	-	9	9
	aggregate	5.9030 ± 0.0550	5.8553 ± 0.0177	> 45	> 45	90.0 ± 9.24	54.7 ± 5.4	< 0.001	-	9	9
V76E	dimer	7.5641 ± 0.0441	7.5060 ± 0.0127	41.3 ± 0.5	42.0 ± 0.2	0.8 ± 0.2	4.3 ± 1.2	< 0.001	-	8	9
	aggregate	5.8882 ± 0.0214	5.8720 ± 0.0241	> 45	> 45	98.8 ± 0.8	90.0 ± 2.2	< 0.001	-	9	9

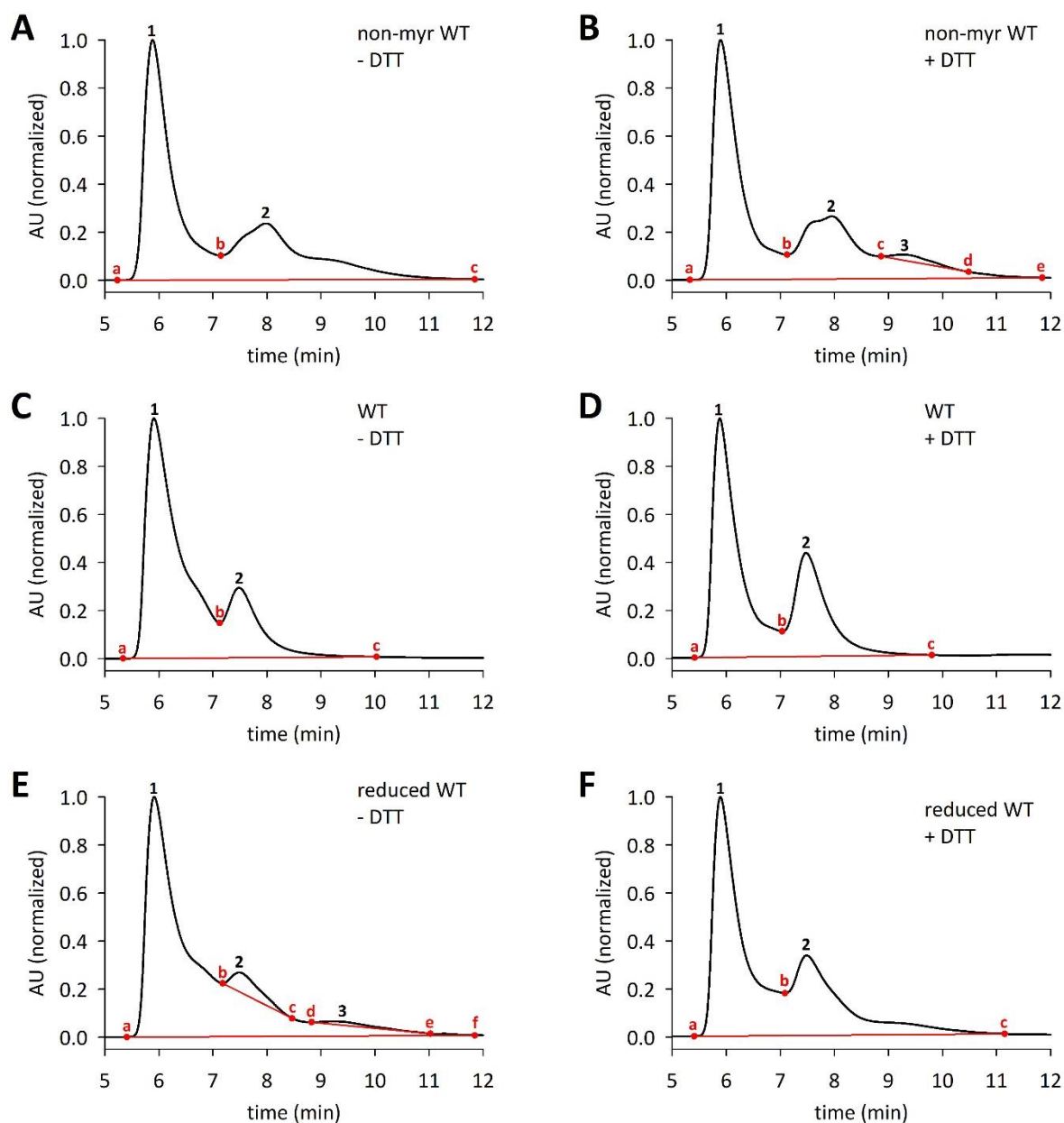


Figure A5: Analytical SEC analysis of GCAP5 - chromatograms of non-myristoylated WT, WT, and reduced WT.

Representative analytical SEC chromatograms of recombinant GCAP5 from five to twelve min after GCAP5 injection normalized to the maximum of the peak at around 5.9 min (peak number 1) for comparison. GCAP5 (50 μg) (**A+B**) non-myristoylated WT, (**C+D**) WT, and (**E+F**) reduced WT were analyzed in the absence (- DTT) and in the presence of DTT (5 mM, + DTT), respectively. The absorbance in AU at 280 nm was recorded over time in min. The peaks of each chromatogram (black numbers), their start and end times (red points and red small letters), and the base lines (red line) were determined by the software Primaide (data listed in Table A5).

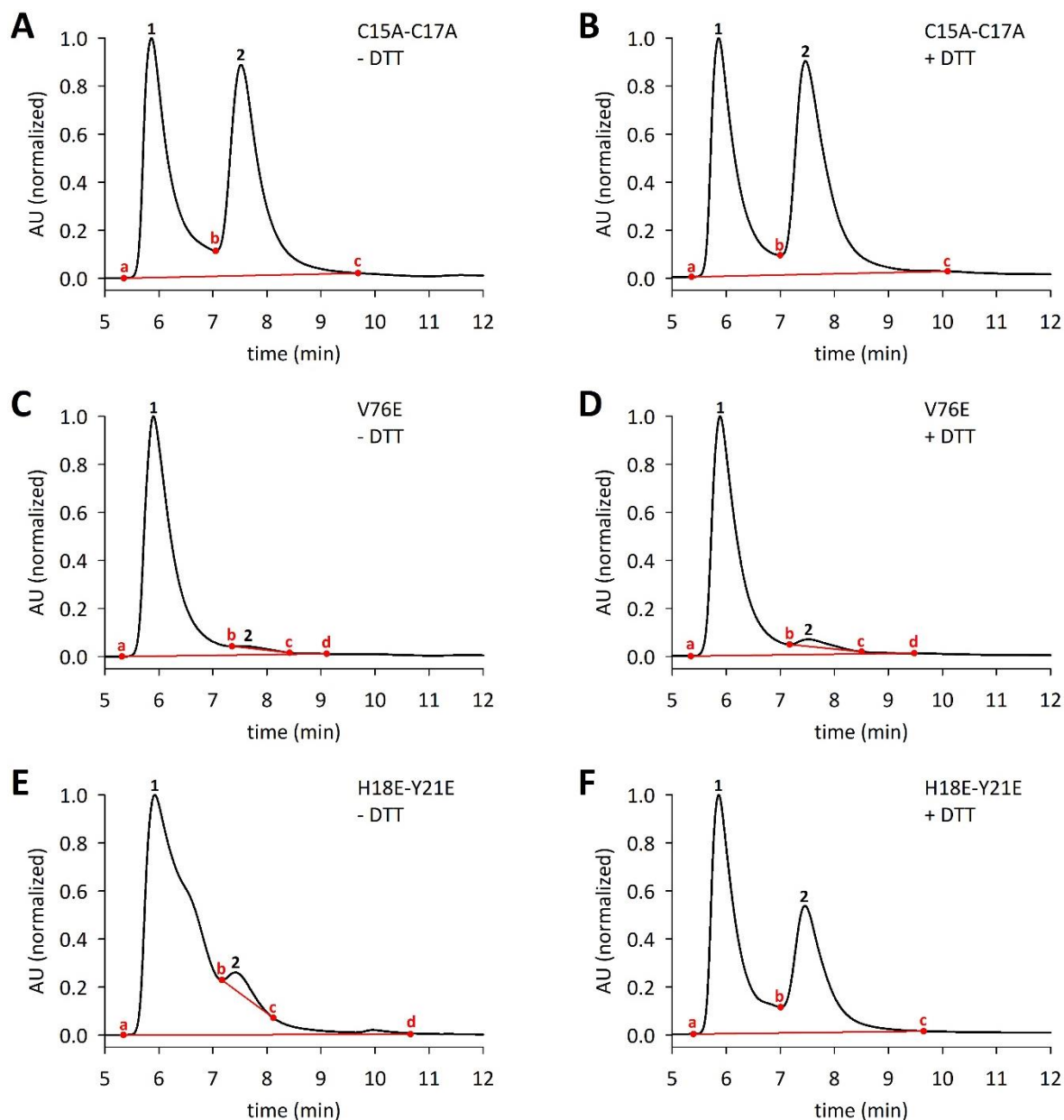


Figure A6: Analytical SEC analysis of GCAP5 - chromatograms of C15A-C17A, V76E, and H18E-Y21E.

Representative analytical SEC chromatograms of recombinant GCAP5 from five to twelve min after GCAP5 injection normalized to the maximum of the peak at around 5.9 min (peak number 1) for comparison. GCAP5 (50 μ g) (**A+B**) C15A-C17A, (**C+D**) V76E, and (**E+F**) H18E-Y21E were analyzed in the absence (- DTT) and in the presence of DTT (5 mM, + DTT), respectively. The absorbance in AU at 280 nm was recorded over time in min. The peaks of each chromatogram (black numbers), their start and end times (red points and red small letters), and the base lines (red line) were determined by the software Primaide (data listed in Table A5).

Table A5: Analytical SEC analysis of GCAP5 - data.

For GCAP5 non-myr WT, WT, reduced WT, C15A-C17A, V76E, and H18E-Y21E, the retention times in minutes, the area of the integration in $\mu\text{V} \cdot \text{s}$, and the start and end time in minutes (small letters refer to red small letters in Figure A5 and Figure A6) of each peak in the chromatograms are listed as well as the start and end times of the base lines. Data of Figure A5 and Figure A6.

		retention time (min)	area ($\mu\text{V} \cdot \text{s}$)	start time (min)	end time (min)
non-myr WT - DTT	general base line	-	-	5.2333 (a)	11.8467 (c)
	peak 1	5.887	4,264,293	5.2333 (a)	7.1467 (b)
	peak 2	7.98	2,598,642	7.1467 (b)	11.8467 (c)
non-myr WT + DTT	general base line	-	-	5.3267 (a)	11.8467 (e)
	peak 1	5.893	4,072,140	5.3267 (a)	7.1267 (b)
	peak 2	7.953	2,908,992	7.1267 (b)	8.8667 (c)
	base line peak 3	-	-	8.8667 (c)	10.4867 (d)
	peak 3	9.247	142,784	8.8667 (c)	10.4867 (d)
WT - DTT	general base line	-	-	5.3400 (a)	10.0267 (c)
	peak 1	5.860	3,624,437	5.3400 (a)	7.1267 (b)
	peak 2	7.460	803,784	7.1267 (b)	10.0267 (c)
WT + DTT	general base line	-	-	5.4133 (a)	9.8067 (c)
	peak 1	5.8800	3,007,153	5.4133 (a)	7.0333 (b)
	peak 2	7.4733	1,677,415	7.0333 (b)	9.8067 (c)
reduced WT - DTT	general base line	-	-	5.4067 (a)	11.8467 (f)
	peak 1	5.913	6,629,652	5.4067 (a)	7.1800 (b)
	base line peak 2	-	-	7.1800 (b)	8.4667 (c)
	peak 2	7.487	333,985	7.1800 (b)	8.4667(c)
	base line peak 3	-	-	8.8267 (d)	11.0267 (e)
	peak3	9.233	91,174	8.8267 (d)	11.0267 (e)
reduced WT + DTT	general base line	-	-	5.4067 (a)	11.1533 (c)
	peak 1	5.893	3,874,564	5.4067 (a)	7.0867 (b)
	peak 2	7.487	2,301,602	7.0867 (b)	11.1533 (c)
C15A-C17A - DTT	general base line	-	-	5.3533 (a)	9.6867 (c)
	peak 1	5.867	2,229,676	5.3533 (a)	7.0533 (b)
	peak 2	7.520	2,278,462	7.0533 (b)	9.6867 (c)
C15A-C17A + DTT	general base line	-	-	5.3600 (a)	10.1000 (c)
	peak 1	5.860	1,910,053	5.3600 (a)	7.0000 (b)
	peak 2	7.467	2,206,751	7.0000 (b)	10.1000 (c)
V76E - DTT	general base line	-	-	5.3200 (a)	9.1067 (d)
	peak 1	5.900	4,346,674	5.3200 (a)	7.3533 (b)
	base line peak 2	-	-	7.3533 (b)	8.4200 (c)
	peak 2	7.540	31,262	7.3533 (b)	8.4200 (c)
V76E + DTT	general base line	-	-	5.3467 (a)	9.4800 (d)
	peak 1	5.887	4,769,703	5.3467 (a)	7.1733 (b)
	base line peak 2	-	-	7.1733 (b)	8.5067 (c)
	peak 2	7.520	148,362	7.1733 (b)	8.5067 (c)
H18E-Y21E - DTT	general base line	-	-	5.3467 (a)	10.6600 (d)
	peak 1	5.927	4,955,245	5.3467 (a)	7.1667 (b)
	base line peak2	-	-	7.1667 (b)	8.1200 (c)
	peak 2	7.413	166,217	7.1667 (b)	8.1200 (c)
H18E-Y21E + DTT	general base line	-	-	5.3933 (a)	9.6533 (c)
	peak 1	5.860	2,384,564	5.3933 (a)	7.0067 (b)
	peak 2	7.453	1,625,252	7.0067 (b)	9.6533 (c)

Myristoylation rate

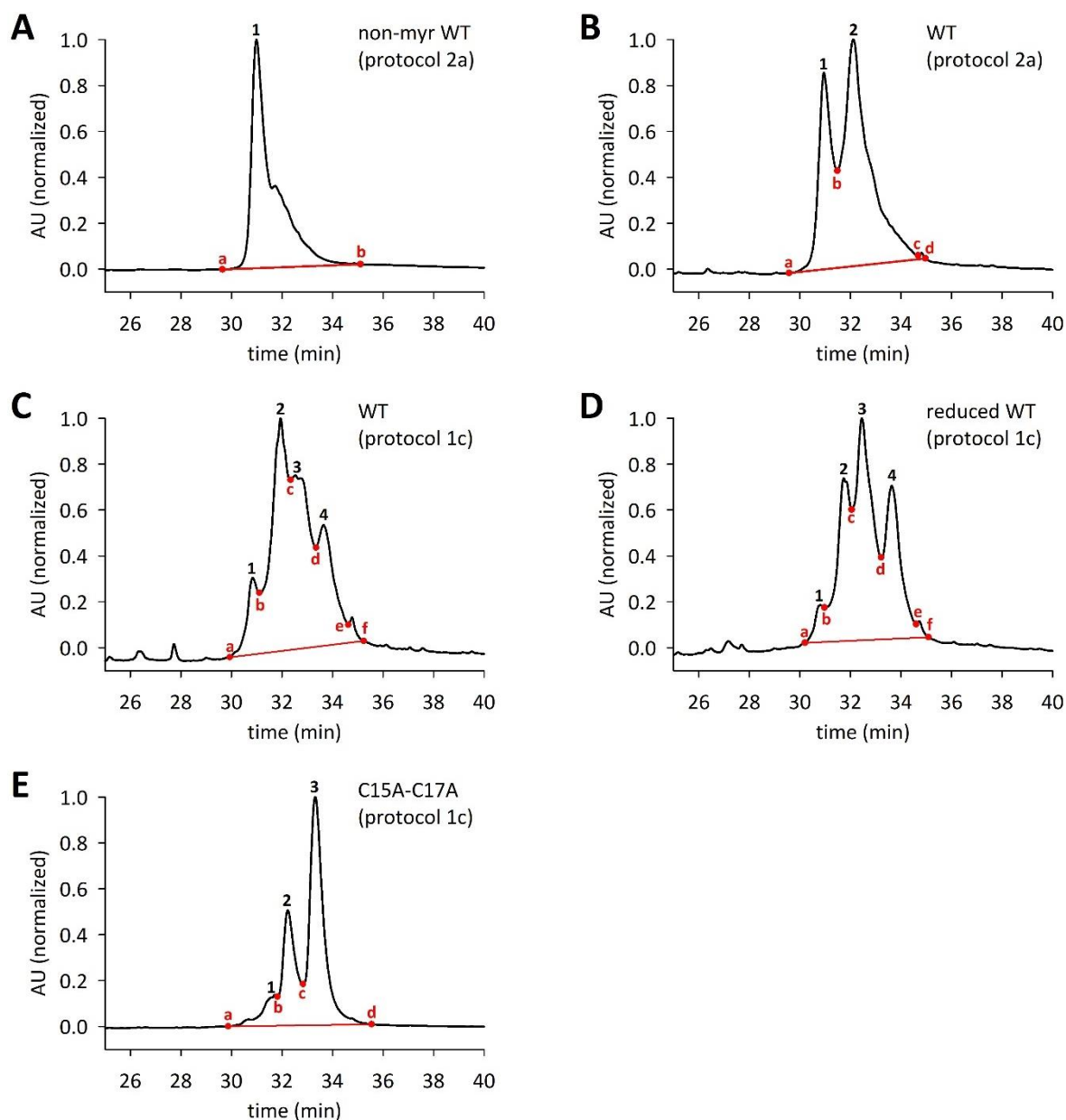


Figure A7: Myristoylation rate analysis of GCAP5 - chromatograms.

Reversed phase-HPLC chromatograms (black line) of recombinant GCAP5 from 25 to 40 min after GCAP5 injection normalized to the maximum of the highest peak within this time range for comparison. GCAP5 (160 μ g) was analyzed using a gradient from 100 % double distilled H₂O/0.1 % TFA to 100 % Acetonitrile/0.1 % TFA in 55 min. GCAP5 (**A**) non-myr WT, (**B** and **C**), WT, (**D**) reduced WT, and (**E**) C15A-C17A were analyzed. They were purified either according to purification protocol 2a from the soluble fraction after expression (Table 3) or according to purification protocol 1c (see Table 2 and section 3.1). The absorbance in AU at 280 nm was recorded over time in min. The peaks of each chromatogram (black numbers), their start and end times (red points and red small letters), and the base line (red line) were determined by the software Primaide (data listed in Table A6).

Table A6: Myristoylation rate analysis of GCAP5 - data.

Data of the myristoylation rate analysis chromatograms (Figure 16, Figure A7), determined by the software Primaide. For GCAP5 non-myr WT, WT reduced WT, and C15A-C17A purified either according to purification protocol 2a (Table 3) or purification protocol 1c (see Table 2 and section 3.1), the retention times in minutes, the area of the integration in $\mu\text{V} \cdot \text{s}$, and the start and end time in minutes (small letters refer to red small letters in Figure A7) of each peak in the chromatograms are listed as well as the start and end times of the base lines. For the peak non-myr WT (purification protocol 2a), only the retention time is needed, the other values were not determined (n. d.).

		retention time (min)	area ($\mu\text{V} \cdot \text{s}$)	start time (min)	end time (min)
non-myr WT (protocol 2a)	base line	-	-	29.6467 (a)	34.7067 (b)
	peak 1	30.993	n. d.	n. d.	n. d.
WT (protocol 2a)	base line	-	-	29.5733 (a)	35.0600 (d)
	peak 1	30.953	446,921	29.5733 (a)	31.4867 (b)
	peak 2	32.113	991,882	31.4867 (b)	34.6800 (c)
WT (protocol 1c)	base line	-	-	29.9400	35.2400 (f)
	peak 1	30.840	58,908	29.9400 (a)	31.1067 (b)
	peak 2	31.947	274,309	31.1067 (b)	32.3467 (c)
	peak 3	32.533	227,131	32.3467 (c)	33.3533 (d)
	peak 4	33.653	150,416	33.3533 (d)	34.6333 (e)
reduced WT (protocol 1c)	base line	-	-	30.2067	35.0933 (f)
	peak 1	30.807	34,956	30.2067 (a)	30.9800 (b)
	peak 2	31.733	231,881	30.9800 (b)	32.0533 (c)
	peak 3	32.453	400,811	32.0533 (c)	33.2200 (d)
	peak 4	33.640	264,927	33.2200 (d)	34.6067 (e)
C15A-C17A (protocol 1c)	base line	-	-	29.8733	35.5533
	peak 1	31.713	260,263	29.8733 (a)	31.8267 (b)
	peak 2	32.233	838,072	31.8267 (b)	32.8400 (c)
	peak 3	33.320	1,775,614	32.8400 (c)	35.5533 (d)

Cysteine accessibility

Table A7: Number of accessible cysteines for the GCAP5 variants.

The cysteine accessibility was measured in the absence (100 μM EGTA) and in the presence (1 mM CaCl_2) of calcium, respectively. Myristoylated zebrafish GCAP3 (myr GCAP3) served as a negative control. GCAP5 non-myr WT, WT, reduced WT, and C15A-C17A were investigated. The mean, the standard deviation (s. d.) of the number of accessible cysteines, and the sample size (n) are listed. Data of Figure 17.

	100 μM EGTA			1 mM CaCl_2			p-value	
	mean	s. d.	n	mean	s. d.	n	M-W test	t-test
myr GCAP3	0.03	0.07	9	0.03	0.07	9	0.965	0.985
non-myr WT	2.69	0.34	9	2.35	0.17	9	0.052	-
WT	1.31	0.09	9	0.90	0.02	6	0.002	-
reduced WT	3.33	0.40	8	2.59	0.31	8	0.005	0.001
C15A-C17A	2.56	0.50	9	1.48	0.16	9	< 0.001	-

Tryptophan fluorescence

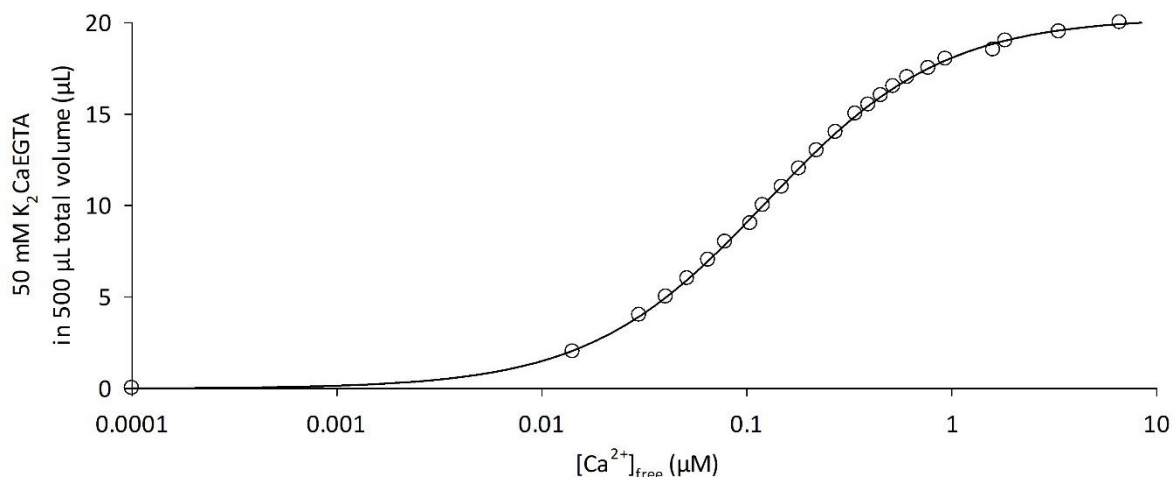


Figure A8: $[Ca^{2+}]_{free}$ calibration curve determined with fura-2.

The volume in μL of 50 mM $K_2CaEGTA$ in a total volume of 500 μL of sample solution is plotted against the free calcium-ion concentration ($[Ca^{2+}]_{free}$) in μM calculated with Equation 6. X-axis scale is logarithmic. The calculated values (black circles, listed in Table A8) were fitted according to Hill with four parameters (black line):

$$\mu\text{L}_{K_2CaEGTA} = \frac{-0.0141 + 20.3026 \cdot (\mu\text{M}_{[Ca^{2+}]_{free}})^{1.0043}}{0.1233^{1.0043} + (\mu\text{M}_{[Ca^{2+}]_{free}})^{1.0043}}$$

Table A8: Pipetting scheme of the Ca^{2+} -EGTA buffer system components and $[Ca^{2+}]_{free}$ determined with fura-2.

The free calcium-ion concentration ($[Ca^{2+}]_{free}$) in μM was determined with fura-2 for specific compositions of the Ca^{2+} -EGTA buffer system components (50 mM $K_2CaEGTA$ and 50 mM K_2H_2EGTA). *The value was calculated with the program WEBMAXC STANDARD (<https://somapp.ucdmc.ucdavis.edu/pharmacology/bers/maxchelator/webmaxc/webmaxcS.htm>, Temperature = 22, pH = 7.5, Ionic = 0.04, EGTA: 2 mM, Ca2: 10 μM , access: 16.02.2020).

$K_2CaEGTA$ in μL	K_2H_2EGTA in μL	$[Ca^{2+}]_{free}$ in μM	$K_2CaEGTA$ in μL	K_2H_2EGTA in μL	$[Ca^{2+}]_{free}$ in μM
0*	20*	$\sim 0.0001^*$	14	6	0.2752
2	18	0.0144	15	5	0.3499
4	16	0.0313	15.5	4.5	0.3989
5	15	0.0414	16	4	0.4592
6	14	0.0529	16.5	3.5	0.5354
7	13	0.0661	17	3	0.6345
8	12	0.0815	17.5	2.5	0.7689
9	11	0.0995	18	2	0.9615
10	10	0.1211	18.5	1.5	1.2606
11	9	0.1472	19	1	1.7887
12	8	0.1796	19.5	0.5	2.9725
13	7	0.2209	20	0	8.0504

Table A9: Ca²⁺-dependent tryptophan fluorescence of GCAP5 - fluorescence intensity maxima of all single measurements.

The absorbance of the fluorescence intensity maximum (F_{max}) in AU of each smoothed spectrum is listed for each measured free calcium concentration ([Ca²⁺]_{free}) in μM. GCAP5 non-myr WT, WT, reduced WT, and C15A-C17A were tested. Lyophilized recombinant GCAP5 (500 μg) was resuspended in fluorescence buffer, potential aggregates were pelleted, and the supernatant was filled up to 15-17 mL. Tryptophans were excited at 280 nm, the emission spectrum was recorded from 300 to 420 nm in 2 nm steps and smoothed (FeliX32). Data points of graphs in Figure 18.

non-myr WT				WT				reduced WT				C15A-C17A			
[Ca ²⁺] _{free} (μM)	F _{max 1} (AU)	F _{max 2} (AU)	F _{max 3} (AU)	[Ca ²⁺] _{free} (μM)	F _{max 1} (AU)	F _{max 2} (AU)	F _{max 3} (AU)	[Ca ²⁺] _{free} (μM)	F _{max 1} (AU)	F _{max 2} (AU)	F _{max 3} (AU)	[Ca ²⁺] _{free} (μM)	F _{max 1} (AU)	F _{max 2} (AU)	F _{max 3} (AU)
0.0001	13299.1	6264.63	16350.1	0.0001	17156	12096.8	11545.9	0.0001	4886.64	10132.7	19834	0.0001	19081.5	14816.4	15615.4
0.0144	13417.1	6462.59	16337.2	0.0144	16702.3	12368.6	11605.9	0.0144	4805.13	10504.8	21190.6	0.0144	17903.3	14223.4	14122.8
0.0313	12980.1	7219.42	15859.2	0.0313	17119.5	11984.7	11708.4	0.0313	5039.85	11257	20724.7	0.0313	18893.8	14166.6	14720.1
0.0414	13150.3	6471.63	16291.2	0.0414	18214.4	11513.2	11253.1	0.0414	-	10936	21373.8	0.0414	-	13978.4	14584
0.0529	13025.2	6422.34	16894.6	0.0529	16890.7	12040.2	11516.5	0.0529	5128.76	10146.9	21228	0.0529	18429.5	13791.7	14047.4
0.0661	12774.5	6397.48	16628.5	0.0661	-	11823.2	11147.7	0.0661	-	11737	20019.9	0.0661	-	13705.1	14193.8
0.0815	13533.9	6358.71	16077.3	0.0815	17530.2	11850.7	13008.8	0.0815	5096.08	10010.2	20802.6	0.0815	17636.1	14011.7	14345.9
0.0995	13015.8	6372.9	16859.3	0.0995	-	12041.5	12268.8	0.0995	-	10044.2	20254.7	0.0995	-	13598.9	14081.7
0.1211	13652.9	6366.88	16617.8	0.1211	18074	12057.6	11471	0.1211	5098.52	10124.1	20268.4	0.1211	18079.3	13380.2	14022.4
0.1335	-	6624.19	16786.6	0.1472	-	11716	11076.9	0.1472	-	10051.4	20335.1	0.1472	-	13943.8	14458.8
0.1472	12611.5	6408.15	16984.4	0.1796	18247.4	11931	11607.1	0.1796	5189.39	9974.82	20428.7	0.1796	18414.7	13806.5	14067
0.1625	-	6309.66	16779.8	0.2209	17594.2	11849.9	11336.3	0.2752	5228.24	10064.2	19510.6	0.2209	-	14168.4	14835.9
0.1796	12687.9	6318.31	16622.1	0.2752	16751	12690.2	11650.3	0.3499	-	10445.1	19764.2	0.2752	18298.9	13831.8	14906.2
0.1989	-	6140.57	17380.2	0.3499	18682.1	12085.6	11983.4	0.4592	5105.07	9834.12	20439.9	0.3499	-	14240.7	16689.3
0.2209	10486.1	7634.51	16690.3	0.4592	17662.3	12439.3	11690.6	0.6345	-	10005.2	20001.6	0.4592	19106.7	13978.3	14469.6
0.2461	-	6347.52	16243.8	0.6345	17863.8	12445.4	11737.2	0.9615	4955.1	9879.72	19749.4	0.6345	-	14104.7	14794.8
0.2752	10913.7	6442.61	16879.8	0.7689	-	12329.7	11841.3	1.2606	-	10895	20093.3	0.9615	18976.2	14690.2	14881.1
0.3093	-	6262.04	16032.2	0.8753	-	11810.4	12180.1	1.7887	-	9716.53	20588.4	1.2606	-	14384	14723
0.3499	12734.3	6301.92	16391.5	0.9615	14719.5	12456.9	10821.6	2.9725	-	10419.8	20809.3	1.7887	-	14766	15562.5
0.3989	-	6426.07	16880.1	1.2606	-	11898.4	11563.5	3.4108	-	10328.2	20775.6	2.9725	-	15538.3	15955
0.4592	13611.8	7311.82	16413.2	1.5354	-	12081.3	11564.1	3.9943	-	10854.5	19905.1	3.4108	-	16509.8	16131.3
0.6345	-	6252.01	16351.1	1.7887	18221.4	11868.5	11863.3	4.8094	-	9978.74	20100.8	3.9943	-	14722	15717.2
0.9615	13463.1	6408.67	16409.4	2.9725	-	12186.4	11947.9	6.0282	-	9967.53	20083	4.8094	-	15581.5	16249.2
1.7887	-	6431.18	16402.2	3.4108	-	12123	11934.2	8.0504	5403.61	10062.9	20091.4	6.0282	-	14941.2	15770.1
2.9725	-	7593.7	16763.4	3.9943	-	12269.8	12034.7	10	5151.12	10188.3	22325.6	8.0504	19882.3	15418.3	16309.7
6.0282	-	6457.04	16529.5	4.8094	-	14086.4	12085.2	50	5169.95	11518.8	21553.5	10	20411.1	15268.8	15425.8
8.0504	13928.8	6421.86	16512.3	6.0282	-	12030.8	11691.2	100	5321.99	10001.6	20282.7	50	19848.6	14701.8	19589.5
10	13987.1	6433.43	16407.2	8.0504	18552.9	12086.4	11542.4	1000	5169.47	9958.11	24297.8	100	19863.2	14010.4	14984.2
50	13315	6810.73	16208.1	10	19121	11898.3	12218.4	-	-	-	-	1000	18997.6	14595.7	14159.9
100	13519.5	6285.04	16618	50	19392.2	12108	11640.1	-	-	-	-	-	-	-	-
1000	13511.1	6373.04	15802.3	100	19476	12333.2	11807.8	-	-	-	-	-	-	-	-
-	-	-	-	1000	19362.7	11776.4	11961	-	-	-	-	-	-	-	-

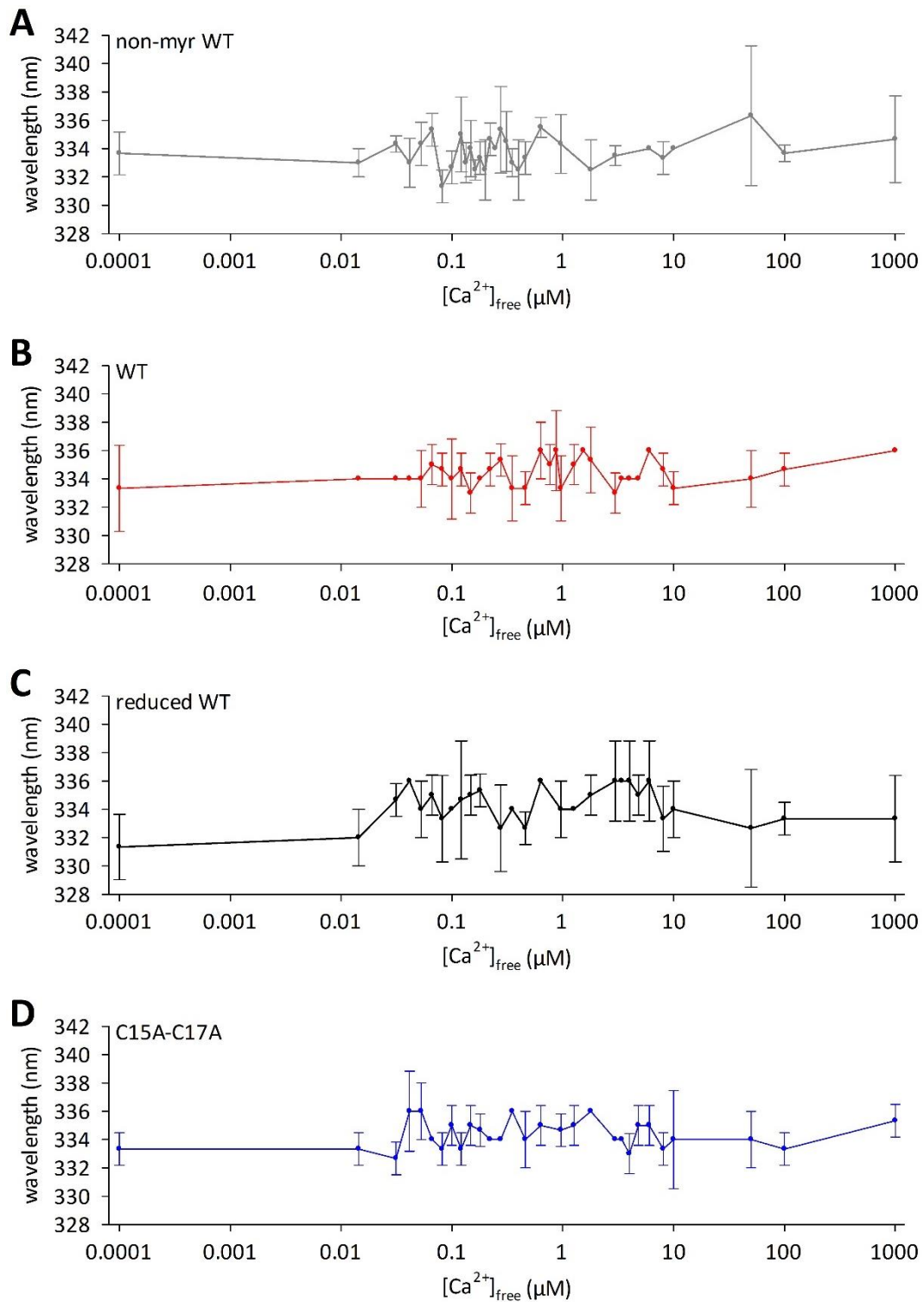


Figure A9: Ca^{2+} -dependent tryptophan fluorescence of GCAP5 - wavelength of fluorescence intensity maxima.

Lyophilized recombinant GCAP5 (**A**) non-myr WT (grey), (**B**) WT (red), (**C**) Reduced WT (black), and (**D**) C15A-C17A (blue) were each resuspended in fluorescence buffer, potential aggregates were pelleted, and the supernatant was filled up to 15-17 mL. Tryptophans were excited at 280 nm, the emission spectrum was recorded from 300 to 420 nm in 2 nm steps and smoothed (FeliX32). The wavelength in nm of the fluorescence intensity maximum of each smoothed spectrum is plotted against the $[Ca^{2+}]_{free}$ in μM . Data points are listed in Table A10.

Table A10: Ca²⁺-dependent tryptophan fluorescence of GCAP5 - wavelength of fluorescence intensity maxima.

The mean wavelength in nm of the fluorescence intensity maximum of two to three (n) smoothed spectra is listed for each measured free calcium concentration ([Ca²⁺]_{free}) in μM. GCAP5 non-my WT, WT, reduced WT, and C15A-C17A were tested. Lyophilized recombinant GCAP5 (500 μg) was resuspended in fluorescence buffer, potential aggregates were pelleted, and the supernatant was filled up to 15-17 mL. Tryptophans were excited at 280 nm, the emission spectrum was recorded from 300 to 420 nm in 2 nm steps and smoothed (FeliX32). Data points of graphs in Figure A9.

non-my WT				WT				reduced WT				C15A-C17A			
[Ca ²⁺] _{free} (μM)	mean (nm)	s. d.	n	[Ca ²⁺] _{free} (μM)	mean (nm)	s. d.	n	[Ca ²⁺] _{free} (μM)	mean (nm)	s. d.	n	[Ca ²⁺] _{free} (μM)	mean (nm)	s. d.	n
0.0001	333.6667	1.5275	3	0.0001	333.3333	3.0551	3	0.0001	331.3333	2.3094	3	0.0001	333.3333	1.1547	3
0.0144	333.0000	1.0000	3	0.0144	334.0000	0.0000	3	0.0144	332.0000	2.0000	3	0.0144	333.3333	1.1547	3
0.0313	334.3333	0.5774	3	0.0313	334.0000	0.0000	3	0.0313	334.6667	1.1547	3	0.0313	332.6667	1.1547	3
0.0414	333.0000	1.7321	3	0.0414	334.0000	0.0000	3	0.0414	336.0000	0.0000	2	0.0414	336.0000	2.8284	2
0.0529	334.3333	1.5275	3	0.0529	334.0000	2.0000	3	0.0529	334.0000	2.0000	3	0.0529	336.0000	2.0000	3
0.0661	335.3333	1.1547	3	0.0661	335.0000	1.4142	2	0.0661	335.0000	1.4142	2	0.0661	334.0000	0.0000	2
0.0815	331.3333	1.1547	3	0.0815	334.6667	1.1547	3	0.0815	333.3333	3.0551	3	0.0815	333.3333	1.1547	3
0.0995	332.6667	1.1547	3	0.0995	334.0000	2.8284	2	0.0995	334.0000	0.0000	2	0.0995	335.0000	1.4142	2
0.1211	335.0000	2.6458	3	0.1211	334.6667	1.1547	3	0.1211	334.6667	4.1633	3	0.1211	333.3333	1.1547	3
0.1335	333.0000	1.4142	2	0.1472	333.0000	1.4142	2	0.1472	335.0000	1.4142	2	0.1472	335.0000	1.4142	2
0.1472	334.0000	2.0000	3	0.1796	334.0000	0.0000	3	0.1796	335.3333	1.1547	3	0.1796	334.6667	1.1547	3
0.1625	332.5000	0.7071	2	0.2209	334.6667	1.1547	3	0.2752	332.6667	3.0551	3	0.2209	334.0000	0.0000	2
0.1796	333.3333	1.1547	3	0.2752	335.3333	1.1547	3	0.3499	334.0000	0.0000	2	0.2752	334.0000	0.0000	3
0.1989	332.5000	2.1213	2	0.3499	333.3333	2.3094	3	0.4592	332.6667	1.1547	3	0.3499	336.0000	0.0000	2
0.2209	334.6667	1.1547	3	0.4592	333.3333	1.1547	3	0.6345	336.0000	0.0000	2	0.4592	334.0000	2.0000	3
0.2461	334.0000	0.0000	2	0.6345	336.0000	2.0000	3	0.9615	334.0000	2.0000	3	0.6345	335.0000	1.4142	2
0.2752	335.3333	3.0551	3	0.7689	335.0000	1.4142	2	1.2606	334.0000	0.0000	2	0.9615	334.6667	1.1547	3
0.3093	334.5000	2.1213	2	0.8753	336.0000	2.8284	2	1.7887	335.0000	1.4142	2	1.2606	335.0000	1.4142	2
0.3499	333.0000	1.0000	3	0.9615	333.3333	2.3094	3	2.9725	336.0000	2.8284	2	1.7887	336.0000	0.0000	2
0.3989	332.5000	2.1213	2	1.2606	335.0000	1.4142	2	3.4108	336.0000	0.0000	2	2.9725	334.0000	0.0000	2
0.4592	333.3333	1.1547	3	1.5354	336.0000	0.0000	2	3.9943	336.0000	2.8284	2	3.4108	334.0000	0.0000	2
0.6345	335.5000	0.7071	2	1.7887	335.3333	2.3094	3	4.8094	335.0000	1.4142	2	3.9943	333.0000	1.4142	2
0.9615	334.3333	2.0817	3	2.9725	333.0000	1.4142	2	6.0282	336.0000	2.8284	2	4.8094	335.0000	1.4142	2
1.7887	332.5000	2.1213	2	3.4108	334.0000	0.0000	2	8.0504	333.3333	2.3094	3	6.0282	335.0000	1.4142	2
2.9725	333.5000	0.7071	2	3.9943	334.0000	0.0000	2	10	334.0000	2.0000	3	8.0504	333.3333	1.1547	3
6.0282	334.0000	0.0000	2	4.8094	334.0000	0.0000	2	50	332.6667	4.1633	3	10	334.0000	3.4641	3
8.0504	333.3333	1.1547	3	6.0282	336.0000	0.0000	2	100	333.3333	1.1547	3	50	334.0000	2.0000	3
10	334.0000	0.0000	3	8.0504	334.6667	1.1547	3	1000	333.3333	3.0551	3	100	333.3333	1.1547	3
50	336.3333	4.9329	3	10	333.3333	1.1547	3	-	-	-	-	1000	335.3333	1.1547	3
100	333.6667	0.5774	3	50	334.0000	2.0000	3	-	-	-	-	-	-	-	-
1000	334.6667	3.0551	3	100	334.6667	1.1547	3	-	-	-	-	-	-	-	-
-	-	-	-	1000	336.0000	0.0000	3	-	-	-	-	-	-	-	-

GC assay

Table A11: Pipetting scheme for IC₅₀ measurements.

The free calcium concentrations ($[Ca^{2+}]_{free}$) in μM for the GC assay were adjusted with the Ca^{2+} -EGTA buffer system components, 10 mM K_2H_2EGTA and 10 mM $K_2CaEGTA$, or with 10 mM $CaCl_2$ and double distilled water (H_2O).

$[Ca^{2+}]_{free}$ (μM)	10 mM K_2H_2EGTA (μL)	10 mM $K_2CaEGTA$ (μL)	10 mM $CaCl_2$ (μL)	H_2O (μL)
0.00177	10	-	-	-
0.029	9	1	-	-
0.058	8	2	-	-
0.099	7	3	-	-
0.159	6	4	-	-
0.255	5	5	-	-
0.405	4	6	-	-
0.705	3	7	-	-
1.491	2	8	-	-
7.688	1	9	-	-
33	-	10	-	-
100	-	-	0.5	9.5
1 000	-	-	5	5

Table A12: IC₅₀ measurement normalized to mean of lowest $[Ca^{2+}]$ - data.

Mean and standard deviation (s. d.) of produced amounts of cGMP by recombinant human GC-E at increasing free calcium concentrations ($[Ca^{2+}]_{free}$) in μM normalized to the mean value at the lowest $[Ca^{2+}]_{free}$. GCAP5 non-myr WT, WT, reduced WT, and C15A-C17A were tested. Data of Figure 19 A-D.

$[Ca^{2+}]_{free}$ (μM)	non-myr WT		WT		reduced WT		C15A-C17A	
	mean	s. d.	mean	s. d.	mean	s. d.	mean	s. d.
0.00177	1	0.0655	1	0.1307	1	0.0621	1	0.0634
0.029	1.1034	0.0757	1.1545	0.0472	1.1144	0.0429	0.8742	0.1751
0.058	1.1879	0.1196	1.1819	0.1766	1.1227	0.094	0.7697	0.1364
0.099	1.3177	0.0564	1.0952	0.0956	1.1835	0.1203	0.5962	0.0815
0.159	1.3693	0.0828	1.0215	0.1301	1.1004	0.0647	0.4828	0.0532
0.255	1.3677	0.0549	1.0174	0.3399	1.0784	0.1607	0.3468	0.0101
0.405	1.4456	0.1117	0.9081	0.2315	1.1008	0.1539	0.2532	0.0427
0.705	1.5486	0.1438	1.0115	0.2057	1.0485	0.1765	0.2063	0.017
1.491	1.5604	0.1447	0.8851	0.0559	1.1014	0.2508	0.1333	0.0234
7.688	1.5033	0.1922	1.2809	0.4615	1.0339	0.1745	0.0994	0.0277
33	1.7236	0.271	1.5214	0.5305	0.9505	0.1936	0.0794	0.0147
100	2.3127	0.2794	1.5054	0.0478	0.9473	0.0871	0.1008	0.0035
1 000	1.1882	0.1338	0.8872	0.0211	0.4264	0.0462	0.0609	0.0025

Table A13: IC₅₀ measurement normalized to the mean of the lowest [Ca²⁺] of non-myr WT GCAP5 - data.

Mean and standard deviation (s. d.) of produced amounts of cGMP by recombinant human GC-E at increasing free calcium concentrations ([Ca²⁺]_{free}) in μM normalized to the mean value at the lowest [Ca²⁺]_{free} of non-myr WT of the same measurement series. GCAP5 non-myr WT, WT, reduced WT, and C15A-C17A were tested. Data of Figure 19 E.

[Ca ²⁺] _{free} (μM)	non-myr WT		WT		reduced WT		C15A-C17A	
	mean	s. d.	mean	s. d.	mean	s. d.	mean	s. d.
0.00177	1	0.0153	3.4091	0.0839	19.3775	0.1108	39.2128	0.8961
0.029	1.0748	0.0521	3.8206	0.1897	20.8051	0.1285	38.8159	0.2204
0.058	1.0556	0.0561	3.5291	0.2421	20.1418	0.3521	31.5476	1.3819
0.099	1.3189	0.0686	3.6217	0.1859	22.5277	1.4935	23.7481	0.3751
0.159	1.2774	0.0175	3.0993	0.0921	20.4117	0.2151	18.267	0.1719
0.255	1.3301	0.0548	2.897	0.0843	19.251	0.4777	13.5348	0.0176
0.405	1.361	0.0812	3.0907	0.2666	18.0632	0.3222	11.4681	0.3033
0.705	1.5524	0.0267	2.9316	0.1029	19.8043	0.9976	8.4503	0.9245
1.491	1.5165	0.0607	2.9237	0.1583	18.7223	0.4136	6.2748	0.1666
7.688	1.473	0.0945	3.9707	0.1865	18.2269	0.2479	5.1263	0.3158
33	1.5604	0.0755	4.7502	0.1667	17.1191	0.0813	3.8271	0.0521
100	2.3095	0.2908	5.1319	0.1628	16.759	0.0289	3.9529	0.1376
1 000	1.0423	0.0604	3.0247	0.0719	7.4562	0.1456	2.3885	0.0962

Table A14: Fe²⁺ and Ca²⁺-dependent GC assay - data.

Produced amounts of cGMP by recombinant human GC-E in $\text{nmol} \cdot \text{min}^{-1} \cdot \text{mg}_{\text{total protein}}^{-1}$ in the presence (+ Fe²⁺) and absence of ferrous iron (- Fe²⁺), respectively, and in the presence (+ Ca²⁺) and absence of calcium (EGTA), respectively, modulated by GCAP variants resuspended either in Mes buffer (Mes) or in sodium phosphate buffer (NaP). GCAP variants tested are GCAP5 WT, C15A-C17A, and myristoylated bovine GCAP1 (myr bovine GCAP1). Control reactions were performed without any GCAPs (- GCAP). Data of Figure 20.

	- Fe ²⁺		+ Fe ²⁺	
	EGTA	+ Ca ²⁺	EGTA	+ Ca ²⁺
WT in Mes	1.9657 \pm 0.1584	2.0896 \pm 0.0568	0.0709 \pm 0.0243	0.0975 \pm 0.0013
C15A-C17A in Mes	1.9470 \pm 0.0284	0.8033 \pm 0.0111	1.0464 \pm 0.0345	0.6706 \pm 0.0087
myr bovine GCAP1 in NaP	4.3150 \pm 0.0971	1.0763 \pm 0.0068	-	-
myr bovine GCAP1 in Mes	4.5974 \pm 0.2249	1.1186 \pm 0.1873	1.3840 \pm 0.0921	1.2612 \pm 0.0675
- GCAP in Mes	0.1051 \pm 0.0017	0.1086 \pm 0.0008	0.1032 \pm 0.0046	0.1102 \pm 0.0041

Ca²⁺-shift of GCAP5

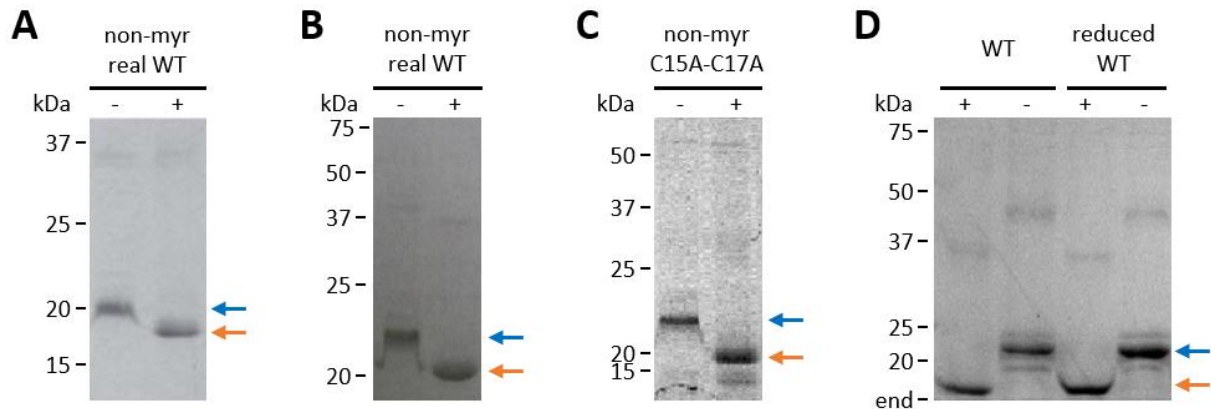


Figure A10: Ca²⁺-shift of GCAP5.

(A) Two μg of recombinant non-myristoylated wildtype GCAP5 without D3N mutation (non-myristoylated WT) in the absence (-, 1 mM EGTA and 1 mM MgCl_2) and presence (+, 1 mM CaCl_2) of Ca^{2+} , respectively, were applied onto a 15 % SDS-polyacrylamide gel. Modified from Scholten and Koch (2011). (B) Five μg of GCAP5 non-myristoylated WT in the absence (-, 2 mM EGTA) and presence (+, not specified) of Ca^{2+} , respectively, were applied onto a 12 % SDS-polyacrylamide gel. Modified from Lange (2012). (C) Five μg of GCAP5 non-myristoylated C15A-C17A, (D) WT, and reduced WT in the absence (-, 1 mM EGTA and 1 mM MgCl_2) and presence (+, 1 mM CaCl_2) of Ca^{2+} , respectively, were applied onto 12 % SDS-polyacrylamide gels. Modified from Gripenstroh (2016). Mobilities and sizes of the standard proteins (kDa) are shown to the left of each gel. The lower end of D is also the end of the gel (end). In 12 % SDS-polyacrylamide gels, Ca^{2+} -loaded GCAP5 has a mobility between 15 and 20 kDa (orange arrow), and the Ca^{2+} -free GCAP5 has a mobility around 23 kDa (blue arrow). Non-myristoylated GCAP5 shows a slightly lower mobility compared to myristoylated GCAP5. In 15 % SDS-polyacrylamide gels, non-myristoylated WT GCAP5 shows higher mobilities, around 20 kDa in the absence and around 18 kDa in the presence of Ca^{2+} .

Western Blot

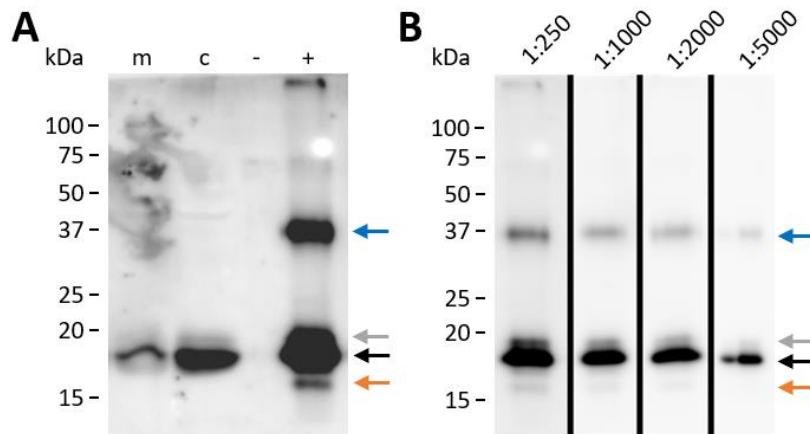


Figure A11: Testing the primary antibody rabbit anti-GCAP5.

(A) Western blot after 15 min of illumination showing GCAP5 immunoreactivity (primary antibody rabbit anti-GCAP5, 1:250, secondary antibody goat anti-rabbit POD, 1:5000) in subcellular fractions of the zebrafish retina (5 μ g of total protein; m: membrane fraction, c: cytosolic fraction). Monomeric myristoylated GCAP5 has a mobility of around 18 kDa in SDS-polyacrylamide gels appearing as a triple band. These three bands possibly represent the apo-state of the myristoylated GCAP5 (black arrow), the calcium-bound state (orange arrow), which, however, could also be a degraded GCAP5, and the non-myristoylated part of the purified GCAP5 (grey arrow). The dimeric GCAP5 has a mobility of around 37 kDa (blue arrow). The positive control is purified recombinant GCAP5 (+, 2 ng), the negative control purified recombinant zebrafish GCAP3 (-, 2 ng). (B) Western blot after 3 min of illumination. Two ng of purified, recombinant myristoylated GCAP5 were detected by the primary antibody rabbit anti-GCAP5 (second antibody goat anti-rabbit POD, 1:5000) at differing dilutions: 1:250, 1:1000, 1:2000, and 1:5000. Colors of the arrows in A also apply to B.

Immunohistochemistry

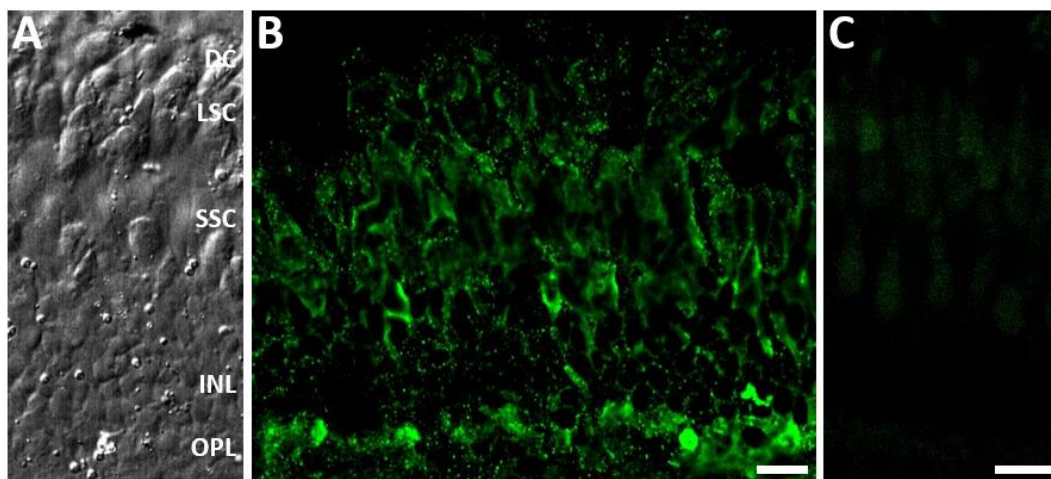


Figure A12: Detection of GCAP5 in the zebrafish retina by anti-GCAP5 and donkey anti-rabbit Alexa Fluor®488.

(B) Immunoreactivity pattern of anti-GCAP5 (primary antibody rabbit anti-GCAP5, 1:2000, secondary antibody donkey anti-rabbit Alexa Fluor®488, *Invitrogen*, 1:1000) in sections of the zebrafish retina. Images present projections of 7 x 0.3 μ m. (A) Layers of the retina are indicated in the transmissions (DC: double cone, LSC: long single cone, SSC: short single cone, OPL: outer plexiform layer, INL: inner nuclear layer). (C) The control without the primary antibody shows background in the photoreceptors (projection of 7 x 0.3 μ m). Scale bars: 10 μ m. Scale bar in B also applies to A.

Publikationen

Lim, S., Scholten, A., Manchala, G., Cudia, D., **Zlomke-Sell, S.-K.**, Koch, K.-W. and Ames, J. B. (2017). "Structural characterization of ferrous ion binding to retinal guanylate cyclase activator protein 5 from zebrafish photoreceptors." Biochemistry **56**(51): 6652-6661.

Cudia, D., Roseman, G. P., Assafa, T. E., Shahu, M. K., Scholten, A., **Menke-Sell, S.-K.**, Yamada, H., Koch, K.-W., Milhauser, G. and Ames, J. B. (2021). "NMR and EPR-DEER Structure of a Dimeric Guanylate Cyclase Activator Protein-5 from Zebrafish Photoreceptors." Biochemistry **60**(41): 3058-3070.

Danksagung

Als erstes danke ich Prof. Dr. Karl-Wilhelm Koch. Du hast mir ein sehr interessantes Thema überlassen und meine Doktorarbeit konstruktiv betreut. Außerdem danke ich dir für das Vertrauen und die Geduld.

Außerdem danke ich apl. Prof. Dr. Ulrike Janssen-Bienhold, zum einen für die Übernahme des Zweitgutachtens, aber auch dafür, dass du mir bei meinen immunhistochemischen Färbungen so gut geholfen hast. Die Zusammenarbeit mit dir hat mir sehr viel Spaß gemacht.

Dr. Alexander Scholten, seit ich für meine Bachelorarbeit zum ersten Mal in die Abteilung Biochemie gekommen bin, hast du mich bei allen möglichen Problemen rund um die Forschung unterstützt. Danke dafür.

Werner Säftel, deine Erfahrung im Labor war sicherlich für uns alle von unschätzbarem Wert. Wenn man auf ein Problem gestoßen ist, konnte man sich immer auf deine Hilfsbereitschaft und auf deinen Ideenreichtum verlassen. Danke, dass du immer da warst.

Jutta Appelt, mit der Pflege und der allmorgendlichen Vorbereitung der Zellkultur hast du sicherlich uns allen sehr viel Arbeit abgenommen. Auch bei Fragen rund um die Zellkultur konnte man sich immer auf dich verlassen. Vielen Dank.

Dr. Stefan Sulmann, auch du hast mir seit meiner Bachelorarbeit sehr viel geholfen. Die Zusammenarbeit mit dir war immer sehr angenehm und hat mir sehr viel Spaß gemacht. Danke, dass du meinen Start in der Abteilung Biochemie so gut unterstützt hast.

Auch allen weiteren Mitgliedern der Abteilung Biochemie danke ich für die Zusammenarbeit. Besonders danke ich neben den oben genannten Personen der Abteilung Biochemie auch Dr. Michael Müller, Astrid Sulmann, Dr. Maike Köster, Dr. Patrick Zägel und Dr. Farina Vocke-Dörries für die herzliche Aufnahme in die AG. Außerdem danke ich Vanessa Schnarre, Dr. Seher Abbas, Dr. Charlotte Beelen und Malte Lübben. Ihr habt mir mehr als ihr euch vielleicht vorstellen könnt durch eine schwierige Zeit geholfen.

Natalie Schmidt, Michela Cumerlato, and Jennifer Richter, it was a pleasure to work with you and to tutor your Bachelor theses. Thank you for your help in the lab and for your curiosity.

Prof. Dr. James B. Ames, thank you for the great collaboration and a lot of ideas to investigate the biochemical properties of zebrafish GCAP5.

Prof. Dr. Yogendra Sharma, Dr. Anand Kumar Sharma, and Dr. Radhika Khandelwal, I want to thank you for the opportunity to visit Hyderabad in India and to work in a highly inspiring and interdisciplinary workplace. Additionally, I want to thank Dr. Amrutha H. Chidananda, Dr. Asmitta D. Pawar, Sai Uday Kiran, and Manisha Kumari Shahu. All of you spared no effort to make my stay in India unforgettable in the most positive way. I enjoyed every single day. Also, I am happy that Manisha found her way into our group.

Ganz besonders danke ich meinem Mann, meiner Familie und meinen Freunden.

Erklärung

Hiermit erkläre ich, dass ich die vorliegende Dissertation selbstständig verfasst und nur die angegebenen Hilfsmittel und Quellen benutzt habe. Ich versichere, dass die vorliegende Dissertation weder in ihrer Gesamtheit noch in Teilen einer anderen Hochschule zur Begutachtung in einem Promotionsverfahren vorliegt oder vorgelegen hat. Weiterhin versichere ich, dass mir die Leitlinien guter wissenschaftlicher Praxis der Carl von Ossietzky Universität Oldenburg bekannt sind und von mir befolgt wurden. Außerdem erkläre ich, dass im Zusammenhang mit dem Promotionsvorhaben keine kommerziellen Vermittlungs- oder Beratungsdienste (Promotionsberatung) in Anspruch genommen worden sind.

Teile dieser Arbeit wurden bereits veröffentlicht (siehe Abschnitt Publikationen auf S. 128).

Oldenburg (Oldb), den 31. Januar 2023

Ort, Datum

Sarah-Karina Menke-Sell